Modelling the movements of flapper skate (*Dipturus intermedius*) in relation to a Scottish Marine Protected Area

Edward Lavender

A thesis submitted for the degree of PhD
at the
University of St Andrews

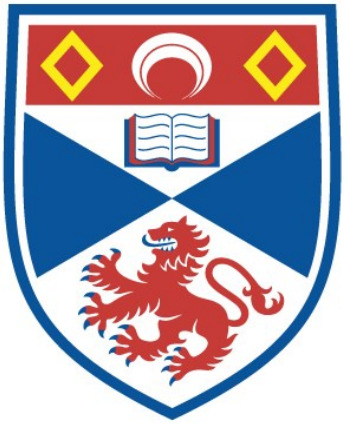

2022

Identifier to use to cite or link to this thesis:

DOI: https://doi.org/10.17630/sta/201

Abstract

1. Movement shapes the lives of animals and their interactions with human activities. In recent decades, the emergence of movement ecology as a discipline and developments in electronic tagging and tracking have led to substantial improvements in our understanding of animal movement and its implications for species conservation. Yet while research has burgeoned for many taxa, including sharks, other groups in aquatic ecosystems, such as skate (Rajidae), remain comparatively understudied.
2. The flapper skate (*Dipturus intermedius*) is a large, Critically Endangered elasmobranch. The species has been extirpated from much of its former range, but individuals are still found off west Scotland where the Loch Sunart to the Sound of Jura Marine Protected Area (MPA) has been designated for flapper skate conservation. However, skate movements within and around the MPA remain poorly understood.
3. This thesis investigates the movements of flapper skate in relation to the MPA using electronic tagging and tracking data from passive acoustic telemetry, archival (depth and temperature) tags and mark-recapture angling. Objectives include the examination of site affinity, vertical movements and responses to disturbance. Research in these areas motivates the development of a flexible, mechanistic modelling framework for passive acoustic telemetry systems.
4. For flapper skate, the key finding is the prevalence of site affinity to the MPA. Vertical movements are shaped by depth-specific periodic behaviours and individual variation. These movements can be perturbed by angling, but on the whole skate appear to be behaviourally resilient to this practice.
5. Beyond flapper skate, this thesis highlights multifarious uses of electronic tagging and tracking data, brings underutilised analytical methods to the attention of the movement ecology community and establishes a holistic framework for movement modelling in passive acoustic telemetry systems. This work demonstrates the wide-ranging contributions of species-specific studies in the fields of movement ecology and conservation.

Candidate's declaration

I, Edward Lavender, do hereby certify that this thesis, submitted for the degree of PhD, which is approximately 60,000 words in length, has been written by me, and that it is the record of work carried out by me, or principally by myself in collaboration with others as acknowledged, and that it has not been submitted in any previous application for any degree. I confirm that any appendices included in my thesis contain only material permitted by the 'Assessment of Postgraduate Research Students' policy.

I was admitted as a research student at the University of St Andrews in September 2018.

I received funding from an organisation or institution and have acknowledged the funder(s) in the full text of my thesis.

Date 31/05/2022 Signature of candidate

Supervisor's declaration

I hereby certify that the candidate has fulfilled the conditions of the Resolution and Regulations appropriate for the degree of PhD in the University of St Andrews and that the candidate is qualified to submit this thesis in application for that degree. I confirm that any appendices included in the thesis contain only material permitted by the 'Assessment of Postgraduate Research Students' policy.

Date 06/06/2022 Signature of supervisor

Permission for publication

In submitting this thesis to the University of St Andrews we understand that we are giving permission for it to be made available for use in accordance with the regulations of the University Library for the time being in force, subject to any copyright vested in the work not being affected thereby. We also understand, unless exempt by an award of an embargo as requested below, that the title and the abstract will be published, and that a copy of the work may be made and supplied to any bona fide library or research worker, that this thesis will be electronically accessible for personal or research use and that the library has the right to migrate this thesis into new electronic forms as required to ensure continued access to the thesis.

I, Edward Lavender, confirm that my thesis does not contain any third-party material that requires copyright clearance.

The following is an agreed request by candidate and supervisor regarding the publication of this thesis:

Printed copy

No embargo on print copy.

Electronic copy

Embargo on all of electronic copy for a period of 2 years on the following ground(s):

- Publication would preclude future publication

Supporting statement for electronic embargo request

Publication would preclude further publication of thesis chapters as peer-reviewed papers.

Title and Abstract

- I agree to the title and abstract being published.

Date 31/05/2022 Signature of candidate

Date 06/06/2022 Signature of supervisor

Underpinning Research Data or Digital Outputs

Candidate's declaration

I, Edward Lavender, hereby certify that no requirements to deposit original research data or digital outputs apply to this thesis and that, where appropriate, secondary data used have been referenced in the full text of my thesis.

Date 31/05/2022 Signature of candidate

Acknowledgements

This thesis owes a great deal to many people. Academic mentorship from Alex Rogers, Owen Lewis, Ada Grabowska-Zhang, Ella Cole, Ben Sheldon, Michael Morrissey, Clive Fox, Michael Burrows and many others encouraged me to pursue a PhD and I am grateful to you all. Many thanks to my supervisors James Thorburn, Sophie Smout, Mark James, Janine Illian and Peter Wright for your steadfast support over the years. I could not have wished for a kinder team of supervisors. Jane Dodd was helpful throughout my studies and, together with Rachel Mawer, greatly facilitated the use of angler mark-recapture data. Samuel Iglésias graciously shared data and analyses of size–maturity relationships in flapper skate. Dmitry Aleynik provided model outputs and assistance with the West Scotland Coastal Ocean Modelling System, which was integral to Chapters Two and Three. Clinton Blight provided model outputs from POLTIPS.3 tidal prediction software, supporting Chapters Two, Four and Five. Advice from Julien Martin, David Miller, Dimitrios Stasinopoulos, Cecilia Pinto and Luigi Spezia informed Chapter Four. Feedback from John Baxter and several anonymous reviewers refined material in Chapters Three–Five. Chapter Six was inspired by a conversation with Jason Matthiopoulos and the particle filtering methodology was suggested by Richard Glennie. Stanisław Biber stepped in to help bring this together with refreshing enthusiasm and the chapter benefited enormously from your inputs. Many other colleagues advised me throughout the years, especially Andy Seaton and members of the Movement Ecology of Flapper Skate and the Flapper Skate steering groups, and I am grateful to you all.

For time in the field, I am indebted to James Thorburn, Jane Dodd and Roger Eaton. Thanks to Mark James for sharing field kit and to Georgina Cole and Adam Naylor for accommodating me during fieldwork. Lisa Kamphausen's photograph of a flapper skate from a recent field trip graces Chapter One and I am grateful for her permission to include it in this thesis. John Boyd created an opportunity to join the Irish Groundfish Survey during the final year of my PhD, which provided welcome respite from my studies and greatly supported my wider scientific development.

Throughout my PhD, I benefited from discussions with members of the Bayesian Statistics Reading Group, especially James Rimmer, Janneke Ransijn and Edith Invernizzi. In the Scottish Oceans Institute, David Patterson made me feel welcome and the Marine Alliance for Science and Technology for Scotland (MASTS), the MASTS Graduate School and administrative staff at the University of St Andrews, especially Rhona Rodger and Jess Fenton, provided helpful assistance throughout my studies.

Supportive family and friends have been the bedrock for my academic development. For many people this is not a given and this thesis owes more to you than me. It is dedicated to you.

At the time of writing (May 2022), material from Chapters Three, Four and Five has been published in the following publications, which are here acknowledged:

- **Lavender, E.**, Aleynik, D., Dodd, J., Illian, J., James, M., Wright, P. J., et al. (2021). Movement patterns of a Critically Endangered elasmobranch (*Dipturus intermedius*) in a Marine Protected Area. *Aquat. Conserv. Mar. Freshw. Ecosyst.* 32, 348–365. doi:10.1002/aqc.3753.
- **Lavender, E.**, Aleynik, D., Dodd, J., Illian, J., James, M., Wright, P. J., et al. (2021). Environmental cycles and individual variation in the vertical movements of a benthic elasmobranch. *Mar. Biol.* 168, 164. doi:10.1007/s00227-021-03973-1.
- **Lavender, E.**, Aleynik, D., Dodd, J., Illian, J., James, M., Wright, P. J., et al. (2022). Behavioural responses of a large, benthic elasmobranch to catch-and-release angling. *Front. Mar. Sci.* 9, 864344. doi:10.3389/fmars.2022.864344.

The work was conducted during a PhD studentship at the University of St Andrews, jointly funded by NatureScot (via MASTS) and the Centre for Research into Ecological and Environmental Modelling. Data were collected as part of research funded by NatureScot (project 015960) and Marine Scotland (projects SP004 and SP02B0) via the Movement Ecology of Flapper Skate project. Additional funding was provided from MASTS and Shark Guardian.

Contents

Chapter One

Introduction

Abstract

1. A principal aim of movement ecology is to reconstruct the movements of animals and understand their drivers. In recent years, research in this discipline has been driven by rapid developments in methods of data collection and analysis, with significant implications for ecology and conservation. At a time when animal populations are under unprecedented pressure and studies of animal movement have never been more important, there is a pressing need to review these developments and their implications to guide future research, as laid out in this thesis.
2. In Scotland, the flapper skate (*Dipturus intermedius*) is one of the most threatened marine species. In 2016, the Loch Sunart to the Sound of Jura Marine Protected Area (MPA) was designated for this species, but the movements of skate in relation to this area remain poorly understood.
3. The aim of this thesis is to investigate the movements of flapper skate using electronic tagging and tracking data from the MPA collected as part of the Movement Ecology of Flapper Skate project.
4. This introductory chapter establishes the context for this investigation within the field of movement ecology. Technological developments in data collection methods and their relationship to the specific approaches applied to flapper skate are reviewed. Movement modelling frameworks for electronic tagging and tracking data are reviewed to guide research and highlight areas ripe for development that are tackled in subsequent chapters. The taxonomy, distribution, life history, diets and movements of flapper skate are reviewed to define thesis objectives.
5. This chapter demonstrates the potential for recent developments in movement ecology to support research on flapper skate and the opportunities for this line of research to contribute

towards improved understanding of a wide range of theoretical and applied issues in movement ecology as a whole.

Keywords
conservation, *Dipturus intermedius*, electronic tagging and tracking, modelling, movement ecology, Rajidae

1. Introduction

Movement ecology seeks to understand the causes and consequences of movement in nature (Nathan et al., 2008). This ambition requires research into the proximate and ultimate explanations for why, how, when and where movement occurs and their implications (Nathan et al., 2008). This field of work spans multiple levels of biological organisation, from the run-and-tumble propulsion of bacteria (Sidortsov et al., 2017) to the dispersal of plant seeds (Treep et al., 2021) and the multifarious activities of animals (Nathan et al., 2008). However, it is among the latter group that movement reaches its most spectacular and varied, unifying the subterranean burrowing of star-nosed moles (*Condylura cristata*) (Catania, 2005) with the sprint of the cheetah (*Acinonyx jubatus*) (Wilson et al., 2018), the murmurations of starlings (*Sturnus vulgaris*) (Mora et al., 2016) and the explosive predatory movements of great white sharks (*Carcharodon carcharias*) (Semmens et al., 2019).

In the study of animal movement, recent decades have seen a shift from a Eulerian perspective of movement patterns, which treats animals as agglomerations, to a Lagrangian perspective, which considers movement from the perspective of individuals (Turchin, 1998). This shift has been coupled with tremendous enhancements in the capacities of electronic tags designed to be attached to individuals and collect quantitative data on movement and the environment (Hussey et al., 2015; Kays et al., 2015; Nathan et al., 2022). One of the most basic applications of these technologies lies in the identification of where animals go. In aquatic ecosystems, satellite tracking has reconstructed the major flyways of threatened shorebirds (Chan et al., 2019), the transoceanic movements of marine turtles (Hays and Hawkes, 2018), journeys undertaken by the great whales (Mate et al., 2015) and the wide-ranging movements of sharks (Hammerschlag et al., 2022). At the same time, acoustic telemetry and archival tags have revealed fine-scale movements in coastal areas (Matley et al., 2022), record-breaking dives (Quick et al., 2020) and ocean-wide movements of pelagic taxa such as tuna (Block et al.,

2005). Yet the collection of movement data is only one part of the story and, increasingly, sophisticated modelling approaches are required to translate these data into information that can be interpreted and used to support conservation (Patterson et al., 2017).

Reconstructing the movements of animals has significant implications for ecology and conservation. Many rhythms of life pulse through movement: limpets (*Patella sp.*) forage with the tides (Sempere-Valverde et al., 2019), the daily movements of juvenile Atlantic salmon (*Salmo salar*) define and reflect territories (Valdimarsson and Metcalfe, 2001) and groupers (Epinephelidae) concentrate at specific lunar phases in aggregations to spawn, driving the movements of predatory sharks (Rhodes et al., 2019). Increasingly, movement also affects the stressors to which individuals are exposed and their interactions with humans (Rutz et al., 2020; Bates et al., 2021; Doherty et al., 2021). Among vertebrates, chondrichthyans (sharks, skates, rays and chimeras) are one of the most threatened groups, with many large, K-selected, shallow-water species decimated by years of overexploitation (Dulvy et al., 2014; Pacoureau et al., 2021). There has never been a more important time to investigate the exposure of these taxa to threats and to develop conservation solutions.

In Scotland, the flapper skate (*Dipturus intermedius*) is one of the largest and most threatened elasmobranchs, despite only being recently recognised as a distinct species within the common skate (*D. batis*) species complex that includes both flapper and common blue skate (*D. batis*) (Iglésias et al., 2010; Last et al., 2016). Once widespread, the common skate was the first marine fish species to be declared locally extinct in an area (Brander, 1981). Yet the skate remain off the west coast of Scotland, where historical mark-recapture data indicating site affinity supported the designation of the Loch Sunart to the Sound of Jura Marine Protected Area (LStSJ MPA) (Neat et al., 2015). In line with this action, in 2016 the Movement Ecology of Flapper Skate (MEFS) project was established to improve our understanding of flapper skate movement through the deployment of acoustic and archival tags in the MPA.

As part of the MEFS project, the aim of this PhD is to investigate the movements of flapper skate in relation to the MPA, and their ecological and conservation implications, using electronic tagging and tracking data. Key objectives include the definition of reproducible data processing protocols and consideration of the influence of the environment in movement analyses (Chapter Two), investigations into time spent in the MPA (Chapter Three) and vertical movements (Chapter Four), an examination of responses to disturbance (Chapter Five) and the

reconstruction of fine-scale movements and emergent patterns of space use (Chapter Six). Beyond flapper skate, this research touches on a wide range of theoretical and applied issues in movement ecology, including the links between the environment and movement (Chapter Two), the design of MPAs for mobile species (Chapter Three), the links between movement and activity levels (Chapter Four), underutilised uses of electronic tagging and tracking data (Chapters Two and Five) and roles of holistic movement modelling frameworks (Chapter Six). At the same time, this research illustrates underutilised analytical methods (Chapters Four–Five) and develops new modelling frameworks that have widespread applications in movement ecology (Chapter Six).

The aim of this chapter is to set the scene for this investigation within the field of movement ecology, introducing types of electronic tagging and tracking data and their relationship to the specific technologies applied to flapper skate, movement modelling frameworks and the implications of this line of research for ecology and conservation. The taxonomy, distribution, life history, diets and movements of flapper skate are reviewed to define project objectives, as tackled in subsequent chapters.

2. Biologging and biotelemetry

A central component of movement ecology is the identification of where animals go (Nathan et al., 2008). Historically, animal movements were inferred from mark-recapture data (Hammond, 2009) but recent technological development has led to a proliferation of technologies revealing animal movements in unprecedented detail in a diverse array of settings (Hussey et al., 2015; Kays et al., 2015; Nathan et al., 2022). Nevertheless, two broad categories of electronic tagging and tracking technologies have been distinguished on the basis of whether or not they transmit data to an external station (biotelemetry) or store data onboard (biologging) (Cooke et al., 2021). Key examples include satellite tracking, acoustic telemetry and archival tagging (Figure 1).

Satellite tags, in association with the Advanced Research and Global Observation Satellite and Global Navigation Satellite Systems (such as the Global Positioning System), have been a major development (Hussey et al., 2015; Kays et al., 2015). These tags record and in some cases transmit data from tagged individuals via satellites. In aquatic ecosystems, these technologies have been exploited to study the movements of seabirds (Phillips et al., 2007),

marine mammals (Mate et al., 2015), turtles (Hays and Hawkes, 2018) and elasmobranchs (Hammerschlag et al., 2022). However, their application is restricted by the attenuation of radio signals in water (Hussey et al., 2015). Consequently, in aquatic ecosystems, acoustic telemetry and archival tags are often used to study movement instead.

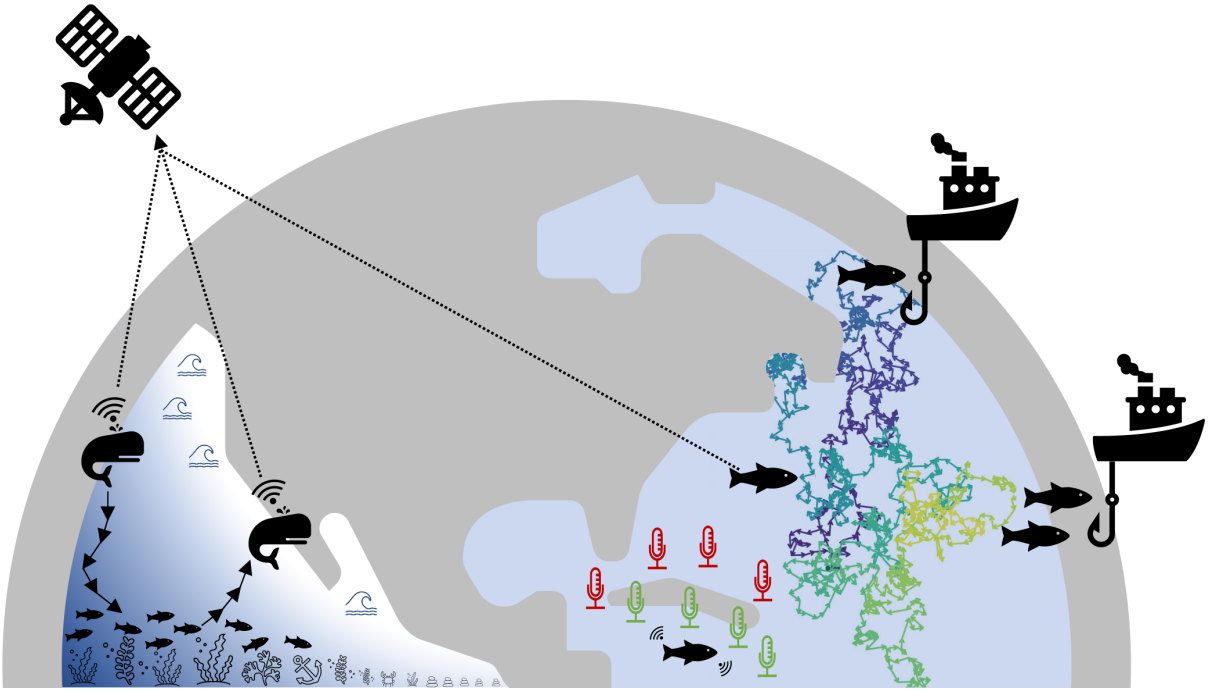

Figure 1. Electronic animal tracking in marine ecosystems. Satellite tracking is widely used for seabirds, turtles, marine mammals (pictured) and other taxa but is limited by the time that individuals spend at the surface (left). In coastal areas, passive acoustic telemetry is widely deployed (middle). For demersal and pelagic species, archival tags (global location sensors) are widely used to track movements over larger spatial scales and to study vertical movement. Pop-up satellite tags release from tagged animals after a preprogramed interval and relay data packets to satellites, but standard archival tags require tagged individuals to be recaptured for data retrieval (pictured). Images sourced from Microsoft.

Acoustic telemetry is the use of sound underwater to study movement (Johnson et al., 2009). Active acoustic telemetry involves following acoustically vocal or acoustically tagged animals from the surface and marking their positions at defined intervals—a cost and time-intensive operation (Morrissey and Gruber, 1993). Passive acoustic telemetry involves the deployment of static hydrophone arrays underwater, which record individual-specific detections of acoustically tagged individuals that move within range (Heupel et al., 2006). These systems are now widely deployed in coastal aquatic ecosystems (Matley et al., 2022).

Archival tags or global location sensors record pressure (depth) and environmental data (such as light-levels and temperature) at pre-programmed intervals (Hussey et al., 2015). Pop-up

satellite archival tags detach from tagged animals after a defined time period, at which point they float to the surface and transmit processed data packets via satellites (and may be retrieved by beach combers). Meanwhile, standard archival tags remain on tagged individuals until those individuals are recaptured (or the tags are lost). Archival tags from recaptured animals can then be removed and the stored data downloaded. Data from both tag types can be used to reconstruct the tracks of tagged individuals (geolocation) over hundreds of kilometres and study vertical movement (Hussey et al., 2015).

3. Movement modelling

When it comes to studying animal movement, the collection of movement data is only one side of the coin. Increasingly, secure data storage infrastructures, reproducible data processing protocols and sophisticated modelling approaches are required to safeguard and interpret movement datasets (Chapter Two; Williams et al., 2020). From a statistical perspective, the properties of modern tracking data can be complex, including spatiotemporal autocorrelation in high-resolution movement time series, non-linearity of observations and their relationships with predictors, and non-normality of movement metrics (Chapters Four and Six; Pinto and Spezia, 2016; Patterson et al., 2017). For this reason, early studies in the movement ecology literature were largely descriptive and many have opted to separate temporal and spatial analyses (Figure 2, Tables 1–2).

In the context of passive acoustic telemetry, temporal analyses query trends in the detections of individuals (Figure 2, Table 1). Detection histories are plotted to depict the detections of each individual through time and summarised using residency indices (Kessel et al., 2016), such as the number of days that individuals spent around receivers (Chapter Three). Descriptive statistics are widely used to investigate trends. For instance, one relatively common approach aggregates detections into time intervals and tests whether the frequency of detections at certain time intervals is greater than expected by chance (i.e., null-hypothesis significance testing), though other approaches have also been exploited (Table 1). The consistency of patterns across individuals is interpreted qualitatively (Collins et al., 2007). However, more sophisticated statistical models can support these types of approaches by investigating trends in detections in relation to their drivers (such as temporal biological rhythms) while adjusting for confounding variables (Chapter Three).

For spatial analyses of passive acoustic telemetry data, mapping detection histories is a useful starting point (Figure 2, Table 1) (Chapter Three). Nevertheless, recently, there has been a push towards the adoption of a common quantitative framework based on centres of activity (COAs) (Udyawer et al., 2018). In this framework, an individual's COAs are estimated over pre-defined time intervals from the locations of receivers at which it was detected. Typically, the mean-position algorithm is used for estimation (Simpfendorfer et al., 2002), though other algorithms have also been suggested (Table 1). COAs are then incorporated into home range analyses, usually by treating COAs as 'relocations' for kernel utilisation distribution estimation (Udyawer et al., 2018). Despite the widespread use of this approach, in non-uniform arrays COAs may be severely constrained by the locations of receivers and thus relatively uninformative about movement patterns across an area (Chapter Six). Alternative approaches, such as network analysis and latent-variable models, have also been proposed (Pedersen and Weng, 2013; Lea et al., 2016; Hostetter and Royle, 2020). However, a comprehensive modelling framework for passive acoustic telemetry remains lacking (Chapter Six).

Analyses of archival time series have followed a similar trajectory (Figure 2, Table 2). Temporal analyses focus on trends in vertical movement and their drivers. Many studies have favoured visual approaches and descriptive statistics (Scott et al., 2016). Signal processing techniques are widely applied to support qualitative interpretation of movement patterns (Shepard et al., 2006; Subbey et al., 2008). These methods can be highly effective at revealing trends in vertical movement, but they are less effective at quantifying potential drivers of variation. For this reason, these kinds of descriptive analyses are increasingly complemented by sophisticated statistical modelling approaches that represent movement metrics as functions of possible explanatory variables and/or underlying processes. Hidden Markov models have become particularly popular (Patterson et al., 2017). These models conceptualise observations as manifestations of hidden states (usually interpreted as behaviours) and model the transition probabilities between states. These approaches are well-suited to time series data but the absence of information on underlying states can constrain interpretation. Markov switching autoregressive models are a generalisation of this approach recently brought to the attention of ecologists by Pinto and Spezia (2016). In an analysis of depth time series from archival tags, their model indicated vertical movements associated with diel and lunar cycles. The model outperformed a hidden Markov model, but currently requires specialist expertise, discrete covariates and commercial libraries, which has limited its use. Nevertheless, other modelling approaches such as generalised additive models that are more familiar to ecologists also offer

potential in this area (Wood, 2017; Pedersen et al., 2019), particularly if used in combination with other flexible regression techniques (Chapter Four).

Over broad spatial scales (typically on the order of hundreds or thousands of kilometres), archival time series can also be used to infer individual location (Figure 2, Table 2). Geolocation approaches come in two main types. For shallow-water species, light-level data can be used to estimate day lengths and the time of noon/midnight, from which latitude and longitude can be estimated (Braun et al., 2018). For demersal or benthic species, tidal geolocation methods that relate observed sinusoidal signatures in vertical movement time series (from periods of sedentary behaviour on the seabed) to background variation are used instead (Pedersen et al., 2008). Yet while these approaches have yielded significant insights at broad spatial scales, at smaller spatial scales geolocation algorithms are limited by the spatial uncertainty around estimated locations (which may exceed tens of kilometres). However, considerable scope remains to combine archival time series with passive acoustic telemetry to reconstruct movements at smaller spatial scales (Chapter Six).

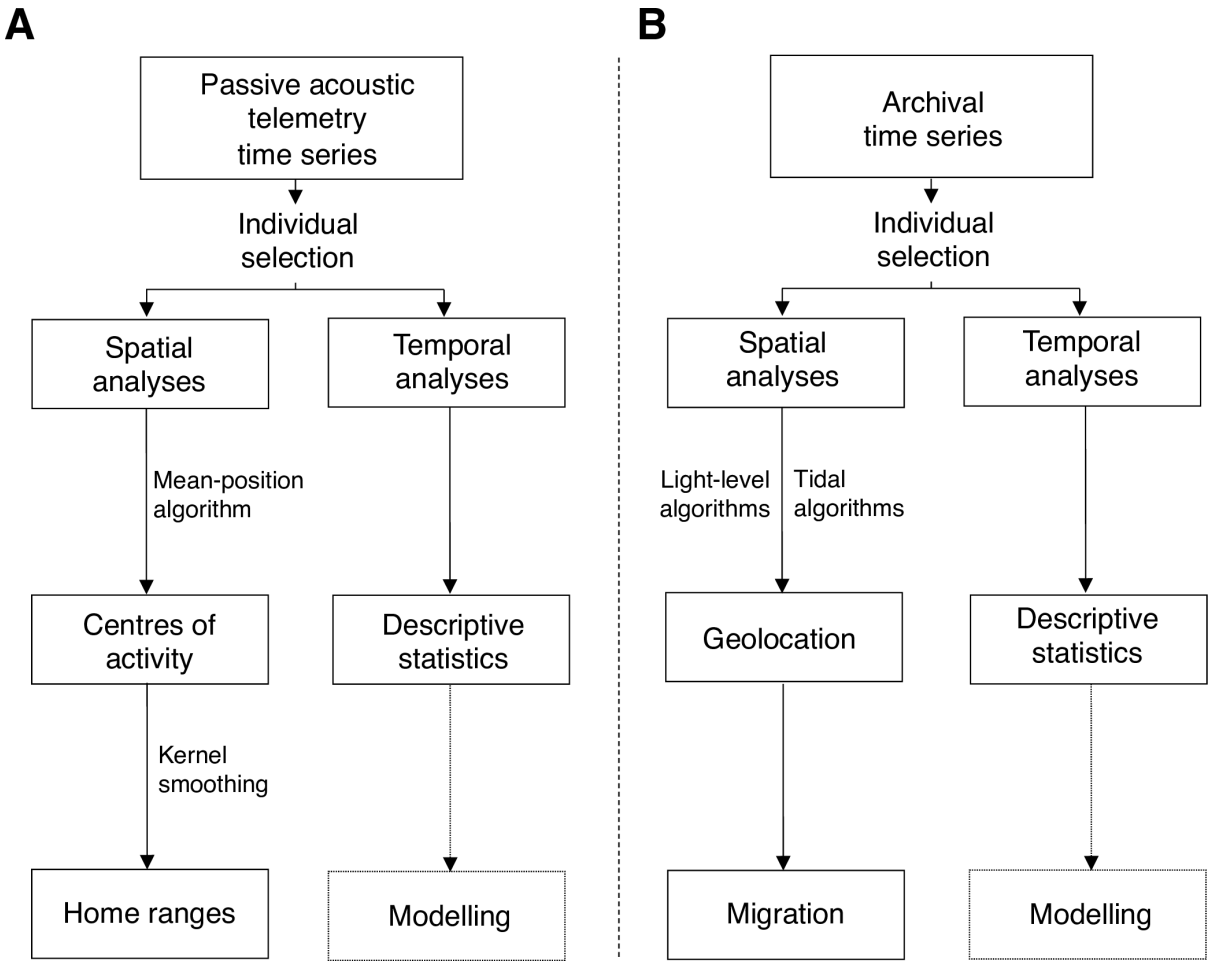

Figure 2. Conventional schemes for the analysis of (A) passive acoustic telemetry and (B) archival time series. For both data types, conventional workflows typically consider each individual and spatial and temporal analyses separately. Spatial analyses typically reconstruct movement paths or patterns of space use via the estimation of centres of activity (in the case of passive acoustic telemetry) or geolocation algorithms (in the case of archival time series). Temporal analyses typically use descriptive statistics to describe trends. These approaches are increasingly being extended via sophisticated statistical modelling techniques.

Table 1. Conventional approaches for the analysis of passive acoustic telemetry data. For each broad category of analysis (temporal, spatial and spatiotemporal), common ecological motivations, general approaches, example techniques and references are listed. Techniques highlighted in italics are particularly common.

Category	Motivation & approach	Example techniques	Example references
Temporal	Residency & visualisation	*Detection histories*	(Kessel et al., 2016)
		Residency indices	
	Periodic patterns & descriptive statistics	Binned summarises	(Collins et al., 2007)
		Circular statistics	(Barnett et al., 2012)
		Signal processing (e.g., fast Fourier transformation)	
Spatial	Spatial patterns & visualisation	*Mapping*	(Barnett et al., 2012)
	Centres of activity & estimation algorithms	*Mean-position algorithm*	(Simpfendorfer et al., 2002)
		Nonparametric algorithms (e.g., local polynomial regression)	(Hedger et al., 2008)
		Random sampling	(Becker et al., 2016)
	Home ranges & smoothing	Minimum convex polygons	(Udyawer et al., 2018)
		Kernel utilisation distributions	
		Brownian bridge movement models	
		Grid occupancy analysis	(Lea et al., 2016)
Spatio-temporal	Home ranges & network analysis or regression modelling	Network analysis	(Lea et al., 2016)
		Flexible regression	(Kock et al., 2018)
		Latent-variable models	(Pedersen and Weng, 2013; Winton et al., 2018; Hostetter and Royle, 2020)

Table 2. Conventional approaches for the analysis of archival data. As for passive acoustic telemetry data, studies have typically analysed temporal trends and spatial patterns using different frameworks, although many analyses blur these boundaries.

Category	Motivation & approach	Examples	References
Temporal	Periodic patterns & descriptive statistics	Visualisation	(Scott et al., 2016)
		Binned summarises	(Humphries et al., 2017)
		Circular statistics	(Tennessen et al., 2019)
		Signal processing (e.g., fast Fourier transformation)	(Graham et al., 2006; Subbey et al., 2008)
	Behaviour & classification	Classification	(Humphries et al., 2017)
		Latent-variable models (e.g., hidden Markov models)	(Pinto and Spezia, 2016)
	Drivers & flexible regression	Locally weighted smoothing	(Neat et al., 2006)
		Generalised additive models	(Thorburn et al., 2019)
Spatial	Geolocation	Light-level geolocation	(Teo et al., 2004; Block et al., 2005; Braun et al., 2018)
		Tidal geolocation	(Hunter et al., 2003; Pedersen et al., 2008)

4. Ecological implications

Reconstructing the movements of animals is important because movements reflect how animals perceive, respond to and influence their surroundings (Figure 3) (Nathan et al., 2008; Riotte-Lambert and Matthiopoulos, 2020). For example, movements define and reflect home ranges (Chapter Three and Six). Burt (1943) defined the home range as the 'area traversed by an individual in its normal activities of food gathering, mating, and caring for young'. Other authors have taken this definition further, linking movements with a multilayered cognitive map that reflects the very way an animal perceives its landscape (Powell and Mitchell, 2012). Under either definition, movement plays a critical role in the way animals interact with their surroundings and home ranges have emerged as a widely documented feature of animal movement, even in far-ranging species such as tiger sharks (*Galeocerdo cuvier*) (Hammerschlag et al., 2022) and other large elasmobranchs (Chapman et al., 2015).

Activity levels and behavioural changes (such as resting versus foraging) are often expressed through movement too (Chapter Four; Hertel et al., 2020). In aquatic environments, for vertically mobile species (or species that move over the substrate in areas with varying bathymetry), these changes are particularly apparent in the vertical dimension and closely associated with periodic environmental cycles (Scott et al., 2016). Diel vertical migration (DVM) is perhaps the movement pattern most commonly exhibited by aquatic species and often linked to species interactions (especially predation) and bodily processes such as thermoregulation (Neilson and Perry, 1990; Graham et al., 2006; Arostegui et al., 2020). However, a wide range of related patterns exist that are collectively termed depth-specific periodic behaviours (Scott et al., 2016).

The ways in which animals respond to disturbances are also partly expressed through changes in movement (Chapter Five; Doherty et al., 2021). For example, in multiple pelagic species, aberrations in movement have been noted following tagging indicative of behavioural change and irregular post-release behaviour (Hoolihan et al., 2011; Whitney et al., 2016, 2017). These changes are associated with both short-term and long-term consequences, such as increased predation risk and reduced survivability (Cooke and Philipp, 2004; Musyl and Gilman, 2019).

Biological characteristics, habitat preferences and ecological processes shape animal movement, which means that studies of movement can shed light on many wider areas of

interest in ecology (Shaw, 2020). For example, studies on diverse taxa—from sharks to seabirds—have indicated personality differences among individuals that appear to be at least partly expressed through differences in movement (Chapters Four–Five; Jacoby et al., 2014; Patrick and Weimerskirch, 2014). At the same time, the connections movement creates within (and between) ecosystems have many broader ecological implications, influencing trophic interactions, competition and other processes (Williams et al., 2018). For example, a study on lemon sharks (*Negaprion brevirostris*) suggested links between movements into shallow water with the flowing tide and the exploitation of prey in intertidal areas (Carlisle and Starr, 2010), while studies on skate (Rajiae) movements have revealed fine-scale spatial partitioning and pointed towards the structuring influence of competition in aquatic ecosystems (Chapter Six; Humphries et al., 2016). Collectively, these studies indicate the important contributions the field of movement ecology can make to the wider science of ecology.

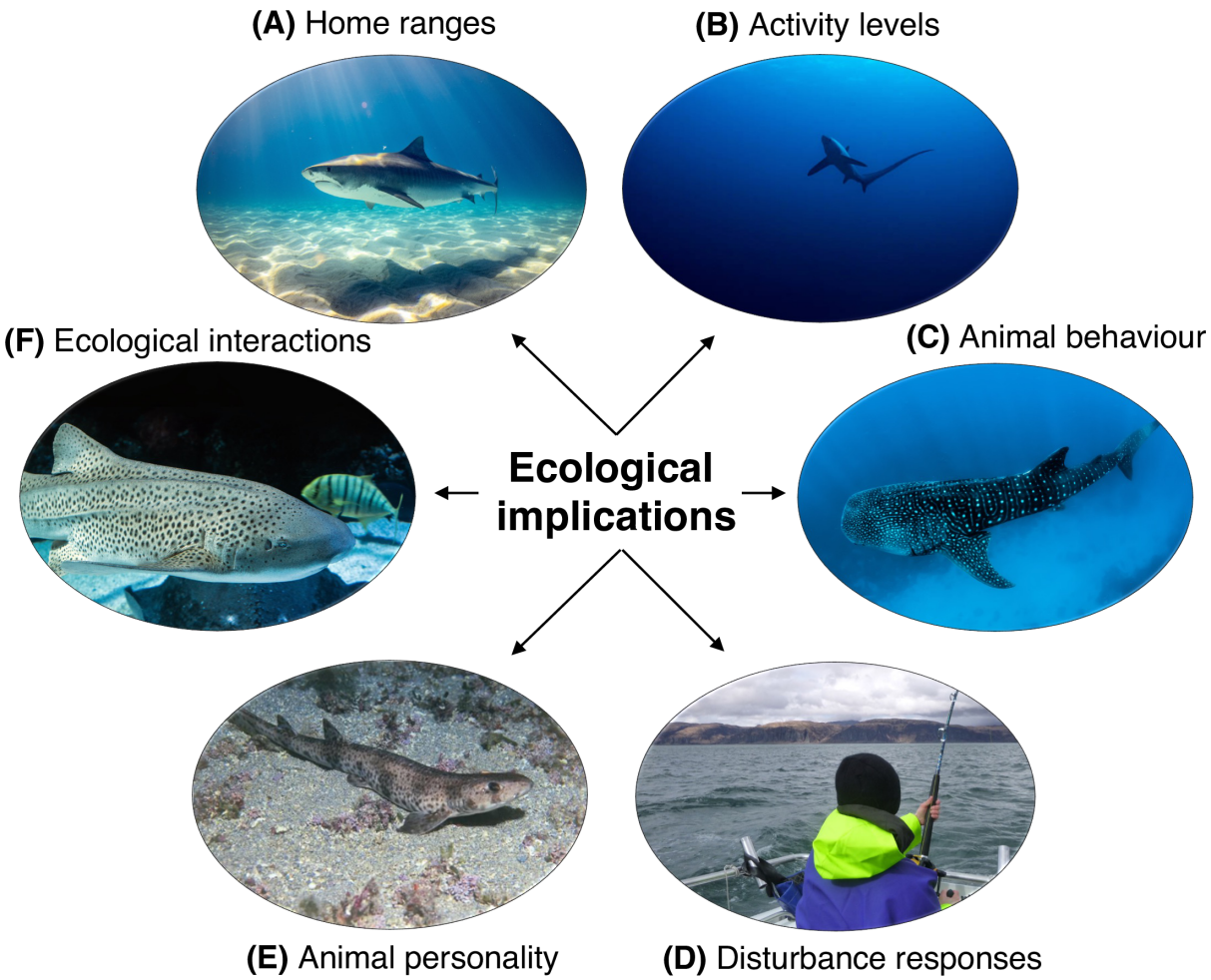

Figure 3. Ecological implications of animal movement, with examples from elasmobranchs. A, movements define and shape home ranges, including in tiger sharks (*Galeocerdo cuvier*) (Hammerschlag et al., 2022). **B**,

activity levels (such as increased crepuscular activity) are expressed through movement (e.g., diel vertical migration) in many species, including thresher sharks (*Alopias sp.*) (Arostegui et al., 2020). **C**, behaviours (such as foraging) are often exhibited in movement too, including in whale sharks (*Rhincodon typus*) (Graham et al., 2006). **D**, animal movement plays an important role in responses to disturbances, such as catch-and-release angling (Hoolihan et al., 2011). **E**, movement is associated with animal personality in small-spotted catsharks (*Scyliorhinus canicula*) (Jacoby et al., 2014). **F**, animal movement shapes and is shaped by ecological interactions, such as predation (Carlisle and Starr, 2009), as illustrated for a leopard shark (*Triakis semifasciata*). Credits: (**A**) Gerald Schömbs, (**B**) Bearacreative; (**C**) Sebastian Lambarri; (**D**) James Thorburn; (**E**) Atese; (**F**) David Clode. Photograph of author (**D)** used with permission from James Thorburn; other photographs sourced from Unsplash.

5. Conservation implications

Alongside ecology, understanding animal movement is pivotal for conservation (Figure 4) (Fraser et al., 2018; Hays et al., 2019). In aquatic ecosystems, many large-bodied, mobile species have been decimated, predominately as a result of overfishing and destructive fishing practices (Estes et al., 2011; McCauley et al., 2015). Elasmobranchs—especially large, coastal species—have emerged as among the most threatened vertebrate groups (Dulvy et al., 2014; Pacoureau et al., 2021). Declines in these species represent a dramatic shift in the structure of marine ecosystems, with potentially substantial consequences for ecosystem functioning and services (Baum and Worm, 2009; Pimiento et al., 2020).

MPAs are a widely promoted conservation option that could combat this crisis (Edgar et al., 2014; MacKeracher et al., 2019). While it remains difficult to quantify the contribution of MPAs to population recovery for mobile species, it is widely recognised that MPA effectiveness is likely to depend on the time that individuals spend in MPAs, the management measures within MPAs and the exposure of individuals to threats within and beyond MPA boundaries, including fisheries, marine pollution and climate change (Chapter Three) (Chapman et al., 2015; MacKeracher et al., 2019). For example, studies on the vertical movements of elasmobranchs have shown how the vulnerability of individuals to bycatch can change through time (Siskey et al., 2019; Arostegui et al., 2020). This information can support the implementation of mitigation strategies, such as technical measures (e.g., fishing gear modifications), designed to support MPAs (Chapter Four; Kynoch et al., 2015). Responses to other forms of disturbance are also important. In the field of movement ecology, the responses of individuals to capture and tagging are of particular interest (Hoolihan et al., 2011; Whitney et al., 2016, 2017). Especially for threatened species, there is a need to balance data deficiencies

against the impacts of data collection (Heupel and Simpfendorfer, 2010; Hammerschlag and Sulikowski, 2011). However, fortunately, electronic tagging and tracking data themselves contain indicators of species' response to capture that can guide management (Chapter Five; Hoolihan et al., 2011; Whitney et al., 2021).

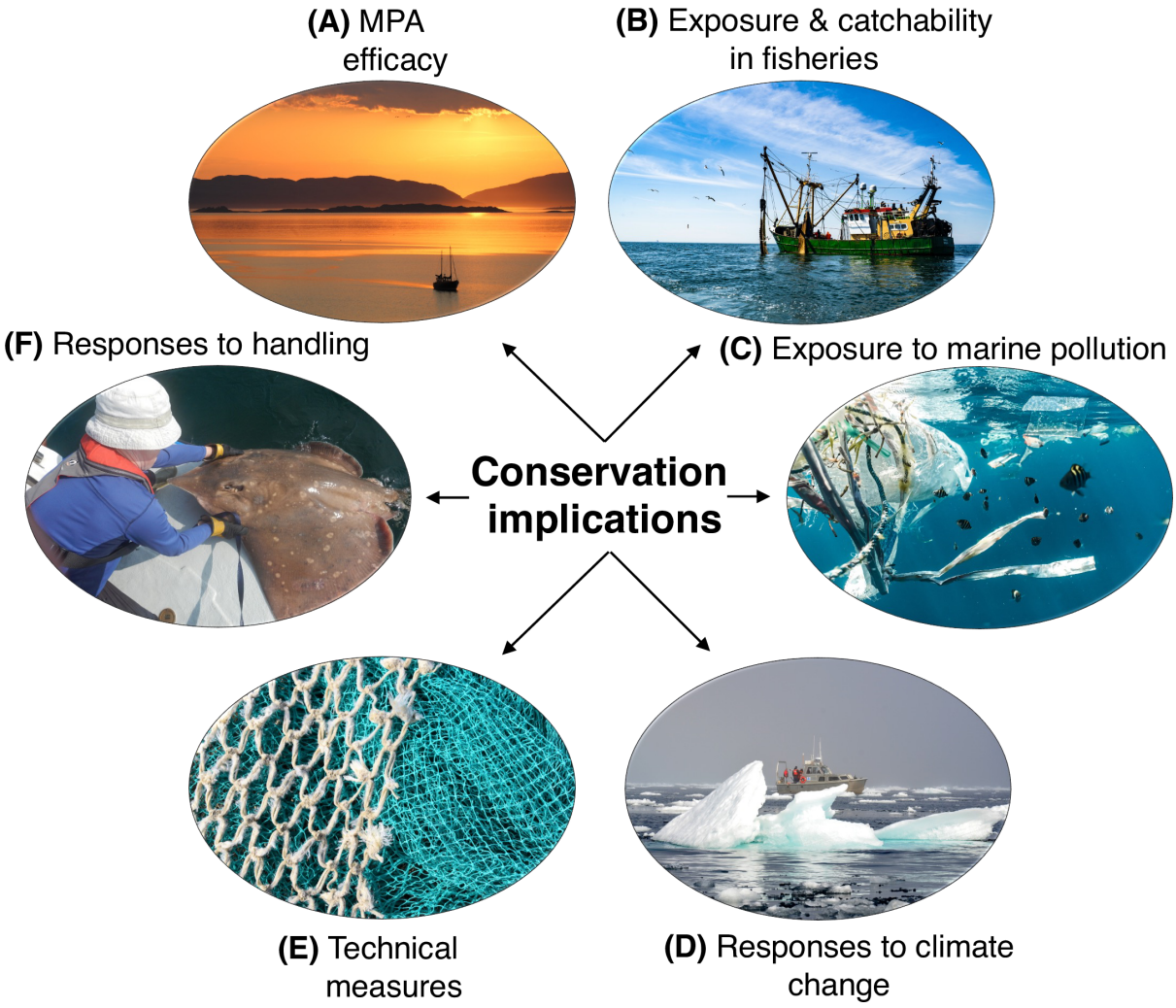

Figure 4. Conservation implications of movement ecology research, with examples from marine ecosystems. **A**, the efficacy of Marine Protected Areas (MPAs) for mobile species depends on the spatiotemporal scale of movement with respect to MPA boundaries, including for the Loch Sunart to the Sound of Jura MPA in Scotland. **B–D**, movement underpins exposure to threats (both within and beyond MPAs) such as fisheries, marine pollution and climate change. **E**, movement can inform technical measures designed to reduce bycatch of mobile species. **F**, movement indicates behavioural responses to capture and handling. Credits: (**A**) Lucas Salmin; (**B**) Paul Einerhand; (**C**) Waldemar Brandt; (**D**) Naja Jensen; (**E**) National Oceanic and Atmospheric Administration; (**F**) James Thorburn. Photograph of author (**F**) used with permission from James Thorburn; other photographs sourced from Unsplash.

6. The flapper skate

6.1. Taxonomy and distribution

The flapper skate is one of two species previously aggregated in the common skate species complex (Iglésias et al., 2010) (Figure 5). The contemporary distribution of flapper skate is uncertain, complicated by this history and massive historical overexploitation (Frost et al., 2020; Bache-Jeffreys et al., 2021; Ellis et al., 2021). Common skate were once distributed across continental shelf and slope habitats in the North-East Atlantic, from Morocco to northern Norway (Dulvy et al., 2006). Fishing pressure subsequently drove substantial declines in abundance and distribution (Dulvy et al., 2006). In the mid-1900s, records show a dramatic decrease in landings. For example, between 1959 and 1997, landings in the Irish Sea and Bristol Channel decreased 10-fold (Dulvy et al., 2000). Similarly, in the 1970s, landings at Concarneau (France) decreased by 91 % (Brander, 1981). By the 1980s, the common skate became the first marine fish species to disappear from the Irish Sea (Brander, 1981). Subsequent surveys in British waters in the 1980s and 1990s landed only six common skate (Dulvy et al., 2000). In 2006, the common skate was categorised as Critically Endangered (Dulvy et al., 2006). Since 2009, European Union (EU) regulations have prohibited the retention of common skate on vessels in EU waters. Now, only remnant flapper skate populations remain, most noticeably around western and northern Scotland (Neat et al., 2015; Frost et al., 2020; Ellis et al., 2021). In 2021, the flapper skate was assessed by the International Union for Conservation of Nature for the first time and categorised as Critically Endangered (Ellis et al., 2021). However, for the common skate species complex, alongside other *Dipturus* species in the North-East Atlantic, there are early indications of recovery (Rindorf et al., 2020).

6.2. Life history

Flapper skate begin life as eggs that are thought to be laid in shallow water (25–50 m deep) in areas with cobble or boulder substrate (NatureScot, 2021; Phillips et al., 2021a). Juveniles hatch at about 20–30 cm in length (Benjamins et al., 2021) and males and females reach maturity at 185.5–197.5 cm in length (Iglésias et al., 2010) and 14–21 years in age (Régnier et al., 2021) respectively. This slow development is associated with a low fecundity and high longevity, perhaps exceeding 40 years (Régnier et al., 2021). Individuals grow throughout life,

with females reaching more than 250 cm in length and 100 kg in weight, becoming the world's largest rajids.

Figure 5. Flapper skate (*Dipturus intermedius*) were decimated by overexploitation, but they can still be found off the west coast of Scotland where they are prized by recreational anglers. This specimen is released in the Loch Sunart to the Sound of Jura Marine Protected Area following capture by the Movement Ecology of Flapper Skate project (Lavender et al., 2021a). © Lisa Kamphausen/NatureScot 2021.

6.3. Foraging ecology and diet

The foraging ecology and diet of flapper skate are poorly understood. Studies of common skate suggest that the species forages on a wide range of benthic and demersal prey, including invertebrates, cephalopods, teleosts and elasmobranchs (Steven, 1947; Wheeler, 1969). In other skate species, ontogenetic shifts in diet are known, with small benthic invertebrates more prevalent in the stomachs of smaller individuals and benthic and demersal teleosts more prevalent in the stomachs of larger individuals (Orlov, 2003; Treloar et al., 2007; Brown-

Vuillemin et al., 2020). For example, common blue skate appear to forage mainly on shrimps and prawns, crabs and teleost fish, but this shifts with ontogeny: shrimps and prawns (such as Norway lobster, *Nephrops norvegicus*) dominate in the diets of small, immature individuals; crabs (such as flying crab, *Liocarcinus holsatus*) are more prevalent in medium-sized individuals; and teleosts, including Gadiformes (such as blue whiting, *Micromesistius poutassou*), Perciformes (such as boar fish, *Capros aper*) and Pleuronectiforms (such as megrim, *Lepidorhombus whiffiagonis*), appear to be favoured by large individuals (Brown-Vuillemin et al., 2020). However, while similar shifts seem likely for flapper skate, at the present time this remains uncertain.

6.4. Movement

On the west coast of Scotland, mark-recapture data from the catch-and-release angling of flapper skate has been collated since the 1970s by Glasgow Museum, the Scottish Shark Tagging Programme and, most recently, NatureScot, Marine Scotland Science and the Scottish Association for Marine Science. In the early days, data were collected using external tags (Little, 1995), but since 2011 these have gradually been replaced with passive integrated transponders and photo-identification (Neat et al., 2015; Benjamins et al., 2018). Collectively, these data demonstrate a remarkable level of site affinity to an area between the Isle of Jura and Loch Sunart, where individuals have been repeatedly recaptured (Little, 1995, 1997; Wearmouth and Sims, 2009; Scottish Natural Heritage, 2014; Neat et al., 2015; Benjamins et al., 2018). In 2016, this information underpinned the designation of the LStSJ MPA for skate conservation (Figure 6) (The Loch Sunart to the Sound of Jura Marine Conservation Order, 2016). Current management measures in the MPA prohibit the use of mobile fishing gear except in eight, seasonally fished areas in which mechanical dredges and demersal trawls (excluding beam trawls), without tickler chains, are permitted. However, angling is still common from spring–autumn. Vessel-based angling principally occurs in three areas around the islands of Kerrera, Insh and Crinan. Shore-based angling is also known to occur but its prevalence remains unclear.

Although there is a clear pattern of site affinity among flapper skate to the LStSJ MPA, movements between captures remain poorly understood. In early spring, mating is believed to occur in inshore areas (Day, 1884). Following mating, it is thought that females may move into shallow water to lay approximately 40 eggs, possibly every other year (Brander, 1981; Little,

1995; NatureScot, 2021). Meanwhile, it has been suggested that males move offshore over the summer, given reduced catches of males at this time (Little, 1997). Over winter, the historical view was that skate move offshore (Wheeler, 1969) and extensive movements have certainly been documented (Little, 1995). However, a recent acoustic study of 20 tagged individuals in the Sound of Jura found that over 50 % were resident on a day-by-day basis for months at a time and identified three long-term, mature female residents (Neat et al., 2015). These results point towards a mixture of movement patterns, with at least some individuals remaining in the MPA over prolonged periods. However, despite these studies, the scale of movements with respect to the MPA has remained unclear (Chapters Three and Six).

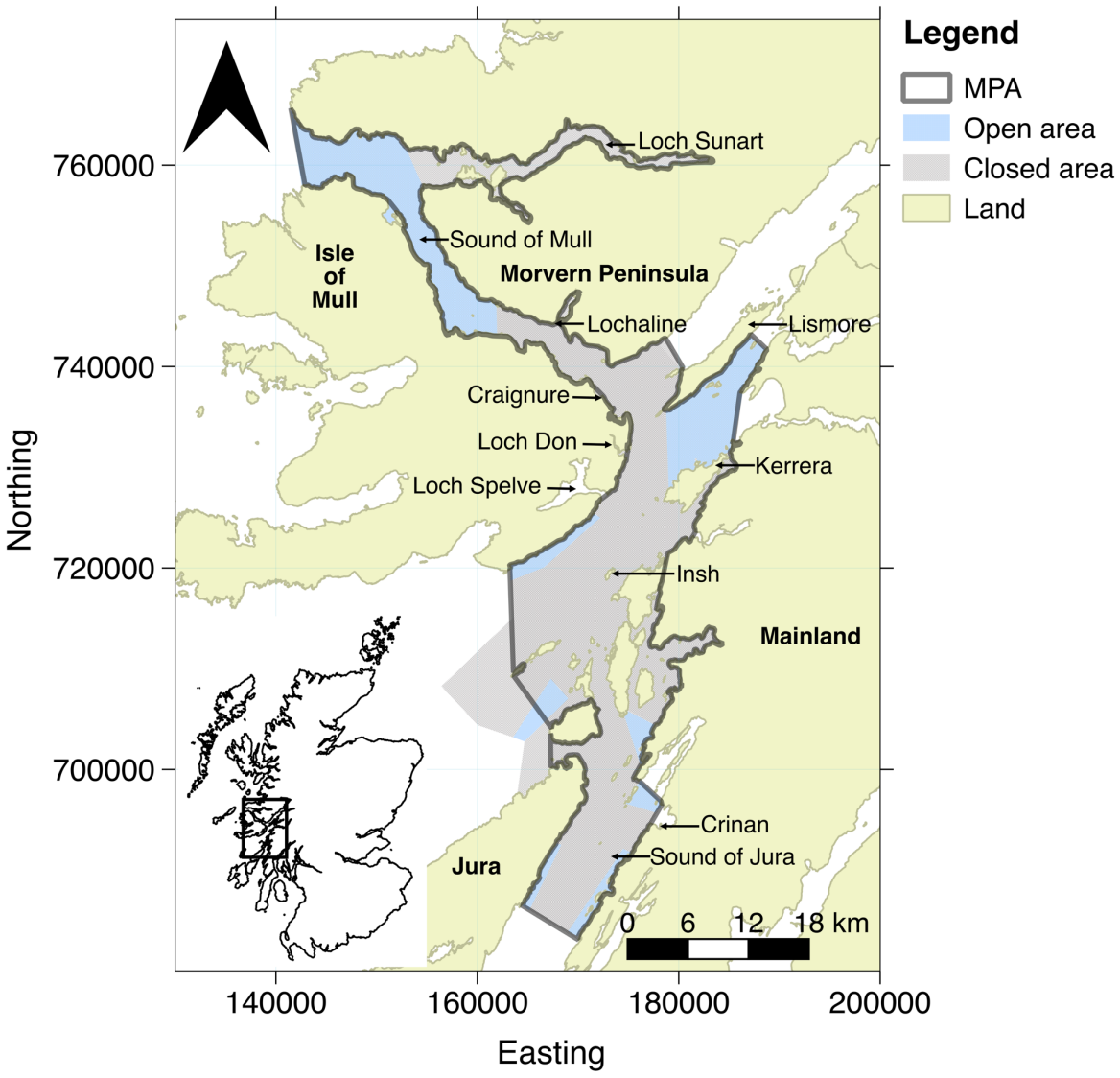

Figure 6. The Loch Sunart to the Sound of Jura Marine Protected Area (MPA). The inset shows the location of the MPA within Scotland. The main figure outlines the MPA in grey. Mobile fishing gear is prohibited throughout the MPA, with the exception of mechanical dredges and demersal trawls (excluding beam trawls) in eight seasonally open areas (shown in blue). These measures extend beyond the MPA to the southwest through

the Firth of Lorn Special Area of Conservation. The coordinate reference system is British National Grid. Background Ordnance Survey maps © Crown copyright and database rights [2019] Ordnance Survey (100025252).

Vertical movement patterns are also poorly understood, but several studies have examined the vertical distribution and depth preferences of flapper skate (Neat et al., 2015; Pinto et al., 2016; Thorburn et al., 2021). They are thought to inhabit depths from the surface to 1,500 m (Ellis et al., 2021), but off the west coast of Scotland mark-recapture data suggest a preference for depths from 100–300 m in close proximity to the coast (Pinto et al., 2016). Within the LStSJ MPA, Neat et al. (2015) reported a daily depth range of 50–180 m for three individuals tagged with archival tags. More recently, Thorburn et al. (2021) reported a depth range of 1–312 m across 25 tagged individuals. However, core depth ranges (25–225 m) varied seasonally and across size classes, with shallow-water (25–75 m) use increasing in winter, especially by large females. Only two studies have examined individual-specific trends in vertical movement and their drivers (Wearmouth and Sims, 2009; Pinto and Spezia, 2016). In archival time series from 4–6 individuals, these studies identified periods of sedentary and active movement that appeared to be associated with tidal and diel cycles, but the prevalence of these patterns among flapper skate more widely remains unclear (Chapter Four). Similarly, the influence of catch-and-release angling on skate movements remains unstudied (Chapters Five–Six).

7. Aims and objectives

Following the designation of the LStSJ MPA, the MEFS project was established to improve our understanding of skate movements in relation to the MPA via acoustic and archival tag deployments. As part of this project, the principal aim of this PhD is to investigate flapper skate movements using acoustic and archival data alongside mark-recapture records. This aim is addressed in the following chapters:

- **Chapter Two** introduces the movement and environmental datasets upon which this research is based, explaining data collection, processing and environmental conditions.
- **Chapter Three** investigates the occurrence of flapper skate in the MPA, analysing detection patterns of skate at acoustic receivers to infer the prevalence and spatiotemporal scale of residency and the roles of life history, environmental conditions and social interactions as drivers of the distribution of detections.

- **Chapter Four** investigates the vertical movements of flapper skate, analysing depth and vertical activity time series to unpick trends in vertical movement and their drivers.
- **Chapter Five** extends the analysis of vertical movements to consider behavioural responses to catch-and-release angling.
- **Chapter Six** integrates horizontal and vertical analyses of movement patterns through the development of a novel, holistic modelling framework for the reconstruction of fine-scale movements over the seabed and emergent patterns of space use.
- **Chapter Seven** discusses key findings, remaining knowledge gaps and future directions for this research.

Chapter Two

Data collection, quality control and the environment

Abstract

1. In movement ecology, technological innovation is driving the collection of enormous volumes of data, but the long-term value of these data and successful analyses, including model development and inference, are contingent on robust data management and careful consideration of environmental conditions through space and time.
2. These requirements are particularly evident for multi-stakeholder projects such as the Movement Ecology of Flapper Skate project, which has pioneered the collection of passive acoustic telemetry, archival and angler mark-recapture data from the Critically Endangered flapper skate (*Dipturus intermedius*) to provide information on individual movements in relation to the Loch Sunart to the Sound of Jura Marine Protected Area in Scotland.
3. To guarantee the long-term value of these data and build the foundation for their analysis, this chapter records data collection, defines protocols to ensure data quality and examines environmental conditions, including those resolved by a hydrodynamic model. To validate hydrodynamic model predictions, movement and oceanographic tag data are integrated in one of the most extensive validations of bottom-temperature predictions for the west coast of Scotland.
4. The outputs of this work include four widely applicable R packages ('prettyGraphics', 'flapper', 'Tools4ETS' and 'fvcom.tbx') that facilitate data processing and analysis. Processed data are provided and documented as an R package ('MEFS') comprising acoustic detections from 33 individuals (205,323 observations) and archival data for 21 individuals (3,908,294 observations). Environmental analyses contextualise these data, suggesting possible drivers of movement, important scales of variation and guiding model development. For bottom temperatures, model predictions are within ± 1 °C of observations and recent model updates have dramatically improved model predictive skill.

5. This chapter provides the foundation and tools for movement ecology research on flapper skate and demonstrates the multidisciplinary benefits of electronic tagging and tracking data.

Keywords

data management, environment, FVCOM, hydrodynamic model, movement ecology, WeStCOMS

1. Introduction

Movement ecology aims to reveal the proximate and ultimate explanations of organismal movement and its consequences (Chapter One). Capture-mark-recapture, in which individuals are repeatedly sampled, marked, released and resampled, forms a cornerstone of this research that has elucidated spectacular examples of movement across taxa (Kohler and Turner, 2001; Hammond, 2009). Recently, with technological developments in electronic tagging and tracking, a new 'Golden Era' for movement ecology has been heralded (Hays et al., 2019). In aquatic environments, passive acoustic telemetry and archival tags have dramatically expanded the realm of movement ecology (Hussey et al., 2015; Matley et al., 2022). Expansive receiver arrays that continuously listen for individual-specific transmissions from acoustically tagged individuals have become widespread (Matley et al., 2022) and the collection of high-resolution archival (depth/temperature/light level) time series has become increasingly commonplace (Hussey et al., 2015). However, realising the promise of these technologies for movement ecology depends upon robust data management, detailed understanding of study systems and thorough consideration of the context from which movement data are sampled.

Robust data management is the prerequisite for successful analyses and a guarantor of the long-term value of movement datasets (Wilkinson et al., 2016; Williams et al., 2020). Detailed records of data collection procedures are the foundation of this process since data collection methodologies often directly underpin and inform analyses. For example, in the case of passive acoustic telemetry, data interpretation depends on details such as the acoustic transmission interval (Simpfendorfer et al., 2015). Clear, reproducible protocols to guarantee data quality are equally important. For long-term usability, stable data storage infrastructures are also necessary (Wilkinson et al., 2016; Williams et al., 2020).

Alongside data management, a detailed understanding of the study system and consideration of the environmental and ecological context from which movement data are sampled are essential for successful analyses. In practice, contextual considerations typically focus on environmental conditions that are related to sampling or animal movement, either directly or indirectly as surrogates for ecological variables (e.g., prey), since information on ecological variables is often unavailable (Patterson et al., 2016). In passive acoustic telemetry studies, a key consideration is the extent to which the environmental conditions surrounding receivers are representative of larger areas of interest because this underpins the interpretation of movement patterns and their wider applicability. For animal movement, an understanding of the environment can also suggest causes or consequences of movement and guide model development (Riotte-Lambert and Matthiopoulos, 2020).

For aquatic taxa, such as elasmobranchs, important environmental data comprise static variables that define habitat structure and spatiotemporal variables that describe how conditions change in space and time (Schlaff et al., 2014). Depth is a major driver of distribution in aquatic environments (Saeedi et al., 2019) and has been identified as an important influence on movement in elasmobranchs (Sundström et al., 2001; Humphries et al., 2017). The complexity of seafloor environments, captured through variables such as rugosity, also affects elasmobranch movement, particularly for benthic species (Grohmann et al., 2011; Humphries et al., 2017). These variables are closely related to environmental conditions such as tidal dynamics and current velocity (Gille et al., 2004), which can affect energy landscapes through the ease of movement (Gibson, 2003) and the availability of prey (Sundström et al., 2001; Schlaff et al., 2014). For example, rugosity and current velocity are often related to sediment type, with low rugosity, low velocity environments typically associated with soft sediments and higher rugosity, higher velocity environments associated with harder sediments (Lauria et al., 2015). In turn, sediment type can influence the movements of benthic predators such as skate (Rajidae), with different sediments favouring different types of behaviour, such as foraging or resting (Kotwicki and Weinberg, 2005; Greenway et al., 2016). Hydrodynamic variables, such as temperature, thermocline strength and salinity, affect metabolism and productivity and, in turn, may affect elasmobranch movement too (Sundström et al., 2001; Schlaff et al., 2014). For example, vertical movements are commonly linked to temperature gradients through the differential effects of warm versus cool temperatures on metabolic efficiency and gastric evacuation (Sims et al., 2006; Papastamatiou et al., 2015). Similarly,

meteorological variables, such as light levels, are widely associated with elasmobranch movement over short (diel) and long (seasonal) timescales (Sundström et al., 2001; Schlaff et al., 2014).

For the integration of environmental fields in studies of animal movement in aquatic ecosystems, hydrodynamic models are a valuable resource that move beyond the information provided by point samples to predict environmental conditions across space and time (Moll and Radach, 2003). For example, the Finite Volume Coastal Ocean Model (FVCOM) is a numerical, hydrostatic, primitive-equation model that resolves hydrodynamic conditions hourly across an unstructured, triangular, vertically layered mesh (Chen et al., 2003). Mesh resolution is highest around the coastline and near the surface and the seabed (where prisms are more closely spaced). Scalar variables (e.g., salinity) are resolved at prism nodes and vectors (e.g., current velocity) are resolved at prism centroids (elements), in each case, either across the mesh surface or 11 vertically spaced, terrain-following Sigma layers (from the first layer at the surface to the deepest layer below the seabed) that rise and fall with the tides. Yet despite the value of these kinds of models, their integration with ecological research remains a substantial learning curve in many cases, especially since hydrodynamic models and ecological inference typically require different software. Even when this can be achieved, model outputs require validation (Radach and Moll, 2003).

However, electronic tagging and tracking data can contribute to hydrodynamic model validation and support the use of hydrodynamic models in movement ecology (Harcourt et al., 2019). Existing research in this field has predominately targeted diving mammals, such as elephant seals (*Mirounga sp.*), which can transmit locational and environmental data packets via satellite tags upon surfacing (Harcourt et al., 2019). The use of animals as sources of oceanographic data in other settings remains underdeveloped, especially when it comes to the validation of near-seabed conditions. However, benthic animals represent a hitherto underappreciated resource for the study of hydrodynamic conditions at the seabed if methods can be developed to link movement and environmental data from these animals to hydrodynamic models.

The flapper skate (*Dipturus intermedius*) is a Critically Endangered benthic elasmobranch that has been the subject of research spanning the development of movement ecology (Chapter One). Beginning in the 1970s, the flapper skate became the subject of a recreational catch-and-

release sport fishery that continues to this day (Little, 1995, 1997; Neat et al., 2015). Originally, skate were identified via external tags, but since 2011 the use of passive integrated transponder (PIT) tags and photo-identification has been promoted by NatureScot, Marine Scotland Science and the Scottish Association for Marine Science (Benjamins et al., 2018). Most recent recorded angling occurs from anchored charter vessels over areas of relatively deep (> 100 m) water. Following hooking, skate typically dig into the sediment for a period of time (typically less than 10 minutes in duration) before the tension from the line forces ascent. The high recapture rate of individuals off the west coast of Scotland ultimately underpinned the designation of a Marine Protected Area (MPA) for skate conservation known as the Loch Sunart to the Sound of Jura (LStSJ) MPA (Neat et al., 2015). Subsequently, angler mark-recapture data from this area have been complemented by small-scale deployments of archival tags and passive acoustic telemetry (Wearmouth and Sims, 2009; Neat et al., 2015; Pinto and Spezia, 2016). Collectively, these studies suggest that some skate show high affinity to the LStSJ MPA and prefer areas close to coastline adjacent to deep (100–300 m) water (Chapter One). There is also limited evidence for depth-specific periodic behaviours (Wearmouth and Sims, 2009; Pinto and Spezia, 2016). However, in general, the fine-scale movements of skate within the LStSJ MPA and their drivers remain poorly known.

Recently, the flapper skate has been the focus of a substantial acoustic and archival tagging programme within the MPA conducted by the Movement Ecology of Flapper Skate (MEFS) project (Chapter One). Data from this project are complemented by high-resolution environmental datasets (Howe et al., 2014; Boswarva et al., 2018) and model predictions from the West Scotland Coastal Ocean Modelling System (WeStCOMS) that implements FVCOM to resolve environmental conditions (Aleynik et al., 2016). For this model, previous comparisons between observations and predictions have revealed a high degree of accuracy (Aleynik et al., 2016). Nevertheless, gaps remain in validation datasets, especially for conditions resolved near the seabed, such as bottom temperatures, where skate are thought to spend most time. For temperatures, there is concern that predictions pre-2017 may be positively biased by the influence of a parent model (Dabrowski et al., 2014). In 2017, the boundary forcing was adjusted to mitigate biases detected in temperature profiles interpolated from the parent model revealed by data from gliders deployed near the model's south-western boundary. However, the benefits of these changes across the rest of the model's domain and their implications for understanding the flapper skate's environment remain to be evaluated.

The aim of this chapter is to secure the long-term value of the MEFS datasets and build the foundation for successful analyses by detailing data collection procedures, processing protocols and the environmental characteristics of the study site. There are four objectives:

A. **Data collection**—to provide a full and detailed record of data collection.
B. **Data processing**—to define data processing protocols for passive acoustic telemetry, archival time series and mark-recapture records and provide quality-controlled datasets.
C. **Environmental context**—to develop methods for the integration of hydrodynamic model outputs and ecological analyses in order to investigate the environmental context within which movement data were collected.
D. **Model validation**—to contextualise hydrodynamic model predictions with observations.

2. Methods

2.1. Study site

The LStSJ MPA occupies a 741 km^2 area on the west coast of Scotland (Figure 1). This is situated in a complex coastal environment, surrounded by a convoluted coastline punctuated by sea lochs, peninsulas and narrow straights. Within this area, passive acoustic telemetry, archival data and mark-recapture data from recreational angling provide information on skate movement (Figure 1).

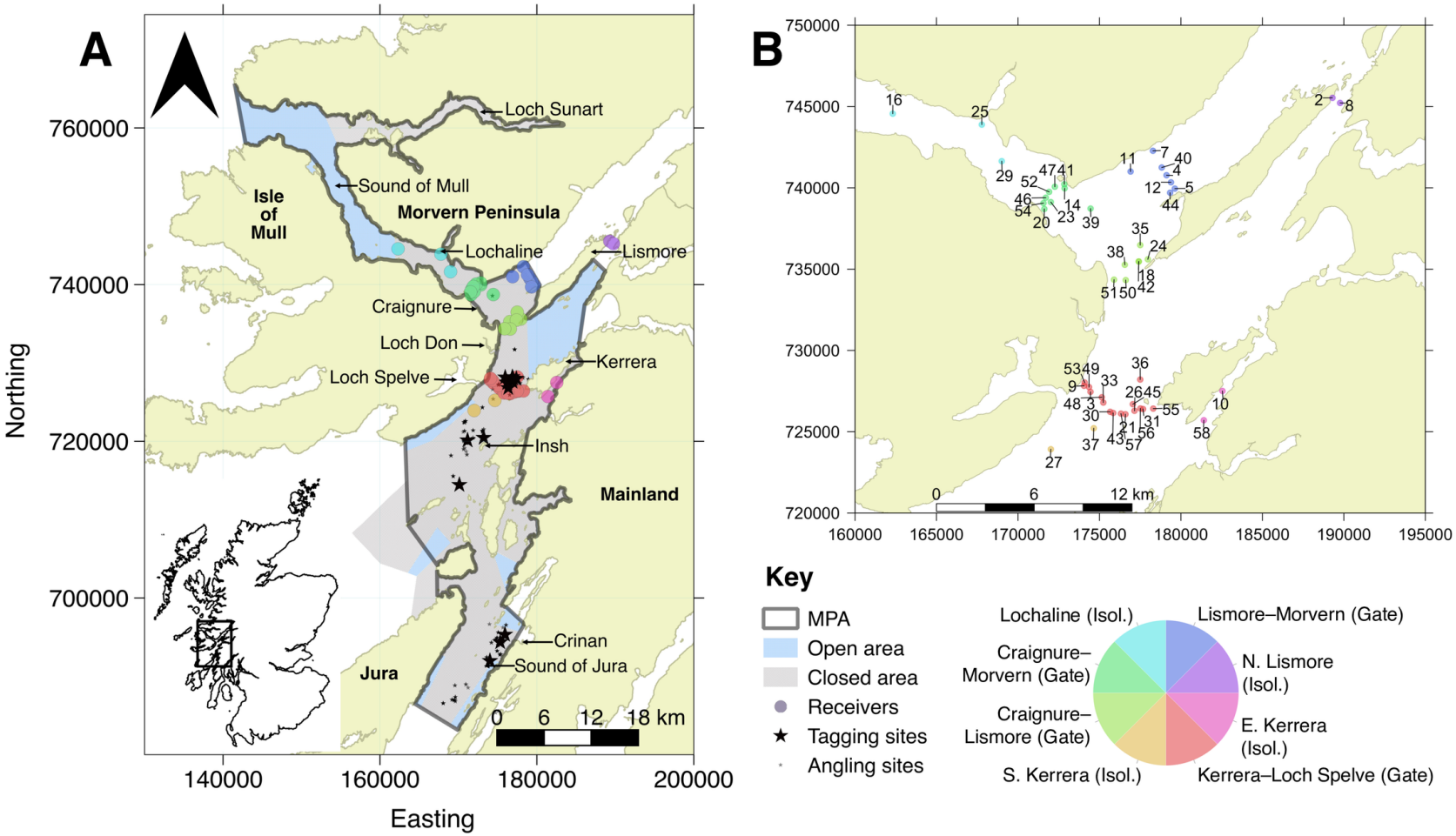

Figure 1. The study site. A, the Loch Sunart to the Sound of Jura Marine Protected Area (MPA). The MPA is delineated by the grey boundary. Mobile fishing gear is prohibited throughout the MPA, with the exception of mechanical dredges and demersal trawls (excluding beam trawls) in eight seasonally open areas (shown in blue) (see Chapter One). The coloured points mark receivers and the 425 m detection range. Small stars mark the locations of recreational angling events recorded in the PIT tag/photo-identification database collated by NatureScot, Marine Scotland Science and the Scottish Association for Marine Science. Large stars mark tag deployment/retrieval sites. **B**, the receiver array. Receivers are grouped into eight main sites identified according to a colour wheel which approximately relates to site location (see key). The coordinate reference system is British National Grid. Background Ordnance Survey maps © Crown copyright and database rights [2019] Ordnance Survey (100025252).

2.2. Data collection

2.2.1. Passive acoustic telemetry

A passive acoustic telemetry array comprising 58 Vemco 69 kHz receivers was deployed from March 2016–July 2017 in the MPA by the MEFS project (Figure 1, Table S1). Three types of receivers were deployed in water depths ranging from 5–180 m. Vemco VR2 and VR2W receivers were deployed 25–50 m below the surface on a line connecting a weighted ballast on the seabed to a surface buoy. These moorings were vulnerable to drag on the line and buoy loss. VR2AR receivers were deployed 5–10 m above the seabed on a line connecting a weighted ballast to an acoustic release. In all cases, receiver hydrophones were orientated towards the surface.

Receivers were deployed in phases (Table S1). In the initial deployment phase (beginning 27th February 2016), 34 receivers were deployed. Eight of these receivers were later lost. Two other receivers were lost but later recovered. One receiver was found to have drifted slightly during the study and returned to its original position. A further 24 receivers were deployed during the course of the study to replace lost receivers and increase array coverage. Overall, 48/58 receiver deployments were successfully deployed and retrieved. The operational end date for most receivers was 2nd June 2017, although the final two receivers remained operational until 23rd July 2017. However, neither receiver recorded any detections in this time. For this reason, 2nd June 2017 is treated as the effective end date of the passive acoustic telemetry study.

Receiver deployments concentrated in four main clusters in the centre of the MPA (Figure 1). These clusters formed ‘gates’ between Craignure and Morvern in the northwest (the ‘Craignure–Morvern Gate’), Lismore and Morvern in the northeast (the ‘Lismore–Morvern Gate’), Craignure and Lismore in the centre (Craignure–Lismore Gate) and Kerrera and Loch Spelve in the south (the ‘Kerrera–Loch Spelve Gate’). Nine isolated receivers were placed further west in the Sound of Mull, at the northern end of Lismore, on the eastern side of Kerrera and south of Loch Spelve. Collectively, the Kerrera–Loch Spelve Gate and the two southernmost receivers form an area defined as the ‘southern receiver curtain’. Receiver deployments were driven by logistics, receiver loss and replacement, and the requirements of another research project on Atlantic salmon (*Salmo salar*).

Preliminary analyses of range testing data for deployed receivers suggest that the probability of a detection event at a receiver (k) at a given time (t), following a transmission from a given location ($\boldsymbol{s}$), i.e., $\Pr(E[k,t]|\boldsymbol{s})$, is strongly associated with the distance between the receiver and the transmitter (Klöcker, 2019). Next to receivers, $\Pr(E[k,t]|\boldsymbol{s}) \sim 0.97$; but by 400–450 m $\Pr(\mathrm{E[k,t]}|\mathbf{s}) \sim 0.5$. In this chapter and Chapter Three, a median value of 425 m is taken as an estimate of the detection range around receivers (Figure 1). In Chapter Six, this assumption is relaxed through the development of a modelling framework that can incorporate a model for $\Pr(E[k,t]|\boldsymbol{s})$.

2.2.2. Electronic tagging

In three sites in the MPA (around Kerrera, Insh and Crinan), 66 skate were captured and tagged during the study following the methods of Neat et al. (2015) (Figure 1, Table S2). Skate were captured from two chartered angling vessels using 50–80 Ib class rods with lever drag multiplier reels. A braided main line was used that terminated in a 3 m 250 Ib rubbing length. A standard lead weight (12 oz) was attached via a sliding boom so that it could drop off in the case of a broken line. The tackle terminated in a 10/0 O'Shaughnessy hook with the barb removed. Whole mackerel (*Scomber scombrus*) were used as bait.

During angling, individuals were typically hooked in the mouth, although deep hooking (in the throat/gut) has been observed (personal observation). Once hooked and reeled to the surface, skate were brought onto the vessel, either via a custom-made mat that was slipped under the skate or by pushing a gaff (hook) through the edge of the wing, with the mat or gaff then used to pull the skate aboard.

Visual inspection of captured individuals suggested that all individuals were flapper skate rather than common blue skate (*D. batis*). The disc width (wing tip to wing tip) and total length (snout tip to tail tip) of the dorsal surface of each skate were measured with a tape measure. Maturation status (immature, mature) was later predicted from a model for maturation with total length (Iglésias et al., 2010). For mature males, there was one individual for which the predicted maturation status was uncertain (≤ 0.95), but post-hoc examination of photographs of the individual's claspers suggested it was mature (Table S2). For mature females, there was

also one individual for which the predicted maturation status was uncertain (Table S2). However, electronic tagging and tracking data were not recovered from this individual.

Following measurement, all individuals were tagged with a PIT tag (if necessary) and photographed as part of ongoing monitoring. Forty-three individuals were tagged with acoustic transmitters on the leading edge of the right wing (Table S2). Each tag was attached externally to the dorsal surface on top of a silicon pad and a Petersen disc via a stainless-steel pin pushed through the wing and secured on the ventral surface with another Petersen disc. Vemco V13 and Thelma Biotel MP-13 miniature (13 x 25 mm) coded acoustic transmitters were used. Tag power output was 147 dB re 1 Pa and 153 dB re 1 Pa at 1 m for the V13 and MP-13 tags respectively. Both tags operated at 69 kHz. Each tag was programmed to transmit an individual-specific acoustic signal with a nominal delay of 60 s (i.e., at random intervals between every 30–90 s) for the duration of the study. (Battery life was guaranteed for 18 months.) Random transmission was used to minimise the probability of transmission collisions which can cause detection failure or false detections (Pincock, 2012; Simpfendorfer et al., 2015). Following tagging, one tag immediately detached from an individual, leading to a sample of 42 individuals that could have been detected by the acoustic array (Table S2). When tagged individuals passed within the detection radius of a receiver, the date/time and an individual-specific identifier were recorded. Both V13 and MP-13 tags could be detected by all receivers.

Sixty-three individuals (including 40 acoustically tagged individuals and a further 23 individuals) were tagged with archival tags (Table S2). The tag attachment method was similar to that used for the acoustic tags, with each archival tag attached to the dorsal surface on the leading edge of the left wing on top of a silicon pad via two stainless steel pins pushed through the wing and secured on the ventral surface with another silicon pad and a base plate. Star Oddi milli-TD, CEFAS G5 and G6A tags were used. However, due to programming issues, only 45 successful Star Oddi milli-TD tag deployments are recognised (Table S2). These tags recorded pressure (depth) to a resolution of 0.24 m and an accuracy of 4.77 m (0.6 % of the 5–800 m depth range), and temperature, to a resolution of 0.032 °C and an accuracy of 0.1 °C, every two minutes during deployment. Tagging took approximately 5 minutes per individual.

Capture and tagging were approved by the ethics committee of the University of St Andrews (number SEC21024). All regulated procedures involving animals were carried out in

compliance with The Animals (Scientific Procedures) Act 1986 under the Home Office Project License number 60/4411 by competent Personal License holders.

2.2.3. Recreational angling

Alongside electronic tagging data from the MEFS project, mark-recapture (PIT and photo-identification) records collated from recreational angling between 2011–2018 were obtained from NatureScot, the Marine Scotland Science and the Scottish Association for Marine Science as a largely independent source of information on flapper skate movement in relation to the MPA across a larger number of individuals, a longer timescale and a wider area. Raw data comprised 1,771 captures of 884 individuals.

2.3. Data processing

2.3.1. Detection time series

Raw data were collated by the MEFS project and partner organisations in Microsoft Excel. Data processing and analyses were implemented in R, version 4.0.2 (R Core Team, 2020). The prettyGraphics package was developed to support visualisation (Lavender, 2020a). For passive acoustic telemetry data, the flapper package was developed to support data processing and analysis (Lavender, 2020b). A 7-stage protocol was defined to process detection time series:

A. **Receiver identity.** Only detections from receivers deployed by the MEFS project in the MPA were used. Detections from receivers deployed elsewhere or used for range testing were excluded.
B. **Receiver loss.** Only detections from successful receiver deployments were used. Two receivers were excluded from all analyses because they were lost for a period of time (Table S1). (Neither receiver recorded any detections over the study period.)
C. **Receiver operation window.** Only detections within receiver deployment windows were used. Receiver deployment windows were defined from five days after receiver deployment until five days before retrieval, excluding all data from 0600 hours until 1800 hours on any servicing dates. Receiver servicing dates were identified from receiver metadata where possible. This definition was used to ensure detection validity because receiver deployment/retrieval dates were only recorded for groups of receivers deployed/retrieved over several days. Detections at receivers outside of deployment

windows associated with receiver checks, range testing or deployment elsewhere were excluded.

D. **Tag identity.** Only detections from tags deployed on skate by the MEFS project were used. All detections of unknown tags from unrecorded receiver checks, range testing, other tagging programmes or Type A false detections (Simpfendorfer et al., 2015) were excluded.

E. **Tag loss.** Only detections from successfully deployed tags were used. Tag 252 was excluded from all analyses because the tag immediately detached following deployment (Table S2).

F. **Tag operation window.** Only detections recorded within tag operation windows were included. Tag operation windows were defined from midnight on the day of tag deployment until 0600 hours on the day of capture (or the end date of the study).

G. **False detections.** Only detections that passed the short-interval criterion filter for type B false detections (which arise from transmission collisions or noise-induced errors) were used. For each tagged individual, this interval flags any detections at a receiver that are unrepeated within a specified time threshold as potentially false (Pincock, 2012). The criterion was implemented with a time threshold of 1,800 s (30 x 60 s) via the `false_detections` function in the glatos package (Holbrook et al., 2020). The criterion identified 1,504 detections as potentially false. Further analysis with the flapper package showed that 1,249 of these detections (83 %) were not accompanied by any detections at nearby receivers over the same time interval, supporting the view that most are likely to be false. However, since the possibilities of collision activity and spurious noise-induced detections could not be excluded, all putative false detections were excluded (Pincock, 2012).

For the detections that passed data processing filters, the potential influence of sampling effort (including receiver coverage and the number of individuals at liberty) on detection patterns was investigated by reconstructing trends in (a) the area sampled by receivers (accounting for receiver number and placement given a detection range of 425 m) and (b) the number of individuals at liberty during the study using the flapper package (Lavender, 2020b).

2.3.2. Archival time series

The Tools4ETS package was developed to facilitate the processing and analysis of ecological (especially archival) time series (Lavender, 2020c). Raw time series comprised timestamped depth and temperature observations and were processed to ensure a consistent representation of these variables. Data around angling events were removed to focus on undisturbed vertical movements in a two-stage process:

A. **Tag deployment/retrieval events.** Data were filtered around all tag deployment/retrieval events by excluding all observations from 0600 hours until midnight on the day of capture/recapture.
B. **Recreational angling.** Data were filtered around recreational angling events that occurred during individuals' time at liberty (when individuals were captured and released with archival tags attached). Angling events were identified from the PIT/photo-identification mark-recapture database maintained by NatureScot, Marine Scotland Science and the Scottish Association for Marine Science (see §2.2.3). Recorded capture dates were validated using the archival time series and the Visualise Time Series interactive application in the prettyGraphics package; angling events should be visible as peaks in the depth time series as individuals are pulled to the surface (Lavender, 2020c). Using the archival data, the precise time of each event was defined from the peak in the depth time series using a semi-automatic approach implemented by the `define_recapture` function in Tools4ETS package. Since ascents in the depth time series are only realised after a period of tension from a rod and line, all data from two hours before each event until midnight on the day of the event (a median of 9.33 hours ± 1.21 median absolute deviation) were excluded for analyses of vertical movement (Chapters Three–Four). A slightly larger window was used to investigate post-release behaviour (see Chapter Five). Putative unrecorded angling events were not removed from the archival time series, but their prevalence and potential influence on analyses were investigated and are likely to be minimal (Chapter Five).

2.3.3. MEFS

Processed datasets from the MEFS project were stored and documented in the MEFS R package (Lavender, 2020d). This includes datasets that define receiver deployments, tagged individuals, and the detection and archival time series. Each dataset was stored with an object identifier and associated observations, excluding calculated fields.

2.3.4. Mark-recapture time series

Mark-recapture records from recreational angling were processed for analysis to include only angling events with all required information (i.e., individual identity, size, angling location and date). For each record, the probability that the angled individual was mature was predicted from its length, as previously described (see §2.2.2). To avoid including captures from individuals whose predicted maturation status was ambiguous, capture records were only used from individuals for which the probability that they were either immature or mature exceeded 0.75.

2.4. Environmental conditions

Environmental conditions in the area were explored using available datasets and modelling. High-resolution (5 x 5 m) bathymetry data and sediment maps were obtained from the Ireland, Northern Ireland and Scotland Hydrographic surveys (Howe et al., 2014; Boswarva et al., 2018). Using the bathymetry data, slope angles were calculated as a metric of rugosity using Horn's (1981) algorithm, implemented by the `terrain` function in the raster package (Hijmans, 2020). For each variable (depth, slope and sediment type), the distribution of habitats across the MPA was mapped and frequency distributions were scrutinised. The relative area occupied by each sediment type across different depths and slopes was also examined.

Spatiotemporal variation in hydrodynamic and meteorological conditions in the MPA was explored using modelling. The fvcom.tbx package was developed for this analysis (Lavender, 2020e). Variation in tidal elevation, temperature, salinity, current velocity, precipitation, wind and light levels was considered since these variables are widely linked to movements in elasmobranchs (Sundström et al., 2001; Schlaff et al., 2014) and could be resolved for the study site (Table S3). For tidal elevation, 15-minute predictions were obtained from POLTIPS.3 tidal prediction software for the standard port in the area (Oban) alongside the times of low and high tide for the two secondary ports in the area (Seil Sound and Craignure). Hourly predictions were also extracted from WeStCOMS over a one-year period from March 2016–17. For other variables, hourly predictions were resolved in the same way, either via WeStCOMS directly (e.g., temperature), by processing WeStCOMS predictions (e.g., current velocity vectors were translated into current speeds) or via alternative algorithms (e.g., photoperiod) provided by

fvcom.tbx (Table S3). For each variable, summary statistics, time series plots and animated maps were used to explore spatiotemporal variation in environmental conditions.

2.5. WeStCOMS validation

This chapter contributes two sources of validation data for WeStCOMS. The first source of data is bottom-temperature observations collected by archival tags during tag deployment (i.e., when skate are assumed to be living a benthic lifestyle). The second source of data is temperature-depth profiles sampled by archival tags during angling. These data were used to validate WeStCOMS bottom and water-profile temperature predictions at times when the location of observations could be identified.

To validate WeStCOMS bottom-temperature predictions, a dataset with observed data and corresponding predictions was assembled using the fvcom.tbx package. Observed data comprised observations sampled by archival tags when individuals were simultaneously detected at receivers. Corresponding predictions were derived at the nearest hour in time and the nearest node in space for the 10^{th} Sigma layer (i.e., nearest neighbour interpolation). To validate model predictions with this dataset, the frequency distribution of differences between observed and predicted temperatures and the difference between observations and predictions through time and in relation to depth were examined. To contextualise validation 'effort', the total number of validation observations per day though time and at each receiver over time and space was examined.

To validate predicted temperature-depth profiles, observed profiles were compared against predicted profiles. Observations were derived from ascents immediately preceding angling events recorded during individuals' time at liberty and tag retrieval events. (Temperature-depth observations immediately following tag deployment or recreational angling were not considered because archival temperature loggers take time to equilibrate to surrounding temperatures following exposure to air during capture.) Only events for which locational data were recorded were considered. Potentially erroneous locations were flagged if the maximum observed depth in the recorded location was more than 25 m deeper than the depth of the seabed in that location. For each angling event, predicted profiles were obtained from WeStCOMS for the nearest hour (from the start of the angling event) and node. Layer depth was calculated, accounting for tidal elevation at the start of the angling event, using the fvcom.tbx package.

Observed and predicted temperature-depth profiles were visualised together for each angling event. To contextualise validation 'effort', temporal and spatial sample summaries were computed.

3. Results

3.1. Passive acoustic telemetry

From February 2016 until June 2017, the number of operational receivers ranged from 8–28 (median = 23) receivers. Deployment durations ranged from 63–504 (median = 164) days. During deployment, receivers surveyed 3.93–13.88 km^2 (0.53–1.87 % of the MPA) (Figure 2). Over time, sampling effort was highest from March to November 2016 and declined sharply in December, before being partially restored in January 2017 until the end of the study (Figure 2). Over space, sampling effort concentrated in specific areas and was greatest around the southern receiver curtain. The distribution of depths, slopes and sediment types within receiver detection ranges was similar to the background distribution of these conditions.

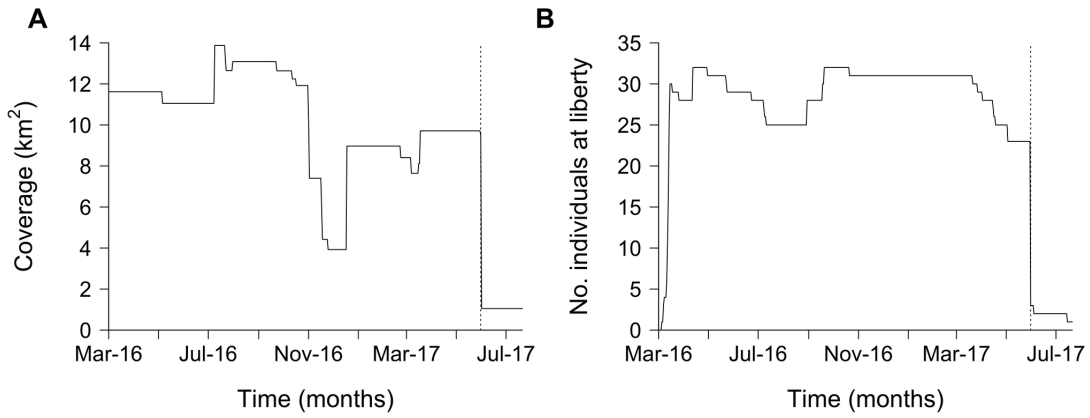

Figure 2. A summary of sampling effort through time. A, receiver coverage through time, assuming a constant 425 m detection radius. Changes in receiver coverage were due to changes in the number and placement of receivers. **B**, the number of acoustically tagged skate at liberty through time. In both panels, the vertical, dotted line marks the operational end date of the study.

3.2. Acoustic records

Forty-two individuals were successfully tagged with acoustic tags, comprising 26 females (11 immature and 15 mature individuals) and 16 males (eight immature and eight mature

individuals). Total length (cm) ranged from 109–221 (median = 202) and 107–198 (median = 182) for females and males respectively. During the study, the number of individuals at liberty ranged from 3–33 individuals (Figure 2). Days at liberty ranged from 3–452 (median = 399) days (Table S2).

In the raw database, 449,063 detections were recorded. Following processing, 205,323 detections (46 %) remained. Overall, 33/42 individuals successfully tagged with acoustic tags were detected at least once. For these individuals, the number of detections ranged from 40–23,840 (median = 1,776). Detections were recorded at 40/48 receivers, with the number of detections per receiver ranging from 9–55,381 (median = 883).

During the study, 21 individuals were recaptured and had their transmitters removed (Table S2). The location of tag removal was recorded for five of these individuals (Table S2). In these cases, tags were recovered within a linear distance of 0.44–0.69 (median = 0.63) km from the tagging location.

3.3. Archival records

Archival data, comprising 4,337,193 observations, were successfully obtained for 21/63 individuals, comprising 15 females (six immature and nine mature individuals) and six mature males (Table S2). Total length ranged from 134–218 (median = 201) and 188–198 (median = 194) for females and males respectively. Five angling events were identified during individuals' time at liberty (Table S4). Following processing, 3,908,294 observations (90 %) remained. Time series spanned 3–772 (median = 164) days, with three time series lasting 100–200 days, two lasting 200–300 days and eight (from six females and two males) longer than 300 days. The location of tag retrieval was recorded for seven individuals (Table S2). In these cases, tags were recovered within a linear distance of 0.41–1.07 (median = 0.66) km from the tagging location.

3.4. Mark-recapture records

The processed mark-recapture database comprised 1,026 records of 555 individuals. This included individuals in all life-history categories but few records for early life stages. Mark-recapture events were distributed from 3 March 2016 until 30 October 2018 and occurred

exclusively within MPA boundaries. Per capita, the number of mark-recapture records ranged from 1 to 12 (median = 1).

3.5. Environmental conditions

The bathymetric environment in the MPA is complex (Figure 3A). Most of the MPA is relatively shallow (< 50 m), but there are also glacially over-deepened basins (< 5 km^2 in area and > 150 m deep), numerous ridges and deep-water channels that range in width from tens to hundreds of metres (Figure 3A). The maximum depth is 290 m. In line with the bathymetry, the frequency distribution of slopes is right skewed, with a large number of relatively flat areas as well as steeper slopes along the edges of channels. Although the spatial extent of sediment data is more limited, available data reveal a complex patchwork of sediment types (Figure 3B). Overall, muddy sediments are most abundant (occupying 135 km^2), but coarser, rockier sediments are found over smaller areas. However, the relative availability of sediment types changes with depth and slope angle, with muddy sediments particularly prevalent between 0–50 m in low rugosity areas (Figure 3C–D).

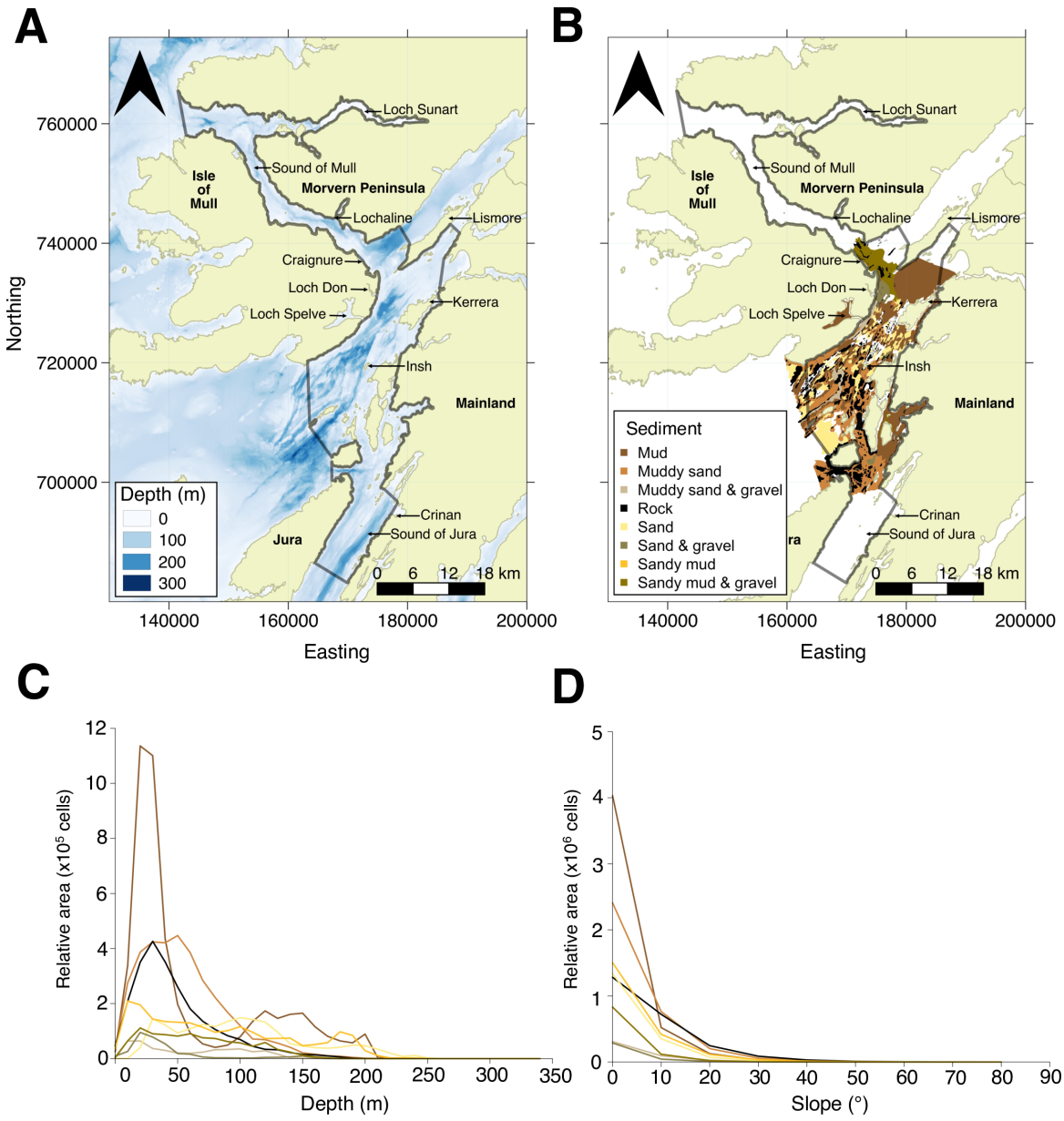

Figure 3. The study site as a habitat. A and **B** are maps of bathymetry and sediment type respectively, with the MPA marked in black. **C** and **D** show the relative area (number of grid cells) covered by each sediment type in each 10 m depth bin and each 10 ° slope angle bin respectively. Bathymetry data are shown at mixed 5 x 5 m and one arc-second resolution, with high-resolution data from Howe et al. (2014) shown where available and lower resolution data from Digimap shown elsewhere. Sediment type data are from Howe et al. (2014) and Boswarva et al. (2018). The coordinate reference system is British National Grid. Background Ordnance Survey maps © Crown copyright and database rights [2019] Ordnance Survey (100025252).

Hydrodynamic conditions in the study site vary across space and time (Figures 4–5). In most cases, temporal variation outweighs spatial variation. Tidal elevation changes at a rate of approximately 0.36 m per hour, oscillating by 3–4 m with the spring and neap tides respectively (Figure 4A–B). Over space, variation is relatively limited. According to POLTIPS predictions, the timing of high and low tide at Oban, Craignure and Seil Sound is similar, although the

magnitude of tidal elevation is smaller at Oban (Figures 4A and 5A). Across the WeStCOMS mesh, tidal elevation varies by up to 2.5 m at any one time, but most of this variation is localised to a few specific areas (e.g., sea lochs) and the daily maximum interquartile range (IQR) in tidal elevation is limited between 0.18–1.27 (median = 0.68) m (Figure 5B). Across all hourly predictions, the median IQR is only 0.15 m.

In terms of light levels, variation in sun angle is dominated by diel and seasonal variation (Figures 4C and 5C). For short-wave radiation, diel and seasonal variation are also the predominant axes of variation, although short-wave radiation is much more variable over space at any one time and over small timescales than sun angle (Figures 4D and 5D). From March 2016–17, the Pearson's correlation coefficient between the hourly means for sun angle and short-wave radiation is 0.743 overall, 0.809 during the day and 0.320 at night. Photoperiod changes gradually through the year, increasing from a minimum of approximately 8 hours in January to a maximum of approximately 20 hours in mid-June, before declining (Figure 4E). Spatial variation in photoperiod is negligible across the study site throughout the year (Figure 5E).

Temporal variation in temperature also predominates over spatial variation (Figures 4F–H and 5F–H). Surface and bottom temperatures change incrementally (by a median value of 3×10^{-3} °C per hour) from a minimum of 6 °C in March to a maximum of 16 °C in late September. Spatial variation in temperature usually extends between 0–1 °C but is occasionally as large as 10 °C. However, most of this variation is confined to a few areas (Figure 5F–G). The upper 100 m experiences up to 2 °C of seasonal stratification (Figures 4H and 5H). However, even at their warmest, surface temperatures lie within the range of predicted bottom temperatures (Figures 4H and 5H).

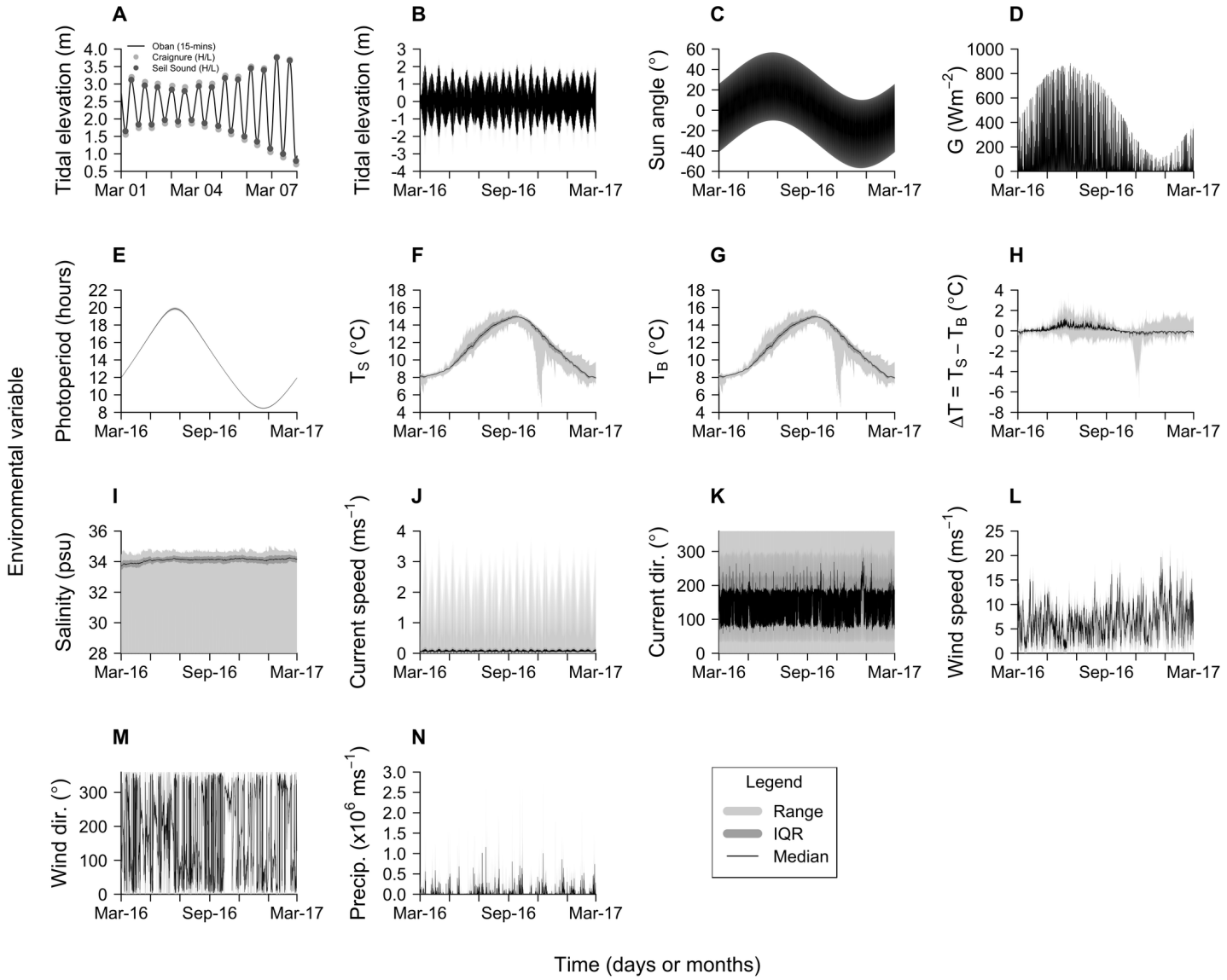

Figure 4. Environmental time series for the study site. A, tidal elevation resolved by POLTIPS.3 tidal prediction software every 15-minutes at Oban (black line) and at high and low tide at Seil Sound and Craignure (dark and light grey points) over a one-week period. **B–N**, conditions resolved across the WeStCOMS mesh: **B**, tidal elevation; **C**, sun angle; **D**, short wave radiation; **E**, photoperiod; **F**, surface temperature; **G**, bottom temperature; **H**, thermocline strength; **I**, salinity; **J**, current speed; **K**, current direction; **L**, wind speed; **M**, wind direction; and **N**, precipitation. For **B–N**, the black line marks the hourly median across the study site. The dark grey envelope marks the hourly interquartile range. This is an approximate measure of the similarity in the values of an environmental variable across most of the study site at any one time. The light grey envelope covers the hourly range. The relative magnitude of short- and long-term temporal change in the median and interquartile range, relative to the variation at any one time, indicates the relative magnitude of these two types of variation.

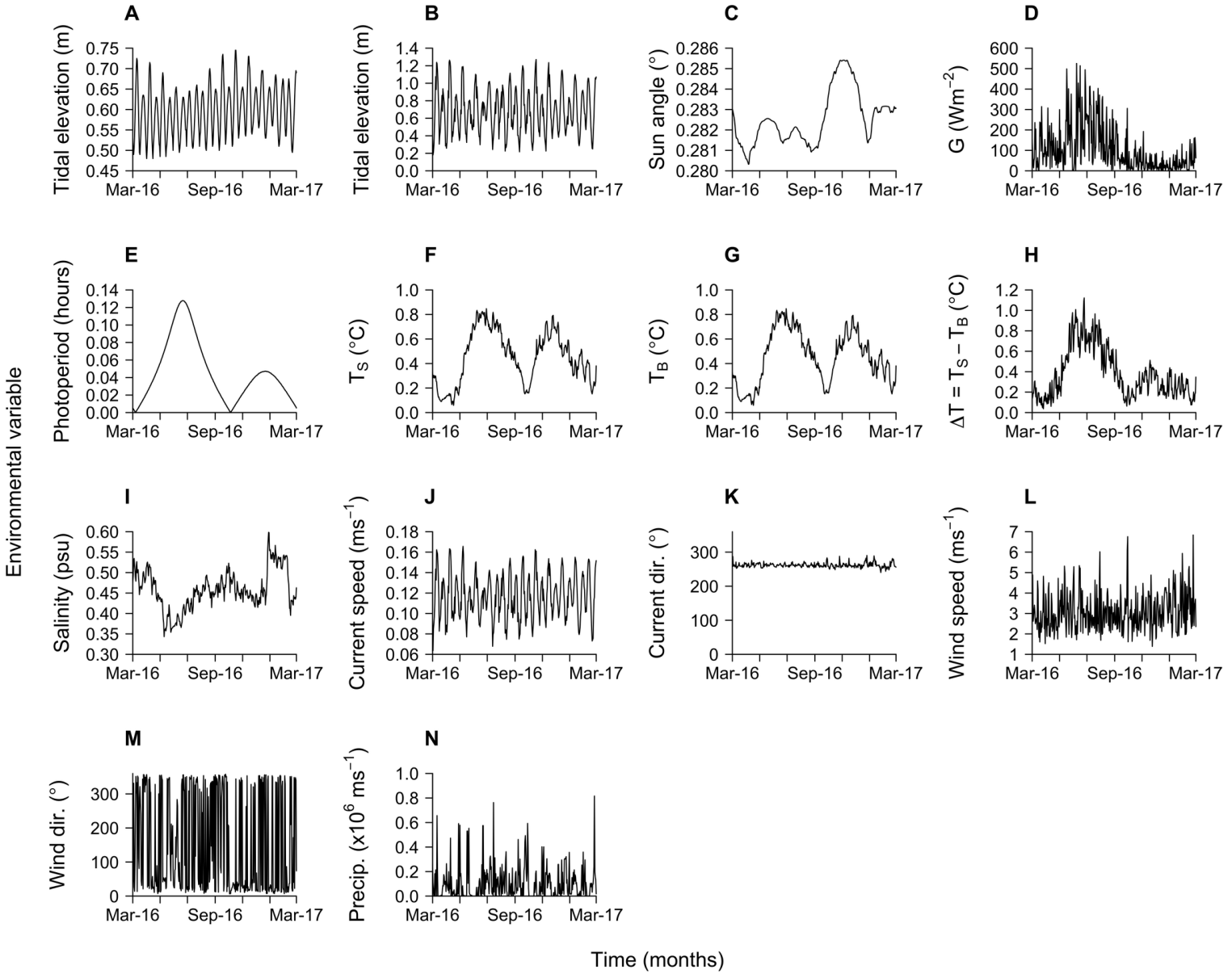

Figure 5. The spatial variation in environmental conditions through time. Panel order follows Figure 4. For each variable, the maximum interquartile range for each day is shown. This is a metric of the magnitude of spatial variation across most of the study site through time. However, the actual range in environmental conditions across the study site may be much larger (e.g., if a few areas differ dramatically from most of the study site).

Bottom salinity is relatively constant across the study site (Figures 4I and 5I). Variation is strongly tied to proximity to sources of freshwater input, such as river discharge, in combination with seasonal precipitation. Consequently, lower salinities and more extreme fluxes are found around the edges of sea lochs, but tend to be highly localised.

The flow regime and meteorological conditions, including wind velocity and precipitation, exhibit higher spatiotemporal variation (Figures 4J–N and 5J–N). The flow regime is dominated by semi-diurnal tides that interact with the bathymetry and incised coastline. In narrow straights such as the Gulf of Corryvreckan, current velocity may exceed eight knots, but elsewhere current velocities are less extreme. Wind velocities and precipitation are similarly influenced by a complex topography and are highly variable.

3.6. WeStCOMS validation

For the validation of WeStCOMS bottom-temperature predictions, the integration of archival and passive acoustic telemetry data led to a validation dataset comprising 102,630 observations from 14 individuals across all hours of the day and 37 nodes. Over time, validation effort spanned over one year in duration (from 15th March 2016 to 1st June 2017), although there were 72 days without any validation observations during this time (Figure 6A). Validation effort was relatively high in spring/summer 2016 and more limited in early winter and 2017. Over space, the distribution of validation effort was strongly right-skewed, with 40 % of observations at one node (22,420), a further 10–15 % of observations at each of two other nodes (22,423 and 22,421) and all other nodes contributing less than 5 % of observations (Figure 6B). The average number of nodes with observations was relatively constant (Figure 6C).

Across the whole time series, the frequency distribution of differences between observed and predicted temperatures was leptokurtic around a mean difference of -0.57 °C, which corresponds to an overprediction of bottom temperatures. Differences ranged between -1.96 and 0.73 °C (Figure 7A). However, WeStCOMS predictive skill varied through time (Figure 7B–C). Specifically, while the differences between observations and predictions were consistently around -0.5 °C in spring (March–May) 2016, they became more variable (while generally remaining negative) in summer (July–September) 2016. Thereafter, the differences gradually declined, especially in 2017. This change is not clearly attributable to changes in the spatial effort (i.e., the number of nodes with observations through time was not higher in

summer 2016 when the distribution of differences was most variable: Figure 6C). It is difficult to synthesise WeStCOMS skill over space given the predominance of observations around the southern receiver array. However, there is no clear relationship between WeStCOMS skill and depth (Figure 7D).

For the validation of predicted temperature-depth profiles, 26 angling events were identified, comprising five events during individuals' time at liberty and 21 tag retrieval events. Of these, locations were available for nine events. However, one of these locations is likely to have been incorrect, with an observed depth more than 100 m deeper than depth of the seabed (Table S4). Therefore, a sample of eight temperature-depth profiles, comprising 64 observations in total, were used for validation. In terms of the temporal validation effort, these samples were collected on four different hours on eight different days from August 2016–April 2017. Spatially, these samples were collected from eight unique locations corresponding to five nodes southeast of Kerrera. Samples spanned a depth range 0–163 m and a temperature range of 7.81–14.05 °C.

The results from a comparison of observed and predicted temperature-depth profiles were largely consistent with the results for bottom temperature (Figure 8). In all cases, predicted temperatures were generally within 1.5 °C of observations. For the four profiles from 2016 (obtained in August and October), WeStCOMS overpredicted the temperature across all depths (Figure 8A–D). This overprediction was stronger for the two samples collected in August and particularly noticeable at the surface where, in contrast to relatively linear observed profiles, WeStCOMS predicted a 0.5 °C increase in temperature in the upper 10–20 m (Figure 8A–B). In October, the shape of the observed profiles was captured more effectively by WeStCOMS, with both observed and predicted temperatures marginally cooler at the surface at this time (Figure 8C–D). In 2017, all four samples (collected in March and April) were accurately predicted by the model (Figure 8E–H), although there was a small discrepancy in the near-surface predictions for the final temperature-depth profile (Figure 8H).

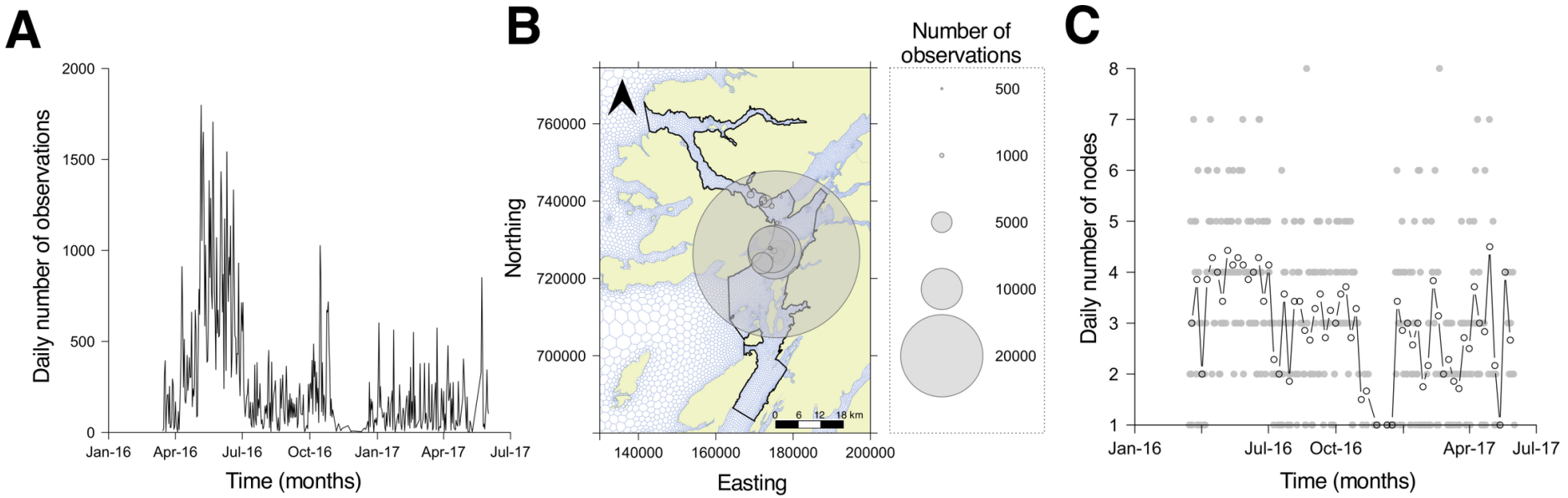

Figure 6. WeStCOMS bottom-temperature validation effort. A, temporal effort expressed as the number of validation observations per day through time. **B**, spatial effort, expressed as the total number of observations at each receiver location. The WeStCOMS mesh (around nodes) is shown in blue. The coordinate reference system is British National Grid. Background Ordnance Survey maps © Crown copyright and database rights [2019] Ordnance Survey (100025252). **C**, spatiotemporal effort, expressed as the total number of nodes with observations per day through time. The filled grey points show the total number of nodes; the open points and the line mark the weekly mean.

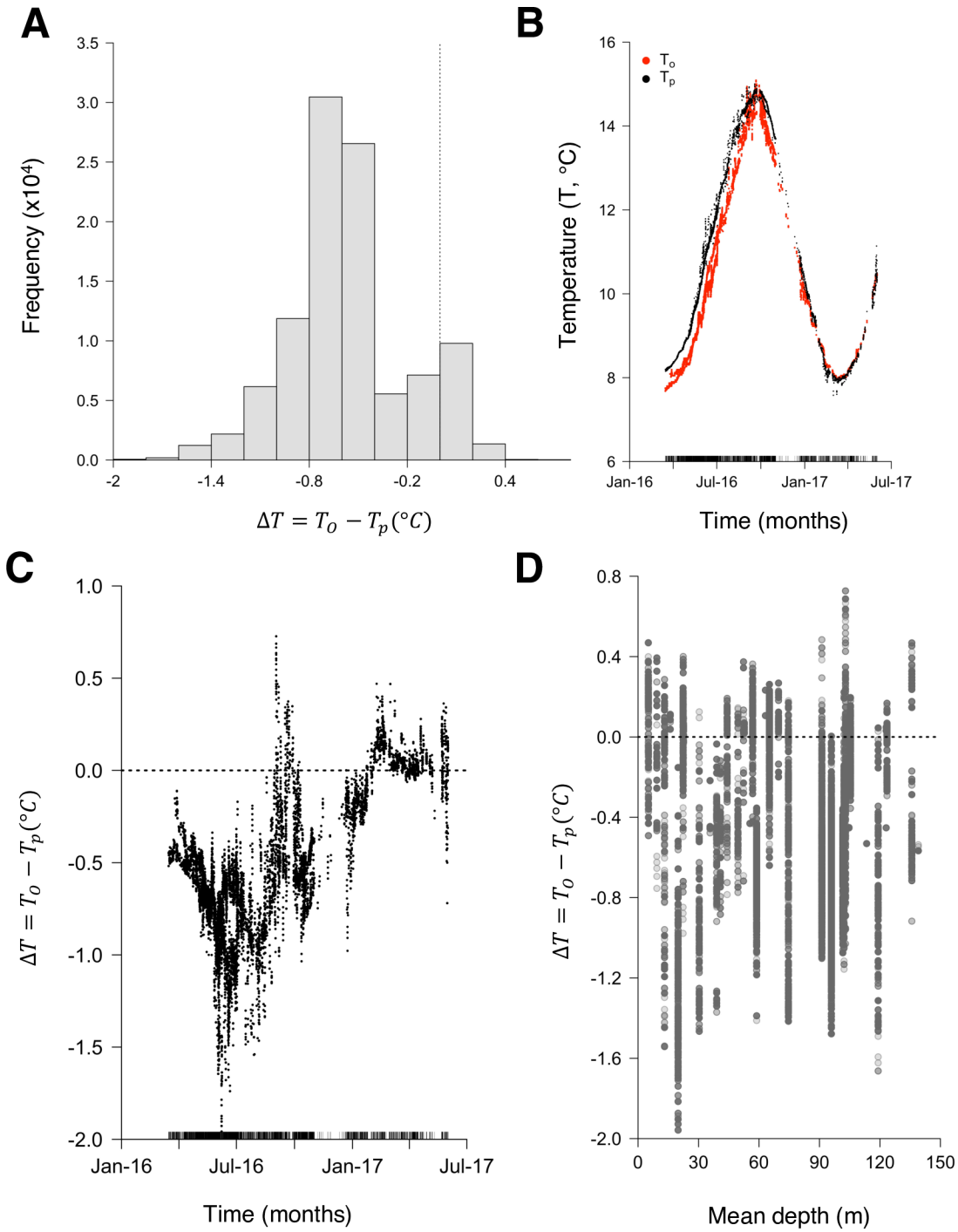

Figure 7. WeStCOMS bottom-temperature validation. A, the frequency distribution of differences between observed and predicted bottom temperatures. The vertical dashed line marks the point of no difference in temperature observations and predictions. **B**, observed and predicted temperature time series (red and black points, respectively). **C**, the difference between observed and predicted temperatures through time. In **B** and **C**, the rug marks times with observations. The horizontal line at $\Delta T = 0$ marks the point of no difference between observations and predictions. **D**, the difference between observed and predicted temperatures in relation to the mean depth (of nodes).

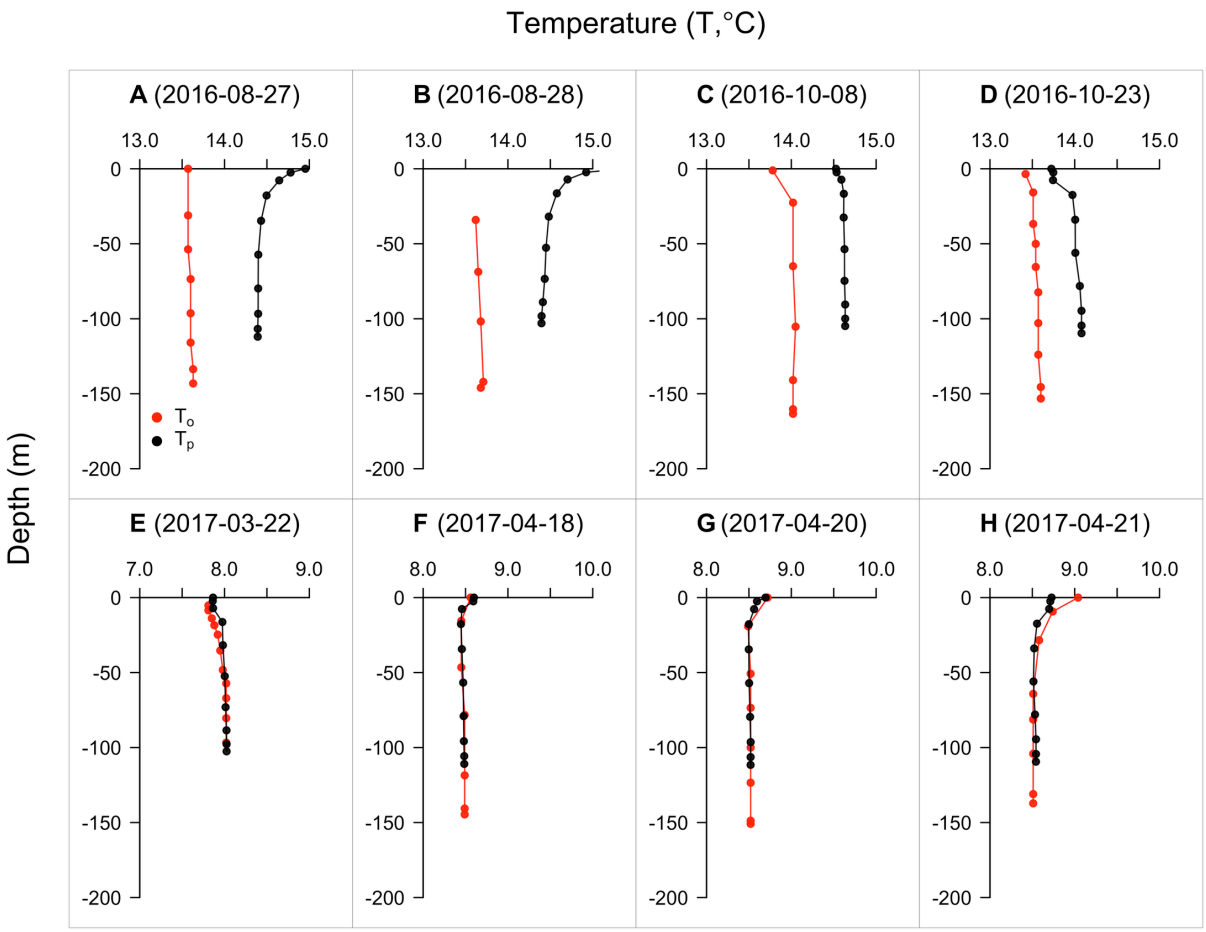

Figure 8. WeStCOMS temperature-depth profile validation. Each panel (**A–H**) shows an observed (red) and predicted (black) temperature-depth profile sampled on a particular date (shown in brackets). For profile **B**, missing observations from the end of available time series mean that near-surface temperature observations are lacking. Note that the temperature axis differs among panels, but the difference between minimum and maximum temperatures in each case is the same (2 °C), so the panels are comparable. Differences between the depth of the bottom WeStCOMS layer and the maximum depth of individuals reflect local variation in bathymetry that is not captured at resolution of the WeStCOMS mesh.

4. Discussion

Technological innovation in electronic tagging and tracking is driving the collection of a wealth of animal movement data (Hussey et al., 2015; Kays et al., 2015; Nathan et al., 2022). These data provide opportunities to understand spatiotemporal patterns in animal movement, alongside their causes and consequences, in a rapidly changing world (Hays et al., 2019). However, the complexity of movement datasets requires a renewed focus on data management, study systems and the context from which movement data are sampled to realise these opportunities (Ogburn et al., 2017; Williams et al., 2020). This chapter expands the set of tools for data processing, visualisation and analysis available to movement researchers through the development of four widely applicable R packages. For flapper skate, the chapter secures the long-term value of movement data collected by the MEFS project by documenting data collection and processing and through the development of the MEFS R package for data storage. At the same time, the chapter demonstrates the importance of analyses of sampling effort and the environment for research into species' movements. For the MEFS datasets, these analyses reveal the need to account for tagging location and receiver coverage in analyses of passive acoustic telemetry data (Chapter Three and Six) and suggest putative causes and consequences of movement, correlations between variables and important scales of variation that underpin model development (Chapters Three, Four and Five). For the integration of environmental analyses with movement modelling, the development of a method for the validation of hydrodynamic models via benthic species in passive acoustic telemetry systems is a notable step forward that expands the range of animal oceanographers in aquatic environments (Harcourt et al., 2019). For WeStCOMS, the bottom-temperature validation dataset assembled using this method is one of the most extensive to date and provides a unique empirical confirmation that recent model updates have dramatically improved model predictive skill. Moving forwards, this work should support the integration of environmental products in movement models for flapper skate and foster multidisciplinary research in the fields of movement ecology and hydrodynamic modelling.

This chapter represents a case study of the importance of data management for movement researchers, advisory bodies and government agencies. Four recommendations for robust data management emerge as lessons from this project. First, every field in a database should be recorded in a single, consistent, computer-readable format, to an unambiguous level of precision (Broman and Woo, 2018). Spreadsheet software, such as Microsoft Excel, can

facilitate inconsistencies or errors because data types are not defined and enforced (Powell et al., 2008; Broman and Woo, 2018), but relational databases and R packages force necessary consistency and scale more effectively with data volume (Cunha et al., 2009; Wickham, 2015). Second, every relevant observation should be accompanied by a time stamp and a location. For example, in this project, capture times were not recorded. Yet post-hoc identification of angling events within archival time series is difficult, especially because prolonged tension from rod and line is required to force skate into ascent. Consequently, exclusion windows around angling events had to be wider than otherwise necessary. Third, in the field, opportunities for data collection should be maximised. For example, the absence of clasper morphometrics and other maturity data in this chapter meant that the definition of maturation status was based on predictive modelling (Iglésias et al., 2010). However, photographs were instructive in guiding the interpretation of model predictions. Fourth, all raw data should be stored in a single, read-only database. All data processing should be implemented subsequently using reproducible protocols (Wilkinson et al., 2016). The prettyGraphics, Tools4ETS and flapper packages facilitate this process with functions for processing archival and passive acoustic telemetry time series, including the identification of angling events, investigation of false detections and automated implementation of quality checks.

The data processed in this chapter, provided and documented in the accompanying MEFS R package, create significant opportunities to examine flapper skate movements and support management. The detection time series provide a means to quantify residency around receivers, underpinning our understanding of the contribution of the LStSJ MPA to flapper skate conservation (Chapter Three). Similarly, the archival time series contain information on vertical movements and responses to catch-and-release angling which may reflect the vulnerability and responses of skate to threats such as bycatch (Chapters Four and Five). Bringing these two datasets together should facilitate the reconstruction of fine-scale movements over the seabed and emergent patterns of space use, providing a means to estimate residency in the MPA as a whole and habitat preferences (Chapter Six).

Analyses of sampling effort contextualise these opportunities and guide the implementation and interpretation of movement ecology research. For example, in this chapter, spatiotemporal variation in tagging location, receiver coverage and the number of individuals at liberty is clearly important for the modelling and interpretation of passive acoustic telemetry data (Chapter Three). Likewise, the clustered arrangement of receivers underpins the analysis and

interpretation of detection patterns and their wider relevance across the MPA (Chapter Three) (Hays et al., 2020). Given the arrangement of receivers, methods that reconstruct movements beyond receivers are required to understand movement patterns across the MPA, residency within this area as a whole and habitat preferences (Chapters Three and Six). These considerations underpin the choice of analyses, and their interpretation, in later chapters.

Analyses of environmental conditions are another prerequisite for movement analyses that can highlight putative causes or consequences of movement, the suitability of environmental metrics for inclusion in models and notable scales of variation. In the LStSJ MPA, this chapter highlights tidal elevation, sun angle, photoperiod and temperature as candidate drivers of temporal variation in movement patterns, with most variation in these variables expressed through time. Moreover, for these variables, metrics derived at a single location are likely to be reasonable representations of the conditions affecting tagged individuals, a necessary prerequisite for their inclusion in movement models for individuals whose precise locations are unknown (Chapter Four). Over space, significant variation in depth, sediments and salinity may influence skate movement in the MPA, as in other systems (Sundström et al., 2001; Schlaff et al., 2014). For example, given that elasmobranchs are stenohaline (Froeschke et al., 2010; Martin et al., 2012), substantial fluctuations in salinity in shallow, inshore areas adjacent to sources of freshwater input may limit flapper skate movements in these areas (Chapter Three). At fine scales, other variables such as current velocity are likely to be important, as shown for other elasmobranchs (Sundström et al., 2001; Schlaff et al., 2014). However, the effects of current velocity and other highly changeable variables on movement may be difficult to quantify given uncertainty in individual locations (Chapters Three and Four).

The investigation of environmental conditions also reveals correlations between variables that are important for model development and interpretation. For example, the correlation between sun angle and short-wave radiation demonstrates that sun angle is a reasonably robust metric for light levels at the surface, notwithstanding other factors, such as cloud cover, which modulate light intensity (Wild, 2009). For modelling elasmobranch movement, this is important because sun angle is a more widely applicable metric of light levels (given relatively limited spatial variation) and light levels are linked to movement perhaps more commonly than any other environmental variable (Schlaff et al., 2014).

For candidate drivers of movement, examination of environmental conditions also suggests potentially important scales of variation. For instance, alongside light levels, temperature is another commonly documented driver of elasmobranch movement over diel and seasonal timescales (Sundström et al., 2001; Schlaff et al., 2014). In the LStSJ MPA, diel change in temperatures is limited and most variation is over seasonal timescales. In the summer, a thermocline is established, but the strength of the thermocline is limited. These results suggest temperature gradients may have limited consequences for metabolic efficiency and gastric evacuation in flapper skate and that diel structure in the vertical movements of tagged individuals may reflect other factors, such as changes in light levels and diel rhythms in prey availability (Chapter Four; Wearmouth and Sims, 2009; Pinto and Spezia, 2016).

This chapter highlights the contributions of hydrodynamic models towards an improved understanding of aquatic environments, alongside their uses in ecological research more broadly (Aleynik et al., 2016; Gallego et al., 2017; Braun et al., 2018). For ecologists familiar with the R programming language, fvcom.tbx greatly streamlines interactions with hydrodynamic model outputs via the provision of functions for processing, exploration and validation (Lavender, 2020e). The latter is essential in oceanography and applied settings (Radach and Moll, 2003). In movement ecology, for instance, an understanding of the accuracy of temperature predictions is required for investigations into the potential influence of temperature on animal movement (Chapter Three). In line with this requirement, the development of a method to integrate passive acoustic telemetry and archival data for model validation is a significant extension of previous research that has focused on the use of diving mammals and global positioning systems (Harcourt et al., 2019) and provides a unique demonstration of the use of benthic species for oceanographic data collection.

The applicability of the model validation method in this chapter depends on the assumption that flapper skate are benthic animals. This assumption is consistent with skate morphology and diet studies of common skate (*D. batis*) and related species (Steven, 1947; Wheeler, 1969; Brown-Vuillemin et al., 2020). The way that skate have to be pulled off the seabed during recreational angling is also consistent with this hypothesis. In addition, recent work has shown that it is possible to reconstruct skate movements under the assumption that skate are living at (or very near) the seabed (Chapter Six). In some situations, burial within the sediment, as documented in other species (Kuhnz et al., 2019), or propulsion above the seabed, as hypothesised to account for the presence of pelagic prey in the stomachs of common skate

(Wheeler, 1969), may cause small discrepancies between observations and predictions, but these are probably limited in most cases. The other main assumption of the validation method developed in this chapter is nearest neighbour interpolation in time and space. In many cases, this choice is likely to be a pragmatic option, given the accuracy of observations, the magnitude of spatiotemporal variation, computational considerations and research objectives, but the method could be refined to implement other interpolation methods if necessary.

From a hydrodynamic modelling perspective, the dataset assembled in this chapter for WeStCOMS bottom-temperature validation is unprecedented in scale, especially through time. The results provide robust confirmation that WeStCOMS bottom-temperature predictions are highly accurate (± 1°C). Pre-2017, there was a tendency to overpredict bottom temperatures, but recent model updates have substantially reduced model bias. This is a unique example of use of animal movement time series to validate empirically changes to the design of a hydrodynamic model. Observed temperature-depth profile data are much more limited, but available data suggest that the results for bottom temperatures may apply throughout the water column. From an ecological perspective, this demonstrates that predicted temperatures are a reasonable representation of available temperatures. This is important because temperature is perhaps the most widespread driver of species' distributions in aquatic ecosystems, at least at large spatial scales (Stuart-Smith et al., 2017; Lavender et al., 2021b), and clearly influences movement in many elasmobranch species (Sundström et al., 2001; Schlaff et al., 2014). However, understanding spatiotemporal variation in other variables, especially those near the seabed such as bottom current velocities, remains an active research area, with model predictions less extensively validated (Aleynik et al., 2016).

Appendices

1. Supporting tables

Table S1. Summary of the acoustic array. For each unique receiver deployment (ID = 1,…,58), the receiver, easting and northing (coordinates on the British National Grid coordinate reference system), operational start and end dates (year-month-day), the duration of the operational period, receiver depth and seabed depth are shown. Note that some receivers were not retrieved. [a]Two receivers were lost during the course of the study and later retrieved elsewhere; these are excluded from analyses. [b]One receiver drifted during the course of the study; on 2016-04-08 the receiver was found near to its deployment location (171366.3, 721435.5) and returned to this location. This receiver is included in acoustic analyses. The operational end date for most receivers was 2017-06-02; the operational end date for the final two receivers was 2017-07-23, but these receivers made no additional detections over that period. For this reason, 2017-06-02 is considered the end point of acoustically tagged individuals' time at liberty. The duration of the operational period is defined as the number of days between the operational start and end dates, inclusive, excluding any receiver servicing dates. Seabed depth was extracted from one arc-second resolution Ordnance Survey bathymetry data because not all receivers lie within the domain of higher resolution data (Howe et al., 2014). Note that the depths of receivers 2 and 8—the two receivers placed in very shallow water off North Lismore—are greater than extracted water depths; this is due to inaccuracies in the bathymetry data.

ID	Receiver	Easting	Northing	Date (start)	Date (end)	Duration (days)	Receiver depth (m)	Seabed depth (m)
1	VR2-5536	178825	741251	16-03-03	-	-	-	-
2	VR2-5626	189301	745534	16-03-03	16-07-23	142	5	2
3	VR2-5629	174453	727455	16-03-03	16-11-02	243	50	109
4	VR2-5630	179118	740776	16-03-03	17-03-08	367	50	160
5	VR2-5633	179628	739952	16-03-03	17-07-23	506	25	74
6[a]	VR2-5634	178500	741760	16-03-03	16-07-10	129	-	180
7	VR2-5635	178285	742279	16-03-03	16-11-26	265	50	147
8	VR2-5636	189769	745220	16-03-03	16-07-23	142	5	7
9	VR2-5637	174056	727826	16-03-03	16-10-13	223	10	26
10	VR2-5638	182550	727508	16-03-03	16-11-19	260	10	28

ID	Receiver	Easting	Northing	Date (start)	Date (end)	Duration (days)	Receiver depth (m)	Seabed depth (m)
11	VR2-6720	176913	741002	16-03-03	16-11-18	258	50	173
12	VR2-6723	179393	740340	16-03-03	17-03-08	367	50	151
13	VR2-6724	176411	730286	16-03-03	-	-	-	-
14	VR2W-107823	172866	739971	16-03-03	17-07-23	505	25	55
15	VR2W-107824	172442	739547	16-03-03	-	-	-	-
16	VR2W-107825	162319	744560	16-03-03	16-05-07	65	25	70
17	VR2W-107826	176014	726158	16-03-03	-	-	-	-
18	VR2W-108155	177417	735470	16-03-03	16-11-18	258	25	46
19	VR2W-108156	174876	727085	16-03-03	-	-	-	-
20	VR2W-108157	171622	738701	16-03-03	17-06-01	451	10	23
21	VR2W-108158	176597	726079	16-03-03	17-06-02	453	25	56
22	VR2W-108159	175643	735022	16-03-03	-	-	-	-
23	VR2W-108160	172019	739124	16-03-03	16-09-24	203	25	35
24	VR2W-108161	177972	735604	16-03-03	17-06-02	452	25	41
25	VR2W-108162	167784	743887	16-03-03	16-11-19	261	50	102
26	VR2W-108163	177152	726290	16-03-03	16-10-18	227	25	48
27 [b]	VR2W-110825	172019	723925	16-03-03	16-11-02	242	50	103
28 [a]	VR2W-112985	178263	726581	16-03-03	16-04-16	44	-	72
29	VR2W-113141	169007	741641	16-03-03	17-02-23	356	50	117
30	VR2W-113142	175658	726227	16-03-03	16-11-02	242	50	126
31	VR2W-120722	177681	726396	16-03-03	16-11-19	259	25	37
32	VR2W-128784	176887	735339	16-03-03	-	-	-	-
33	VR2W-128786	175241	726794	16-03-03	16-07-24	142	50	94
34	VR2W-128787	176172	735191	16-03-03	-	-	-	-

ID	Receiver	Easting	Northing	Date (start)	Date (end)	Duration (days)	Receiver depth (m)	Seabed depth (m)
35	VR2AR-546131	177505	736478	16-07-11	16-11-03	115	25	33
36	VR2AR-546132	177505	728210	16-07-11	16-11-03	115	95	103
37	VR2AR-546133	174655	725219	16-07-11	16-11-03	115	50	86
38	VR2AR-546134	176558	735268	16-07-11	16-11-03	115	40	66
39	VR2AR-546136	174458	738725	16-07-11	16-11-03	115	105	109
40	VR2W-113898	178825	741251	16-08-02	16-11-18	108	50	171
41	VR2-5637	172846	740221	16-12-20	17-06-02	164	25	28
42	VR2W-108155	177412	735472	16-12-20	17-06-02	164	25	46
43	VR2W-108160	175846	726156	16-12-20	17-06-02	164	50	128
44	VR2W-108163	179339	739700	16-12-20	17-06-02	163	25	86
45	VR2AR-546131	177052	726697	16-12-20	17-06-02	164	35	55
46	VR2AR-546132	171711	739397	16-12-20	17-06-02	164	25	34
47	VR2AR-546133	172264	740066	16-12-20	17-06-02	164	90	101
48	VR2AR-546134	175146	727121	16-12-20	17-06-02	164	145	133
49	VR2AR-546135	174362	727748	16-12-20	17-06-02	164	85	83
50	VR2AR-546136	176616	734328	16-12-20	17-06-02	164	75	65
51	VR2AR-546380	175897	734355	16-12-20	17-06-02	164	25	28
52	VR2AR-546586	171915	739751	17-03-18	17-06-02	76	20	23
53	VR2AR-546587	174096	728027	17-03-18	17-06-02	76	15	24
54	VR2AR-546591	171568	739061	17-03-18	17-06-02	76	20	27
55	VR2AR-546583	178302	726425	17-03-20	17-06-02	74	60	81
56	VR2AR-546584	177516	726434	17-03-20	17-06-02	74	30	39
57	VR2AR-546585	176322	726119	17-03-20	17-06-02	74	75	83
58	VR2AR-546589	181407	725711	17-03-20	17-06-02	74	20	24

Table 2. Summary of tagged skate. For each individual (ID = 1,…,66), the tag deployment date (year-month-day), deployment site, sex, disc width, total length, maturation probability, acoustic identifier (number and tag type: Vemco V13 [V] or Thelma Biotel MP-13 [T]), archival identifier (number and tag type: Star Oddi [S] or CEFAS [C]), whether or not the archival tag was recovered, and the dates and sites of acoustic and archival tag retrieval, if known, are provided. The coordinates of angling locations are not provided because anglers' favoured angling locations are sensitive. Body sizes were measured on the vessel but, for one individual[a], the total length appears to be erroneous for its disc width (or vice versa), given the length–width relationship shown by other individuals. However, since neither acoustic nor archival data were successfully recovered for this individual, this issue has not been corrected. Overall, 43 individuals were tagged with acoustic tags, but for one individual[b] the acoustic tag detached from the animal as soon as it was released. Thus, 42 successful acoustic tag deployments are recognised. Another individual[c] was recaptured without an acoustic or archival tag on 2016-05-02; this date is given as the date of acoustic tag retrieval. Archival tags were attached to 63 individuals. However, for 18 individuals[d], programming issues were discovered. Therefore, 45 successful archival (Star Oddi milli-TD) tag deployments are recognised. Following archival tag deployments, 31 tagged individuals were recaptured, but this number includes nine individuals with tags that had programming issues and the individual that was recaptured without its archival tag. Therefore, 21 successful archival (Star Oddi milli-TD) tag retrievals are recognised.

ID	Dep. date	Dep. site	Sex	DW (cm)	TL (cm)	Pr (mature)	Acc ID	Arc ID	Arc recovered	Ret. date acc	Ret. date arc	Ret. site acc	Ret. site arc
1	16-03-03	Kerrera	F	170	213	1.00	-	1566 [S]	0	-	-	-	-
2	16-03-03	Kerrera	F	159	211	1.00	-	1567 [S]	0	-	-	-	-
3	16-03-03	Kerrera	M	152	201	1.00	-	1562 [S]	0	-	-	-	-
4	16-03-03	Kerrera	M	137	180	0.00	-	1568 [S]	0	-	-	-	-
5	16-03-03	Kerrera	F	152	203	1.00	-	1563 [S]	0	-	-	-	-
6	16-03-03	Kerrera	F	160	203	1.00	-	1574 [S]	1	-	2016-06-09	-	-
7	16-03-07	Kerrera	M	155	198	1.00	251 [V]	1572 [S]	0	18-06-07	-	-	-
8	16-03-07	Kerrera	F	168	221	1.00	250 [V]	1560 [S]	0	18-06-07	-	-	-
9	16-03-09	Insh	F	79	109	0.00	255 [V]	1564 [S]	0	18-06-07	-	-	-
10	16-03-09	Insh	F	170	221	1.00	254 [V]	1570 [S]	0	17-06-06	-	-	-
11 [b]	16-03-09	Insh	F	165	208	1.00	252 [V]	1571 [S]	0	16-03-16	-	-	-
12	16-03-10	Insh	M	137	175	0.00	253 [V]	1546 [S]	0	18-06-07	-	-	-
13	16-03-13	Insh	F	135	174	0.00	249 [V]	1558 [S]	1	17-07-17	16-05-28	-	-

ID	Dep. date	Dep. site	Sex	DW (cm)	TL (cm)	Pr (mature)	Acc ID	Arc ID	Arc recovered	Ret. date acc	Ret. date arc	Ret. site acc	Ret. site arc
14	16-03-13	Insh	F	137	185	0.00	247 [V]	1552 [S]	1	16-07-11	16-04-02	-	-
15	16-03-14	Kerrera	F	140	180	0.00	246 [V]	1555 [S]	0	18-06-07	-	-	-
16 [c]	16-03-14	Kerrera	M	79	107	0.00	245 [V]	1528 [S]	0	16-05-02	-	-	-
17	16-03-14	Kerrera	M	146	188	0.98	244 [V]	1536 [S]	1	16-10-23	16-10-23	Kerrera	Kerrera
18	16-03-14	Kerrera	F	155	206	1.00	248 [V]	1532 [S]	0	16-03-28	-	-	-
19	16-03-14	Kerrera	F	119	155	0.00	564 [V]	1533 [S]	1	16-05-25	16-10-08	-	Kerrera
20	16-03-15	Kerrera	F	114	155	0.00	242 [V]	1538 [S]	1	16-06-25	17-07-19	-	-
21	16-03-15	Kerrera	M	155	198	1.00	241 [V]	1545 [S]	0	18-06-07	-	-	-
22	16-03-15	Kerrera	F	163	213	1.00	552 [V]	1537 [S]	0	17-05-05	-	-	-
23	16-03-15	Kerrera	M	75	108	0.00	559 [V]	1513 [S]	0	18-06-07	-	-	-
24	16-03-15	Kerrera	F	155	201	0.98	535 [V]	1539 [S]	1	17-04-17	16-04-29	Kerrera	-
25	16-03-15	Kerrera	F	163	208	1.00	555 [V]	1547 [S]	1	18-04-26	18-04-26	-	-
26	16-03-16	Kerrera	F	114	160	0.00	532 [V]	1499 [S]	0	18-06-07	-	-	-
27	16-03-16	Kerrera	M	142	190	1.00	563 [V]	1520 [S]	1	16-07-13	16-07-13	-	-
28	16-03-16	Kerrera	F	130	160	0.00	560 [V]	1522 [S]	1	17-04-18	17-04-18	Kerrera	Kerrera
29	16-03-16	Kerrera	M	145	193	1.00	542 [V]	1523 [S]	1	16-05-26	16-05-26	-	-
30	16-03-16	Kerrera	M	147	185	0.47	545 [V]	1521 [S]	0	18-06-07	-	-	-
31	16-03-16	Kerrera	F	160	206	1.00	550 [V]	1526 [S]	1	16-03-19	16-03-19	-	-
32	16-03-16	Kerrera	M	150	196	1.00	549 [V]	1548 [S]	1	18-06-07	17-04-21	-	Kerrera
33	16-03-16	Kerrera	F	118	160	0.00	541 [V]	1531 [S]	0	18-06-07	-	-	-
34	16-03-16	Kerrera	M	149	198	1.00	539 [V]	1518 [S]	1	17-03-22	17-03-22	Kerrera	Kerrera
35	16-03-17	Kerrera	F	100	135	0.00	540 [V]	1509 [S]	1	17-04-20	17-04-20	Kerrera	Kerrera
36	16-03-17	Kerrera	F	170	213	1.00	543 [V]	1512 [S]	1	17-05-05	16-07-13	-	-

ID	Dep. date	Dep. site	Sex	DW (cm)	TL (cm)	Pr (mature)	Acc ID	Arc ID	Arc recovered	Ret. date acc	Ret. date arc	Ret. site acc	Ret. site arc
37	16-03-17	Kerrera	F	165	213	1.00	558 [V]	1508 [S]	0	18-06-07	-	-	-
38	16-03-17	Kerrera	F	160	206	1.00	547 [V]	1507 [S]	1	16-07-10	16-05-18	-	-
39	16-03-17	Kerrera	M	149	196	1.00	-	1511 [S]	1	-	16-08-28	-	Kerrera
40	16-03-17	Kerrera	F	175	226	1.00	-	1505 [S]	0	-	-	-	-
41 [d]	16-04-13	Crinan	F	160	213	1.00	-	A07099 [C]	1	-	-	-	-
42 [d]	16-04-13	Crinan	F	163	211	1.00	-	A07107 [C]	0	-	-	-	-
43 [d]	16-04-13	Crinan	F	165	211	1.00	-	A07097 [C]	0	-	-	-	-
44 [d]	16-04-13	Crinan	F	157	208	1.00	-	A07098 [C]	1	-	-	-	-
45 [d]	16-04-14	Crinan	F	163	213	1.00	544 [V]	A09291 [C]	0	18-06-07	-	-	-
46 [d]	16-04-14	Crinan	F	160	211	1.00	546 [V]	A09278 [C]	1	17-04-04	-	-	-
47 [d]	16-04-14	Crinan	F	160	203	1.00	548 [V]	A09301 [C]	0	18-06-07	-	-	-
48 [d]	16-04-14	Crinan	F	152	198	0.68	561 [V]	A02298 [C]	0	18-06-07	-	-	-
49 [d]	16-04-14	Crinan	F	163	208	1.00	-	A09281 [C]	1	-	-	-	-
50 [d]	16-04-14	Crinan	F	165	211	1.00	-	A09289 [C]	0	-	-	-	-
51 [d]	16-04-14	Crinan	F	168	221	1.00	-	A11716 [C]	0	-	-	-	-
52 [d]	16-09-01	Insh	M	100	136	0.00	41261 [T]	1520 [S]	1	18-06-07	-	-	-
53 [d]	16-09-01	Insh	M	115	156	0.00	41269 [T]	1574 [S]	1	18-06-07	-	-	-
54 [d]	16-09-01	Insh	F	117	157	0.00	41268 [T]	1512 [S]	1	18-06-07	-	-	-
55	16-09-20	Insh	M	86	112	0.00	41265 [T]	-	-	18-06-07	-	-	-
56	16-09-20	Insh	F	156	211	1.00	41264 [T]	-	-	18-06-07	-	-	-
57 [d]	16-09-22	Insh	M	139	177	0.00	41262 [T]	1526 [S]	1	17-03-29	-	-	-
58 [d]	16-09-22	Insh	M	142	178	0.00	41297 [T]	1552 [S]	1	18-06-07	-	-	-
59 [a,d]	17-04-18	Crinan	M	122	201	1.00	-	A11714 [C]	1	-	-	-	-

ID	Dep. date	Dep. site	Sex	DW (cm)	TL (cm)	Pr (mature)	Acc ID	Arc ID	Arc recovered	Ret. date acc	Ret. date arc	Ret. site acc	Ret. site arc
60 [d]	17-04-18	Crinan	F	163	210	1.00	-	A11710 [C]	0	-	-	-	-
61	17-04-19	Crinan	F	163	201	0.98	-	1525 [S]	1	-	17-05-03	-	-
62	17-04-19	Crinan	F	165	216	1.00	-	1502 [S]	1	-	19-02-26	-	-
63	17-04-19	Crinan	F	170	-	-	-	-	-	-	-	-	-
64	17-04-19	Crinan	F	159	193	0.00	-	1514 [S]	0	-	-	-	-
65	17-04-19	Crinan	F	170	218	1.00	-	1519 [S]	1	-	19-03-31	-	-
66	17-04-19	Crinan	M	145	191	1.00	-	1508 [S]	0	-	-	-	-

Table S3. A summary of the environmental variables that were resolved across the WeStCOMS mesh. For each variable, the abbreviation (if applicable), the units, source, type and category are provided. The source is given as 1–4, which indicates that the variable was (1) resolved by WeStCOMS, (2) computed from WeStCOMS predictions, (3) computed across the WeStCOMS mesh using alternative algorithms or (4) resolved by other means. Wind/current direction are defined as the direction of mass flow; sun angle is the angle of the sun above the horizon; and photoperiod is the duration between the start of morning civil twilight and the end of evening civil twilight.

Category	Variable type	Variables	Source
Hydrodynamic	Tides	Tidal elevation (m)	1, 4
	Temperatures	Surface temperature (°C)	1
		Bottom temperature (°C)	1
		Thermocline strength (°C)	2
	Salinity	Salinity (psu)	1
	Currents	Current speed (ms^{-1})	2
		Current direction (°)	2
Meteorological	Precipitation	Precipitation (Precip., ms^{-1})	1
	Winds	Wind speed (ms^{-1})	2
		Wind direction (°)	2
	Light levels	Sun angle (°)	3
		Short-wave radiation (G, Wm^{-2})	1
		Photoperiod (hours)	3

Table S4. Summary of recreational angling events that occurred during archival tag deployments for the 21 individuals for which archival data were recovered. For each individual (Arc ID), the angling site (if known) and the date of capture (year-month-day) are shown. Note that the angling location recorded for 1536 (Loch Sween*) is inconsistent with the depth time series around the angling event for that individual given that the maximum reported depth for the area is 40 m (Scottish Natural Heritage, 2013).

Arc ID	Site	Date
1522	-	16-07-13
1522	Kerrera	16-08-27
1523	-	16-05-16
1533	-	16-05-10
1536	Loch Sween*	16-04-29

Chapter Three

Detection patterns, residency around receivers and wider range movements

Abstract

1. Marine Protected Areas (MPAs) are widely used in marine management, but for mobile species understanding the spatiotemporal scale of management measures that is required to deliver conservation benefits depends on a detailed knowledge of species' movements that is often lacking. This is especially the case for species of skate (Rajidae) for which relatively few movement studies have been conducted.
2. In Scotland, the Loch Sunart to the Sound of Jura MPA has been designated for the conservation of the Critically Endangered flapper skate (*Dipturus intermedius*), but localised movements and residency within this area remain poorly understood.
3. A passive acoustic telemetry study which coupled acoustic tagging of 42 individuals and a static array of 58 receivers was conducted in the MPA from March 2016–June 2017. Using acoustic detection time series alongside depth time series from archival tags and angler mark-recapture records, localised movements and residency were investigated.
4. Overall, 33 of the 42 tagged individuals were detected. Residency, site fidelity and transiency were documented. Residency around receivers, lasting from three months to more than 12 months, was documented in 16 acoustically detected individuals (48 %) and all life-history categories but was most noticeable among females. Localised movements around receivers were associated with depth, salinity and season, but there was no evidence that individuals formed close-knit groups in the areas in which they were detected.
5. Taken together with historical occurrence records of flapper skate, the prevalence and scale of residency documented here suggest that the MPA is sufficiently large to benefit a notable percentage (38 [24–52] %) of skate found in the study site over monthly and seasonal

timescales. This result strengthens the case for the use of MPAs to support the conservation of flapper skate and other skate species that display similar movement patterns.

Keywords

detection, management, marine protected area, passive acoustic telemetry, Rajidae, residency

1. Introduction

Elasmobranchs are among the most threatened vertebrates (Dulvy et al., 2014; Pacoureau et al., 2021). One quarter of species are threatened with extinction, principally due to overfishing (Dulvy et al., 2014). The most threatened species are predominately large-bodied species in shallow, coastal areas (Dulvy et al., 2014). The decline of these species has potentially serious consequences for ecosystem structure, function and services (Baum and Worm, 2009; Pimiento et al., 2020). Consequently, there is an urgent need for research into the efficacy of management approaches designed to reduce the pressures on these species (Chapter One).

In coastal marine ecosystems, spatial management approaches, such as Marine Protected Areas (MPAs), are a popular option for elasmobranch conservation (Ferretti et al., 2018; MacKeracher et al., 2019). Their central objective is to reduce the pressures to which species or habitats of conservation concern are exposed. For mobile elasmobranchs, successful spatial management depends on the time that individuals in different life-history categories spend in protected areas, which is contingent upon the scale of movement in space and time with respect to these areas (Chapman et al., 2015).

A plethora of terms has been introduced to describe animal movements at different scales (Chapman et al., 2015). A key term is the ‘home range’, which is most widely defined as the ‘area traversed by an individual in its normal activities of food gathering, mating, and caring for young’ (Burt, 1943). Localised home ranges reflect site-attached behaviour while more diffuse home ranges reflect movements across wider areas. ‘Site affinity’ is a general term for site-attached behaviour that encompasses both prolonged and repeated periods of localised space use (Chapman et al., 2015). The interpretation of ‘localised’ is context-specific, but affinity to specific sites such as MPAs is often of particular interest. Prolonged periods of localised space use are usually distinguished by the duration over which they last, with ‘short-

term residency' lasting for three months and 'long-term residency' lasting for more than one year. Repeated periods of localised space use interspersed with substantial movements away from an area are termed 'site fidelity'. In contrast, a brief, unrepeated visit to an area is termed 'transiency' (Chapman et al., 2015).

Research on elasmobranch movements has increased in recent years, but most studies have focused on sharks (Papastamatiou and Lowe, 2012; Chapman et al., 2015) and the movement patterns of batoids, especially skates (Rajidae), remain poorly understood (Flowers et al., 2016; Siskey et al., 2019). A number of studies have investigated skate movement using mark-recapture data (Siskey et al., 2019; Bird et al., 2020). In addition, archival depth and temperature tags have been used to examine depth use (Thorburn et al., 2021), vertical movement (Peklova et al., 2014; Humphries et al., 2017) and long-range movements over hundreds of kilometres (Hunter et al., 2005a, 2005b; Pinto et al., 2016). However, uncertainty in the gaps between recaptures and archival geolocation algorithms limits the application of these approaches to the study of residency in small coastal areas (spanning tens of kilometres). At these spatial scales, passive acoustic telemetry is well-suited to the study of movement patterns and residency (Matley et al., 2022). This system comprises a static array of acoustic receivers which listen continuously for individual-specific acoustic transmissions from tagged individuals. Detections at receivers demonstrate occupancy and can be used to evaluate the potential benefits of MPAs for mobile species (Matley et al., 2022). However, few studies have exploited passive acoustic telemetry to study the movements of rajids (Morel et al., 2013; Neat et al., 2015; Sousa et al., 2019).

The Critically Endangered flapper skate (*Dipturus intermedius*) is one of the most threatened rajids (Chapter One; Ellis et al., 2021). Once widespread in the North-East Atlantic, flapper skate were extirpated across much of their former range (Ellis et al., 2021). They inhabit depths from the surface to 1,500 m, but they are thought to prefer coastal habitats adjacent to deep (100–300 m) basins (Pinto et al., 2016; Ellis et al., 2021). They are considered largely benthic, with a broad diet comprising benthic and pelagic species, including crustacea, cephalopods, teleosts and elasmobranchs, which may be ambushed, actively hunted or scavenged (Steven, 1947; Wheeler, 1969; Ellis et al., 2021).

On the west coast of Scotland, angler mark-recapture records demonstrate that flapper skate show affinity to the Loch Sunart to the Sound of Jura Marine Protected Area (LStSJ MPA)

(Chapter One; Neat et al., 2015). This MPA was designated in 2016, in large part on the basis of historical (1975–2015) angler mark-recapture records from Glasgow Museum and the Scottish Shark Tagging Programme that demonstrated skate are repeatedly caught throughout the area (Little, 1995; Little, 1997; Wearmouth & Sims, 2009; Scottish Natural Heritage, 2014; Neat et al., 2015). However, movements between captures remain poorly understood. Extensive movements have been documented (Little, 1995) and the historical view was that skate move offshore over winter (Wheeler, 1969); yet an acoustic study of 20 tagged individuals in the Sound of Jura found that over 50 % were resident on a day-by-day basis for months at a time and identified three long-term, mature female residents (Neat et al., 2015). However, the extent of residency among other life-history categories and over time and space remains uncertain. Seasonal movement patterns in particular have been identified as an important knowledge gap for management (Thorburn et al., 2021). In early spring, mating is thought to occur in inshore areas (Day, 1884), after which point a seasonal movement of males offshore over the summer has been suggested (Little, 1997). Following mating, it is thought that females may move into shallow water (25–50 m deep) to lay eggs, possibly every other year (Little, 1995; NatureScot, 2021). There is circumstantial evidence for associations among pairs of individuals and single-sex groups from angling (Little, 1995), but the extent to which individuals associate underwater remains unknown.

The aim of this chapter is to investigate localised movements and residency of flapper skate within the LStSJ MPA using acoustic, archival and angler mark-recapture data. There are two objectives:

A. **Residency—**to examine the scale(s) of movement with respect to the MPA, with a focus on the prevalence and scale of residency in this area.
B. **Drivers—**to examine the drivers of localised movements in the MPA from detections at receivers, including the roles of sex, maturity, habitat preferences and social interactions.

2. Methods

2.1. Study site

The LStSJ MPA covers a 741 km^2 area off the west coast of Scotland (Figure 1). Current management measures prohibit the use of mobile fishing gear except in eight, seasonally fished areas in which mechanical dredges and demersal trawls (excluding beam trawls), without tickler chains, are permitted (Chapters One–Two). The bathymetric environment is complex, including areas of shallow water less than 50 m in depth alongside glacially over-deepened basins and channels up to 290 m in depth (Chapter Two). Water temperatures vary between 6 °C (March) and 16 °C (September). In summer and autumn, the upper 100 m experiences 1–2 °C of thermal stratification (Chapter Two). Salinity variation in the upper layers (from 0.0–34.5 psu) is most strongly associated with proximity to sources of freshwater input and seasonal precipitation, which peaks in winter (Chapter Two). The flow regime is dominated by semi-diurnal tides that interact with the bathymetry and incised coastline, with current velocities in narrow straights such as the Gulf of Corryvreckan sometimes exceeding 8 knots (Chapter Two).

2.2. Data collection

A passive acoustic telemetry array comprising 58 Vemco receivers was deployed from March 2016–July 2017 in the MPA in water depths ranging from 5–180 m (Figure 1) (Chapter Two). Receivers were deployed in four main phases and clustered into eight sites (Figure 1). Most deployments concentrated in two sites—the Kerrera-Loch Spelve Gate and an area to the south—forming an area referred to as the 'southern receiver curtain' that spanned the deep-water basin between Kerrera and the Isle of Mull (Figure 1). Previous analyses of detection probability in this area have estimated a detection range of 425 m (Chapter Two). According to this estimate, receiver coverage during the study ranged between 3.93–13.88 km^2 (0.53–1.87 % of the MPA). Coverage was highest in March–November 2016 before a significant decline in December 2016, after which time coverage was partially restored (Chapter Two).

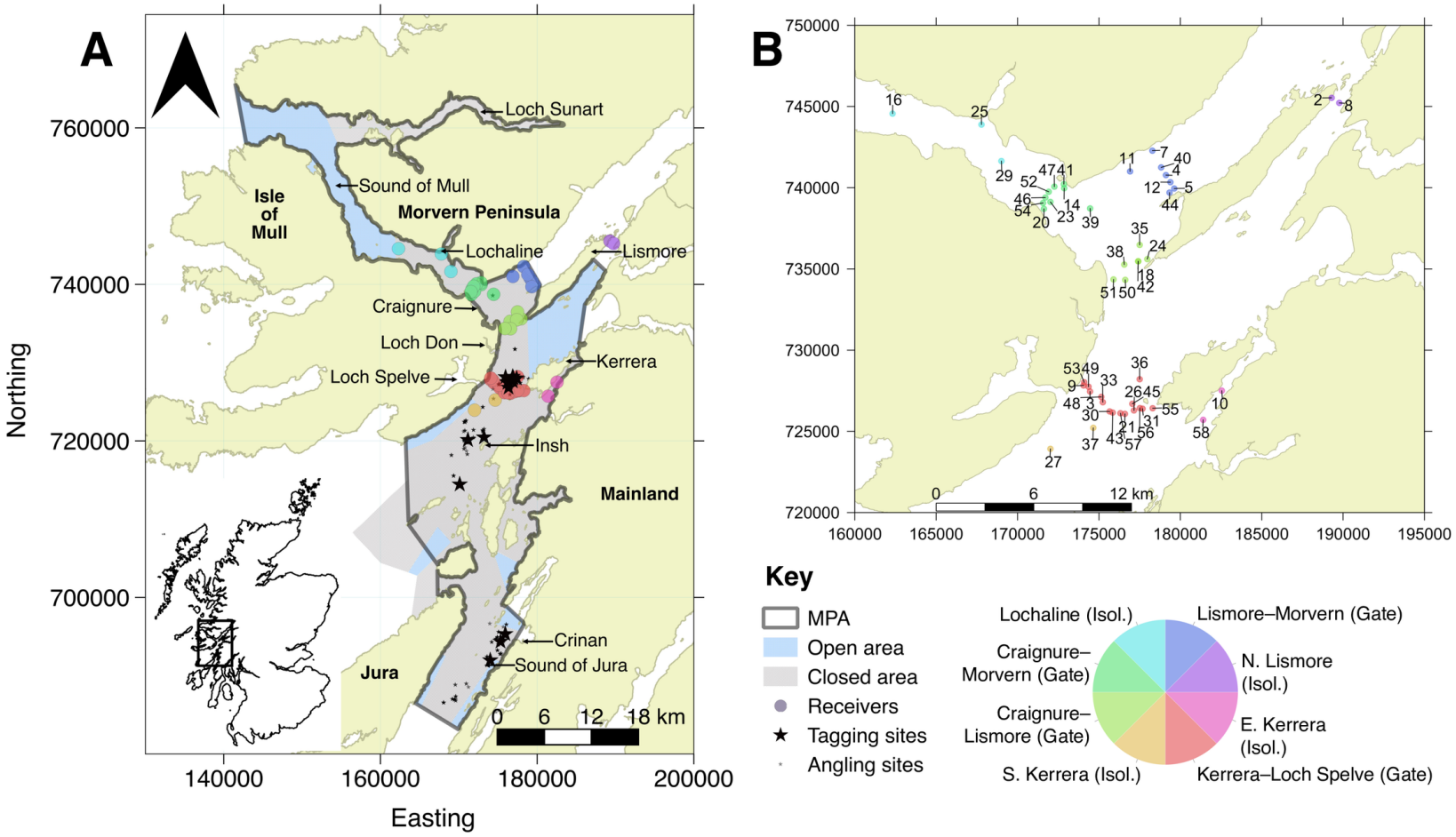

Figure 1. The study site. A, the Loch Sunart to the Sound of Jura Marine Protected Area (MPA). The MPA is delineated by the grey boundary. Mobile fishing gear is prohibited throughout the MPA, with the exception of mechanical dredges and demersal trawls (excluding beam trawls) in eight seasonally open areas (shown in blue) (see Chapter One). The coloured points mark receivers and the 425 m detection range. Small stars mark the locations of recreational angling events recorded in the PIT tag/photo-identification database collated by NatureScot, Marine Scotland Science and the Scottish Association for Marine Science. Large stars mark tag deployment/retrieval sites. **B**, the receiver array. Receivers are grouped into eight main sites identified according to a colour wheel which approximately relates to site location (see key). The coordinate reference system is British National Grid. Background Ordnance Survey maps © Crown copyright and database rights [2019] Ordnance Survey (100025252). Figure taken from Chapter Two.

Within the MPA, 42 skate were successfully caught and tagged from March–September 2016 (Chapter Two). Skate were captured using baited angling lines with barbless hooks, sexed and measured (Chapter Two). Maturation status (immature, mature) was later defined using a model for maturation with total length (Chapter Two) (Iglésias et al., 2010). Together, sex and maturation status were taken to distinguish four life-history categories (immature females, 'I, F'; mature females, 'M, F'; immature males, 'I, M'; and mature males, 'M, M'). Following measurement, individuals were tagged with Vemco V13 or Thelma Biotel MP-13 coded acoustic transmitters, programmed to transmit an individual-specific acoustic signal at random intervals every 30–90 s (Chapter Two). Forty of the individuals were also tagged with Star Oddi milli-TD or CEFAS G6A archival tags, programmed to record depth and temperature every two minutes. Tagging occurred in three phases at three sites around Kerrera, Insh and Crinan (Figure 1). Most individuals were tagged off Kerrera (25/42) or Insh (6/42) in March 2016. Later that spring, four large females were tagged off Crinan. In the summer, seven individuals, including 6/7 immature males, were tagged off Insh. After tagging, individuals remained at liberty until they were recaptured and the tag removed or until the end of the study in June 2017. During this time, the number of individuals at liberty varied from 3–33 individuals (Chapter Two).

Alongside passive acoustic telemetry and archival tagging, angler mark-recapture records from PIT tagging and photo-identification (comprising 1,771 captures of 884 individuals between 2011–2018) were obtained from NatureScot, Marine Scotland Science and the Scottish Association for Marine Science as a largely independent source of information on site affinity across a larger number of individuals, a longer timescale and a wider area.

2.3. Data processing

Data processing was implemented in R, version 4.0.2 (R Core Team, 2020). Raw acoustic data were quality controlled to exclude any detections from receivers or tags outside of their deployment periods, during servicing, from unknown sources or that were potentially false (Chapter Two). Angler mark-recapture records were processed for analysis to exclude any angling events without all required information (individual identity, size, angling location and date). The maturation status of each angled individual was predicted from its length and only

records for which the probability that the individual was either immature or mature exceeded 0.75 were retained (Chapter Two).

2.4. Individual movement patterns

Visual and statistical analyses were implemented using the prettyGraphics, robmixglm and mgcv packages (Wood, 2017; Lavender, 2020a; Beath, 2021). Undetected and detected individuals were compared in terms of their time at liberty, the location and timing of tagging, sex and size to investigate the drivers of acoustic detection. For undetected individuals, angler mark-recapture records were examined to evaluate the plausibility of different explanations for a lack of detections. For detected individuals, acoustic detection, depth and angler mark-recapture time series were visualised to infer movement patterns. Over the acoustic study, 'short-term residents' were identified as individuals with 'periods of detections, spaced less than 31 days apart, lasting for more than 3 months'. Long-term residents were identified as individuals with 'periods of detections, spaced less than 31 days apart, lasting for more than 12 months'.

2.5. Collective spatiotemporal patterns

The overall amount of time that males and females spent around receivers was investigated using a Poisson generalised linear model of the total number of days with detections (hereafter, 'detection days' or $count_{days}$ in equations) for each individual in relation to a three-way interaction between time at liberty, tagging site and sex. The model was formulated according to the equations:

$$count_{days_i} \sim P(\lambda_i) \quad (1)$$

$$\log(\lambda_i) = \alpha + \beta_1 liberty_i + \beta_2 site_{\mathrm{Insh}_i} + \beta_3 sex_{\mathrm{M}_i} + \beta_4 liberty_i site_{\mathrm{Insh}_i} + \beta_5 liberty_i sex_{\mathrm{M}_i} + \beta_6 site_{\mathrm{Insh}_i} \mathrm{sex}_{\mathrm{M}_i} + \beta_7 liberty_i site_{\mathrm{Insh}_i} \mathrm{sex}_{\mathrm{M}_i}$$

where $liberty$ refers to the number of days over which each individual was at liberty, $site$ refers to the location in which each individual was tagged (Kerrera or Insh) and sex_M is a factor that identifies males. α is the model intercept, $\beta_{1,\ldots,7}$ are coefficients and i indexes individuals. This model was motivated by the recognition that movement past receivers drove detections and the expectation that the manifestation of movement patterns as 'detection days' should differ depending on tagging site and sex. Based on previous research (Neat et al., 2015),

localised, residential movements were expected to be more common in females than males. Under this movement pattern, detection days should be positively related to time at liberty for individuals tagged near to the array. This relationship should be weaker for individuals tagged further afield. In contrast, a pattern of transiency should not induce a relationship between detection days and time at liberty at any tagging site, irrespective of distance from the array. The model was fitted using a robust regression framework to restrict the impact of influential observations (see Appendix §1.1) (Beath, 2021).

Temporal trends in the use of areas around receivers for different life-history categories were investigated using a binomial generalised additive model (GAM) of the number of detected individuals in each life-history category per day ($count_{detected}$), out of the total number that could have been detected in that category on each day ($count_{liberty}$), in relation to life-history category (grp), time of year (day), and the area surveyed by receivers at each time point, assuming a detection range of 425 m ($area$). This model was formulated as follows:

$$count_{detected_i} \sim B(count_{liberty_i}, p_{detected_i}) \tag{2}$$

$$\begin{aligned} logit(p_{detected_i}) &= \alpha + \beta_1 grp_{M,F_i} + \beta_2 grp_{I,M_i} + \beta_3 grp_{M,M_i} + s(day_i, grp_{I,F_i}) \\ &+ s(day_i, grp_{M,F_i}) + s(day_i, grp_{I,M_i}) + s(day_i, grp_{M,M_i}) \\ &+ \beta_4 (area_i) \end{aligned}$$

where $p_{detected}$ denotes the expected proportion of detected individuals; $grp_{I,F}$, $grp_{M,F}$, $grp_{I,M}$ and $grp_{M,M}$ denote immature females, mature females, immature males and mature males respectively; day denotes Julian day; and i indexes observations (one for each life-history category on each date). Julian day was implemented as a group-level smoother using a cyclic cubic regression spline (s) with a basis dimension of k = 15 and boundary knots at 0.5 and 366.5 (to account for the 2016 leap year). Tagging site was not included in the model since tagging sites were unbalanced across life-history categories. For this GAM (and those described below), model fitting, prediction and diagnostic checks (including the k-index diagnostic used to check the adequacy of basis dimensions) were implemented using the mgcv package (see Appendix §1.2.1) (Wood, 2017).

Seasonal patterns in angler mark-recapture time series were examined in a similar way using a negative binomial GAM of the number of individuals caught per unit time ($count_{angled}$) in

relation to life-history category and a group-specific smoother for time. Since angling effort is unknown, the purpose of this model was to explore relative differences among life-history categories through time, which should be independent of effort, rather than the specific trends exhibited by each category. For modelling, time was expressed in months, rather than days, given the concentrated seasonal distribution of observations, with the boundary knots at 0 and 12 and a basis dimension of $k = 10$. The model was implemented as follows:

$$count_{angled_i} \sim NB(\theta_i) \tag{3}$$

$$\begin{aligned} logit(\theta_i) = \alpha + \ & \beta_1 grp_{M,F_i} + \beta_2 grp_{I,M_i} + \beta_3 grp_{M,M_i} + s\left(month, grp_{I,F_i}\right) \\ & + s\left(month, grp_{M,F_i}\right) + s\left(month, grp_{I,M_i}\right) + s\left(month, grp_{M,M_i}\right) \\ & + \beta_4\left(year_{2017_i}\right) + \beta_6\left(year_{2018_i}\right) \end{aligned}$$

where $month$ is an integer that refers to time in months (1–12); $year$ refers to the year (2017 or 2018); and i indexes observations (one for each life-history category and month in the time series from 2016–2018). Other terms are as defined previously (see Appendix §1.2.2).

To summarise spatial movement patterns, the distribution of acoustic detections was mapped and angler mark-recapture records were visually examined for evidence of skate presence beyond the array. This visual approach was used to explore the spatial scale of movements because the clustered arrangement of receivers rendered the other most widely used approach (the mean-position algorithm) uninformative (Chapters Two and Six; Simpfendorfer et al., 2002). The influence of tagging site and habitat preferences as drivers of the spatial distribution of acoustic detections was investigated by considering the number of days on which there were detections of each individual at each receiver in relation to the distance between each individual's tagging site and receiver, and environmental conditions around receivers. Distances were calculated as the shortest distances between tagging sites and receivers, assuming skate move over the seabed, using the bi-directional Dijkstra algorithm provided by Larmet (2019), as implemented by the `lcp_over_surface` function with the '`cppRouting`' method in the flapper package (Lavender, 2020b). Seabed bathymetry data at one arc-second resolution were sourced from Digimap for this analysis since available higher resolution data do not cover the whole area (Howe et al., 2014). Within each receiver's 425 m detection range, depth and hydrodynamic conditions (thermocline strength, bottom temperature, salinity and current speed) were identified as plausible environmental drivers of skate presence. For each receiver, depths were extracted from within its detection range using the raster package

(Hijmans, 2020) and hourly hydrodynamic model predictions over a one-year period from March 2016–17 were extracted from the West Scotland Coastal Ocean Modelling System (Aleynik et al., 2016) via the fvcom.tbx package (Lavender, 2020e). Model outputs were extracted from the 10th Sigma layer or the deepest element layer, since flapper skate are thought to be predominately benthic animals (Chapter Two). Visualisation suggested that detection days by receivers were associated with depth, salinity and current speed; therefore, these variables were taken as candidate explanatory variables for model development. For each variable, the average and variability around each receiver were summarised using the median and median absolute deviation respectively. For hydrodynamic variables, collinearity analyses showed moderate to strong correlations for these two statistics; therefore, only the average conditions were considered. Median depths and salinities were also strongly correlated, but both were retained for model development as variables of biological interest.

These exploratory analyses led to four competing models for the spatial pattern (SP) of detections, which were compared qualitatively and using Akaike's Information Criterion (AIC). Model SP1 was a negative binomial GAM of the number of detections of each individual at each receiver ($count_{days\_by\_receivers}$), offset by the overlap (in days) between each individual's time at liberty and each receiver's operational period, in relation to life-history category and smooth functions of distance, median depth, the median absolute deviation in depth, median salinity and current speed. Smooth functions were implemented using thin plate regression splines with a basis dimension of k = 10. This model was formulated as follows:

$$count_{days\_by\_receivers_i} \sim NB(\theta_i) \quad (4)$$

$$\begin{aligned} logit(\theta_i) = \alpha + {} & \beta_1 grp_{M,F_i} + \beta_2 grp_{I,M_i} + \beta_3 grp_{M,M_i} + s(id\_rec\_dist\_lcp_i) \\ & + s(depth\_median_i) + s(depth\_mad_i) + s(sal\_median_i) \\ & + s(cs\_median_i) + \zeta_{id} + \log(id\_rec\_overlap_i) \end{aligned}$$

where $id\_rec\_dist\_lcp$ refers to the shortest distance between the location at which each individual was tagged and each receiver; $depth\_median$ is the median depth in the detection range around each receiver; $depth\_mad$ is the median absolute deviation in depth; sal_median and cs_median are the median bottom salinity and bottom current speed from the nearest WeStCOMS node/element to each receiver across all hourly predictions over the course of a year (from March 2016–17); ζ is a random effect for individual; $id\_rec\_overlap$ is the temporal overlap (in days) between each individual's time at liberty and each receiver's

operational period; and *i* indexes observations (one for each individual/receiver combination) (see Appendix §1.3.1). Building on this model, three others were implemented. To allow for potential differences in relationships by life-history category, a model with group-specific smoothers was fitted (Model SP2) (see Appendix 1.3.2). Since depth and salinity were strongly correlated, models with only one of each of these variables were also evaluated (Models SP3 and SP4) (see Appendix 1.3.2)

To investigate the occurrence of social interactions among flapper skate and their potential influence on spatial patterns, angler mark-recapture records were used to quantify the extent to which specific pairs of individuals have been caught together (i.e., in the same location and on the same day) through time. (Higher resolution information on the timing of angling events was not available.) Using acoustic detections, the total number and percentage of detections 'shared' among all pairs of detected individuals (n = 1,056) was also examined using the `make_matrix_cooccurrence` function in the flapper package (Lavender, 2020b). 'Shared' detections were defined as detections at the same receiver within 90 s of each other (the upper limit for the delay between sequential acoustic transmissions) (Chapter Two). Among the individuals who shared a high proportion of detections, overlapping acoustic and depth time series were visually examined further for evidence of coupled movement patterns.

3. Results

3.1. Movement datasets

The processed passive acoustic telemetry dataset comprised 205,323 detections from 33 individuals (Chapter Two). Archival time series were retrieved from 15 acoustically tagged individuals and totalled 2,709,676 observations. The processed angler mark-recapture database comprised 1,026 records of 555 individuals, including individuals in all life-history categories (though few young juveniles) (Chapter Two).

3.2. Individual movement patterns

Nine successfully tagged individuals were undetected by receivers. Undetected individuals were at liberty for a similar duration (3–449, median = 385, days) to detected individuals (71–452, median = 398, days). Summary statistics suggest that detection may have been affected

by angling location, season or individual characteristics but the relative importance of these variables is difficult to disentangle. Most individuals tagged near to the array (off Kerrera and Insh) in winter and summer were detected while none of the four individuals (all large females) tagged off Crinan in spring were detected. One of the individuals tagged off Crinan (546) was re-captured (twice) in the same area during the study, suggesting its absence from the array may have been caused by residency in this area. In total, large (≥ 198 cm) females accounted for seven undetected individuals. In contrast, the two undetected males were smaller (≤ 175 cm) than average. Tag shedding or removal probably contributed towards the lack of detections for at least one male (245) that was recaptured without its tags (Chapter Two). However, there was no evidence for transmitter malfunction among recovered tags, nor any angler mark-recapture records of undetected individuals beyond the MPA or mortality. Nevertheless, despite an absence of detections during this study, angler mark-recapture records show that four of the undetected individuals have been caught multiple times in the area over extended periods.

For acoustically detected individuals (n = 33/42, 79 %), movement time series reveal heterogeneous patterns (Figures 2 and S1–4). Among immature females (n = 11), six individuals were identified as short-term (n = 4) or long-term (n = 2) residents during the acoustic study (Figures 2A and S1, Table 1) and five had angler mark-recapture records over multiple years demonstrating site affinity over a longer timescale (Figure S5). During the acoustic study, three individuals, including the two long-term residents (540 and 249) and one short-term resident (560), were detected around the southern receiver curtain for ≥ 150 days, with only one substantial gap in detections during a temporary drop in receiver coverage. Concurrent depth time series for these individuals show repeated movements around a central depth (Figure S1). For these three individuals, angler mark-recapture records suggest that residency probably continued beyond the study (Figure S5). Short-term residency was apparent from detections on 24–70 days in three other immature females (532, 247 and 242) but was not accompanied by clearly repeating patterns of depth use. One of these individuals (242) was caught outside of the MPA near Mallaig in 2017, a shortest swimming distance of approximately 100 km from its tagging site. The five immature females that were not identified as residents were detected less often. Nonetheless, angler mark-recapture records demonstrate that one of these individuals (564) made repeated use of the area over multiple years (Figure S5).

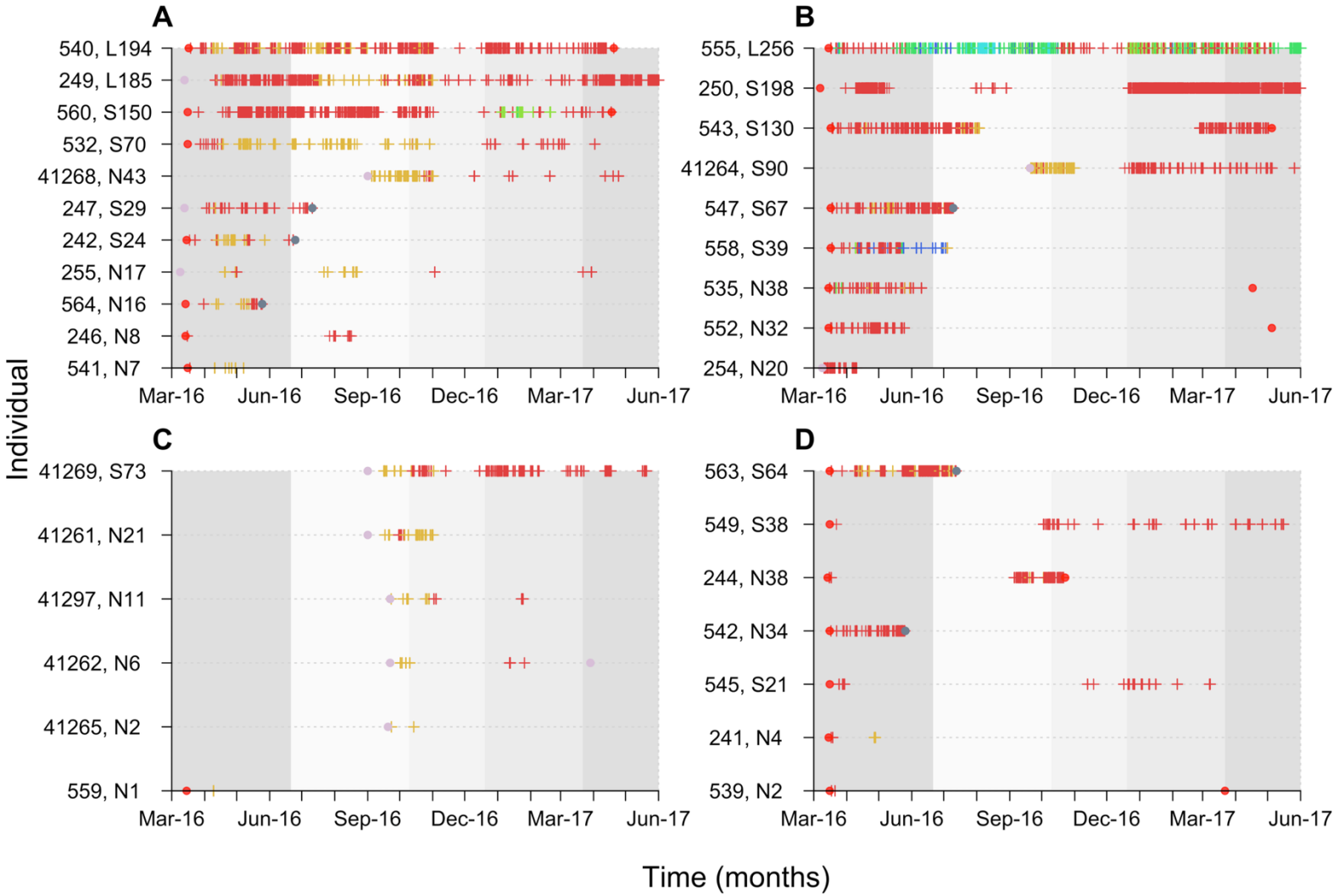

Figure 2. Detection histories for each life-history category. **A**, immature females; **B**, mature females; **C**, immature males; and **D**, mature males. Each point (+) defines the time of a detection for a particular individual. Filled points (•) mark the dates of tagging and tag retrieval (if applicable) respectively. Point colour corresponds to receiver location (see Figure 1), with tagging events off Insh (away from receivers) shown in pink and tag retrieval events in unrecorded locations shown in grey. The background colouration highlights the season. Y-axis labels define individual IDs, residency categories (N, non-resident; S, short-term resident; L, long-term resident) and the total number of days with detections (by which individuals are ordered). Short-term and long-term residents are individuals with periods of detections spaced less than 31 days apart over more than 3 or 12 months, respectively.

Table 1. Statistical estimates of the proportion of short-term and long-term residents within the acoustic array. Short-term and long-term residents were defined as individuals with periods of detections spaced less than 31 days apart over more than three or 12 months, respectively. For each life-history category, the total number (n) of individuals in that category, the number (n_r) and the observed proportion (p_r) of short-term and long-term residents, the estimated proportion ($\hat{p}_r$) and the 95 % confidence intervals (CIs) are shown. Following convention, estimated proportions are given by $\hat{p}_r = p_r$ or $\hat{p}_r = (n_r + 2)/(n + 4)$ if $n_r < 5$ and/or $n - n_r < 5$. Corresponding standard errors are given by $SE = \sqrt{\hat{p}_r(1 - \hat{p}_r)/n}$ or $SE = \sqrt{\hat{p}_r(1 - \hat{p}_r)/(n + 4)}$ respectively and 95 % CIs by $[\hat{p}_r \pm t_{0.975,n-1}SE]$ (truncated between 0 and 1) where t is the critical t value.

Sex	Maturation Status	n	Short-term residents				Long-term residents				Total residents			
			n_r	p_r	$\widehat{p_r}$	CI	n_r	p_r	$\widehat{p}_r$	CI	n_r	p_r	$\widehat{p}_r$	CI
Female	Immature	11	4	0.364	0.400	[0.118,0.682]	2	0.182	0.267	[0.012,0.521]	6	0.545	0.545	[0.211,0.880]
	Mature	9	5	0.556	0.538	[0.220,0.857]	1	0.111	0.231	[0.000,0.500]	6	0.667	0.615	[0.304,0.927]
Male	Immature	6	1	0.167	0.300	[0.000,0.673]	0	0.000	0.200	[0.000,0.525]	1	0.167	0.300	[0.000,0.673]
	Mature	7	3	0.429	0.455	[0.087,0.822]	0	0.000	0.182	[0.000,0.466]	3	0.429	0.455	[0.087,0.822]
Totals		33	13	0.394	0.394	[0.221,0.567]	3	0.091	0.135	[0.021,0.250]	16	0.485	0.485	[0.308,0.662]

Of the nine mature females detected by receivers, six were identified as short-term (n = 5) or long-term (n = 1) residents and eight have angler mark-recapture records over multiple years (Figures 2B, S2 and S5, Table 1). The long-term resident (555) was tagged off Kerrera and detected on more (n = 256) days than any other individual. The depth time series shows extensive use of near-surface depths to approximately 220 m (Figure S2). Five short-term residents were identified from acoustic detections. For two of these individuals (250 and 543), periods of short-term residency were punctuated by long gaps that are consistent with seasonal site fidelity. For individual 250, after a prolonged gap in detections over the summer and autumn of 2016, detections in winter 2016–spring 2017 occurred almost continuously at a single receiver. However, for the other three short-term residents (41264, 547 and 558), seasonality was not apparent. Three individuals were not identified as residents. These individuals were frequently detected during the first few months of the study but then appeared to move away from receivers. However, all non-residents have angler mark-recapture records spanning multiple years (Figure S5).

Detections of males were less frequent (Figures 2C–D and S3–4). Among immature males (n = 6), only one short-term resident (41269) was identified and only two have angler mark-recapture records in multiple years (Figures 2C and S5, Table 1). During the acoustic study, the five non-residents were detected less often. For two individuals (41297 and 41262), an initial bout of detections was repeated after a gap of approximately three months, demonstrating repeated use of the array, but the remaining three individuals (41261, 41265 and 559) were only detected for a short period of time around the southernmost receivers following tagging, suggesting movement to the south. However, one of these individuals (41261) has since been recaptured three times at Kerrera, demonstrating repeated use of the area over a longer timescale (Figure S5).

For mature males (n = 7), movement time series suggest periods of short-term residency, movement beyond the MPA and multi-annual site fidelity (Figures 2D and S4–5, Table 1). Short-term residency was apparent for three individuals (563, 549 and 545). For the two short-term residents (549 and 545) that were at liberty for more than two seasons, there was some evidence for seasonality, with long gaps between detections following tagging in March 2016 and subsequent detections in late summer or thereafter. For individual 549, this seasonal absence was associated with a period of prolonged, limited depth use (Figure S4). There were four non-residents. For individual 542, detections resembled short-term residency but were

constrained by a short period at liberty. Another non-resident (244) exhibited seasonality in the timing of detections, with an absence of detections over spring–summer associated with extensive use of deep (up to 311 m) water, suggesting movement beyond the MPA. The remaining two non-residents (241 and 539) were only detected briefly following tagging. However, as for individual 244, substantial use of waters deeper than 200 m by individual 539 suggests movement beyond the MPA. Nevertheless, while detections were relatively infrequent for mature males, in five cases angler mark-recapture records demonstrate site affinity to the MPA over multiple years (Figure S5).

Overall, detection histories provide evidence for short- or long-term residency in 48 % of detected individuals and multi-annual site fidelity in 64 % of detected individuals. While the sample size of acoustically tagged individuals was small, the estimates for the proportion of detected (0.79) and resident ($\hat{p} = 0.49\,[0.30,0.66]$) individuals (Table 1) suggest that approximately 0.38 [0.24–0.52] of individuals in the study site, or 337 [237–460] of the 884 individuals recorded in the raw angler mark-recapture database, may have exhibited short-term or long-term residency since the onset of PIT tagging.

3.3. Collective spatiotemporal patterns

Across all detected individuals, the number of days with detections ranged between 1–256 (median = 34) days. Detection days were associated with time at liberty, tagging site and sex (Figure 3, Table S1). For females, detection days were positively related to time at liberty for individuals tagged at Kerrera but not individuals tagged at Insh, as expected under a pattern of localised residency. However, there was substantial variability, with high and low detection days indicating both residency and transiency. For males, detection days were consistently lower. For males tagged at Kerrera, detection days were negatively related to time at liberty, suggesting transiency among the males with the longest times at liberty. The detection days of males tagged at Insh were positively related to time at liberty, but there were fewest observations for this category and the range in time at liberty was smallest. Hence, this result is not directly interpreted. Collectively, these results point towards a mixture of residency and transiency (during the acoustic study) in all life-history categories that is difficult explain from time at liberty, sex and tagging site alone.

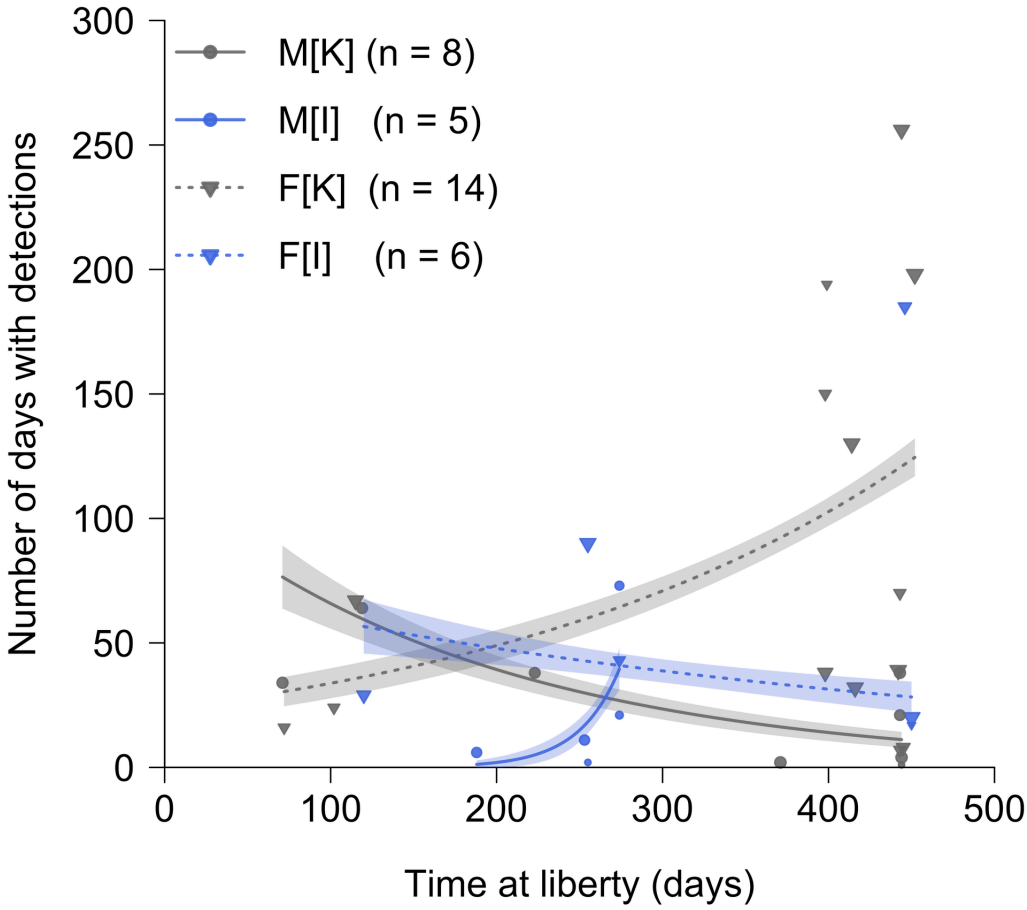

Figure 3. Detection days in relation to time at liberty for each sex and tagging site. Points, lines and envelopes mark the observations, fitted values and 95 % confidence intervals from a robust generalised linear model of detection days in relation to time at liberty, sex (M, male; F, female) and tagging site (K, Kerrera; I, Insh). These are shaped according to sex and coloured according to tagging site. Point size is proportional to the total length (cm) of each individual. Numbers in brackets define the number of individuals in each category. Confidence intervals were estimated from 100 parametric bootstrap simulations.

Over time, the proportion of individuals detected fluctuated significantly for all life-history categories (Figure 4, Table S2). For both female groups, the proportion of individuals detected was broadly highest following tagging in spring/summer before declining in winter and partially increasing thereafter (Figure 4A–B). However, for mature females, the trend was more obviously seasonal. There was a significantly positive effect of receiver coverage on these trends (estimate = 0.21 ± 0.03 standard error), but they remained apparent even after accounting for this effect. Across the time series, the proportion of detected males was lower (Figure 4C–D). This model explained 49 % of the deviance. The model of angler mark-recapture records similarly identified stronger seasonal patterns for females relative to males, particularly mature females for which the number of angler mark-recapture records at their peak in late May was

approximately double that of immature females (Figure S6, Table S3). This model explained 66 % of the deviance. In both cases, standard diagnostics were reasonable.

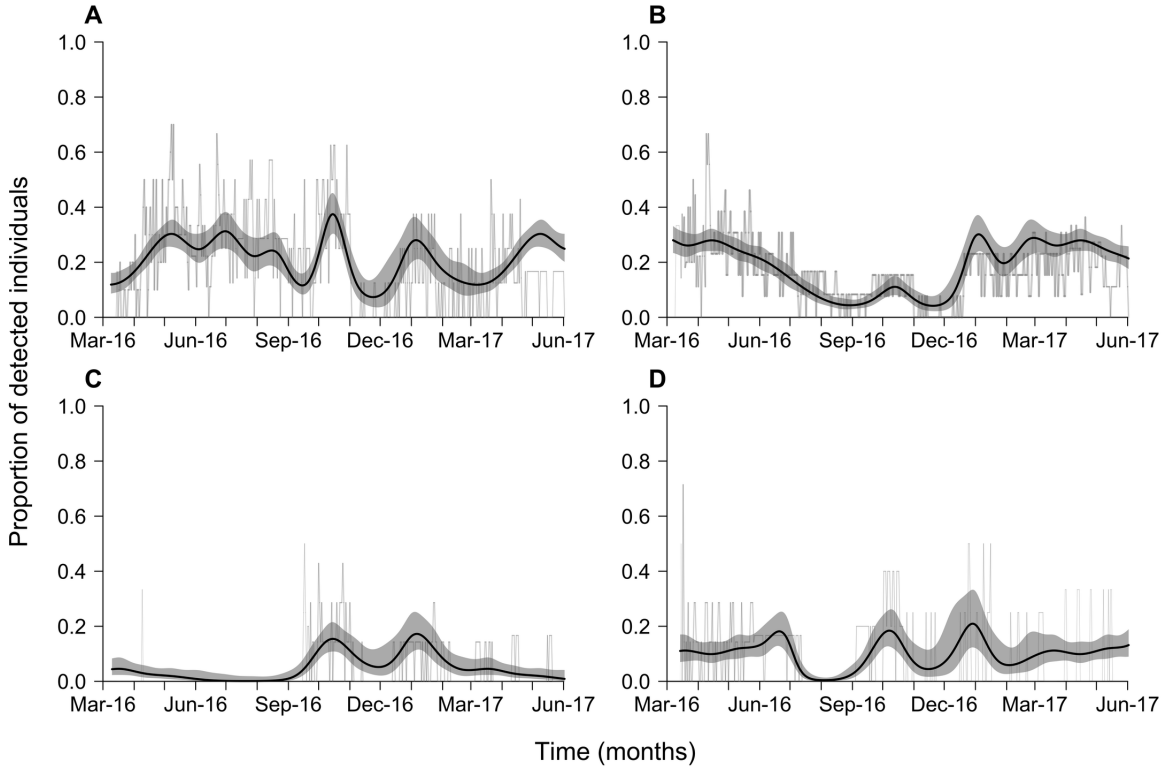

Figure 4. Trends in the proportion of individuals detected in each life-history category. A, immature females; **B**, mature females; **C**, immature males; and **D**, mature males. In each panel, the grey line is the proportion of individuals detected on each day. Line thickness is proportional to the total number of individuals at liberty in each life-history category on each day. The black line and surrounding envelope show the trend in the expected proportion of detected individuals, surrounded by 95 % pointwise confidence bands, from a binomial generalised additive model of the number of detected individuals in each life-history category, out of the total number that could have been detected in that category, while holding the receiver area constant at its median value (11.05 km^2).

Over space, detections and angler mark-recapture records concentrated in specific areas (Figures 5 and S7–S9). All receivers that recorded detections on more than half of their deployment days were located in the southern receiver array. More northerly receivers also recorded detections, though these were attributable to only four individuals (560, 555, 558 and 535). The two receivers furthest east along the Sound of Mull, two receivers on the southern tip of Lismore and both receivers at the northern tip of Lismore and east of Kerrera never recorded detections. Angler mark-recapture records for all life-history categories were concentrated in a similar area off Kerrera and Insh where the two favoured angling marks are found (Figure S9). Fewer angler mark-recapture events were recorded further south in the

Sound of Jura. To the north of the southern receiver curtain, only 13 angler mark-recapture events were recorded.

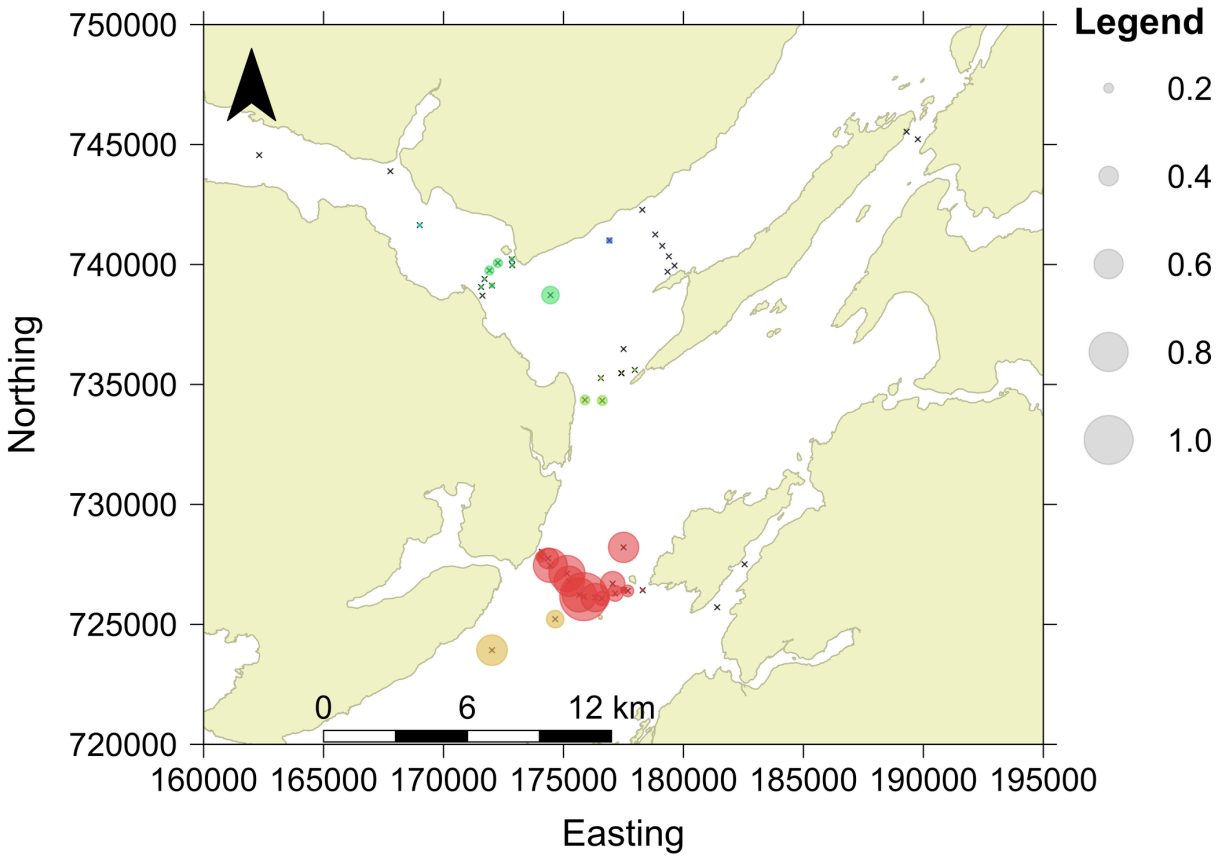

Figure 5. The spatial distribution of detections. Crosses denote receivers and the size of the surrounding bubbles denotes the proportion of days during which there were detections at each receiver over its deployment time, coloured by site (see Figure 1). Proportions are shown rather than counts since receivers were deployed for variable time periods (but the latter show a very similar picture.) The coordinate reference system is British National Grid. Background map © Crown copyright and database rights [2019] Ordnance Survey (100025252).

The predominance of detections around the southern receiver curtain was associated with tagging site and depth and/or salinity. The model with all covariates and global smoothers (SP1) was the best supported model according to AIC (Table S4). This model received substantially more support than the model (SP2) with group-level smoothers (ΔAIC = 211.14). The biological interpretation of this result is that the relationships between detection days by receivers, tagging site and environmental variables were similar among individuals. Across all individuals, the effect of distance on detection days by receivers was clearly negative (Figure 6A, Table S5). In models including either depth or salinity (SP3 and SP4), both variables were identified as significant, with detections occurring on more days at receivers in relatively

deeper, saltier water. However, in the best-supported model with both predictors (SP1), the effect of depth appeared to explain detection patterns less successfully than salinity (Figure 6B versus 6C). While the range in median salinities was small, this result reflects the fact that receivers without detections were predominately located in near-shore areas adjacent to sources of freshwater input that can experience more substantial fluctuations in salinity (Figure 5). This result was also supported by a comparison of Model SP3 versus SP4 in terms of AIC (Table S4). In contrast to the effects of depth/salinity, according to the best-supported model (SP1), bottom roughness and current speed were not clearly related to detections, after conditioning on the effects of other variables (Figure 6D–E). However, concurvity estimates from Model SP1 for all smooth terms (excluding individual) ranged between 0.69 and 0.91, suggesting these effects were difficult to distinguish (Table S6). This model explained 74 % of the deviance but did not fully explain the longest residency times.

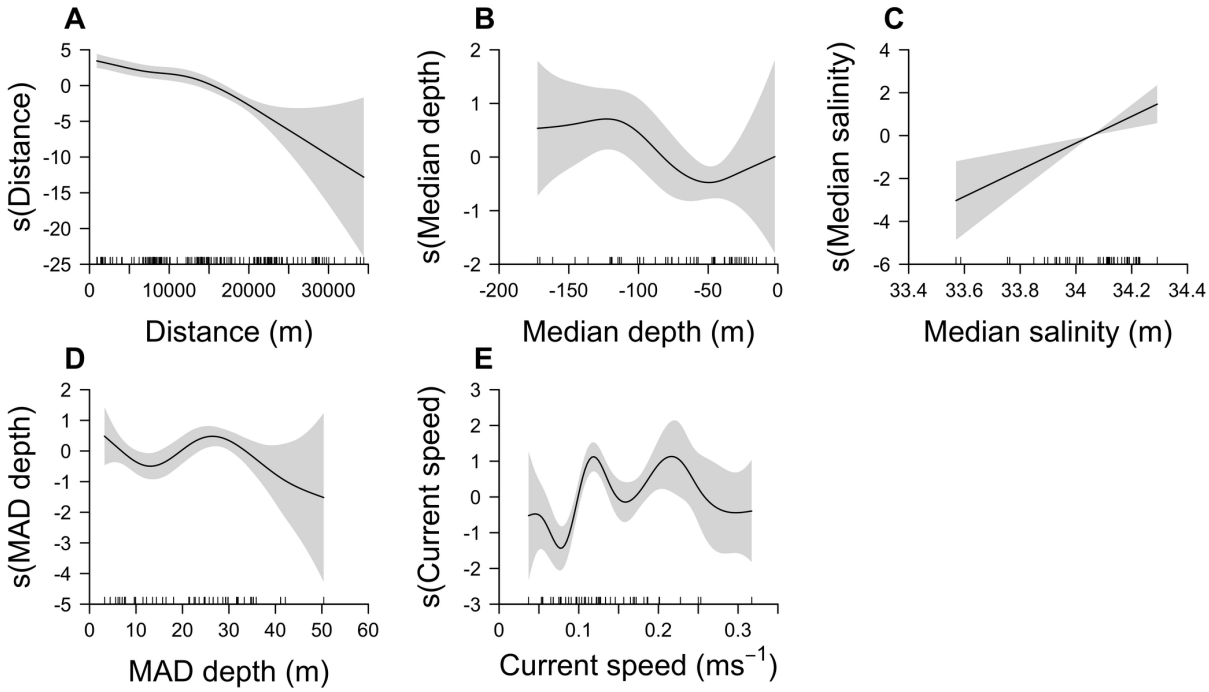

Figure 6. Smooth terms for the effects of tagging site and environmental conditions on the spatial distribution of detections. Smooths for the following variables were estimated: **A**, the shortest distance between receiver and tagging sites; **B**, the median depth; **C**, the median (bottom) salinity; **D**, the median absolute deviation in depth; and **E**, the median (bottom) current speed. In each panel, the smooth shown by the black line represents the change in the expected number of detection days by receivers on the scale of the link function across the range of each explanatory variable. Smooths are shown on the scale of the link function so that the 95 % pointwise confidence bands, marked in grey, relate solely to the uncertainty in the smooth rather than uncertainty in both the smooth and the mean of the response. Thus, expected detection days by receivers are higher at receivers near tagging sites (**A**) and saltier water (**C**), but are not clearly related to the receiver depth (**B**), the metric of bottom roughness (**D**) or current speeds (**E**).

Angler mark-recapture records and detection time series also shed light on the prevalence of social interactions and their possible role as a driver of the spatial distribution of detections. In angler mark-recapture records, 79 cases (comprising 66 individuals) were identified in which the same pair of individuals was re-caught together on two separate occasions. Repeated angler mark-recapture records of pairs of males were least common and only documented for 15 pairs. More common were repeated angler mark-recapture records of pairs of males and females (30 pairs) and pairs of females (34 pairs). Three pairs of individuals were caught as pairs on three separate occasions. Nearly all of these repeated angler mark-recapture records occurred off Kerrera from March–October**.**

Detection time series suggest that associations were probably largely coincidental. Across all pairs of individuals, 0–30 (median = 0) % of detections were shared (Figure 7). Most individuals shared few detections with other individuals, but at least one individual in each of two pairs shared 15–20 % of detections with the other individual and there was one pair of individuals in which an individual shared 30 % of its detections with the other. All shared detections occurred around the southern receiver array and were most prevalent in spring/summer 2016 when most individuals were at liberty. In terms of life-history category, while the percentage of shared detections was generally low, both immature and mature females shared more detections than either category shared with immature or mature males, while detections of males coincided with detections of females more often than with other males (Figure 7).

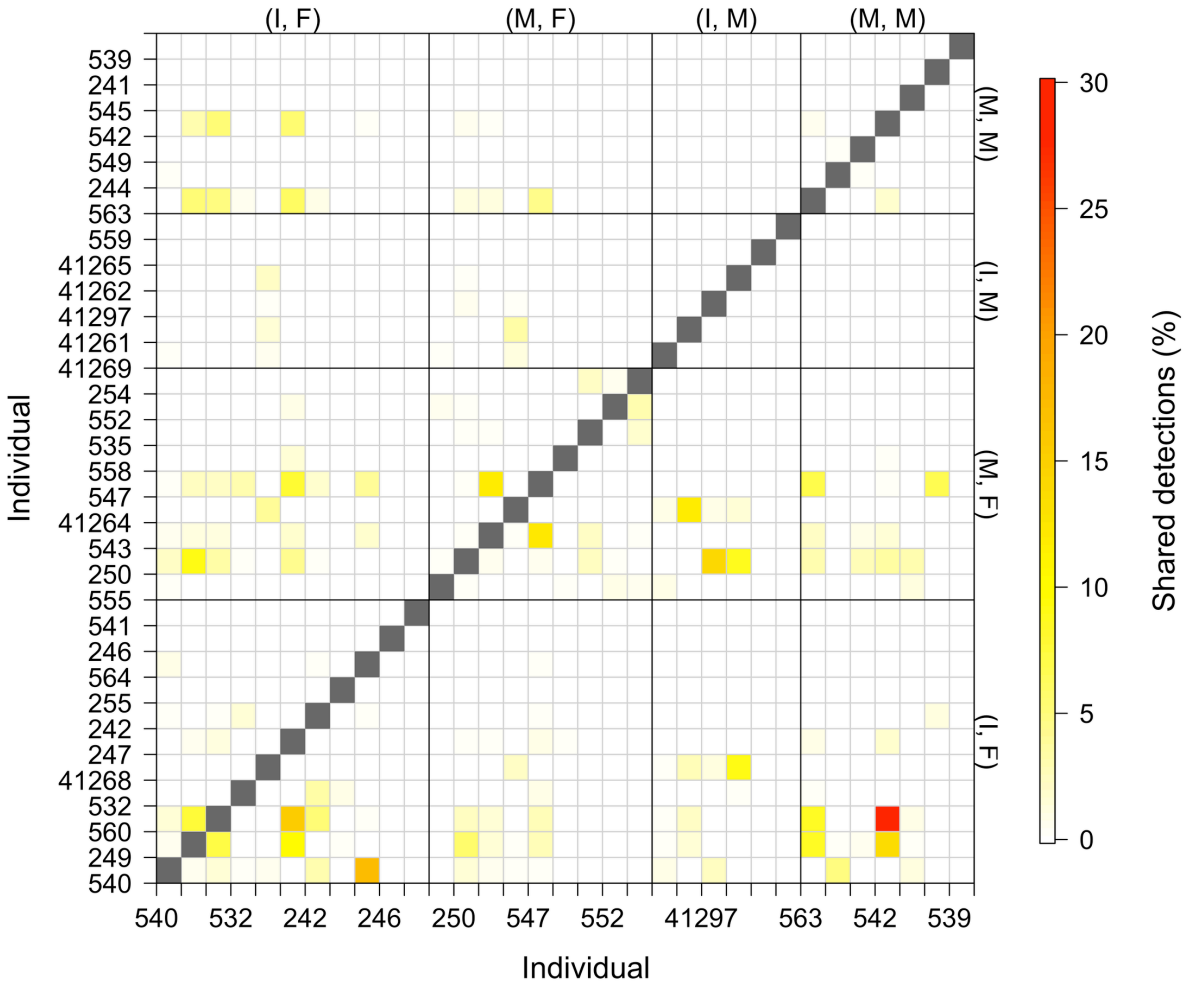

Figure 7. Co-occurrence patterns in detections. Each cell (i, j) shows the percentage of the detections of individual i (on the x axis) that are 'shared' with individual j (on the y axis). The diagonal of the matrix is highlighted in grey. Life-history categories—immature females (I, F), mature females (M, F), immature males (I, M) and mature males (M, M)—are labelled. Within each category, individuals are ordered by the total number of days over which they were detected (i.e., following Figure 2). Note that the percentage of observations shared by pairing i, j may not equal the percentage shared by pairing j, i when individuals have differing numbers of detections.

Among the individuals who shared a high proportion of detections, further examination of overlapping acoustic and depth time series did not suggest that individuals that shared detections were intimately associated in space for prolonged periods. Instead, most acoustic associations appear coincidental, prevailing among individuals occupying similar but distinct areas. In the few cases in which both acoustic and depth time series were similar, there were no consistent patterns in their nature or timing that could be attributed to particular types of interactions, such as mating. However, further reconstruction of fine-scale movements would be beneficial (Chapter Six).

4. Discussion

This is one of the first studies to examine the movements of a skate species at fine spatial scales over prolonged periods. For flapper skate, angler mark-recapture records and acoustic telemetry have previously demonstrated site affinity, especially among mature females, to the LStSJ MPA, but the prevalence, scale and drivers of this pattern remained unclear (Chapter One) (Neat et al., 2015). This chapter provides the first evidence that residency within the LStSJ acoustic array is relatively common among all life-history categories (at least for individuals that have reached more than one metre in size) and extends for periods of three months (short-term residency) to at least 15 months (long-term residency). This result strengthens the evidence that spatial management measures such as the LStSJ MPA should benefit flapper skate over monthly and seasonal timescales and suggests that studies on similar, large-bodied rajids in relation to MPAs would be worthwhile. At the same time, this chapter corroborates evidence for site fidelity and transiency for some individuals in the area (Neat et al., 2015). There is stronger evidence that movement patterns may differ among demographic groups, but the hypothesis that individuals associate closely in pairs or groups is refuted.

The dominant movement pattern in detection time series was short-term residency. This was documented in approximately 50 % of tagged individuals and all life-history categories. In theory, an individual only had to swim into the array once a month for three months to be identified as a ‘short-term resident’, but detection histories demonstrated that short-term residents typically spent weeks or months around receivers, particularly in the southern receiver curtain. In the most extreme case, detections of one female concentrated around a single receiver for five months, though there is a possibility that this individual shed its tag or died in this area. Long-term residency was documented in a further 10–20 % of immature and mature females, respectively, but may have been more common given that 38 % of short-term residents were only at liberty for less than one year. Taken together with previous angler mark-recapture and acoustic analyses (Neat et al., 2015), these results suggest that residential behaviour, especially short-term residency, is common among skate in the LStSJ MPA.

However, the prevalence and spatiotemporal scale of residency remain partially unclear, given the number of tagged individuals and limited receiver coverage. In the gaps between detections, individuals could have moved into other parts of the MPA or beyond MPA boundaries (Williamson et al., 2021). In some settings, alternative array designs, such as paired gated

arrays, provide additional (directional) information that can help to distinguish these possibilities (Heupel et al., 2006). Paired gated designs are particularly common in riverine systems for studies of salmonid movements (Rechisky et al., 2020) but logistically challenging in non-linear, open systems. Hence, new analytical methods that integrate acoustic detections with ancillary data to reconstruct movements in the gaps between detections would also benefit analyses of the prevalence and scale of residency and the estimation of home ranges (Chapter Six).

Residency is emerging as a relatively common movement pattern for many mobile marine species (Abecasis et al., 2015; Chapman et al., 2015; Hartman et al., 2015). Yet much previous research has focused on the movements of reef-associated teleosts (Abecasis et al., 2015; Rojo et al., 2019). Among elasmobranchs, research has also tended to focus on reef-associated species, especially sharks (Flowers et al., 2016). For instance, blacktip (*Carcharhinus melanopterus*), whitetip (*Triaenodon obesus*) and Caribbean (*Carcharhinus perezi*) reef sharks all show strong patterns of residency (Randall, 1997; Papastamatiou et al., 2010; Bond et al., 2012; Heupel et al., 2018). Some wide-ranging species, such as tiger sharks (*Galeocerdo cuvier*) also exhibit residency at certain times of year or in specific locations (Hammerschlag et al., 2022). Among rajids, only a handful of studies have examined residency (Hunter et al., 2005b; Morel et al., 2013; Neat et al., 2015; Sousa et al., 2019). However, a study in the southern North Sea suggested that many thornback rays (*Raja clavata*) remain in the Thames estuary year-round (Hunter et al., 2005b). Similarly, an acoustic study of three white skate (*Rostroraja alba*) revealed short-term residency within a marine park for two individuals and long-term residency lasting over 20 months in a mature female (Sousa et al., 2019). During this time, core activity areas were around 0.4 km^2, within a home range of approximately 3.2 km^2. For flapper skate, detection patterns suggest a similar scale of movement. While evidence is limited, the emerging picture from these studies is that residency may be an important aspect of the biology of rajids.

The drivers of residency remain unclear. Short-term residency may reflect natal, nursery, aggregation or mating philopatry (Chapman et al., 2015). These behaviours are poorly understood in flapper skate, but the use of nursery habitats by immature individuals may contribute towards residency in this group (Kinney and Simpfendorfer, 2009; Speed et al., 2010). Over seasonal and annual timescales, depth time series for three resident immature skate tagged in this study exhibit a pattern of repeated movements around particular depths, which

points towards central foraging or refuging behaviour (Humphries et al., 2017; Papastamatiou et al., 2018b). Amongst other elasmobranchs, long-term residency appears to predominate among tropical or subtropical species (Chapman et al., 2015) but has been documented in a few deep-water, benthic species in higher latitudes, including the bluntnose sixgill (*Hexanchus griseus*) (Andrews et al., 2009), the prickly shark (*Echinorhinus cookei*) (Dawson and Star, 2009) and white skate (Sousa et al., 2019). These patterns suggest that environmental stability, if coupled with a consistent food supply, may promote residency (Chapman et al., 2015).

Another movement pattern apparent from detection time series is one of repeated detections in an area punctuated by gaps. This pattern is difficult to interpret because detections and the gaps between detections varied in duration and the locations of undetected individuals were generally unknown. Nevertheless, there is evidence of seasonal site fidelity that might be attributable to mating. In March/April, when mating is believed to occur (Day, 1884), 8/11 mature females tagged near to the array and all mature males that were at liberty were detected. Thereafter, a clear, seasonal gap in the detections of at least two females (250 and 543) and three males (549, 244 and 545) followed over the summer/autumn, which may be associated with movement offshore (Little, 1997). Seasonal site fidelity has been reported in other elasmobranchs, such as short-tailed (*Dasyatis brevicaudata*) and round (*Urobatis halleri*) stingrays (Vaudo and Lowe, 2006; Le Port et al., 2008) but, for flapper skate, further evidence is needed to understand fully these patterns given the density and scale of the acoustic array used in this chapter.

There was evidence of transiency in all life-history categories. Previous angler mark-recapture analyses from the LStSJ MPA have indicated the presence of transient individuals (Neat et al., 2015). In the present chapter, the biological interpretation of transiency hinges on the interpretation of the lack of detections, which could have been caused by movements outside of receiver detection ranges within the MPA; more extensive movements to areas beyond MPA boundaries, possibly as part of a longer-term pattern of site fidelity; tag shedding, malfunction or removal; or mortality (Chapter Six). Angler mark-recapture and depth time series data shed light on these options. One mature female (546) that was tagged in the Sound of Jura and appeared ‘transient’ from the perspective of acoustic detections probably continued to reside in this region, where she was re-caught by anglers during the study. At least three individuals moved away from the MPA, including two mature males (244 and 539) which moved into deeper waters, and one immature female (242) which moved north to Mallaig. Other

individuals could also have moved beyond MPA boundaries during their time at liberty, given historical evidence for long (> 100 km) northwards journeys (Ritchie, 1923; Wheeler, 1969; Little, 1995). One individual also lost its acoustic tag but the wider extent of tag loss remains unclear (Neat et al., 2015).

There is evidence that movements differed between life-history categories. Across the board, detections were lower for males, reflecting a difference between the sexes in terms of the time they spent around receivers and perhaps more widely. In other elasmobranchs, sex-biased dispersal is relatively common and typically involves wider ranging movements in males (Pardini et al., 2001; Roycroft et al., 2019). A number of hypotheses might explain this behaviour (Wearmouth and Sims, 2010), such as differing habitat requirements in relation to divergent reproductive strategies (Economakis and Lobel, 1998) and the competitive exclusion of males by larger females (Corcoran et al., 2013). For flapper skate, while the prevalence of male-biased dispersal is unclear, this chapter strengthens the evidence that male and female movements differ and points towards other approaches, such as archival tags, as the means to clarify the movements of males.

Despite variation in movement patterns, over space almost all detections occurred around the southern receiver array. Only four tagged skate (560, 555, 558 and 535) were detected at receivers elsewhere and only one of these individuals (555) was detected in most areas of the array. However, the implications of this pattern depend on the relative influences of habitat preferences, detection probability, social interactions and sampling location.

In terms of habitat preferences, detections were more numerous away from shallow, inshore habitats close to sources of freshwater input. While skate certainly use shallow-water habitats, this pattern may reflect a preference for deeper water (Pinto et al., 2016; Thorburn et al., 2021). This hypothesis is consistent with the location of angler mark-recapture sites over deep areas, a species distribution model (Pinto et al., 2016) and observed depth time series (Thorburn et al., 2021), and may be related to prey distribution or refuging behaviour away from storms, water currents or previous mobile fishing activity. Alternatively, this apparent depth preference may have been driven by the complete absence of detections at receivers in shallow, near-shore habitats proximate to sea lochs, a pattern which appeared to be captured more effectively by salinity. In elasmobranchs, salinity variation often correlates with movement (Schlaff et al., 2014). While the causal links between these variables vary among systems (Heupel and

Simpfendorfer, 2008; Knip et al., 2011b; Simpfendorfer et al., 2011), most elasmobranchs are stenohaline (Froeschke et al., 2010; Martin et al., 2012), so it is plausible that flapper skate avoid areas around sea lochs which experience greater salinity variation. Space use may be affected by anthropogenic influences, such as aquaculture (Wearmouth and Sims, 2009), but further research is required to investigate their effects.

Apparent habitat preferences may have been affected by detection probability (Kéry and Schmidt, 2008). For example, receivers in shallow water on the mainland sides of Kerrera and Lismore may be exposed to higher levels of disturbance, which could decrease detection probability (Kessel et al., 2014). However, these factors are likely to influence the daily detection count more than the detection days metric used in this chapter. Moreover, a complete lack of detections in a few areas probably reflects a genuine absence of tagged skate in these areas over the study. Specifically, given the position of the coastline, it is likely that no tagged skate travelled all of the way along the eastern sides of Lismore or Kerrera, despite using the western sides of both of these islands.

Social interactions may have further influenced spatial patterns of detections (Jacoby et al., 2012). Yet despite circumstantial evidence for single-sex groups in flapper skate (Little, 1997) and for grouping behaviour in other elasmobranchs (Jacoby et al., 2012), the hypothesis that individuals closely associate in pairs or groups for substantial periods was unsupported. Even individuals from the same life-history category located in a similar area at the same time generally exhibited distinct depth time series (Chapter Six). However, looser associations, for instance with many immature females remaining in similar areas through time, perhaps due to shared feeding grounds or overlapping territories, may be important and probably explain patterns in angler mark-recapture records.

Sampling location also affected the spatial distribution of detections. Specifically, given the prevalence of localised movement patterns, capture at a few favoured angling sites appeared to contribute towards the appearance of detection hotspots around angling marks. Beyond these areas, localised movement suggests that skate probably remain undersampled by recent PIT tagging efforts (2011–present). The implication is population-level inferences from a handful of sites may be unrepresentative and a wider, more representative spatial distribution of angler mark-recapture effort would benefit analyses of habitat preferences and the estimation of population trends (Sun et al., 2014; Hays et al., 2020). More sampling is also required in the

winter months to clarify seasonal movement patterns, especially for males with sparser detection time series, and for the smallest size classes, which remain understudied.

This research has implications for skate conservation. Taken together with historical angler mark-recapture records that demonstrate skate occur throughout the MPA (Little, 1995; Little, 1997; Scottish Natural Heritage, 2014; Neat et al., 2015), the strength of site affinity revealed by recent angler mark-recapture records and the acoustic time series analysed here suggests that removing pressures such as fishing from areas the size of the MPA has the potential to benefit multiple life-history categories, especially females, over monthly and seasonal timescales. In fact, prolonged residency within particular areas of the acoustic array suggests that smaller protected areas could be beneficial to some individuals over these timescales. At the same time, the spatial scale of residency implies that skate may be particularly vulnerable to localised pressures, especially in areas that are disproportionately important for their life history (Kinney and Simpfendorfer, 2009; Flowers et al., 2016). These results add to the accumulating evidence in support of the use of MPAs for skate (Hunter et al., 2006; Wiegand et al., 2011; Sousa et al., 2018, 2019) and in elasmobranch conservation more broadly (Ferretti et al., 2018; MacKeracher et al., 2019; Dwyer et al., 2020). However, an open question remains regarding the extent to which protection from fisheries over monthly and seasonal timescales supports population recovery.

Within the MPA, the results further confirm the importance of the deep-water basins around angling sites for skate, as found in other parts of the MPA (Neat et al., 2015; Thorburn et al., 2021). In contrast, there were a few specific locations in which tagged skate were not detected. However, further research is required to evaluate the suitability of MPA boundaries given the small sample size, the influence of tagging site on detection patterns and other considerations that affect the benefits of management measures, such as habitat suitability (Lauria et al., 2015; Pinto et al., 2016) and potential fishing pressure (Langton et al., 2020).

There are eight areas in the MPA in which seasonal fisheries are permitted from October–March. Acoustic detections demonstrate that there is the potential for skate–fisheries interactions during this time, especially for mature females for which seasonal detection patterns were strongest. Unfortunately, the absence of angler mark-recapture and acoustic data from fished areas precludes further evaluation in this chapter of the prevalence of these interactions. However, this should be a priority for future research (Chapter Seven).

Beyond the LStSJ MPA, evidence for wider movements suggests that the LStSJ MPA alone is not fully adequate for the protection of flapper skate found in this area. Flapper skate are no longer commerically targeted, but they are caught as bycatch in bottom-trawl fisheries (Bendall et al., 2017) and survivorship estimates for related species (Benoît et al., 2010; Dulvy et al., 2014), along with estimates of vital rates (Régnier et al., 2021), suggest that this has the potential to impede population recovery. If short-term residency in winter/spring typically precedes offshore movement (Wheeler, 1969), flapper skate may be particularly vulnerable to this source of mortality in summer/autumn. For some individuals, localised movements are likely to increase the severity, but reduce the area, of overlaps between skate and fisheries. For other individuals, especially males, longer distance movements away from protected areas may increase the time over which individuals are potentially exposed to fisheries, which has the potential to lead to sex-biased exploitation (Mucientes et al., 2009). However, technical measures, such as the removal of 'tickler' chains, which startle skate resting on the seabed in front of trawls into nets, can substantially reduce the bycatch of skate (Chapter Four; Kynoch et al., 2015) and should be considered as a potential management tool in areas in which flapper skate occur.

Alongside fisheries, in coastal areas flapper skate are potentially exposed to aquaculture farms (Bell et al., 2016), pollutants (Bezerra et al., 2019), electromagnetic cables (Hutchison et al., 2018b) and other anthropogenic stressors such as climate change (Chapter One; Wheeler et al., 2020). For example, recent research has reported notable concentrations of plastic (Smith, 2018) and other pollutants (Gelsleichter and Walker, 2010; Bezerra et al., 2019; Tiktak et al., 2020) in elasmobranchs, which may have physiological and population-level impacts (Wheeler et al., 2020), as reported in marine mammals such as orcas (*Orcinus orca*) (Desforges et al., 2018). As a result, MPAs like the LStSJ MPA need to be embedded within an ecosystem-based management approach that recognises the suite of stressors to which species are exposed in order to deliver management objectives (McLeod et al., 2005; Wheeler et al., 2020).

Appendices

1. Supporting methods

1.1. The overall number of days with detections

A robust Poisson generalised linear model (GLM) was used to investigate how the total number of days with detections varied in relation to time at liberty, tagging site and sex. Time at liberty was centred by the mean number of days at liberty across all individuals. This model was fitted in `R` as follows:

```
library(robmixglm)
mod <- robmixglm(count_days ~ liberty * site * sex,
                 family = "poisson",
                 data = data
                 )
```

where `site` is a factor that distinguishes tagging sites, `sex` is a factor that distinguishes males from females and other variables are as previously described. `data` refers to a dataframe with one row for each individual and columns for the corresponding values of the response and explanatory variables.

1.2. Temporal trends

1.2.1. Temporal trends in the number of acoustically detected individuals

The binomial generalised additive model (GAM) used to investigate temporal trends in the number of acoustically detected individuals was fitted as follows:

```
library(mgcv)
mod <- gam(cbind(count_detected, count_liberty - count_detected) ~
             grp +
             s(day, by = grp, bs = "cc", k = 15) +
             area,
           family = binomial(link = "logit"),
```

```
            knots = list(yday = c(0.5, 366.5)),
            data = data)
```

where all variables are as previously described and `data` refers to a dataframe with one row for each day and life-history category and columns for the response variable and corresponding explanatory variables.

1.2.2. Temporal trends in the number of individuals caught by recreational anglers

The negative binomial GAM used to investigate temporal trends in the number of individuals caught by recreational anglers was fitted as follows:

```
library(mgcv)
mod <- mgcv::gam(count_angled ~
                   grp +
                   s(month, by = grp, bs = "cc") +
                   year,
                 knots = list(month = c(0, 12)),
                 family = nb(),
                 data = data)
```

where `year` is a factor that distinguishes years and other variables are as previously described. `data` refers to a dataframe with one row for each month of the time series and each life-history category and columns for the response variable and corresponding explanatory variables.

1.3. Spatial patterns

1.3.1. Model SP1

The first model of the spatial pattern of detections (Model SP1) was fitted as follows:

```
library(mgcv)
data$id_rec_overlap_log <- log(data$id_rec_overlap)
mod1 <- gam(count_days_by_receivers ~
              grp +
              s(id_rec_dist_lcp) +
              s(depth_median) +
```

```
              s(depth_mad) +
              s(sal_median) +
              s(cs_median) +
              s(id, bs = "re") +
              offset(id_rec_overlap_log),
            family = nb(),
            data = data)
```

where all variables are as previously described and `data` is a dataframe with one row for each individual-receiver combination and columns for the response variable and corresponding explanatory variables.

1.3.2. Model SP2

A similar model with group-level smoothers was also implemented, as follows:

```
mod2 <- gam(detection_days_by_receivers ~
              grp +
              s(id_rec_dist_lcp, by = grp) +
              s(depth_median, by = grp) +
              s(depth_mad, by = grp) +
              s(sal_median, by = grp) +
              s(cs_median, by = grp) +
              s(id, bs = "re") +
              offset(id_rec_overlap_log),
            family = nb(),
            data = data)
```

where all terms are as previously described.

1.3.3. Model SP3 and SP4

Since depth and salinity were strongly correlated, models identical in structure to Model SP1 but including either `depth_median` (SP3) or `sal_median` (SP4) were also implemented.

2. Supporting tables

Table S1. Coefficient estimates from a robust Poission generalised linear model of detection days as a function of a three-way interaction between time at liberty, tagging site and sex. Coefficients were estimated from 33 observations. For each coefficient, the estimate, standard error, *z*-value and *p*-value are shown.

Coefficient	Estimate	SE	*z*-value	*p*-value
Intercept	4.360	0.062	70.643	0.000
Time at liberty	0.004	0.000	7.859	0.000
Site (Insh)	-0.758	0.080	-9.427	0.000
Sex (male)	-1.342	0.104	-12.963	0.000
Time at liberty x site (Insh)	-0.006	0.001	-6.446	0.000
Time at liberty x sex (male)	-0.009	0.001	-11.744	0.000
Site (Insh) x sex (male)	3.545	0.723	4.907	0.000
Time at liberty x site (Insh) x sex (male)	0.051	0.013	3.864	0.000

Table S2. Coefficient estimates from a binomial generalised additive model of the number of acoustically detected individuals in each life-history category, out of the total number that could have been detected in that category, through time. Coefficients were estimated from 1,800 observations. The model explained 49.198 % of the deviance. For parametric coefficients, the estimate, standard error, *z*-value and *p*-value are shown. For smooth terms, the effective degrees of freedom, reference degrees of freedom, χ^2 and *p*-value value are shown. Time is in units of days (Julian day: 0–366).

Parametric coefficients				
Term	***Estimate***	***SE***	***z-value***	***p-value***
(Intercept)	-3.742	0.328	-11.415	0.000
Mature females	-0.304	0.068	-4.485	0.000
Immature males	-2.269	0.261	-8.708	0.000
Mature males	-1.059	0.112	-9.479	0.000
Receiver coverage	0.214	0.031	6.948	0.000
Approximate significance of smooth terms				
Term	***EDF***	***Ref DF***	χ^2	***p-value***
s(time): immature females	12.167	13	87.600	0.000
s(time): mature females	11.906	13	213.220	0.000
s(time): immature males	8.374	13	61.860	0.000
s(time): mature males	11.361	13	52.060	0.000

Table S3. Coefficient estimates from a negative binomial generalised additive model of the number of individuals captured by recreational anglers in each life-history category through time. Coefficients were estimated from 128 observations. The model explained 65.658 % of the deviance. For parametric coefficients, the estimate, standard error, *z*-value and *p*-value are shown. For smooth terms, the effective degrees of freedom, reference degrees of freedom, χ^2 and *p*-value value are shown. Time is in units of months (1–12).

Parametric coefficients				
Term	***Estimate***	***SE***	***z-value***	***p-value***
(Intercept)	2.116	0.115	18.470	0.000
Mature females	-0.532	0.141	-3.763	0.000
Immature males	-0.034	0.124	-0.271	0.786
Mature males	-0.030	0.124	-2.244	0.807
Year (2017)	0.460	0.113	4.066	0.000
Year (2018)	0.649	0.115	5.628	0.000
Approximate significance of smooth terms				
Term	***EDF***	***Ref DF***	χ^2	***p-value***
s(time): immature females	2.646	8	15.891	0.000
s(time): mature females	5.083	8	98.712	0.000
s(time): immature males	2.654	8	11.840	0.002
s(time): mature males	0.993	8	1.517	0.204

Table S4. Akaike's Information Criterion (AIC) scores for the four models of the spatial pattern (SP) of detections. For each model, the degrees of freedom, the AIC score and the difference in the AIC score relative to the best-supported model are shown. Models are ordered by AIC scores. Model SP1 included global smoothers for all variables; Model SP2 included group-specific smoothers for all variables; Model SP3 was identical to Model SP1 but excluded salinity; and Model SP4 was identical to Model SP1 but excluded depth.

Model	**DF**	**AIC**	**ΔAIC**
SP1	55.351	2425.816	0.000
SP2	57.320	2636.954	211.138
SP4	48.781	2641.425	215.609
SP3	53.593	2649.155	223.339

Table S5. Coefficient estimates from a negative binomial generalised additive model of the total number of days with detections of each individual at each receiver (Model SP1). Coefficients were estimated from 1,409 observations. The model explained 74.480 % of the deviance. For parametric coefficients, the estimate, standard error, *z*-value and *p*-value are shown. For smooth terms, the effective degrees of freedom, reference degrees of freedom, χ^2 and *p*-value value are shown.

Parametric coefficients				
Term	***Estimate***	***SE***	***z-value***	***p-value***
(Intercept)	-8.034	0.697	-11.522	0.000
Mature females	0.918	0.824	1.115	0.265
Immature males	-0.637	0.962	-0.663	0.507
Mature males	-1.251	0.900	-1.390	0.164
Approximate significance of smooth terms				
Term	***EDF***	***Ref DF***	χ^2	***p-value***
s(distance)	3.417	4.143	80.340	0.000
s(median depth)	3.167	3.872	17.130	0.001
s(MAD depth)	4.179	5.096	17.020	0.005
s(median salinity)	1.003	1.004	10.960	0.001
s(median current speed)	7.502	8.340	36.940	0.000
s(individual)	26.540	29.000	306.670	0.000

Table S6. Concurvity estimates from a negative binomial generalised additive model of the total number of days with detections of each individual at each receiver (Model SP1). For each smooth term, three concurvity measures are shown.

Concurvity measure	**Smooth term**					
	s(distance)	***s(median depth)***	***s(MAD depth)***	***s(median salinity)***	***s(current speed)***	***s(individual)***
Worst	0.848	0.980	0.949	0.965	0.912	1.000
Observed	0.730	0.837	0.766	0.936	0.789	0.203
Estimate	0.702	0.856	0.843	0.916	0.692	0.159

3. Supporting figures

Figures S1–S4. Movement time series for all acoustically detected individuals in each life-history category over the duration of the acoustic study (S1, immature females; S2, mature females; S3 immature males; and S4, mature males). In each figure, each panel contains the time series for the individual shown. In each panel, the top timeline shows the mark-recapture angling time series; the timeline below shows the acoustic detection time series, with detections shown by crosses and tag deployment/retrieval events marked by filled points; and the plot below shows the depth time series, if successfully recovered for that individual. In the angler mark-recapture and acoustic detection time series, colours correspond to areas of the receiver array as described for Figure 1. The exception is angling events (including some tag deployment and retrieval events) that occurred outside of these areas; namely, off Insh and Crinan. These points are coloured in light pink and orange respectively. Unrecorded angling locations within the Firth of Lorn are shown in grey.

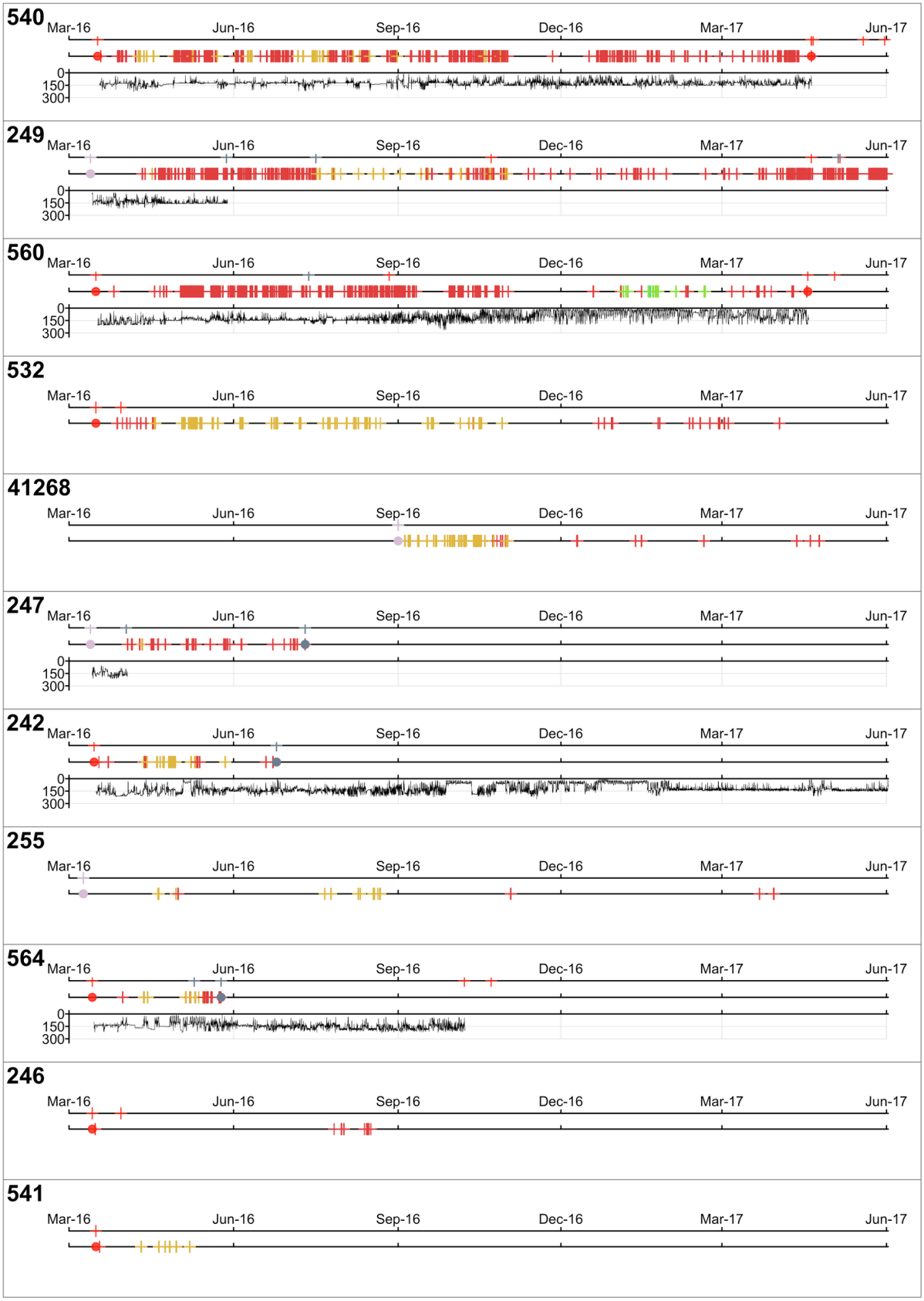

Figure S1. The movement time series for immature females.

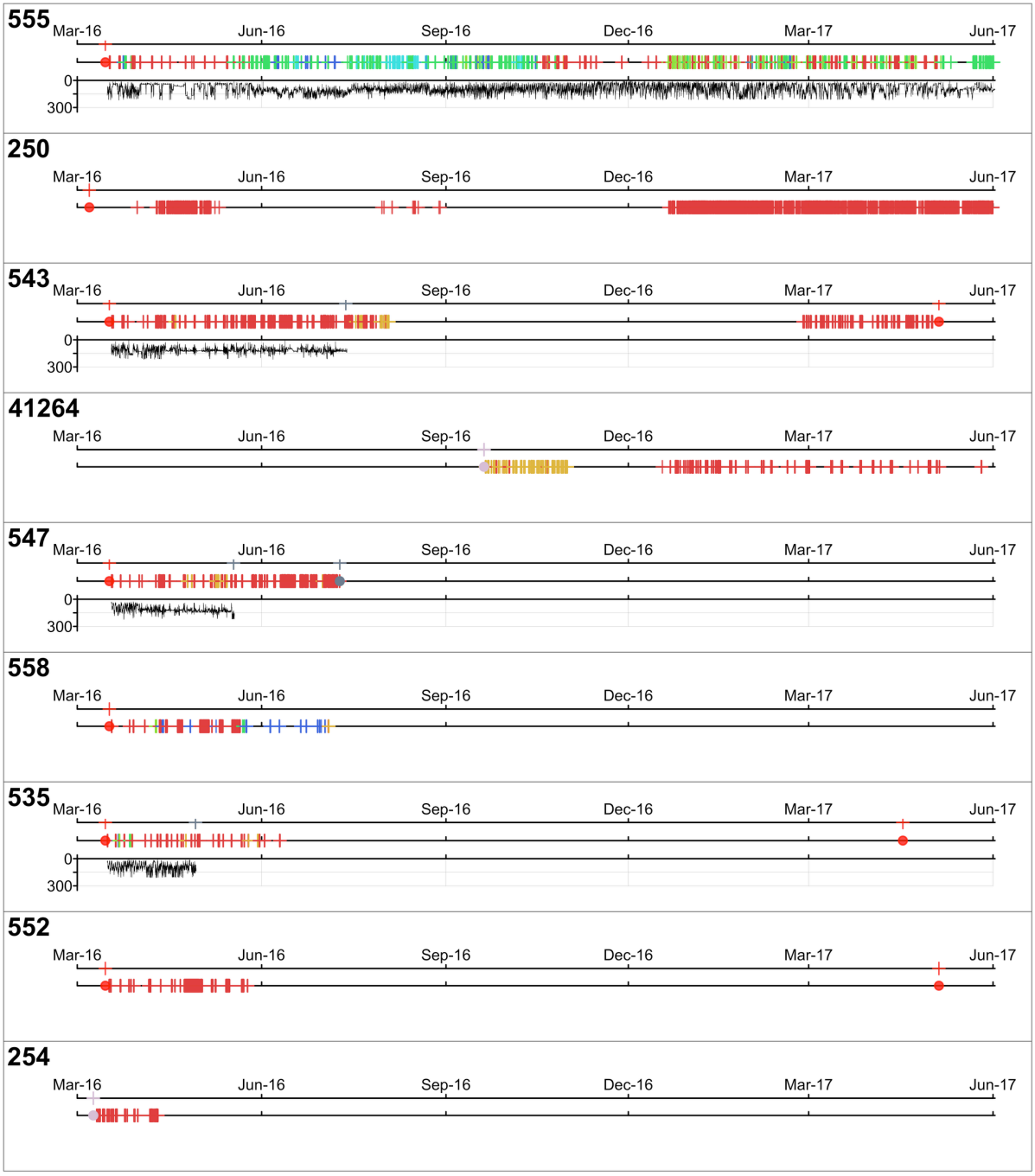

Figure S2. The movement time series for mature females.

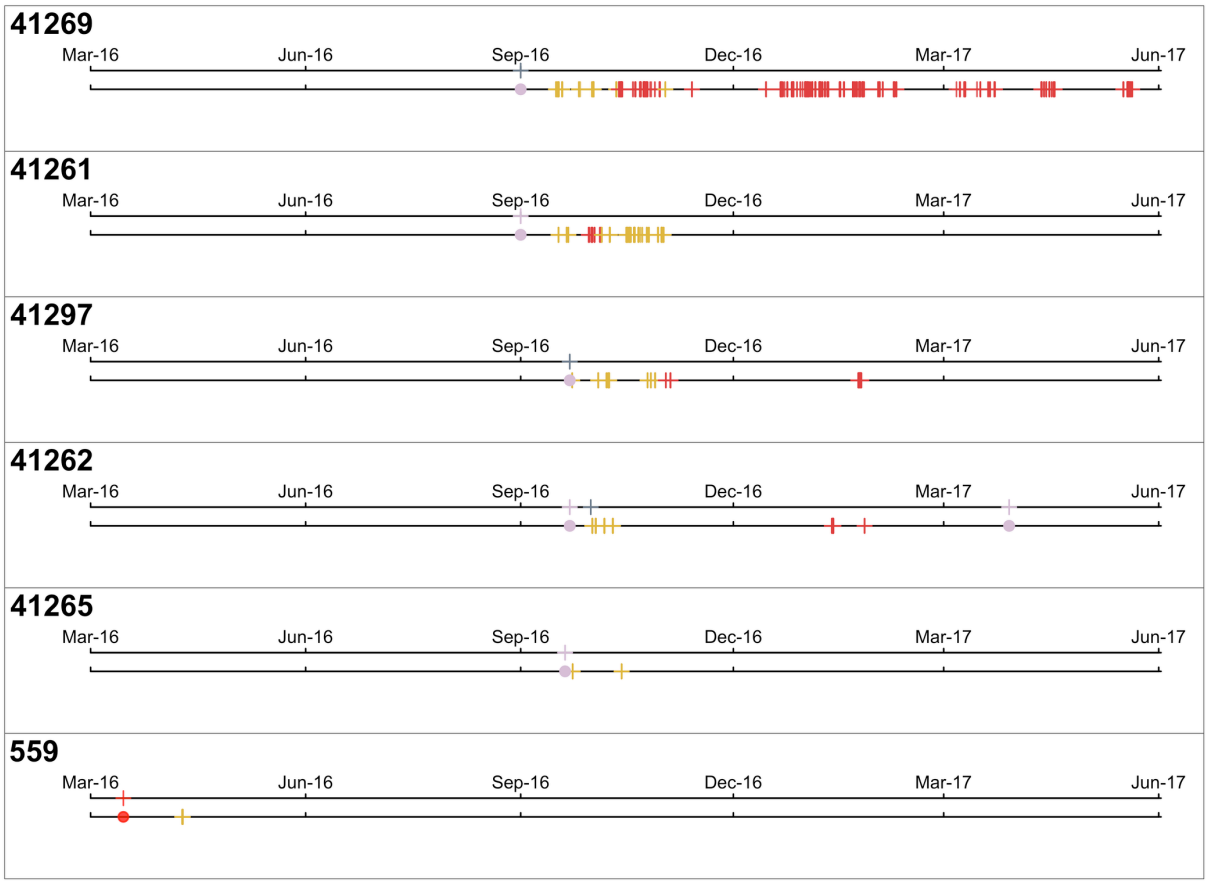

Figure S3. The movement time series for immature males.

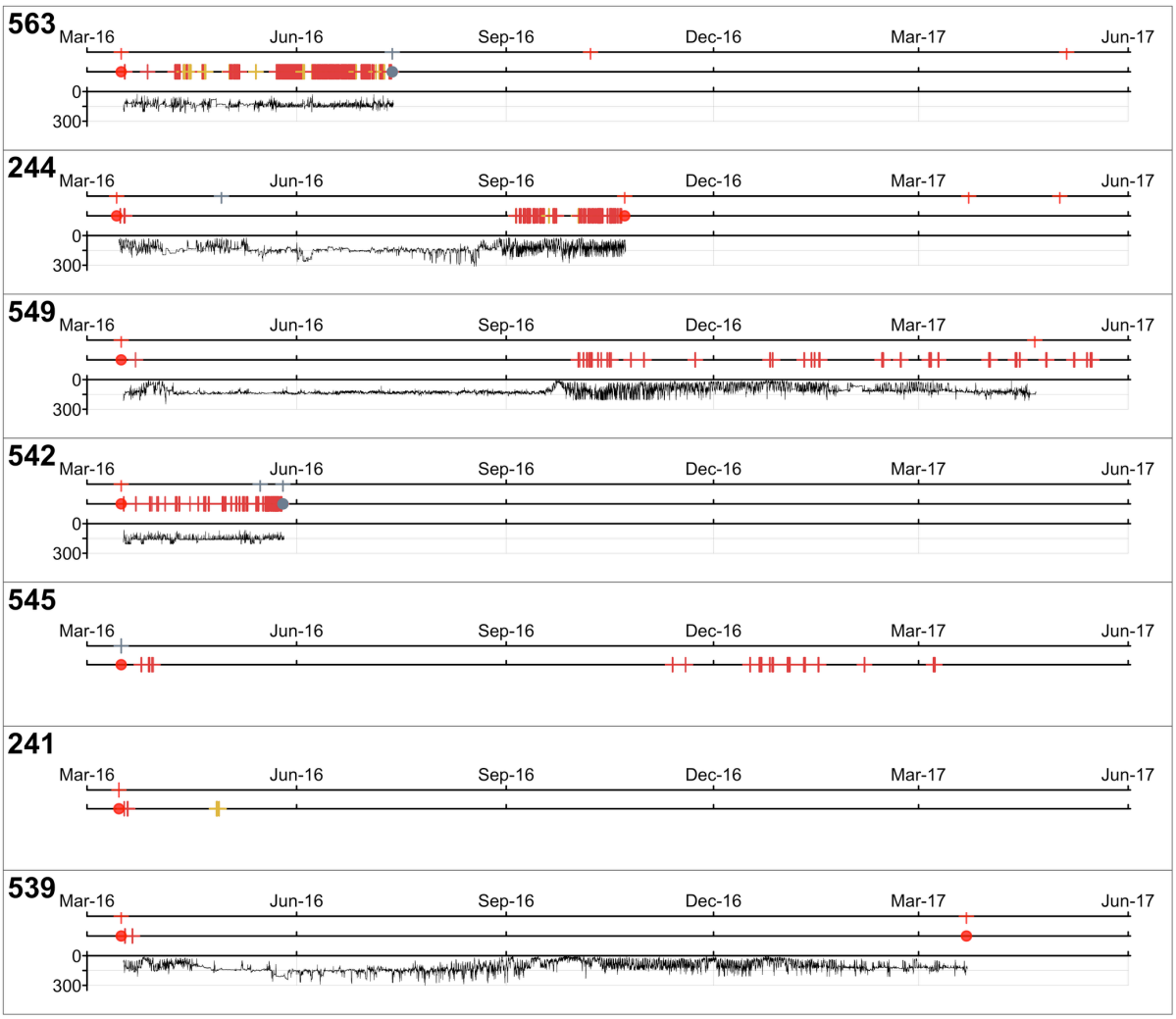

Figure S4. The movement time series for mature males.

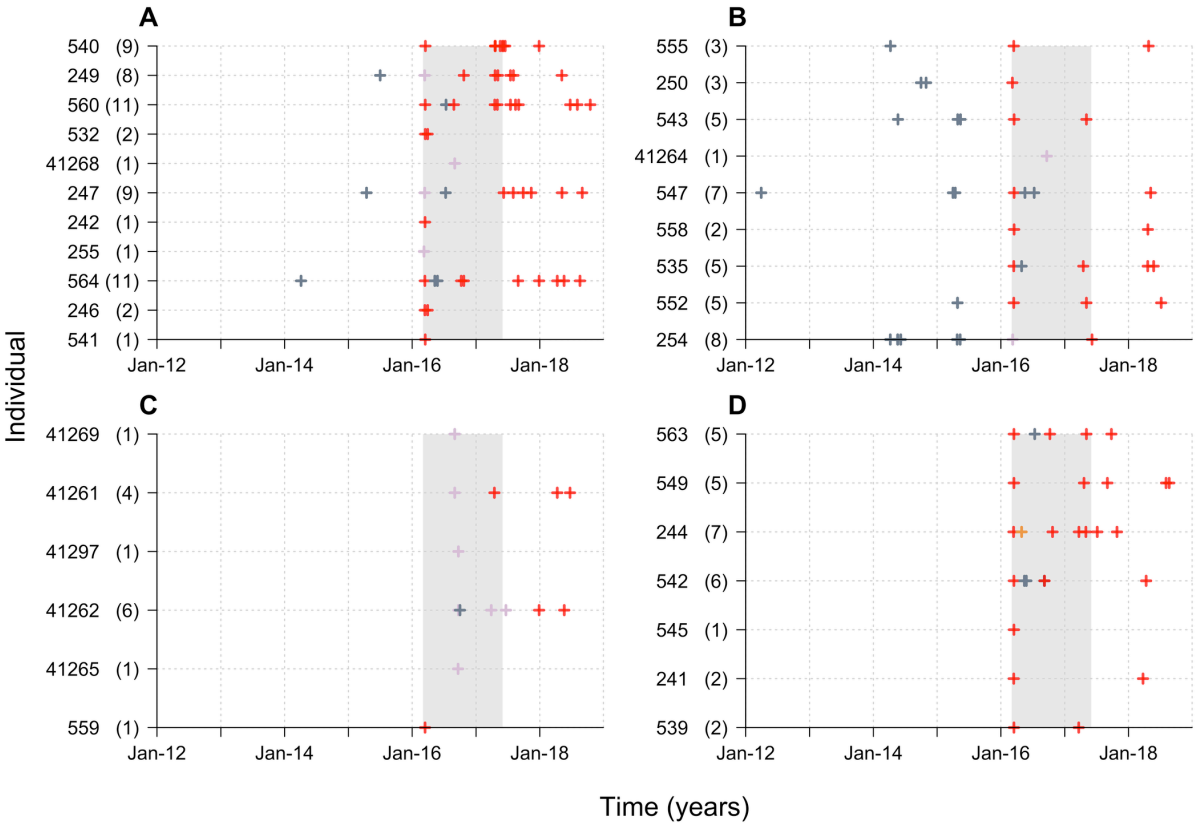

Figure S5. Mark-recapture angling records for acoustically detected individuals in each life-history category, as defined at the onset of the acoustic study. A, immature females; **B**, mature females; **C**, immature males; and **D**, mature males. Each point (+) defines the time of an angler mark-recapture event for a particular individual. Event locations are distinguished by colour following Figures S1–4 (Kerrera, red; Insh, pink; Crinan, orange; unrecorded locations in the Firth of Lorn, grey). The shaded area defines the timing of the acoustic study. Y-axis labels define individual IDs, with the total number of recorded captures for each individual shown in brackets. For convenience, panel and individual order follows Figure 2; however, some individuals may have matured over this timeframe. Note that the inclusion of captures from unrecorded locations in the Firth of Lorn means that angling histories span a longer timeframe (2012–18) than the processed angler mark-recapture database used in models (2016–18).

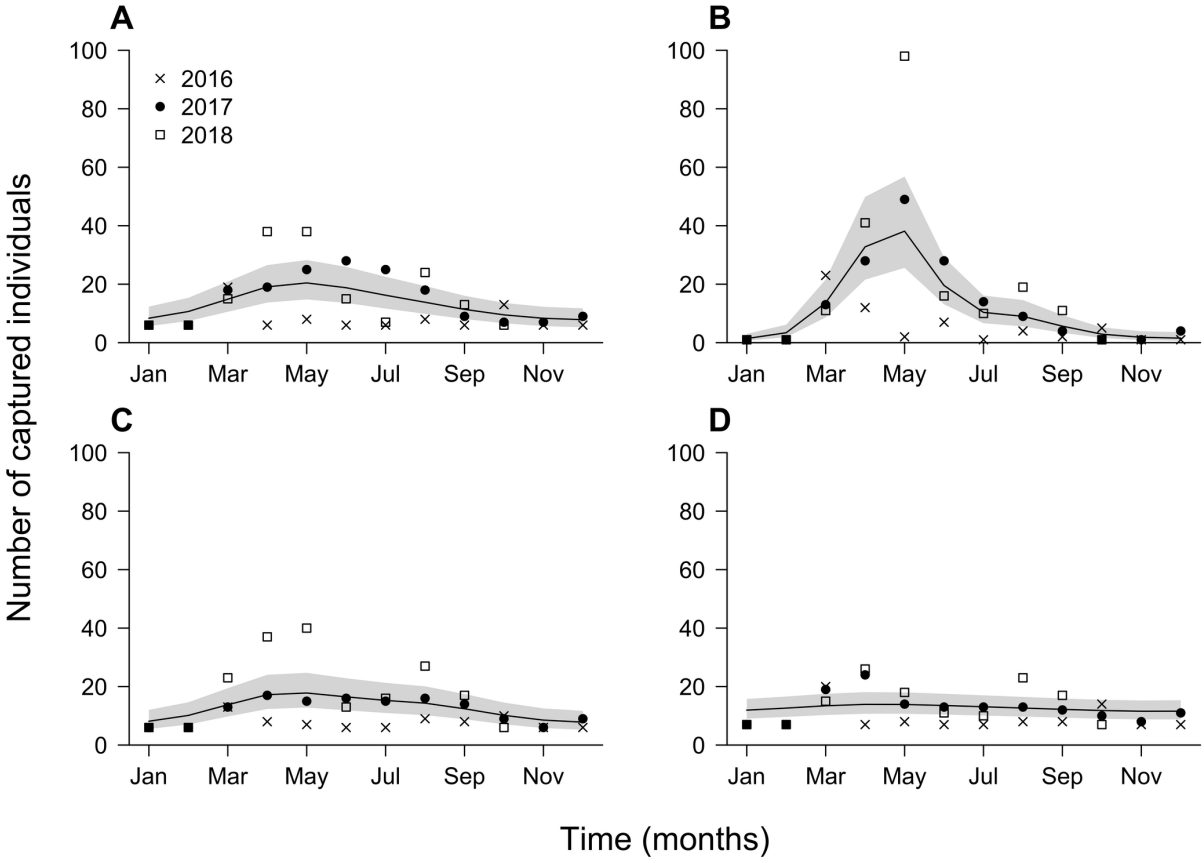

Figure S6. Seasonal differences in the total number of recorded captures in angler mark-recapture records for each life-history category. A, immature females; **B**, mature females; **C**, immature males; and **D**, mature males. Each panel shows the monthly trend in the total number of captured individuals in a particular life-history category for 2016–18. The black line and surrounding envelope are the expected counts and 95 % pointwise confidence bands from a negative binomial generalised additive model of the number of captured individuals in each life-history category through time for 2017.

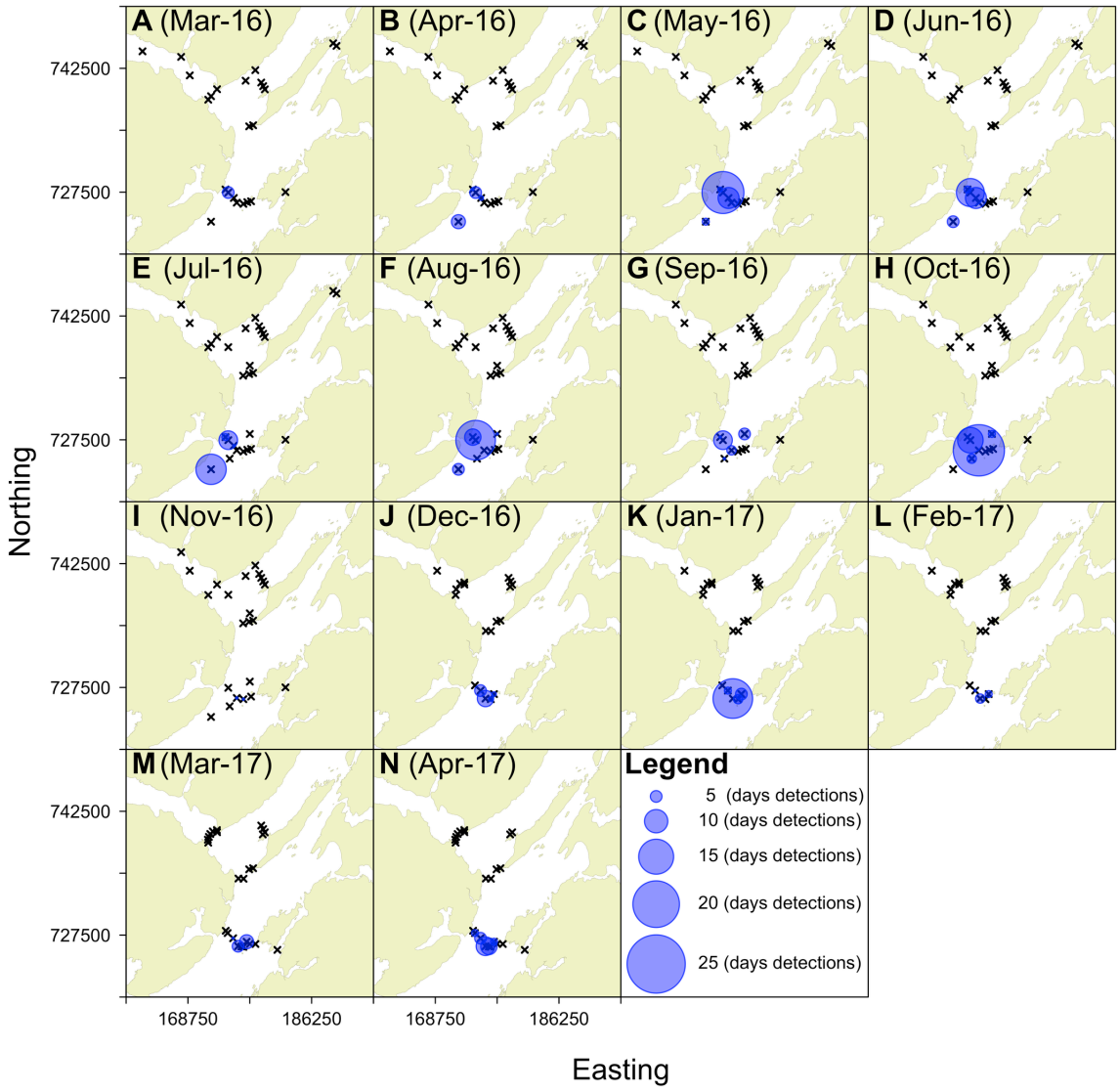

Figure S7. Spatiotemporal patterns in the number of days with detections for an example individual: individual 540, the immature female with the most detection days. Each panel is a different month from March 2016–April 2017. The black crosses mark receivers that were operational in that month. The blue dots mark the receivers at which the individual was detected; their size is proportional to the number of days during which the individual was detected by each receiver in that month. The overall pattern—a predominance of detections around the southern receiver curtain, with detections at multiple (n = 13) receivers and some more prolonged periods at particular receivers—is typical for most sampled individuals. The coordinate reference system is British National Grid. Background map © Crown copyright and database rights [2019] Ordnance Survey (100025252).

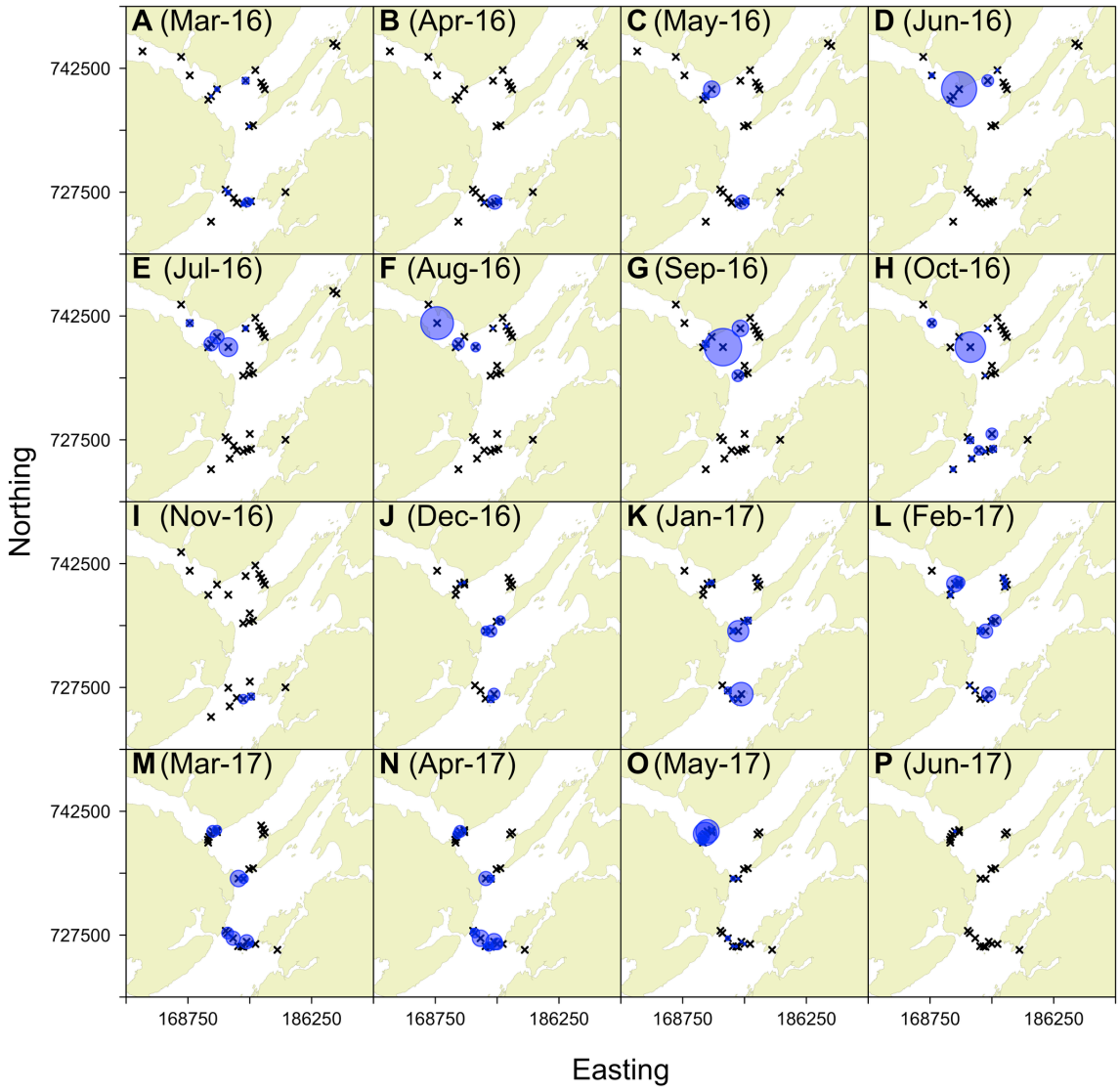

Figure S8. Spatiotemporal patterns in the number of days with detections for another example individual: individual 555, the mature female with the most detection days and detections at the most (n = 37) receivers. Panel characteristics follow Figure S7. The spatiotemporal distribution of detections for this individual is very distinct in terms of the use of most of the receiver array, especially with respect to detections in the northern areas of the array.

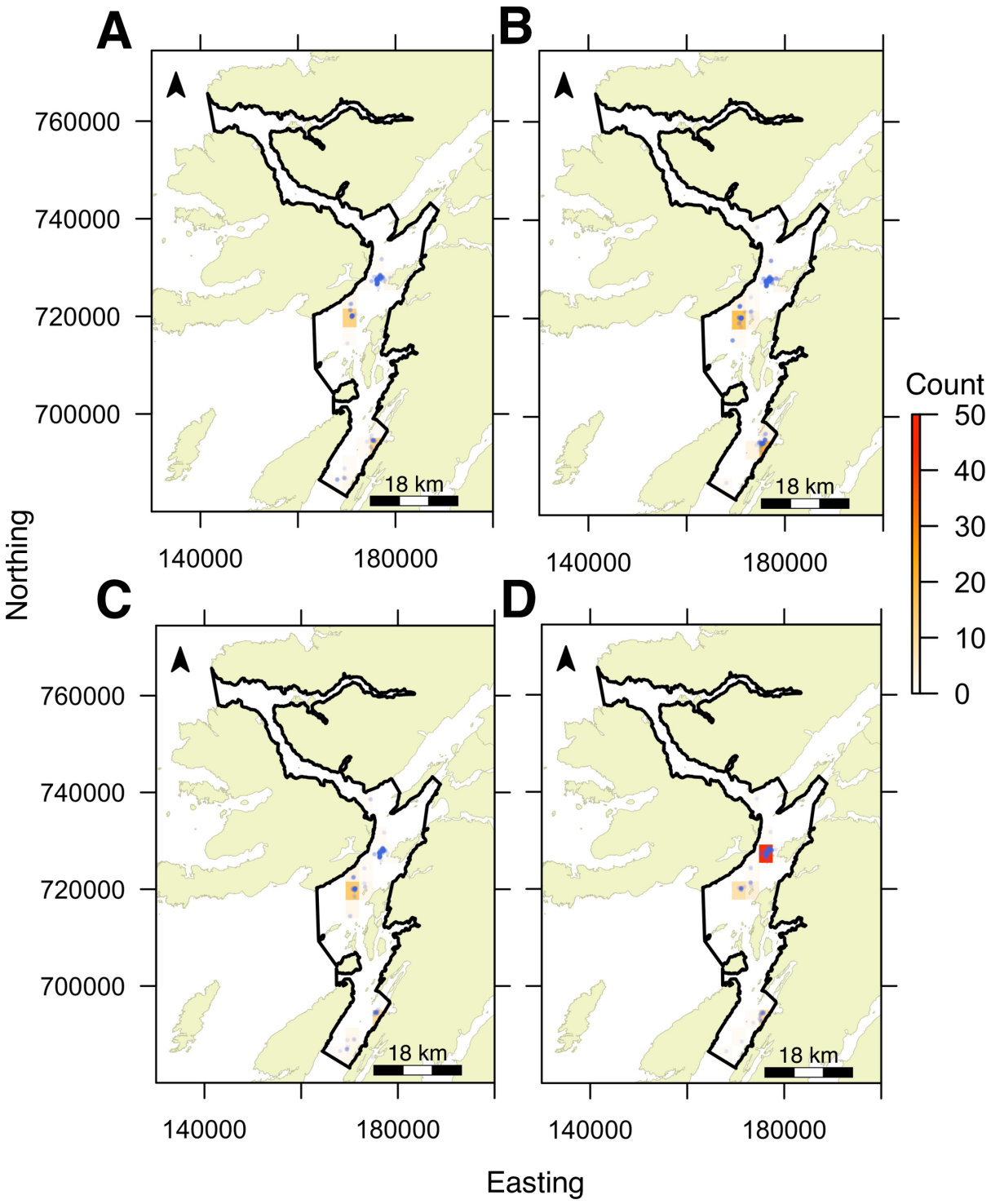

Figure S9. The spatial distribution of recorded captures in mark-recapture angling records for each life-history category. A, immature females; **B**, mature females; **C**, immature males; and **D**, mature males. In each panel, the study site is divided into 25 x 25 grid cells and each cell shows the total number of individuals caught in that cell across the angler mark-recapture time series. Counts are shown, rather than proportions, because proportions can be misleading at low sample sizes. The blue points mark the exact angling locations. The coordinate reference system is British National Grid. Background map © Crown copyright and database rights [2019] Ordnance Survey (100025252).

Chapter Four

Vertical movement

Abstract

1. Trends in depth and vertical activity reflect the behaviour, habitat use and habitat preferences of aquatic organisms. However, among elasmobranchs, research has focused heavily on pelagic sharks, while the vertical movements of benthic elasmobranchs, such as skate (Rajidae), remain understudied.
2. In this chapter, the vertical movements of the Critically Endangered flapper skate (*Dipturus intermedius*) were investigated using archival depth data collected at two-minute intervals from 21 individuals off the west coast of Scotland in 2016–17.
3. Depth records comprised nearly four million observations and included eight time series longer than one year, forming one of the most comprehensive datasets collected on the movement of any skate to date. Additive modelling and functional data analysis were used to investigate vertical movements in relation to environmental cycles and individual characteristics.
4. Vertical movements were dominated by individual variation but included prolonged periods of limited activity and more extensive movements that were associated with tidal, diel, lunar and seasonal cycles. Diel patterns were strongest, with irregular but frequent movements into shallower water at night, especially in autumn and winter.
5. This research strengthens the evidence for vertical movements in relation to environmental cycles in benthic species and demonstrates a widely applicable flexible regression framework for movement research that recognises the importance of both individual-specific and group-level variation.

Keywords

autocorrelation, biologging, depth, functional data analysis, generalised additive model, vertical activity

1. Introduction

Trends in the vertical movements of mobile species are widespread in aquatic ecosystems (Chapter One). They extend across ecological timescales, from the cycles of the tides (Gibson, 2003; Krumme, 2009) to those of the seasons (Hyndes et al., 1999; Milligan et al., 2020) and those exhibited over ontogenetic development (Grubbs, 2010; Frank et al., 2018). They are also prevalent across trophic levels, from the diel vertical migration (DVM) of plankton (Hays, 2003; Bianchi and Mislan, 2016) to the diving patterns of cetaceans (Keen et al., 2019; Caruso et al., 2020) and pelagic sharks (Papastamatiou and Lowe, 2012; Schlaff et al., 2014). An important area of research in aquatic ecology is to understand the drivers of these trends.

Among elasmobranchs, research on vertical movement has focused on pelagic sharks and their diving patterns using animal-borne data loggers (Papastamatiou and Lowe, 2012; Schlaff et al., 2014). This work has demonstrated associations between vertical movement and periodic environmental cycles, individual characteristics and ecological interactions. Associations between vertical movement and environmental cycles are termed depth-specific periodic behaviours (Scott et al., 2016). Over short timescales, many elasmobranchs exhibit tidal-driven movement, moving into shallower waters with incoming tides to minimise energy expenditure or predation risk or to forage (Ackerman et al., 2000; Wetherbee et al., 2007; Carlisle and Starr, 2009, 2010)**.** Over diel scales, solar light levels are often linked to vertical movement via DVM, with crepuscular or nocturnal movement into shallower or deeper water (normal and reverse DVM respectively), and changes in vertical activity (Carey et al., 1990; Andrews et al., 2009; Arostegui et al., 2020). In many cases, these movements are associated with prey availability, but links to thermoregulation and bioenergetic efficiency are also documented (Matern et al., 2000; Sims et al., 2006; Papastamatiou et al., 2015). Over the lunar cycle, movements can be associated with changes in tidal range or moonlight for similar reasons (West and Stevens, 2001; Graham et al., 2006; Weng et al., 2007). Likewise, longer-term seasonal variation in solar light levels through increases or decreases in day length (photoperiod) can be important,

ultimately through the regulation or entrainment of physiological processes such as reproductive cycles (Carey et al., 1990; Kneebone et al., 2012; Nosal et al., 2013).

Alongside environmental cycles, biological characteristics are frequently associated with vertical movement (Papastamatiou and Lowe, 2012; Schlaff et al., 2014). There is increasing interest in the role of individual variation and behavioural plasticity, but this remains poorly studied (Jacoby et al., 2014; Hertel et al., 2020; Shaw, 2020). Sexual segregation in elasmobranchs is also understudied but has the potential to give rise to differences in vertical movement, for instance in association with the movement of gravid females into shallow, sheltered, inshore areas for parturition (Wearmouth and Sims, 2010). Likewise, ontogenetic differences in vertical movements have been documented, especially in association with ontogenetic dietary shifts (Grubbs, 2010; Thorburn et al., 2019). However, in many cases, the links between environmental cycles, individual characteristics and ecological interactions are difficult to demonstrate (Papastamatiou and Lowe, 2012; Schlaff et al., 2014).

The vertical movements of benthic elasmobranchs, such as skate (Rajidae), have received limited attention and generalising patterns from pelagic species is challenging (Humphries et al., 2017; Siskey et al., 2019). Available evidence indicates that in some instances skate undergo DVM in association with diel changes in solar light levels (Peklova et al., 2014; Humphries et al., 2017), perhaps in response to diel rhythms in prey such as Norway lobster (*Nephrops norvegicus*) and sandeels (*Ammodytes spp.*) in the North Atlantic (Winslade, 1974; Aguzzi and Sardà, 2008). In turn, the apparent influence of solar light suggests that lunar phase and photoperiod may be important, as reported for other elasmobranchs (Schlaff et al., 2014) and in aquatic ecosystems more widely (Migaud et al., 2010; Kronfeld-Schor et al., 2013). However, in general, the prevalence of DVM in skate and the influence of other environmental conditions remain poorly understood.

The flapper skate (*Dipturus intermedius*) is a large, benthic rajid, only recently recognised as a distinct species in the common skate (*D. batis*) species complex, which includes both flapper and common blue skate (*D. batis*) (Chapters One–Two). Once widespread in the North-East Atlantic, the flapper skate was strongly affected by overfishing (Ellis et al., 2021). However, the species is still found off the west coast of Scotland where the Loch Sunart to the Sound of Jura Marine Protected Area (LStSJ MPA) has been established for its conservation (Neat et al., 2015). Juveniles hatch at about 20 cm in length (Benjamins et al., 2021) and males and females

reach maturity at 185.5–197.5 cm in length (Iglésias et al., 2010). Mating is thought to occur inshore in early spring, after which point females move into shallow (25–50 m) water to lay eggs and males may move offshore (Day, 1884; Little, 1995; NatureScot, 2021). During this time, individuals are thought to follow a predominately benthic lifestyle, feeding on a variety of prey, including crustaceans, teleosts and elasmobranchs (Steven, 1947; Wheeler, 1969).

The movement ecology of flapper skate is poorly understood, but several studies have examined their vertical distribution and depth preferences (Neat et al., 2015; Pinto et al., 2016; Thorburn et al., 2021). Modelling suggests a preference for depths from 100–300 m in close proximity to the coast (Pinto et al., 2016). Within the LStSJ MPA, Neat et al. (2015) reported a daily depth range of 50–180 m for three tagged individuals. More recently, Thorburn et al. (2021) aggregated data from multiple studies to examine long-term (seasonal and ontogenetic) variation in depth use in terms of how well the MPA covers skate depth preferences. They showed that skate used depths from 1–312 m but core depth ranges (20–225 m) varied seasonally and across size classes, with shallow-water (25–75 m) use increasing in winter, especially by large females. This pattern did not appear to be driven by temperature, but other drivers of depth use were not investigated. However, only two studies have used longitudinal vertical movement time series to examine individual-specific trends in vertical movement and their drivers (Wearmouth and Sims, 2009; Pinto and Spezia, 2016). These studies suggest that skate may exhibit depth-specific periodic trends in relation to tidal, diel and lunar cycles, but the small number of analysed individuals (n = 4–6) limits current understanding of individual-specific trends in vertical movement across ecological timescales.

The aim of this chapter is to characterise the vertical movements of flapper skate in relation to environmental cycles and individual characteristics. There are two objectives:

A. Depth use—to characterise trends in depth and the roles of individual characteristics and environmental conditions as drivers of these trends.

B. Vertical activity—to characterise trends in vertical activity and the roles of individual characteristics and environmental conditions as drivers of these trends.

2. Methods

2.1. Study site

Off the west coast of Scotland, the LStSJ MPA is situated in a complex bathymetric environment that encompasses shallow areas (< 50 m deep), glacially over-deepened basins and channels up to 290 m deep (Chapter Two; Howe et al., 2014). In surveyed regions, muddy sediments are widespread, while coarser, rockier sediments are found over smaller areas (Chapter Two; Boswarva et al., 2018). Tidal ranges vary by 3–4 m with the spring and neap tides (Chapter Two). At any one time, spatial variation in tidal elevations is typically less than 1 m but can reach up to 2.5 m in specific areas. Daylight hours are very similar across the area at any one time, extending from a minimum of eight hours in winter to nearly 20 hours in summer (Chapter Two). Peak variation in sea water temperature occurs between March (~6 °C) and September (~16 °C), with the upper 100 m experiencing 1–2 °C of vertical stratification during the summer and autumn (Chapter Two). Salinity in the upper layers (0–34.5 psu) is strongly associated with proximity to sources of freshwater input, which skate seem to avoid, but remains relatively stable elsewhere (Chapters Two–Three). The flow regime is complex, dominated by winds and tidal currents that interact with the bathymetry and incised coastline (Chapter Two).

2.2. Tagging

Forty-five skate were captured, tagged and released in three locations within the MPA in 2016–17 (Figure 1). Skate were captured using baited angling lines with barbless hooks, measured and sexed (Chapter Two). Star Oddi milli-TD archival tags were programmed to record pressure (depth), to a resolution of 0.24 m and an accuracy of 4.77 m, and temperature (°C), to a resolution of 0.032 °C and an accuracy of 0.1 °C, every two minutes (Chapter Two). Tags were attached externally, via two stainless steel pins through the leading edge of the left wing, and secured on a padded housing. Data from archival tags were recovered from recaptured skate whose tags were removed and returned. For these individuals, maturation status (immature, mature) was defined using a model for maturation with total length (Chapter Two) (Iglésias et al., 2010). In all cases, the predicted maturation status was unambiguous.

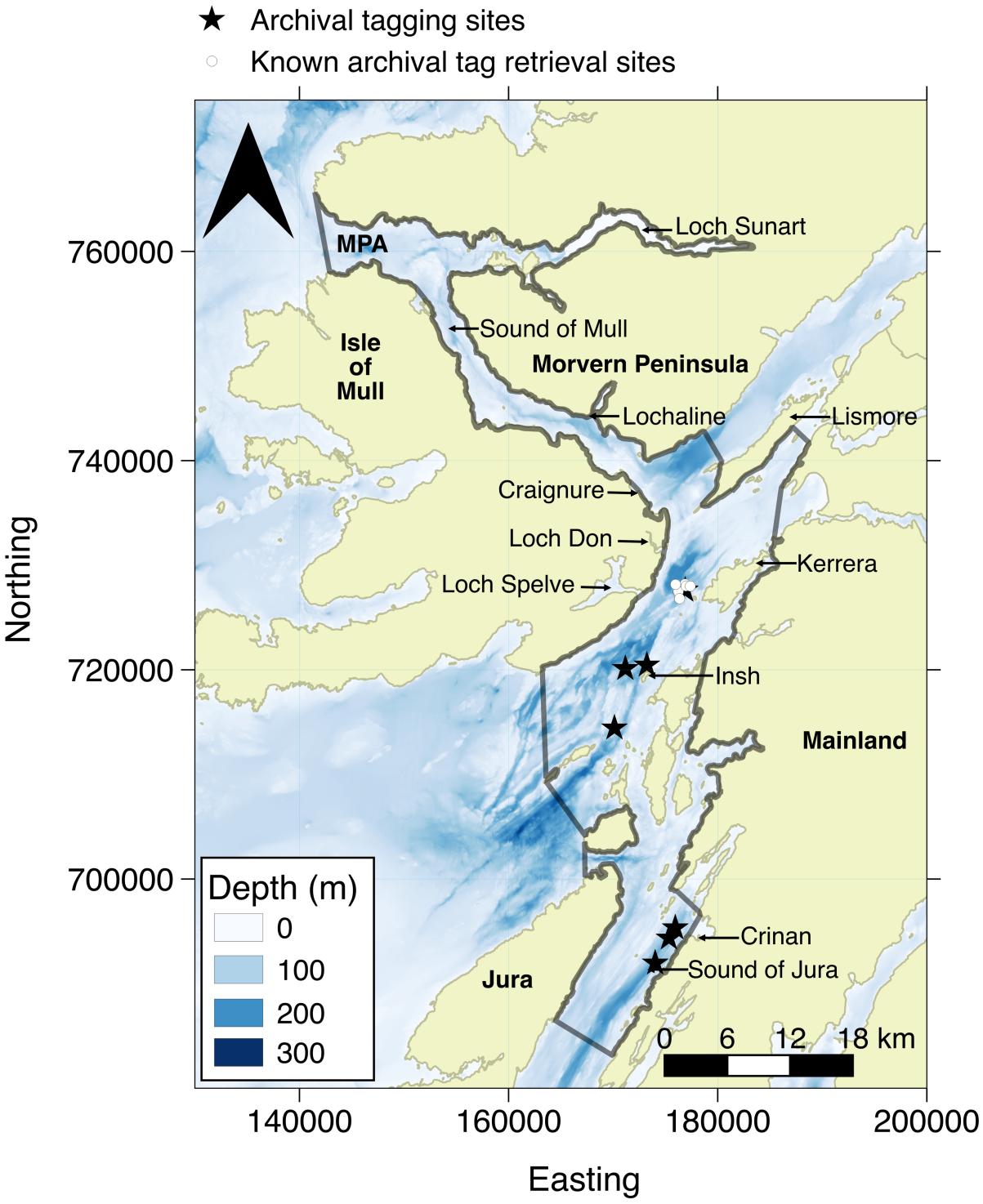

Figure 1. The study site. The grey envelope marks the Loch Sunart to the Sound of Jura Marine Protected Area. Points mark archival tag deployment/retrieval sites. The bathymetry is shown at mixed 5 m and one arc-second resolution, with high-resolution data from Howe et al. (2014) shown where available and lower resolution data from Digimap shown elsewhere (Chapter Two). Background Ordnance Survey map © Crown copyright and database rights [2019] Ordnance Survey (100025252).

2.3. Data processing

Data processing, visualisation and modelling were implemented in R, version 4.0.2 (R Core Team, 2020). The Tools4ETS package was written to facilitate this process (Chapter Two; Lavender, 2020c). For recovered time series, depth was calculated from pressure via pressure/1.01626 (Chapter Two). Vertical activity was calculated as the difference in depth between sequential observations. To focus on undisturbed vertical movements, data in a window around angling events that lasted until midnight on the day of angling were filtered from the time series (Chapter Two).

2.4. Environmental cycles

Tidal, diel, lunar and seasonal cycles were considered as putative periodic environmental drivers of vertical movement. Tidal elevations (m) were extracted from predictions made every 15 minutes for Oban by POLTIPS-3 v.3.6.0.0/13 and linearly interpolated to two-minute time steps. Diel cycles were parameterised with a metric of solar light levels or as diel period (day/night), depending on the model formulation (see §2.6–2.7). For the former, sun angle (degrees above the horizon) was calculated for Oban at each time step using the suncalc package (Thieurmel and Elmarhraoui, 2019). For the latter, 'day' was defined as the time between sunrise and sunset, and 'night' as the time between sunset and sunrise, evaluated at Oban, using suncalc. Thermal stratification was considered as an alternate predictor for diel cycles but not implemented because data exploration indicated diel cycles in vertical movement over winter (when thermal stratification was minimal). Lunar phase (rad) was calculated for each time step using the lunar package (Lazaridis, 2014). Seasonal trends were parameterised in terms of photoperiod (hours between dawn and dusk on each day). Lengthening and shortening days with the same photoperiod were distinguished using a factor ('photoperiod direction') for the direction of change in photoperiod. While there are other correlated drivers of seasonal trends, such as temperature, photoperiod is the least variable across the study site and the most strongly associated with diel cycles through solar light levels (Chapter Two). Furthermore, recent work suggests that depth use is not driven by temperature over seasonal timescales (Thorburn et al. 2021). The expression of these covariates at Oban assumes that skate remained around this area over their time at liberty and that the values of the covariates remained relatively stable across this area at any one time, which is supported by analyses of passive acoustic telemetry data (Chapter Three) and environmental conditions (Chapter Two).

However, other meteorological and hydrodynamic variables that were considered as candidate drivers of vertical movement were not included in models given more substantial variability over space and the uncertain locations of individuals (Chapter Two).

2.5. Exploratory data analysis

Depth time series for each individual were examined visually at multiple temporal scales and in relation to covariates using the Visualise Time Series interactive application in the prettyGraphics package to examine evidence for any relationships between vertical movement and environmental cycles (Lavender, 2020a). Functional principal components analysis (FPCA) was used to compare the structure and shape of observed time series (Ullah and Finch, 2013; Wang et al., 2016), via the fda package (Ramsay et al., 2020). Under this approach, smooth functions are used to describe the shape of individual time series and FPCA is applied to these functions to examine their similarities and differences. This approach was applied to all individuals with sufficient data for each month from 17th March 2016 until 17th February 2017, during which time observations were always available for at least five individuals. For each one-month period, individual time series were represented using 4th order B-splines with 1,000 basis functions. FPCA was then applied to the smoothed time series and PC scores were visualised to examine how time series differed within and between life-history categories (immature/mature males/females) (see Appendix §1.1).

2.6. Depth models

Signal processing techniques (Shepard et al., 2006; Subbey et al., 2008), generalised additive models (GAMs) (Wood, 2017) and Markov switching autoregressive models (Pinto and Spezia, 2016) were considered as analytical approaches for the investigation of vertical movement in relation to periodic environmental variables and individual characteristics (Chapter One). GAMs were chosen because they balance flexibility with accessibility but, despite their familiarity to ecologists (Pedersen et al. 2019), there are relatively few demonstrations of their use in the elasmobranch movement literature. In contrast, signal processing techniques have been widely applied but tend to be used qualitatively (Shepard et al., 2006; Subbey et al., 2008), while the model developed by Pinto and Spezia (2016) requires discrete covariates, commercial software libraries and specialist expertise (Chapter One).

GAMs were fitted to depth time series for each individual to investigate relationships between depth and environmental cycles. The female (1547) with the longest time series (772 days) was taken as an example individual for model development. A five-stage protocol was implemented via the Tools4ETS (Lavender, 2020c) and mgcv (Wood, 2017) packages:

A. **Thinning.** Depth time series were thinned to reduce serial autocorrelation.
B. **$AR0_{DP}$ model fitting.** An initial model of (thinned) depth observations in relation to environmental cycles was fitted. This model did not include an autocorrelation structure and is termed the '$AR0_{DP}$ model'.
C. **AR1 estimation.** The autoregression order 1 (AR1) parameter was estimated from the autocorrelation function (ACF) of the model's residuals.
D. **$AR1_{DP}$ model fitting.** The initial model was re-fitted using the estimated AR1 parameter to capture residual serial autocorrelation. This model is termed the '$AR1_{DP}$ model'.
E. **Inference.** Using the $AR1_{DP}$ model, model smooths, predictions and residual diagnostics were examined.

The first step was to thin the individual's depth time series to reduce serial autocorrelation (A). Thinning was implemented by selecting every 30^{th} observation (accounting for breaks in the time series due to the removal of data around recapture events), since this degree of thinning was sufficiently large to reduce autocorrelation while sufficiently small to not influence model smooths.

An initial Gaussian additive model (the '$AR0_{DP}$ model') was fitted to the thinned depth observations in relation to smooth functions of tidal (height), diel (sun angle), lunar (phase) and seasonal (photoperiod) cycles (B). Tidal elevation was included to account for temporal changes in water depth and to test the hypothesis that vertical movement differs either side of slack tide. A three-way interaction between sun angle, photoperiod and photoperiod direction was included to examine DVM in relation to solar light levels with changes in day length. Following previous results (Wearmouth and Sims, 2009; Peklova et al., 2014; Pinto and Spezia, 2016; Humphries et al., 2017), it was hypothesised that skate would occupy deeper depths during the day when solar light levels are higher. Weaker, more concentrated DVM was expected in summer when nights are shorter and brighter. The incorporation of photoperiod direction in this term allowed the interaction to differ depending on the direction of change in photoperiod. An interaction between sun angle and lunar phase was also included to examine

lunar cycles and test the prediction of this hypothesis that DVM will weaken with increasing moonlight.

The model was implemented using the `bam` function in the mgcv package, which is optimised for big data (see Appendix §1.2.1) (Wood et al., 2015, 2017; Wood, 2017). Tidal elevation, sun angle and photoperiod were implemented with cubic regression splines. Lunar phase was implemented using a cyclic spline, with boundary knots at (0, 2π). Interactions were modelled using tensor smooths. The γ parameter was set to 1.4 to limit overfitting. A basis dimension of k = 10 was sufficient (according to the k-index diagnostic) for most model terms, while k = 5 x 5 was sufficient for interacting terms.

An AR1 correlation structure was used to capture residual serial autocorrelation (see Appendix §1.2.1). To incorporate an AR1 structure, the AR1 parameter was estimated from the ACF of the residuals from the $AR0_{DP}$ model (C). The model was refitted with the estimated AR1 parameter (becoming the '$AR1_{DP}$ model') (D). The final model of depth (*DP*) was:

$$DP_t \sim N(\mu_{DP\,t}, \sigma^2_{DP}) \quad (1)$$

$$\mu_{DP_t} = \alpha + s(tide_t) + te(sun_t, photoperiod_t, direction_t) + te(sun_t, lunar_t) + \hat{\rho} e_{t-1}$$

where $tide$ refers to tidal elevation, sun refers to sun angle, $photoperiod$ refers to the photoperiod, $direction$ refers to the direction of change in photoperiod and $lunar$ refers to lunar phase. α is the model intercept, s is a smooth function, te are tensor product interactions, $\hat{\rho}$ is the AR1 parameter, e refers to residuals and *t* indexes observations.

While a Gaussian likelihood is a convenient option that can be suitable for depth time series (Pinto and Spezia, 2016) and is the only option supported by `bam` for AR1 models, transformation of the response and alternative likelihood formulations were also explored using the flexibility provided by a random effects parameterisation of smooths via the `gamm` function in mgcv (Wood, 2017), GAMs for location, scale and shape (GAMLSS) (Rigby and Stasinopoulos, 2005) and flexible Bayesian approaches (Bürkner, 2017, 2018). However, these model formulations either failed to fit using available routines or else were much more computationally demanding and offered no compensatory benefits in terms of improved model fit. Consequently, alternative model formulations and fitting routines were not pursued further.

Following model fitting, model smooths, predictions and diagnostics were analysed for the $AR1_{DP}$ model using standard mgcv functions. Posterior simulation was used to quantify the magnitude of covariate effects (see Appendix §1.2.2) (Wood, 2017). Expected values of the response (depth) were simulated from the model at contrasting values for covariates of interest (such as low versus high values of tidal elevation), with other covariates fixed at appropriate values. Posterior distributions generated for contrasting values were compared, with the median difference in simulated depths between these values taken as a measure of effect size.

For all subsequent individuals with sufficient data (n = 17), the same protocol (A–E) was followed to generate a set of '$AR1_{DP}$ models' that were analysed in the same way. Models with an identical structure were fitted to enable comparisons among individuals, although the term for photoperiod direction was dropped if there were insufficient data. Using the set of models, ensemble-average effect sizes (for example, the average expected change in depth between low and high values of tidal elevation across all individuals) were estimated for each covariate, by summarising pooled posterior simulations from all individuals, to support graphical interpretation of model predictions (see Appendix §1.2.3). In all cases, ensemble averages overlapped with the posterior distributions from multiple models. FPCA was used to examine how estimated smooths varied in shape among individuals, by representing smooths as B-splines and then applying FPCA to those functions, as described for the observed time series (see Appendix §1.2.4).

2.7. Vertical activity models

For modelling, the total, absolute vertical activity in day/night, averaged over the duration (hours) of each period, was taken as a response variable (VA, mhr^{-1}). This representation of vertical activity increased the signal to noise ratio in each time interval, improved the normality of the response and reduced data volume, while accounting for the effect of diel duration on total absolute vertical activity. For each individual, VA was modelled in relation to diel period (day/night), lunar phase, photoperiod and photoperiod direction, by fitting an '$AR0_{VA}$ model' to the VA time series, estimating the AR1 parameter and then fitting the '$AR1_{VA}$ model', defined below:

$$VA_t \sim N(\mu_{VA_t}, \sigma^2_{VA}) \quad (2)$$

$$\mu_{VA_t} = \alpha + \emptyset_t \delta_{period_{night}} + s(lunar_t, period_t) + s(photoperiod_t, period_t \times direction_t) + \hat{\rho} e_{t-1}$$

where α is the model intercept; $\delta_{period_{night}}$ is the difference in intercept at night; $\emptyset_t$ is an indicator variable which takes a value of 1 when $period_t$ is night and 0 otherwise; and $period \times direction$ is a factor that distinguishes both diel period and photoperiod direction. As for the depth time series, 'AR1$_{VA}$ models' fitted to each individual were then analysed using standard mgcv functions, posterior simulation and FPCA (see Appendix §1.3). Alternative data representations, variable transformations, likelihoods and correlation structures were also explored, but none of alternative modelling options were better than this initial model and are not discussed further.

3. Results

3.1. Archival time series

Archival time series, comprising 4,337,193 observations, were successfully recovered from 21 skate (six immature females, nine mature females and six mature males) (Table 1, Chapter Two). After processing, 3,908,294 observations remained. Time series spanned 3–772 (median = 164) days, with three time series lasting 100–200 days, two lasting 200–300 days and eight (from six females and two males) longer than 300 days. For modelling, the time series for two mature females (1525 and 1526) and one immature female (1552) were insufficient in duration and dropped.

3.2. Exploratory data analysis: visual inspection of the time series

Individuals used a wide depth range within 0–311.82 (median = 115.47) m (Figures 2 and S1–3). Vertical activity was generally low (median = 0.004 ms^{-1}) but ranged from 0.00–1.13 ms^{-1}. Over seasonal timescales, individuals exhibited marked variation in vertical movement and consistent patterns were difficult to identify (Figures 2 and S1–3). Almost all individuals ranged extensively in depth (Figure 2A) but most also used narrow depth ranges over prolonged periods lasting from weeks to months (Figure 2B). There was clear evidence for repeated movements to/from a narrow range of depths. Repetition was most noticeable over daily–weekly timescales and lasted for prolonged periods in four immature females (1538, 1509,

1522 and 1558), two mature females (1512 and 1507) and three mature males (1511, 1520 and 1523) (Figures 2C and S1–3). In general, vertical movement was more restricted in spring and summer, when individuals tended to use deeper water, compared to autumn and winter, when higher vertical movement was associated with increased use of shallower water (Figure 2A–C). Over shorter timescales, individual time series were extremely variable, with periods of relative stasis, sometimes lasting more than one week, punctuated by high vertical activity (Figure 2D). For most individuals, there were times when vertical movements coincided with diel cycles, but this pattern appeared to be irregular through time and varied within and among individuals (Figure 2E).

Individual time series consistently emerged as distinct in monthly FPCAs (Figure S4). In each case, the variation among time series was relatively difficult to characterise effectively with few dimensions, with first and second PCs explaining 37–57 and 14–34 % of variation respectively. There was no evidence for strong similarities within life-history categories at any time; however, there were relatively few individuals within each category.

3.3. Exploratory data analysis: correlations between depth and covariates

Exploratory analysis suggested relationships between depth, sun angle and photoperiod (Figure S5) but not tidal elevation or lunar phase. Most individuals used depths from near the surface (< 25 m) to greater than 200 m in both day and night throughout the year. However, depth at night was shallower on average, especially in autumn and winter when the median difference in depth between day and night was 75 m. This seasonal difference appeared to be driven by fewer visits to the shallowest depths (< 25 m) during the middle of the day, alongside fewer visits to depths beyond 200 m, in autumn and winter.

Table 1. Summary of skate recaptured with archival tags. For each individual, the tag deployment date, site, ID, sex, total length, maturation status and time at liberty are shown.

Dep. Date	Dep. Site	ID	Sex	TL (cm)	MS	Time at liberty (days)
2016-03-15	Kerrera	1538	F	155	Immature	491
2016-03-17	Kerrera	1509	F	135	Immature	399
2016-03-16	Kerrera	1522	F	160	Immature	398
2016-03-14	Kerrera	1533	F	155	Immature	208
2016-03-13	Insh	1558	F	174	Immature	76
2016-03-13	Insh	1552	F	185	Immature	20
2016-03-15	Kerrera	1547	F	208	Mature	772
2017-04-19	Crinan	1519	F	218	Mature	711
2017-04-19	Crinan	1502	F	216	Mature	678
2016-03-17	Kerrera	1512	F	213	Mature	118
2016-03-03	Kerrera	1574	F	203	Mature	98
2016-03-17	Kerrera	1507	F	206	Mature	62
2016-03-15	Kerrera	1539	F	201	Mature	45
2017-04-19	Crinan	1525	F	201	Mature	14
2016-03-16	Kerrera	1526	F	206	Mature	3
2016-03-16	Kerrera	1548	M	196	Mature	401
2016-03-16	Kerrera	1518	M	198	Mature	371
2016-03-14	Kerrera	1536	M	188	Mature	223
2016-03-17	Kerrera	1511	M	196	Mature	164
2016-03-16	Kerrera	1520	M	190	Mature	119
2016-03-16	Kerrera	1523	M	193	Mature	71

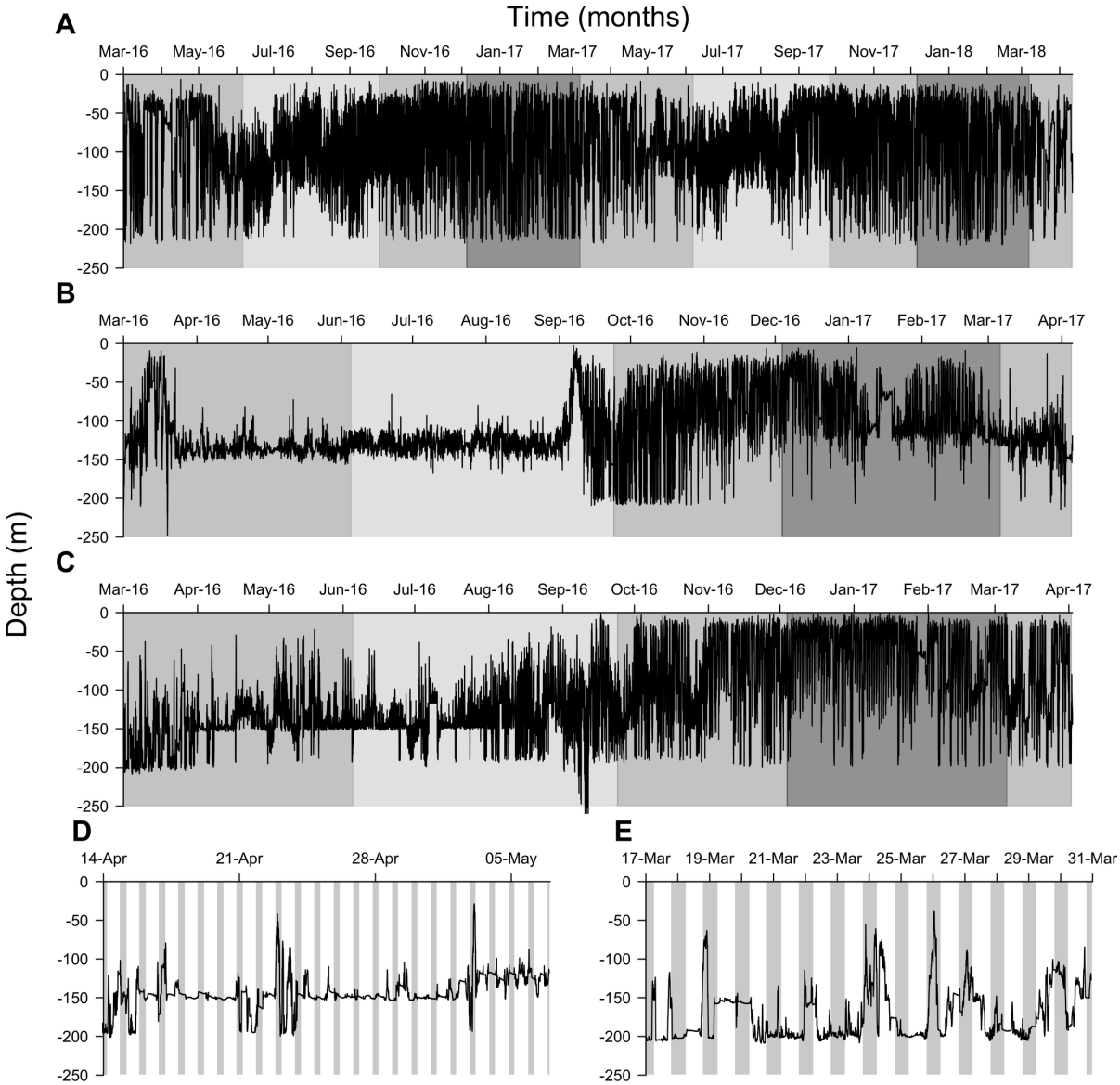

Figure 2. Example vertical movement time series for five individuals. **A**, 1547; **B**, 1548; **C**, 1522; **D**, 1533; and **E**, 1574. **A–D** illustrate distinct long-term patterns, including high vertical activity, prolonged periods of low vertical activity, repeated movements around a central depth and seasonality. The background shading distinguishes the seasons. **D–E** illustrate short-term patterns, including (**D**) periods of stasis interspersed with high vertical activity and (**E**) irregular diel cycles. The background shading distinguishes day (light) from night (dark).

3.4. Depth models

An additive model of depth in relation to tidal, diel, lunar and seasonal cycles for individual 1547 estimated statistically significant effects for all smooth terms (Figure 3, Table S1). The small, positive effect of tidal elevation on depth was consistent with the rise and fall of the tides (Figure 3A). Sun angle had a clear influence on both tensor smooths (Figure 3B–D).

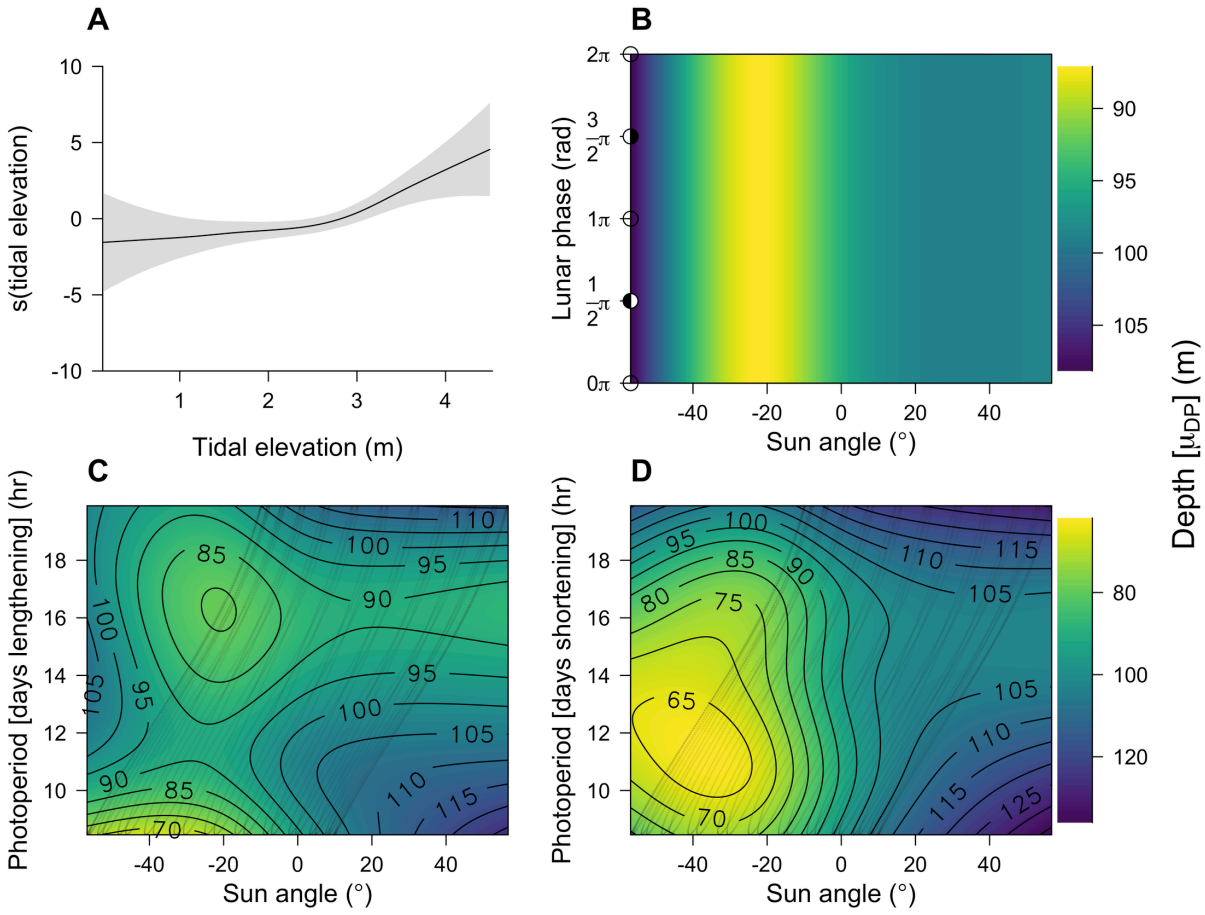

Figure 3. Smooths from the additive model of depth (DP) in relation to environmental cycles for female 1547. A, tidal elevation; **B**, sun angle x lunar phase; **C**, sun angle x photoperiod (for lengthening photoperiod); and **D**, sun angle and photoperiod (for shortening photoperiod). In **A**, the smooth of tidal elevation (the expected change in depth) is shown by the black line with 95 % pointwise confidence bands. (The relationship is centred so that the confidence bands solely reflect uncertainty in the smooth and not the overall mean.) In **B–D**, the expected depth (μ_{DP}) for specific combinations of explanatory variables is shown, with other variables fixed where necessary at the following values: tidal elevation = 2.50 m, lunar phase = 0π radians, photoperiod = 13.22 hours and photoperiod direction = 'lengthening'. In **B**, lunar phase is shown in radians; 0π, π/2, π and 3π/2 refer to the new moon, first quarter, full moon and last quarter respectively (see y axis). In **C–D**, expected depths are defined by lower colour bar and marked by 5 m contours. Diagonal stripes mark observed combinations of sun angle and photoperiod.

The sun angle x lunar phase interaction was driven by a strong diel pattern throughout the lunar cycle (Figure 3C). Even at night, lunar phase did not appear to have influenced depth. However, the estimated effect of sun angle changed over the course of the year (Figure 3C–D). In winter, around the winter solstice (photoperiod = 8.46 hours), there was a clear diel pattern with movement from shallower water (~75 m) at night to deeper water (~120 m) during the day (Figure 3C). The diel cycle weakened over spring and broke down almost entirely in summer.

By the summer solstice (photoperiod = 19.89 hours), the expected depth was deepest and remained deep throughout most of the day (Figure 3C). After the summer solstice, the expected depth remained deep (~120 m) over both day and night (Figure 3D). In autumn, the diel pattern resumed relatively rapidly, strengthening in winter. The deviance explained by this model was 13 % (Table S1). There were some issues with model diagnostics (Figure S6) but these were not improved by any of the alternative model formulations that were implemented.

The relationships between depth and environmental cycles for individual 1547 were borne out for other individuals, despite substantial intra-specific variation (Figure 4). There was a consistently small, positive effect of tidal elevation. Across all posterior simulations, the median difference in depth between the lowest and highest tides was 5.05 m with a median absolute deviation (MAD) of 7.01 m; however, differences from -3.60–26.26 m were supported (Figure 4A). In general, sun angle was positively associated with depth (Figure 4B–C). This effect was strongest in winter (low photoperiod) when the median difference between selected low and high sun angles (-40.42 and 26.93° respectively) was 24.46 ± 26.99 m. However, there was considerable variation among individuals in the strength and shape of this pattern, with limited associations (< 10 m change) between sun angle and depth for four individuals (e.g., 1509 and 1520), moderate associations (10–50 m change) for 11 individuals (e.g., 1502, 1511) and strong associations (> 50 m change) for two mature females and one mature male (1507, 1509 and 1536) (Figures 4B and S7). The diel pattern was weaker in summer when the median difference in depth between low and high sun angles (-10.14 and 57.01°) was 9.37 ± 12.34 m and there were no strong associations between depth and sun angle (Figures 4C and S7). There was no evidence that lunar phase substantially influenced the depth of any individual over extended periods during the night or day (Figure 4D–E). Similarly, depth was only weakly associated with photoperiod on average, with depths on the longest day 8.73 ± 20.79 m and 22.42 ± 36.04 m deeper than when the photoperiod was shorter (13.22 hours) earlier or later in the year respectively (Figure 4E–F). However, while the effect of lengthening photoperiod was small (< 10 m change) for 10 individuals (e.g., 1502 and 1507), for five individuals (e.g., 1511 and 1522) the effect was moderate (10–50 m) and for one mature female and two males (1507, 1536 and 1518) the shift in the mean depth with photoperiod exceeded 50 m. Individual 1536 exhibited the strongest contrast in the expected depth between low and high photoperiods (Figure S8). For 13/18 individuals with sufficient data, these effects mirrored the effect of declining photoperiod as the days shortened, although there were two exceptions (female 1519 and male 1536) (Figure S8). In all cases, variation in the shape of these smooths appeared

principally attributable to individual-level, rather than group-level, variation, with no well-defined clusters attributable to life-history category visually apparent from FPCA scores (Figure S9).

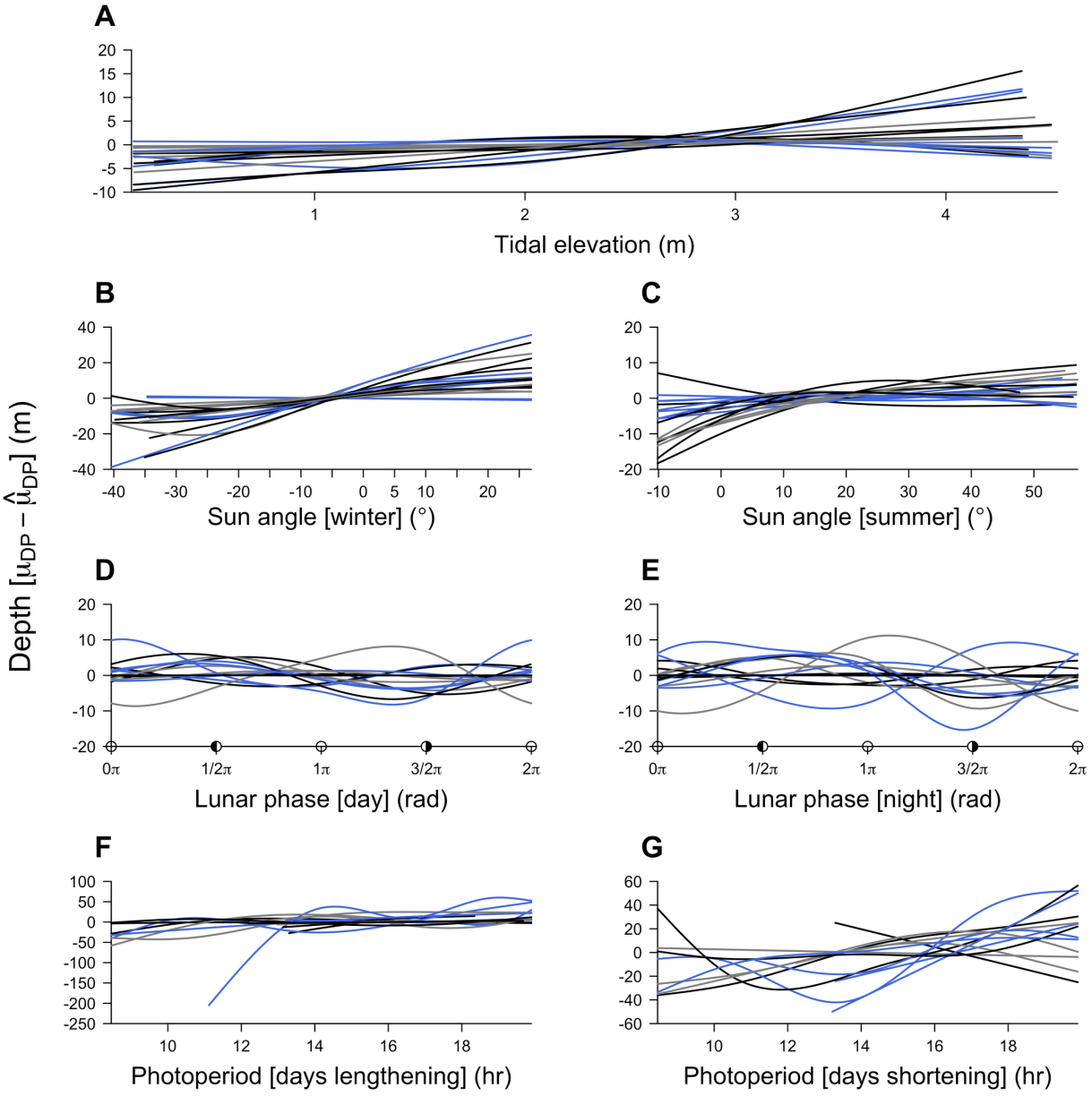

Figure 4. Predicted changes in depth across environmental variables for all individuals. Each panel shows the change in the expected depth (μ_{DP}) of each individual, centred (to enable comparisons among individuals) by the mean of the function for that individual ($\hat{\mu}_{DP}$), given **A**, the effect of tidal elevation; **B–C**, the effect of sun angle (**B**) near the start of the year (2016-03-17) versus (**C**) the summer solstice (2016-06-20); **D–E**, the effect of lunar phase during the day (sun angle: 25.00°) versus the night (sun angle: -25.00°); and **F–G**, the effect of photoperiod under lengthening and shortening day length. Each line shows predictions for an individual in grey (immature females), black (mature females) or blue (mature males) across the range of values for that variable experienced by that individual. Unless otherwise stated, predictions reflect tidal elevation = 2.50 m, sun angle = 0.00°, lunar phase = 0π radians, photoperiod = 13.22 hours and photoperiod direction = 'lengthening'.

The deviance explained by individual models ranged from 4–56 (median = 29) %. There was a moderate correlation between deviance explained and the duration of individuals' time series (Spearman's rank correlation, $rs = 0.49$, $n = 18$, $p = 0.04$). As for individual 1547, there were similar issues with model diagnostics for most individuals.

3.5. Vertical activity models

VA ranged from 2.05–177.08 (median = 74.79) mhr^{-1}. For individual 1547, the estimated mean VA during the day was 69.42 ± 1.27 mhr^{-1} (standard error) (Table S2). The model of VA for this individual suggested that VA was marginally higher at night (difference = 3.80 ± 0. 87 mhr^{-1}, $t = 4.37$) (Figures 5A, Table S2). During the day, VA was approximately 2–5 mhr^{-1} higher during the new and full moon, around spring and neap high tides, but there was no clear effect of lunar phase at night (Figure 5B). In both day and night, posterior simulation showed that VA was 9.09–57.75 mhr^{-1} (2.5^{th}–97.5^{th} quantiles) lower at higher photoperiods (Figure 5C–D). For example, with increasing photoperiod from low values when the individual was tagged (8.46 hours) to the summer solstice (19.89 hours), the median decrease in VA during the day was -47.93 ± 6.66 mhr^{-1} MAD—a 69 % decrease relative to the mean VA during the day across the time series. Moving towards the winter solstice, VA during the day partially increased, but less substantially (17.70 ± 6.72 mhr^{-1}). This model explained 26 % of the deviance and standard residual diagnostics were acceptable (Figure S10, Table S2).

However, relationships between VA and environmental cycles varied among individuals (Figure 6). The distribution of estimated differences between VA at night versus the day was right-skewed, ranging from -1.58–10.93 (median = 3.66) mhr^{-1} or -5–36 % of daytime levels (Figure 6A). Half of the individuals showed little (≤ 5 mhr^{-1}) difference in VA between night and day, but higher (> 5 mhr^{-1}) VA at night was clearly evident for others, especially females 1509 and 1538 for which VA at night was > 25 % higher than daytime levels. Lunar phase was not strongly related to VA (Figure 6B–C). Nine individuals showed weakly cyclical relationships between lunar phase and VA, with VA approximately 2–5 mhr^{-1} deeper at new moon and/or full moon, but these effects were small. The effect of photoperiod differed among individuals (Figure 6D–G). For most (13/18) individuals (e.g., 1502 and 1507), daytime VA declined with photoperiod as the days lengthened; in nine cases (e.g., 1509 and 1519), only weakly (< 10 mhr^{-1}); in eight cases (e.g., 1502 and 1507) moderately (10–50 mhr^{-1}); and in one case (1536) substantially (> 50 mhr^{-1}) (Figures 6D and S11). In contrast, two individuals (1523

and 1533) increased VA by more than 10 mhr^{-1} with photoperiod, while three remaining individuals (1520, 1539, 1538) did not show consistent patterns (Figure S11). In general, these patterns mirrored the expected changes in depth after the summer solstice as photoperiod declined, although there were three exceptions (1502, 1536 and 1548) (Figure S11). In all cases, trends in day and night were similar (Figure 6E and G). There was no clear evidence for clusters in the change in VA with environmental variables by life-history category from visual inspection of FPCA scores (Figure S12). Deviance explained ranged from 0–77 (median = 21) % and was moderately correlated with the duration of individuals' time at liberty (Spearman's rank correlation, $rs = 0.46$, $n = 18$, $p = 0.05$). Model diagnostics were reasonable.

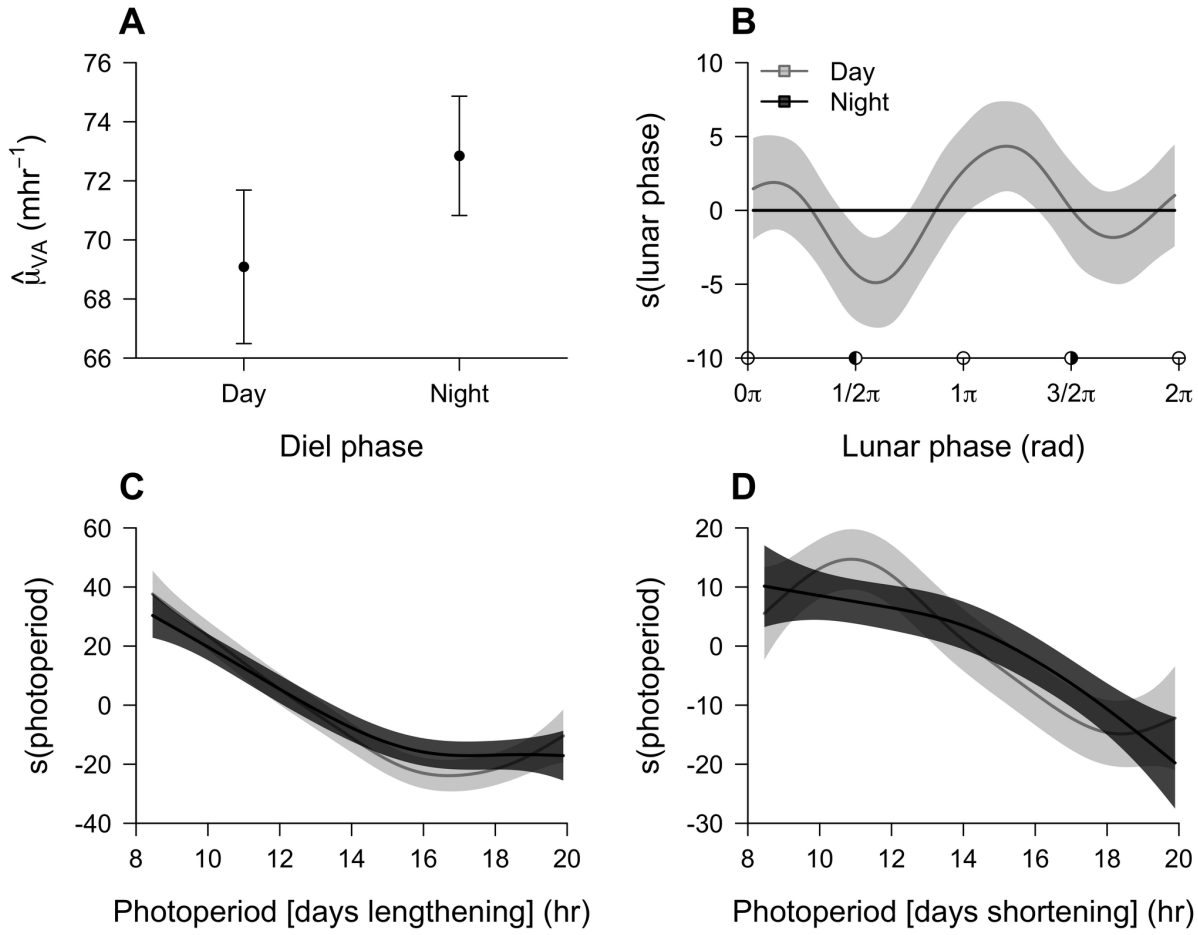

Figure 5. Parametric terms and smooths from the additive model of total absolute vertical activity per hour (VA) in relation to environmental cycles for female 1547. A, diel phase; **B**, lunar phase; **C**, diel phase x photoperiod (lengthening); and **D**, diel phase x photoperiod (shortening). In **A**, the mean expected VA in day/night is shown, surrounded 95 % confidence intervals. In **B–D**, smooths (which depict the expected change in VA with covariates) are shown for day (light grey) and night (dark grey) and surrounded by 95 % pointwise confidence bands. (Smooths are centred so that the confidence bands solely reflect uncertainty in the smooths and not the overall mean.) In **B**, lunar phase is shown in radians: 0π, π/2, π and 3π/2 refer to new moon, first quarter, full moon and last quarter respectively (see x axis).

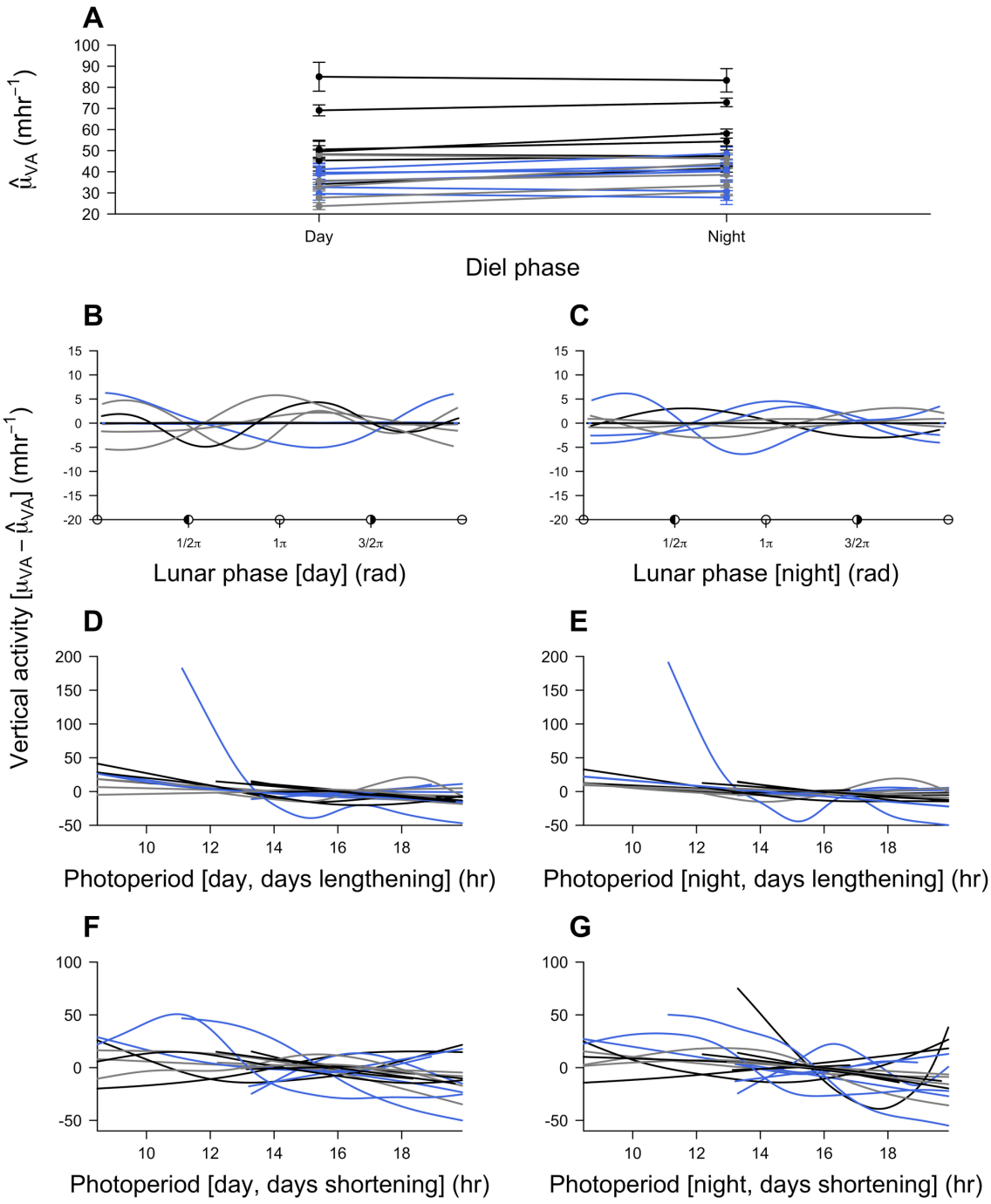

Figure 6. Predicted changes in total absolute vertical activity per hour (VA) across environmental variables for all individuals. Each panel shows the expected VA (μ_{VA}) of each individual given **A**, the effect of diel phase; **B–C**, the effect of lunar phase during (**B**) day versus (**C**) night; **D–E**, the effect of photoperiod, when the day length is increasing, during (**D**) day versus (**E**) night; and **F–G**, the effect of photoperiod when the day length is shortening, during (**F**) day versus (**G**) night. In **A**, the connected points and error bars mark the mean expected VA ± 95 % confidence intervals for each individual. In **B–G**, the lines represent the expected VA for each individual (centred, to enable comparisons, by mean of the function, $\hat{\mu}_{VA}$, for each individual) in grey (immature females), black (mature females) or blue (mature males) across the range of values for that variable experienced by each individual. Unless otherwise stated, predictions are shown for diel phase = 'day'; lunar phase = 0π radians; and photoperiod = 13.22 hours.

4. Discussion

This chapter describes the vertical movements of a Critically Endangered benthic elasmobranch and demonstrates the influence of some environmental cycles alongside individual variation for understanding these movements over daily and seasonal timescales. Vertical movement patterns span periods of low vertical activity that are sometimes restricted around core depths for weeks or months as well as periods of higher vertical activity, providing additional evidence that benthic species may switch between periods of low and high vertical activity over extended timeframes (Kawabe et al., 2004; Wearmouth and Sims, 2009; Humphries et al., 2017). The results further develop the evidence base for vertical movements in relation to environmental cycles in benthic species (Wearmouth and Sims, 2009; Peklova et al., 2014; Humphries et al., 2017), with a significant portion of the variation in flapper skate movement structured over daily and seasonal scales. For flapper skate, this chapter provides the first evidence that interactions between environmental cycles affect vertical movement, extending previous research that has mainly focused on the independent effects of specific predictors (Wearmouth and Sims, 2009; Pinto and Spezia, 2016). In line with recently documented seasonal trends in average depth use (Thorburn et al., 2021), there is a substantial seasonal shift in diel vertical movement patterns, with normal DVM and elevated nocturnal vertical activity weakening in summer when skate tend to be less active and spend more time in deeper water. This points towards solar light as an important correlate of vertical movements and may have implications for their vulnerability as bycatch in other parts of their range (Bendall et al., 2017), as noted for Arctic skate (*Amblyraja hyperborea*) (Peklova et al., 2014) and other elasmobranchs (Gilman et al., 2019; Siskey et al., 2019; Arostegui et al., 2020). There is also evidence for a role for individual variation in movement, alongside ontogenetic segregation in depth use documented previously (Thorburn et al., 2021).

At short timescales, tidal cycles are associated with vertical movement in many elasmobranchs (Ackerman et al., 2000; Wetherbee et al., 2007; Carlisle and Starr, 2009, 2010). Yet proposed explanations for this behaviour typically hinge on the benefits of movement into shallow water with the incoming tide, either for foraging (Ackerman et al., 2000; Carlisle and Starr, 2009, 2010) or predator avoidance (Wetherbee et al., 2007; Knip et al., 2011a; Guttridge et al., 2012), which are unlikely to apply to flapper skate that tend to occupy deeper water (Wearmouth and Sims, 2009; Neat et al., 2015; Thorburn et al., 2021). In agreement with this view, this chapter indicates that the vertical movements of tagged skate were not strongly influenced by tidal

cycles at the resolution considered here. Nevertheless, tidal cycles may influence skate movement in other ways. For example, reports from recreational anglers of higher catches around slack tide suggest that tidal cycles may be associated with fine-scale changes in foraging behaviour. Alongside evidence for tidal influences on the movements of other elasmobranchs (Ackerman et al., 2000; Whitty et al., 2009; Campbell et al., 2012) and benthic flatfish (Metcalfe et al., 1990; Scott et al., 2016), this suggests that the influence of the tides would benefit from further investigation, particularly with accelerometry (Gleiss et al., 2013; Coffey et al., 2020).

DVM is widely documented among elasmobranchs, especially sharks (Carey et al., 1990; Andrews et al., 2009; Arostegui et al., 2020). While flapper skate occupied a range of depths over the diel cycle, this chapter adds to the evidence base for DVM in flapper skate (Wearmouth and Sims, 2009; Pinto and Spezia, 2016) and benthic predators more widely (Sims et al., 2006; Gorman et al., 2012; Harrison et al., 2013; Peklova et al., 2014; Cott et al., 2015; Humphries et al., 2017). Notwithstanding variation, tagged individuals tended to occupy shallower depths and exhibit slightly higher vertical activity levels at night, especially in the autumn and winter when depths were 75 m shallower on average at night. However, at short temporal scales the timing of DVM often appeared irregular, as noticed for other skate species (Peklova et al., 2014; Humphries et al., 2017).

In other elasmobranchs, including batoids, DVM has been attributed to thermoregulation and bioenergetic efficiency (Matern et al., 2000; Sims et al., 2006; Papastamatiou et al., 2015) and foraging (Andrews et al., 2009; Arostegui et al., 2020). For flapper skate, given elevated DVM in winter when vertical temperature gradients are minimal, a role for foraging seems most likely. Studies of common skate suggest a broad, largely benthophagous diet comprising benthic invertebrates, cephalopods, teleosts and elasmobranchs (Steven, 1947; Wheeler, 1969). Switches between different foraging modes for these prey over a diel cycle are one potential driver of DVM. Low activity, opportunistic predation is common in benthic fish (Smale et al., 1995, 2001; Fouts and Nelson, 1999). For flapper skate, depth and vertical activity time series suggest that this behaviour may predominate in deeper water in daytime, perhaps in a central place away from disturbances. However, in the closely related common blue skate the consumption of demersal and pelagic teleosts, especially by larger individuals, points towards the use of more active predation strategies too (Brown-Vuillemin et al., 2020). Coupled with lower vertical activity in deeper water during the day, an increase in the prevalence of more

active predatory behaviour at night could contribute towards DVM since nocturnal movement from deep habitats will naturally cause movement into shallower water. Cyclical trends in prey availability are likely to influence these movements, as noted for other elasmobranchs (Carey et al., 1990). For example, within the LStSJ MPA it is likely that skate respond to the diel rhythms of prey such as Norway lobster (Aguzzi and Sardà, 2008; Thorburn et al., 2021) and sandeels (Winslade, 1974). For example, in shallower (30–70 m) parts of the MPA, the increased availability of sandeels to flapper skate at night in winter, when sandeels remain buried in sand, may contribute towards the emergence of DVM at this time. However, while these examples illustrate some of the potential ecological dynamics that may affect skate, further data on skate diets, prey availability and movement are required to examine fully the links between foraging and movement (Chapter Seven).

Alongside foraging, the avoidance of unfavourable near-surface conditions that prevail in the day and/or summer may influence DVM. There is some support for the hypothesis that skate avoid higher light levels near the surface through seasonal changes in DVM. The absence of appreciable effects of moonlight appears to conflict with this hypothesis, but may be partly attributable to the impact of cloud cover. Other factors, such as seasonal sexual activity, have been postulated as explanations for seasonal trends in DVM (Carey et al., 1990), but their influence remains unknown for flapper skate.

In addition to seasonal patterns in DVM, there was evidence for repeated movements to and from a central depth over daily–weekly timescales for prolonged periods. These kinds of movements have been documented in several skate species (Humphries et al., 2017), but the longevity of the repeated movements illustrated here is exceptional. The pattern is reminiscent of central foraging or refuging behaviour (Humphries et al., 2017). In other taxa, this is typically associated with movement to and from resting, recovery or nesting sites (Boyd et al., 2014; Patrick et al., 2014; Papastamatiou et al., 2018b; Brost et al., 2020). In flapper skate, this behaviour is particularly obvious in immature females, which suggests that it is not associated with reproduction. More reasonable hypotheses include a spatiotemporal separation in the times or areas that are most suitable for resting versus foraging, which may result from the need to avoid intra-specific competition with large individuals (Humphries et al., 2016; Papastamatiou et al., 2018b); territorial behaviour (Martin, 2007); or personality traits, with ‘shy’ individuals remaining in familiar territory (Patrick and Weimerskirch, 2014).

Individual characteristics, such as personality (Jacoby et al., 2014), age (Grubbs, 2010) and sex (Wearmouth and Sims, 2010), can certainly be important drivers of movement. The results presented here demonstrate a significant role for individual variation, with distinctive patterns such as the extensive vertical movements of female 1547 and the prolonged period of low vertical activity of male 1548 not shared by other tagged individuals. One emerging explanation for this kind of variation is personality (Jacoby et al., 2014; Patrick and Weimerskirch, 2014). Individual variation in small samples may also be attributable to characteristics that appear to be associated with specific individuals but are in fact shared more widely among individuals in a population. For example, in this chapter, there was no clear evidence for clustering in individuals' responses to environmental cycles by life-history category, which may partly reflect relatively small sample sizes for each life-history category, especially if differences only emerge at specific times (e.g., in association with reproduction). For this reason, future research would benefit from more data for all life-history categories, especially juveniles, for which data remain sparse (Chapter Seven).

Despite evidence for structure in the vertical movements of flapper skate, unsurprisingly a notable portion of variation remained unexplained by models. The absence of space from models is a significant limitation for benthic organisms: while models implicitly assume that individuals are 'free' to respond to changes in the value of covariates, benthic movements are restricted by bathymetry (Humphries et al., 2017). Building on an earlier study of flapper skate movement inferred from passive acoustic telemetry (Chapter Three) and the analyses of vertical activity developed here, approaches that integrate these two sources of information to reconstruct possible movement pathways over the seabed would further advance our understanding of the ways in which bathymetry shapes vertical movement (Chapter Six). The roles of oceanographic variables and anthropogenic factors, such as aquaculture farms, that are associated with the movements of other elasmobranchs (Dempster et al., 2005; Schlaff et al., 2014) could be also investigated with improved localisations of individuals, in tandem with new tag deployments and parameters derived from regional hydrodynamic models (Aleynik et al., 2016). However, biotic variables, such as prey movement and competition, are likely to be the primary drivers of movement (Papastamatiou and Lowe, 2012; Schlaff et al., 2014). The lack of information on foraging in particular is a major ecological and conservation knowledge gap, not just for flapper skate but also more broadly (Chapter Seven; Papastamatiou and Lowe, 2012). Coupled with improved estimates of individual space use, new data on these biotic processes should help to explain the complex movement patterns exhibited by flapper skate

and the role of environmental conditions as indirect or direct drivers of these patterns (Chapter Seven).

Statistical innovation will complement this ambition. While GAMs are a sophisticated and flexible modelling approach, a caveat with some of the analyses presented here (particularly the depth GAMs) is the violation of some model assumptions. Within the constraints of available software, the models were forced to assume a gaussian error distribution, homoscedascity and an AR1 correlation structure. Statistical developments offer promise for relaxing these assumptions in the future. For instance, GAMLSS model the mean (e.g., depth), variation (e.g., vertical activity) and the shape of a response under a single framework using a diverse array of distributions (Rigby and Stasinopoulos, 2005). These remain underutilised in ecology, although there are examples (Hudson et al., 2010; Barbini et al., 2018; Secor et al., 2021). While initial exploration of this approach in this chapter did not yield major improvements upon GAMs, a new experimental routine that provides an interface to the fast restricted maximum likelihood `bam` model fitting routine in mgcv (Stasinopoulos et al., 2020), as well as a new package for time series (gamlss.ts) that is currently under development provide opportunities for future research (D. Stasinopoulos, personal communication). Developments to other modelling frameworks would also be beneficial. For instance, the Markov switching autoregressive model developed by Pinto and Spezia (2016) is well suited to time series with complex autocorrelation structures. While the current implementation of this model requires specialist expertise, commercial software and specific discrete covariates, future research is likely to make the approach more accessible to ecologists.

The synthesis of vertical movement time series with statistical modelling has important implications for skate management (Chapter One). For many skate species, bycatch is a major conservation concern (Dulvy et al., 2014; Oliver et al., 2015; Bendall et al., 2017). Most bycatch occurs in bottom trawls with a relatively low headline (Silva et al., 2012). The benthic habit of skate makes them particularly vulnerable to this gear, but vertical movements substantially affect their exposure (Bizzarro et al., 2014; Gilman et al., 2019) and catchability (Kynoch et al., 2015; Bayse et al., 2016). The addition of ‘tickler’ chains to the front of trawls to startle fish from the seabed into nets appears to increase skate bycatch in bottom-trawl fisheries (Kynoch et al., 2015). Consequently, in the LStSJ MPA, their use has been prohibited. The results of this chapter suggest that this measure is likely to have the biggest impact during the day and in summer, when vertical activity is lower. Later in the year, when skate are more

active, tickler chain removal may have less of an impact. However, if higher vertical activity is associated with movement off the seabed, the vulnerability of skate to trawling in autumn and winter may actually be lower, as noted for other species such as spurdog (*Squalus acanthias*) (Ellis et al., 2015). This highlights the need for high-resolution data on the vertical movements of skate in relation to the seabed, which could be provided by accelerometers and sonar tags (Gleiss et al., 2013; Lawson et al., 2015; Coffey et al., 2020). This research is essential for the effective implementation of fisheries management measures and spatial management approaches, such as marine protected areas, designed to achieve reductions in bycatch and improve skate conservation (Siskey et al., 2019).

Appendices

1. Supporting methods

1.1. Functional principal components analysis (FPCA) for observed time series

FPCA was used to examine similarities and differences in the shape and structure of observed depth time series, for each month from March 2016 until February 2017, using the protocol shown below for an example month:

```
#### Define observations
# For each time window, all of the observations from that month
# ... were identified. In order to make the time series comparable,
# ... given breaks in some time series associated
# ... with (re)capture events and variable times at liberty,
# ... only individuals with the most common number of observations
# ... in that month were included in the analysis.
# ... These data were coerced into a matrix, with
# ... one row for each depth observation (two-minute resolution)
# ... and one column for each individual. This matrix is named 'mat'.
# ... FPCA was then performed on this matrix, as shown below.

#### Make B splines
# 1,000 basis functions sufficient to represent
# ... complex time series effectively
n_basis    <- 1000
rng        <- 1:nrow(mat)
bs_splines <- fda::create.bspline.basis(range(rng), n_basis)

#### Create a functional data object using the matrix and B-spline basis
fda_df <- fda::Data2fd(mat, argvals = rng, basisobj = bs_splines)

#### Compare smooths and observations
# Extract necessary objects
```

```
fdobj  <- fda_df
y      <- rng
Lfdobj <- fda::int2Lfd(0)
fdmat  <- fda::eval.fd(y, fdobj, Lfdobj)
# Plot first time series and smooth as an example
plot(y, fdmat[, 1], col = "red")
lines(y, mat[, 1])

#### Implement FPCA
pcs_1 <- fda::pca.fd(fda_df)

#### Visualise FPCA scores
plot(pcs_1$scores)
```

1.2. Depth models

1.2.1. Model fitting

Depth (`depth`) was modelled in relation to tidal elevation (`tide`), sun angle (`sun`), lunar phase (`lunar`), photoperiod (`photoperiod`) and photoperiod direction (`direction`) for each individual (`dst_id`), according to the following protocol shown for individual 1547:

```
#### Flag independent time series
# Here, 'arc_1547' is the observed time series for DST ID 1547
# ... and 'date_time' distinguishes time stamps.
# ... Serially independent time series are defined as those
# ... with breaks longer than the duration between regular archival
# ... observations (i.e., due to the removal of data around
# ... recapture events).
flags <- Tools4ETS::flag_ts(x = arc_1547$date_time,
                            duration_threshold = 2)
# Add flags to dataframe:
arc_1547$start_event    <- flags$flag1
arc_1547$start_event_id <- flags$flag3
```

```
#### Thin time series, accounting for breaks
# Here, we thin the time series by n = 30.
# ... This degree of thinning is sufficiently large
# ... to reduce autocorrelation
# ... while sufficiently small not to influence model smooths.
# ... Further, models fitted to datasets thinned by
# ... lesser/greater amounts confirm that
# ... the results are robust to this choice.
arc_1547 <-
  Tools4ETS::thin_ts(dat = arc_1547,
                     ind = "start_event_id",
                     flag1 = "start_event",
                     first = 1,
                     nth = 30)

#### Define model formula
# For tidal elevation, sun angle and photoperiod,
# ... cubic regression splines are used as these are
# ... more computationally efficient than the default
# ... thin plate regression splines.
# ... For lunar phase, a cyclic spline is required.
fdriver <-
  formula(depth ~
            direction +
            s(tide, bs = "cr", k = 10) +
            te(sun, lunar,
               bs = c("cr", "cc"), k = c(5, 5)) +
            te(sun, photoperiod,
               by = direction,
               bs = c("cr", "cr"), k = c(5, 5))
          )
```

```r
fdriver_knots <- list(lunar = c(0, 2*pi))

#### Model fitting
# The models are fitted using mgcv::bam(),
# ... which is optimised for large datasets.
# This function can incorporate an AR1 correlation structure
# ... for models with a Gaussian likelihood, but the AR1 parameter
# ... must be specified: it is not estimated internally, unlike
# ... other commonly used routines, such as mgcv::gamm(). Therefore,
# ... we will implement the model without an AR1 structure, use this model
# ... to estimate the AR1 parameter, and then re-implement the model
# ... using the estimated AR1 parameter.

## Fit model without AR1 parameter
dat_mod <- arc_1547
mod_ar0 <- mgcv::bam(fdriver,
                     gamma = 1.4,
                     knots = fdriver_knots,
                     data = dat_mod)

## Estimate AR1 parameter
ar1     <- Tools4ETS::estimate_AR1(resid(mod_ar0),
                                   AR.start = dat_mod$start_event,
                                   verbose = FALSE)
## Fit model with AR1 parameter
mod_ar1 <- mgcv::bam(fdriver,
                     gamma = 1.4,
                     knots = fdriver_knots,
                     rho = ar1,
                     AR.start = dat_mod$start_event,
                     data = dat_mod)
```

Model smooths, predictions and diagnostics were examined using standard `mgcv` functions, posterior simulation and FPCA (see below). This process was repeated for each individual.

1.2.2. Posterior simulation for each individual

For each individual, posterior simulation was used to estimate the magnitude of covariate effects. In this process, values of the response (depth) were simulated from the $AR1_{DP}$ model for low and high values of variables of interest (e.g., tidal elevation), using the `simulate_posterior_mu` function in the `Tools4ETS` package (Lavender, 2020c). For each variable of interest, this process generated two 'posterior distributions' for depth (e.g., one for low tidal elevation and one for high tidal elevation), from which a 'posterior distribution' of differences in depth was calculated. The median value of this distribution was taken as an estimate of effect size and the median absolute deviation was taken as a measure of uncertainty. This approach was applied to obtain estimates for the following effects:

- **The effect of tidal elevation.** Depths were simulated and compared for tidal elevation = 0.13 versus 4.53 m (the minimum and maximum tidal elevation experienced in the study site), with sun angle = 0.00°, lunar phase = 0π radians, photoperiod = 13.22 hours and photoperiod direction = 'lengthening'.
- **The effect of sun angle when the photoperiod was short.** Depths were simulated and compared for sun angle = -40.41° versus sun angle = 26.93° (the minimum and maximum sun angle experienced near the start of the year, on 2016-03-17, by which time all but two of the individuals with data were tagged and at a photoperiod experienced by all individuals), with tidal elevation = 2.50 m, lunar phase = 0π radians, photoperiod = 13.22 hours (the photoperiod on 2016-03-17) and photoperiod direction = 'lengthening'.
- **The effect of sun angle when the photoperiod was long.** Depths were simulated and compared as above but with sun angle = -10.14° versus sun angle = 57.01° and photoperiod = 19.89 hours, the values for the summer solstice (2016-06-20). Note that this required limited extrapolation beyond the maximum photoperiod experienced for individuals 1507, 1523, 1539, 1558 and 1574.
- **The effect of lunar phase during the day.** Depths were simulated and compared for lunar phase = 0π (new moon) versus lunar phase = π radians (full moon), with tidal elevation =

2.50 m, sun angle = 25.00° (a daytime value broadly applicable throughout the year), photoperiod = 13.22 hours and photoperiod direction = 'lengthening'.

- **The effect of lunar phase at night.** Depths were simulated and compared as above but with sun angle = -25.00°.
- **The effect of photoperiod when days were lengthening.** Depths were simulated and compared for photoperiod = 13.22 hours versus photoperiod = 19.89 hours, with tidal elevation = 2.50 m, sun angle = 0.00°, lunar phase = 0π radians and photoperiod direction = 'lengthening'.
- **The effect of photoperiod when days were shortening.** Depths were simulated and compared as above, for individuals with sufficient data, but with photoperiod direction = 'shortening'.

As an example, the protocol used to estimate the statistical effect of tidal elevation on depth for a given individual is shown below.

```
# Define 'newdata' for which to simulate values of the response (depth)
nd <- data.frame(tide = c(0.13, 4.53),
                 sun = 0,
                 lunar = 0,
                 photoperiod = 13.21528,
                 direction = "lengthening")

# Simulate values of the response (depth) from the model
# ... Here, 'mod' is the 'AR1DP model' for a specific individual
# ... 'nd' is the newdata dataframe defined above.
post <- Tools4ETS::simulate_posterior_mu(model = mod,
                                         newdata = nd,
                                         return = "full")

# Define the posterior distribution of differences
post_diff <- post[2, ] - post[1, ]

# Summarise the posterior distribution of differences in depth
```

```
# ... as a measure of 'effect size'.
# The median difference in simulated depths between
# ... low/high tidal elevations
stats::median(post_diff)
# The median absolute deviation of the differences
stats::mad(post_diff)
```

However, rather than focusing on estimated effect sizes for each individual, the purpose of this exercise was to generate posterior distributions that could be pooled across individuals, to provide an indicator of 'average' effect size to support graphical interpretation of Figure 4 (see §1.2.3, below).

1.2.3. Posterior simulation across individuals

To estimate the average effect size across all individuals, simulated outcomes from posterior simulation were aggregated across individuals, with the following function, and then summarised.

```
#' @title Simulate the posterior distribution of differences between two
values
#' @description This function calculates the posterior distribution of
differences in simulated outcomes between two values of a variable, holding
other variables constant.
#' @param mods A list of models (one for each individual).
#' @param newdata A 2 x n dataframe that defines the values of the model
covariates at which predictions are required.
#' @return The function returns a numeric vector of differences.

get_posterior_difference <- function(mods, newdata){
  # Create a list of posterior distributions (for each model)
  post <- lapply(mods_depth_ar1, function(mod_ar1){
    # Simulate from the posterior of the model, given newdata
    Tools4ETS::simulate_posterior_mu(model = mod_ar1,
                                     newdata = newdata,
                                     seed = 1L,
```

```
                                        return = "full")
  })
  # Aggregate posterior distributions across individuals
  post <- do.call(cbind, post)
  # Return the distribution of differences between the first two rows
  post_diff <- post[2, ] - post[1, ]
  return(post_diff)
}
```

For example, to summarise the distribution of differences in the expected depth between low and high tide, the following approach was implemented:

```
#### E.g. Simulate depths at low versus high tide
# ... setting sun angle to 0
# ... lunar phase to 0 (new moon)
# ... photoperiod to ~ 13.21 (hours of daylight on 2016-03-17)
# ... photoperiod direction to 'lengthening' (increasing photoperiod),
# ... for mods_depth_ar1
# ... (a list of models with one element for each individual)
nd <- data.frame(tide = c(0.13, 4.53),
                 sun = 0,
                 lunar = 0,
                 photoperiod = 13.21528,
                 direction = "lengthening")
post <- get_posterior_difference(mods = mods_depth_ar1, newdata = nd)

#### Examine frequency distribution of differences
graphics::hist(post)
```

The results of this process were taken to provide an indicator of the average effect size across individuals to support graphical interpretation of model predictions.

1.2.4. FPCA of model smooths

FPCA was used to examine how estimated smooths varied in shape, by representing smooths as B-splines and then applying FPCA to those functions, as demonstrated below for tidal elevation:

```
#### Define data for prediction
# Define a regular sequence of tidal elevations
# ... across the range for that variable
# Hold other variables constant at appropriate values
nd <- data.frame(tide = seq(0.13, 4.53, length.out = 100),
                 sun = 0,
                 lunar = 0,
                 photoperiod = 13.21528,
                 direction = "lengthening")

#### Define centred predictions for each individual in a matrix
# Loop over a named list of model objects ('mods_depth_ar1')...
pred_by_id <- lapply(mods_depth_ar1, function(mod_ar1) {
  # Make predictions from nd
  pred <- predict(mod_ar1, newdata = nd)
  # Centre predictions to focus on the shapes of the smooths
  pred <- as.numeric(pred)
  pred <- pred - mean(pred)
  return(pred)
  })
# Convert to matrix
mat           <- do.call(cbind, pred_by_id)
colnames(mat) <- names(mods_depth_ar1)

#### Make B-splines
# 10 basis functions sufficient to represent smooths effectively
rng        <- 1:nrow(mat)
bs_splines <- fda::create.bspline.basis(range(rng), 10)
```

```
#### Create a functional data object
fda_df <- fda::Data2fd(mat, argvals = rng, basisobj = bs_splines)

#### Compare functions with smooths in FDA
# As shown previously.

#### Implement FPCA
pcs_1 <- fda::pca.fd(fda_df)
```

1.3. Vertical activity models

Following the protocol developed above, the total absolute vertical activity per hour (VA) of each individual was modelled similarly in relation to day/night (diel), lunar phase, photoperiod and photoperiod direction, as shown below for individual 1547.

```
#### Define model formula
# ... The response, VA, is va/diel_duration, where
# ... 'va' is the total (absolute) vertical activity in each diel period
# ... (i.e., day 1, night 1, day 2,..., day n, night n)
# ... and 'diel_duration' is the duration of that period (hours).
# ... Note that since VA is expressed in this way,
# ... there is no need to thin the time series prior to modelling,
# ... unlike in the depth time series models.
fdriver <- formula(va/diel_duration ~
                   diel +
                   s(lunar,
                     bs = "cc", by = diel, k = 10) +
                   s(photoperiod,
                     by = interaction(diel, photoperiod),  k = 10)
                   )
fdriver_knots <- list(lunar_phase = c(0, 2*pi))

#### Fit model without AR1 parameter
# ... Use 'dat_mod', a dataframe with the variables defined above
```

```
# ... for individual 1547
mod_ar0 <- mgcv::bam(fdriver,
                     gamma = 1.4,
                     knots = fdriver_knots,
                     data = dat_mod)

#### Estimate AR1 parameter
ar1     <- Tools4ETS::estimate_AR1(resid(mod_ar0),
                                   AR.start = dat_mod$start_event,
                                   verbose = FALSE)
#### Fit model with AR1 parameter
mod_ar1 <- mgcv::bam(fdriver,
                     gamma = 1.4,
                     knots = fdriver_knots,
                     rho = ar1,
                     AR.start = dat_mod$start_event,
                     data = dat_mod)
```

As for the depth time series, models were fitted to each individual and analysed using standard `mgcv` functions, FPCA and posterior simulation.

2. Supporting tables

Table S1. Coefficient estimates from the additive model of depth in relation to periodic environmental variables for female 1547. Coefficients were estimated from 18,513 observations. The model explained 12.937 % of the deviance. For parametric coefficients, the estimate, standard error, *t*-value and *p*-value are shown. For smooth terms, the effective degrees of freedom, reference degrees of freedom and F statistic and *p*-value are shown.

Parametric coefficients				
Term	***Estimate***	***SE***	***t-value***	***p-value***
(Intercept)	93.463	1.215	76.934	0.000
Photoperiod direction: shortening	0.216	1.757	0.123	0.902
Approximate significance of smooth terms				
Term	***EDF***	***Ref DF***	***F***	***p-value***
s(tidal elevation)	2.718	3.562	4.028	0.005
te(sun angle, lunar phase)	3.840	3.934	19.793	0.000
te(sun angle, photoperiod): photoperiod direction lengthening	8.479	10.783	5.719	0.000
te(sun angle, photoperiod): photoperiod direction shortening	10.678	13.589	4.313	0.000

Table S2. Coefficient estimates from the additive model of total, absolute vertical activity per hour (VA) in relation to periodic environmental variables for female 1547. Coefficients were estimated from 1,543 observations. The model explained 26.164% of the deviance. For parametric coefficients, the estimate, standard error, *t*-value and *p*-value are shown. For smooth terms, the effective degrees of freedom, reference degrees of freedom, F statistic and *p*-value are shown.

Parametric coefficients				
Term	***Estimate***	***SE***	***t-value***	***p-value***
(Intercept)	69.426	1.261	55.073	0.000
Night	3.791	0.868	4.368	0.000
Approximate significance of smooth terms				
Term	***EDF***	***Ref DF***	***F***	***p-value***
s(lunar phase: day)	3.756	8.000	2.032	0.001
s(lunar phase: night)	0.000	8.000	0.000	0.778
s(photoperiod: day, days lengthening)	3.725	4.579	34.011	0.000
s(photoperiod: night, days lengthening)	2.799	3.448	29.637	0.000
s(photoperiod: day, days shortening)	3.844	4.724	9.134	0.000
s(photoperiod: night, days shortening)	2.027	2.508	12.762	0.000

3. Supporting figures

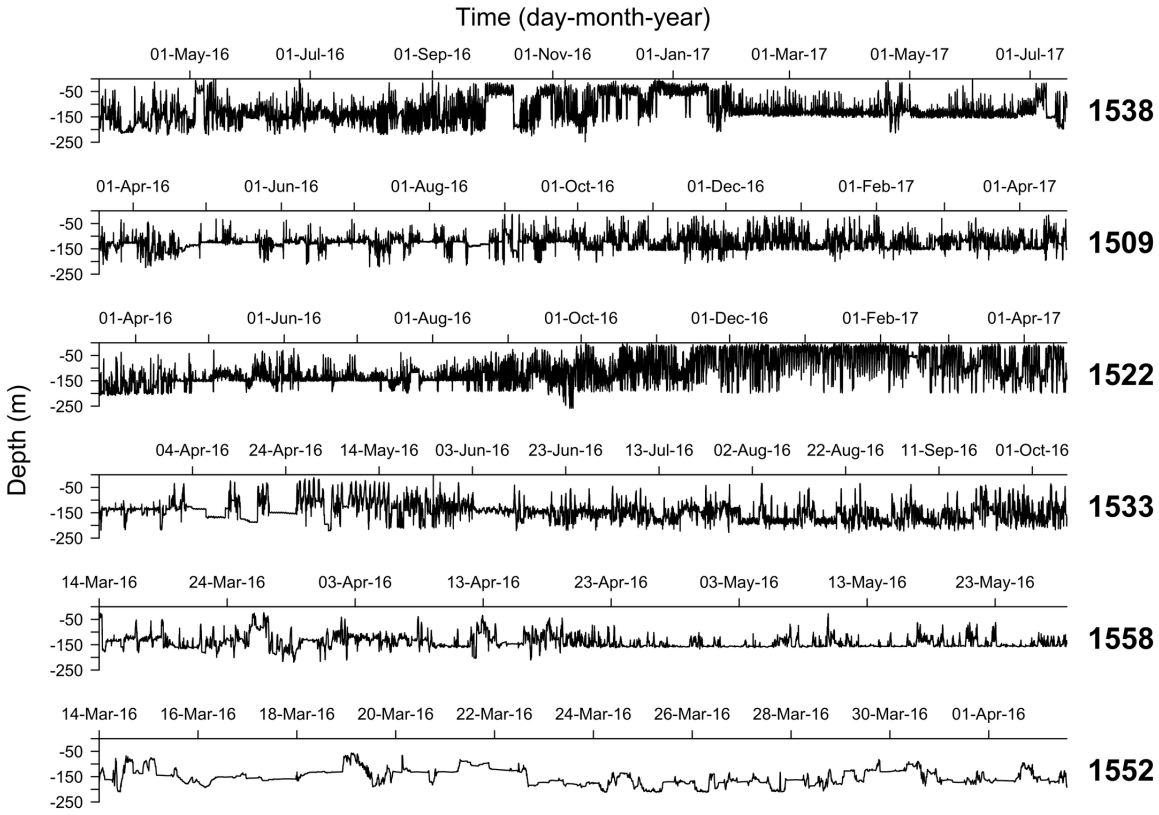

Figure S1. Observed depth time series for immature females. Each panel shows the relationship between depth and time for a specific individual over its time at liberty. Individuals are shown in order of their time at liberty.

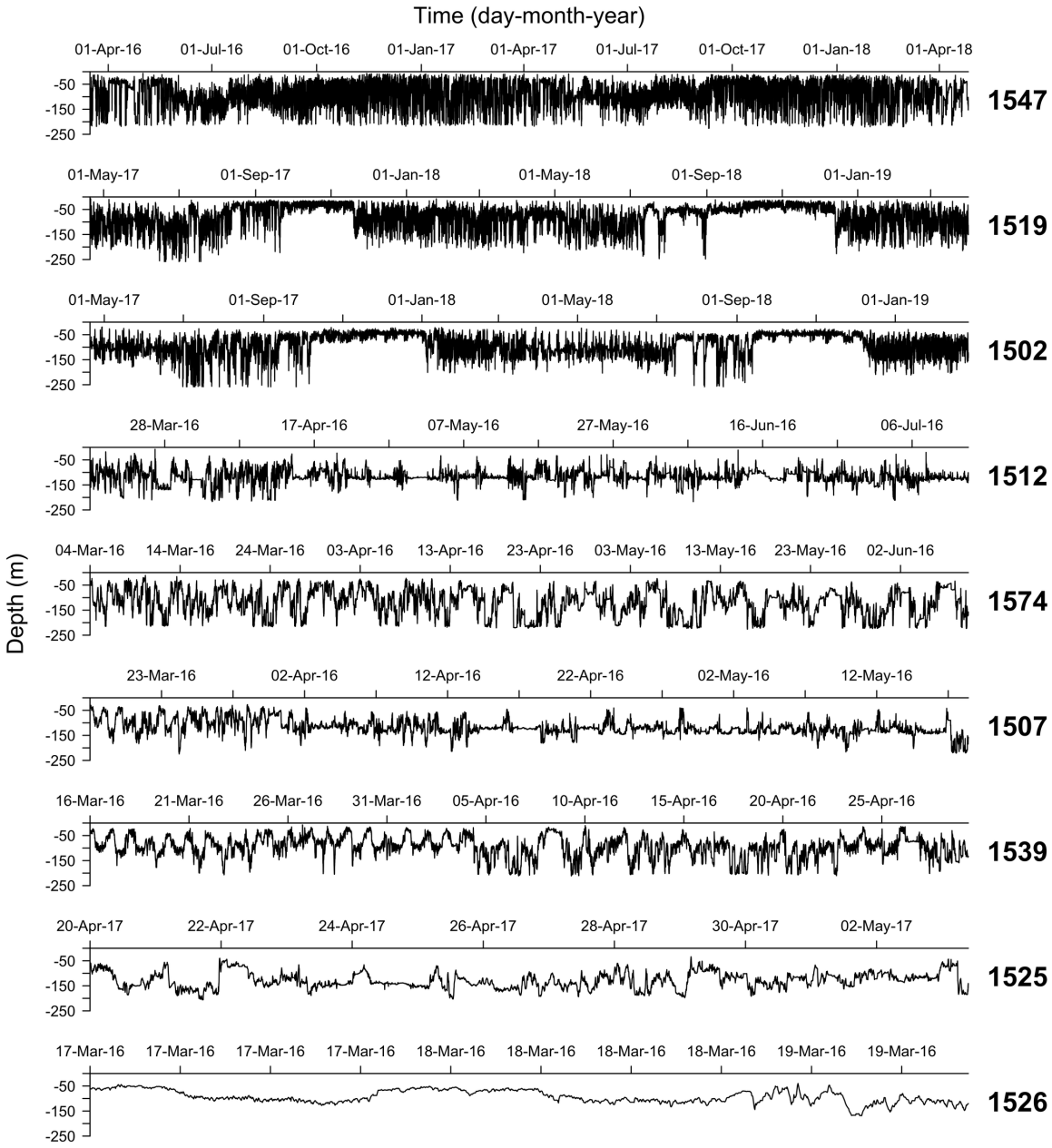

Figure S2. Observed depth time series for mature females. Each panel shows the relationship between depth and time for a specific individual over its time at liberty. Individuals are shown in order of their time at liberty.

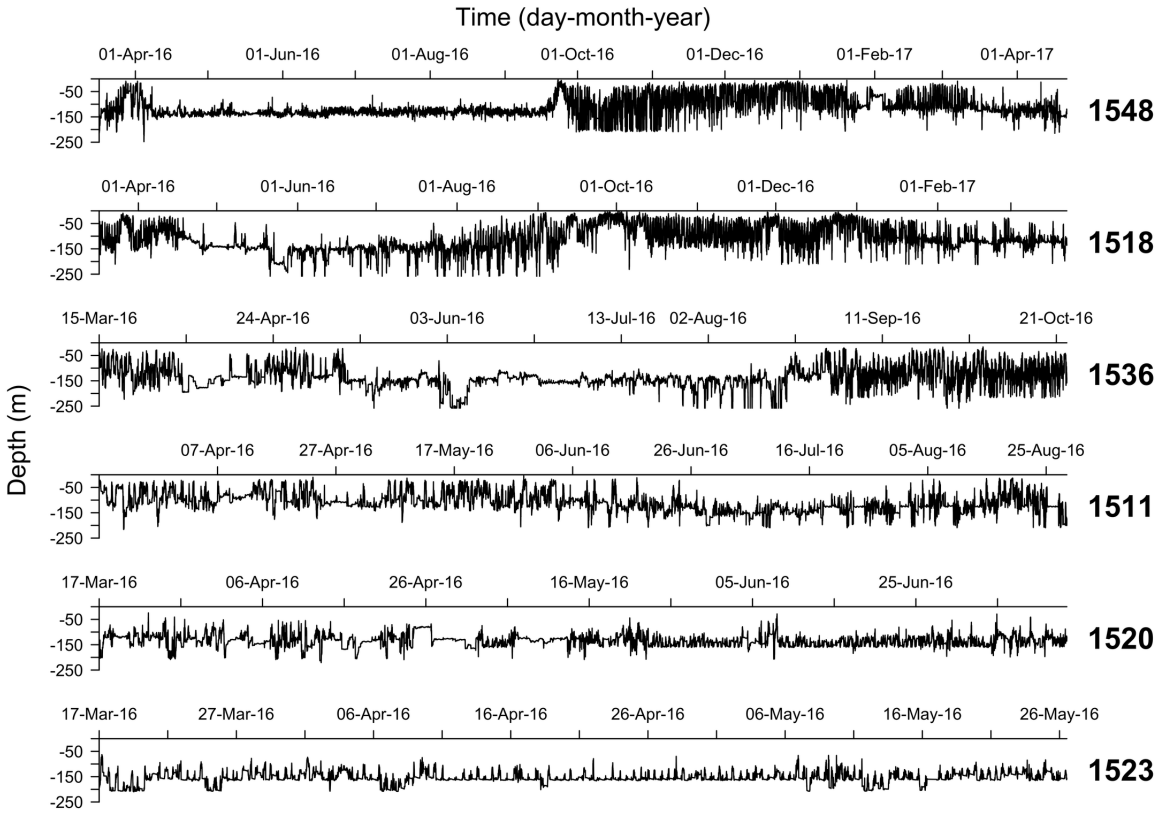

Figure S3. Observed depth time series for mature males. Each panel shows the relationship between depth and time for a specific individual over its time at liberty. Individuals are shown in order of their time at liberty.

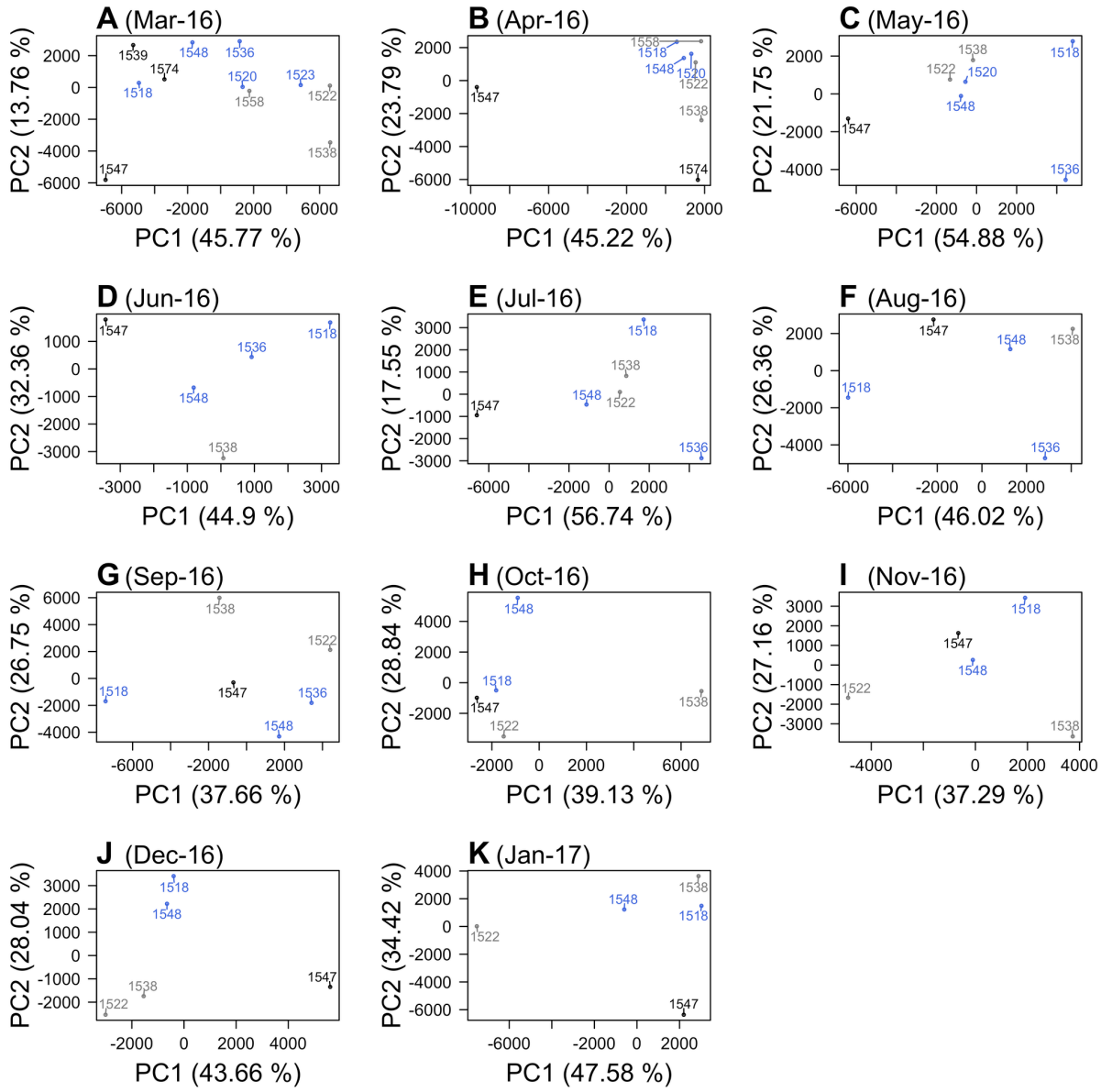

Figure S4. Monthly functional principal component (PC) scores from FPCA of the observed depth time series. Each panel shows, for a given month, for each individual with sufficient data in that month, the score of each individual on the first two PCs, along with the percent of variation explained by each axis. Colours distinguish immature females (grey), mature females (black) and mature males (blue).

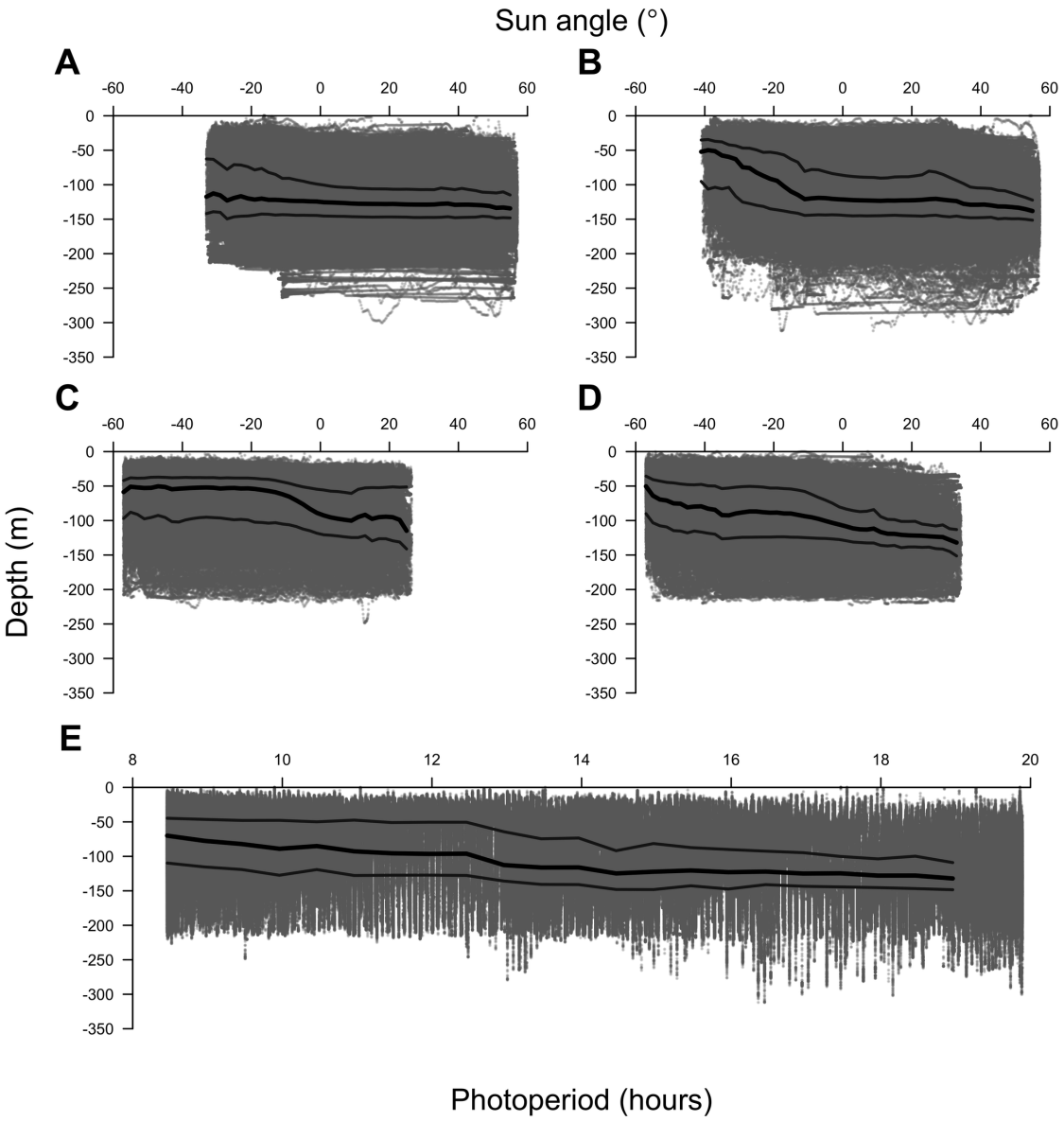

Figure S5. Relationships between depth, sun angle (A–D) and photoperiod (E) across all individuals. In **A–D**, each panel shows the relationship between depth and sun angle for a specific season: **A**, spring; **B**, summer; **C**, autumn; and **D**, winter. In **E**, the relationship between depth and photoperiod is shown over the whole time series. Points mark observations and the thick black line and the surrounding envelope mark the median and the 25th and 75th quantiles of variation in depth for each 2.0° sun angle bin or 0.5 hour photoperiod bin.

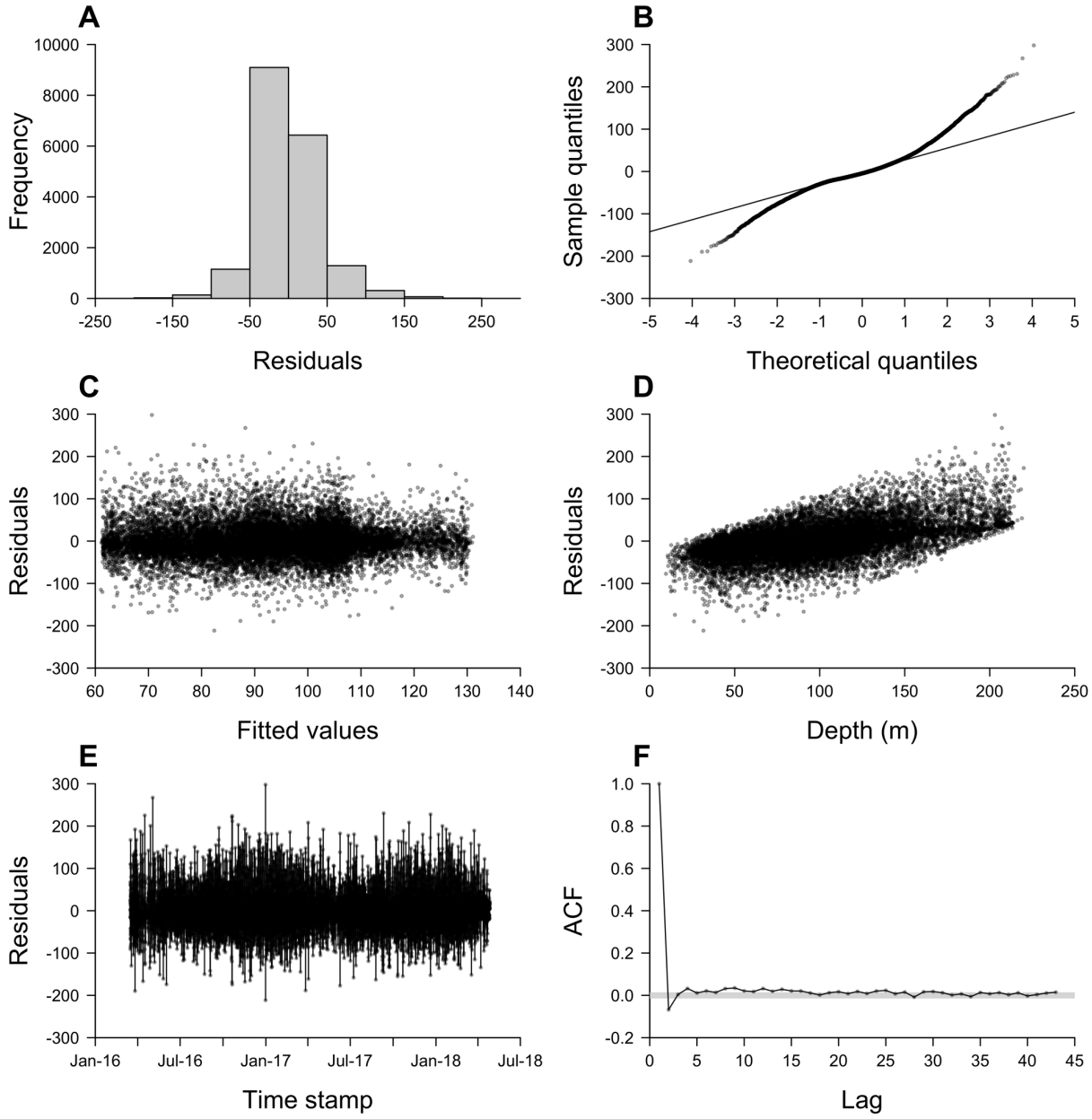

Figure S6. Standard residual diagnostic plots from the additive model of depth in relation to environmental cycles for female 1547. A, a histogram of residuals; **B**, a quantile-quantile plot; **C**, residuals versus fitted values; **D**, residuals versus depth; **E**, residuals versus time stamp; and **F**, the autocorrelation function (ACF) of residuals, with the 95 % confidence intervals for an uncorrelated series of white noise delineated by the grey envelope. In all cases, standardised residuals that are approximately uncorrelated under the correct model are shown.

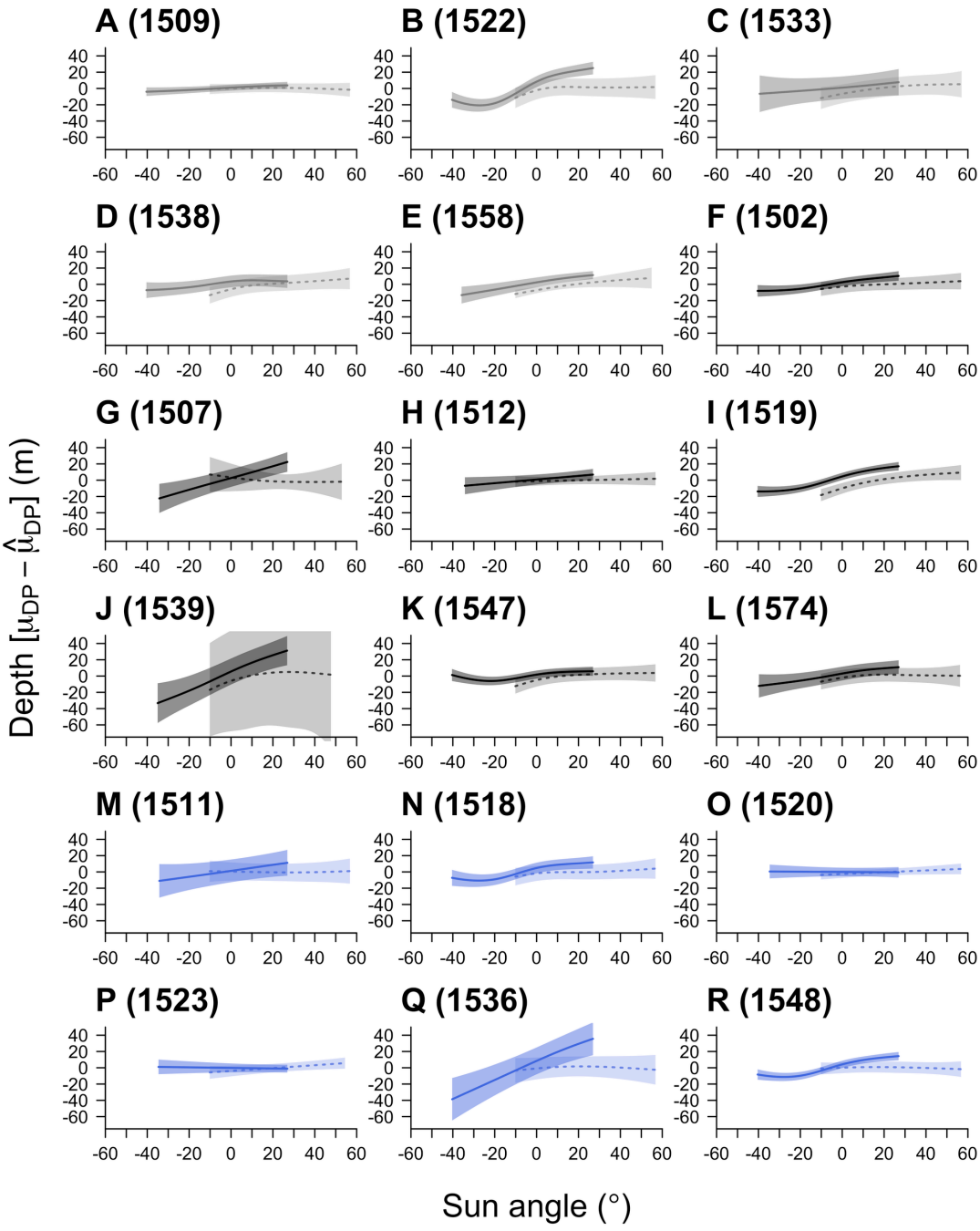

Figure S7. Predictions of the change in depth with sun angle in winter and summer across all individuals. Each panel shows the expected depth (μ_{DP}), centred by the mean ($\hat{\mu}_{DP}$) and surrounded by 95 % pointwise confidence bands, in winter and summer for a single individual, with individuals coloured by population group (immature females, light grey [**A–E**]; mature females, dark grey [**F–L**]; mature males, blue [**M–R**]). Predictions are shown for tidal elevation = 2.50 m, lunar phase = 0π radians, photoperiod = 13.22 (solid line and envelope) or 19.89 (lighter dotted line and envelope) hours and photoperiod direction = 'lengthening'.

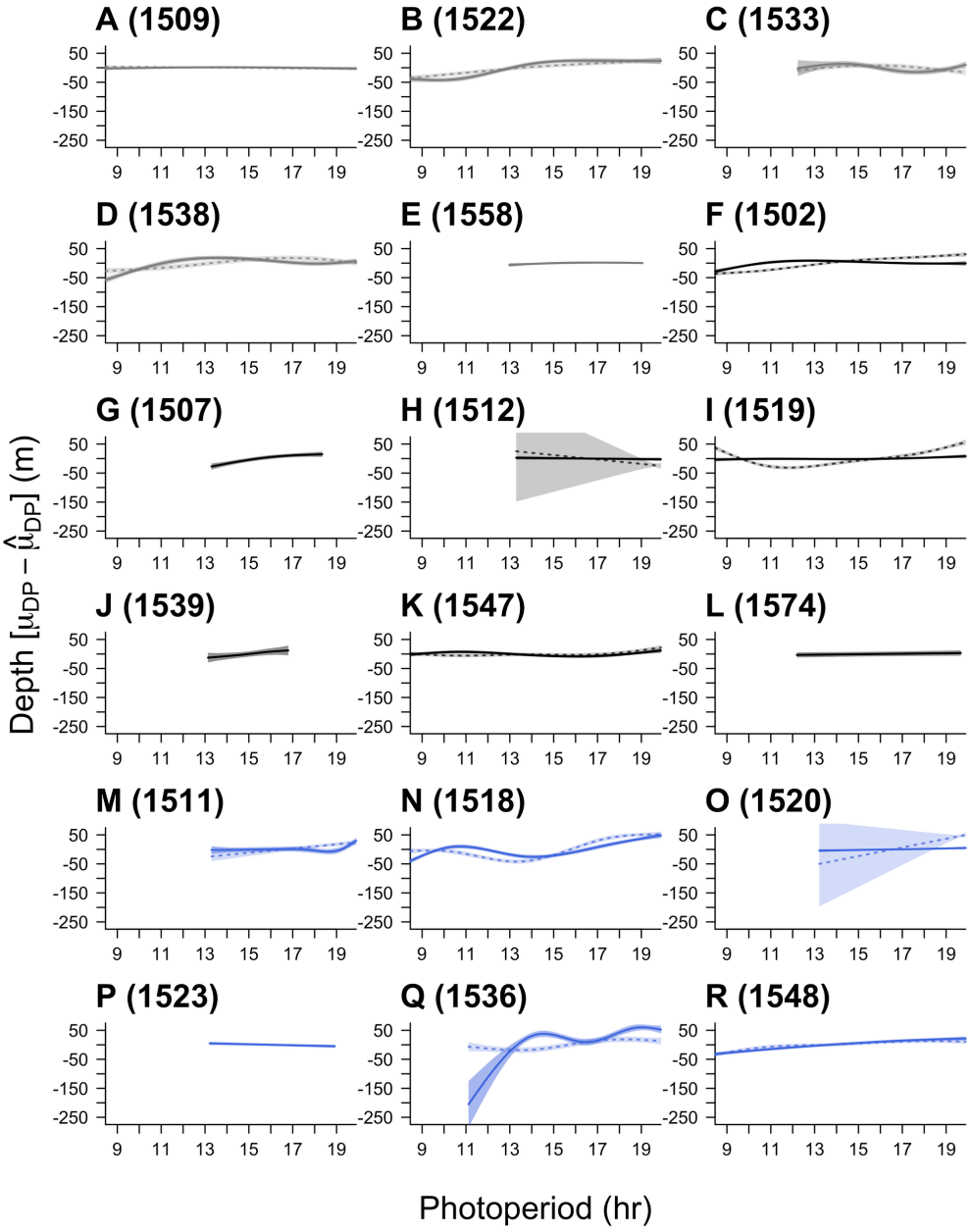

Figure S8. Predictions of the change in depth with photoperiod (lengthening or shortening) across all individuals. Each panel shows the expected depth (μ_{DP}), centred by the mean ($\hat{\mu}_{DP}$) and surrounded by 95 % pointwise confidence bands, for a single individual, with individuals coloured by population group (immature females, light grey [**A–E**]; mature females, dark grey [**F–L**]; mature males, blue [**M–R**]). Predictions are shown for tidal elevation = 2.50 m, lunar phase = 0π radians, sun angle = 0.00°, photoperiod direction = 'lengthening' (solid line and envelope) and, for individuals with sufficient data, photoperiod direction = 'shortening' (lighter dotted line and envelope). Y axis limits are cut at (-275, 75) m to facilitate comparisons among individuals.

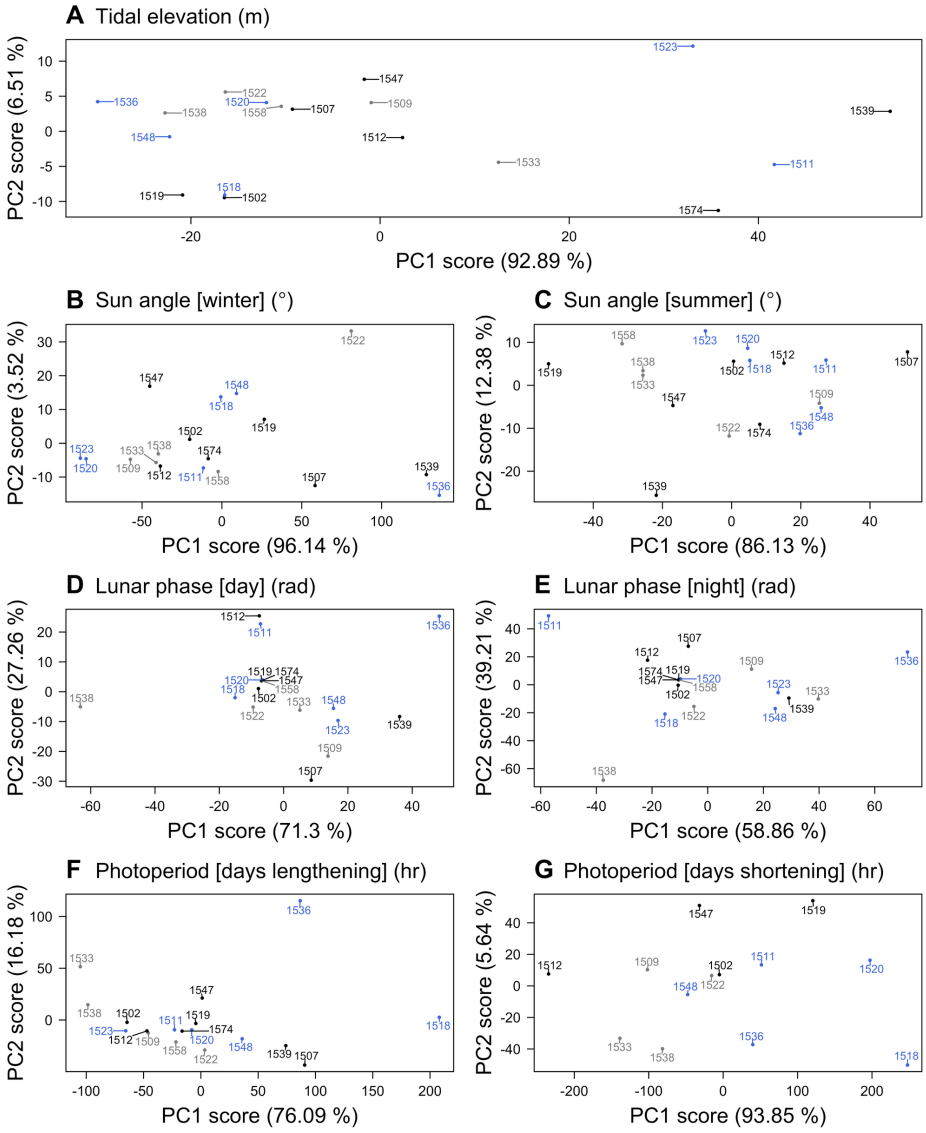

Figure S9. Functional principal component (PC) scores from predictions of the change in depth with environmental cycles across all individuals. Each panel shows the first two PC scores from FPCA of the predicted change in each individual's depth, centred by its mean depth, with change in the following variables: **A**, tidal elevation; **B**, sun angle in winter (photoperiod: 13.22 hours); **C**, sun angle in summer (photoperiod: 19.89 hours); **D**, lunar phase in the day (sun angle: 25°); **E**, lunar phase at night (sun angle: 25°); **F**, photoperiod (lengthening); and **G**, photoperiod (shortening). In each case, PCs are estimated from a B-spline reconstruction of the (centred) predicted change in depth with the change in each variable, while holding other variables constant at the following values: tidal elevation = 2.50 m; sun angle = 0.00°; lunar phase = 0π radians; photoperiod = 13.22 hours; and photoperiod direction = 'lengthening' (unless stated otherwise). Predictions are shown for 18 individuals except in **G**, for which sufficient data were only available for 13 individuals. Note that some FPCA scores are derived from predictions extrapolated by a limited amount beyond the range of observed values for some individuals. Scores should be interpreted as a single realisation of FPCA conducted for predicted values and do not represent statistical uncertainty.

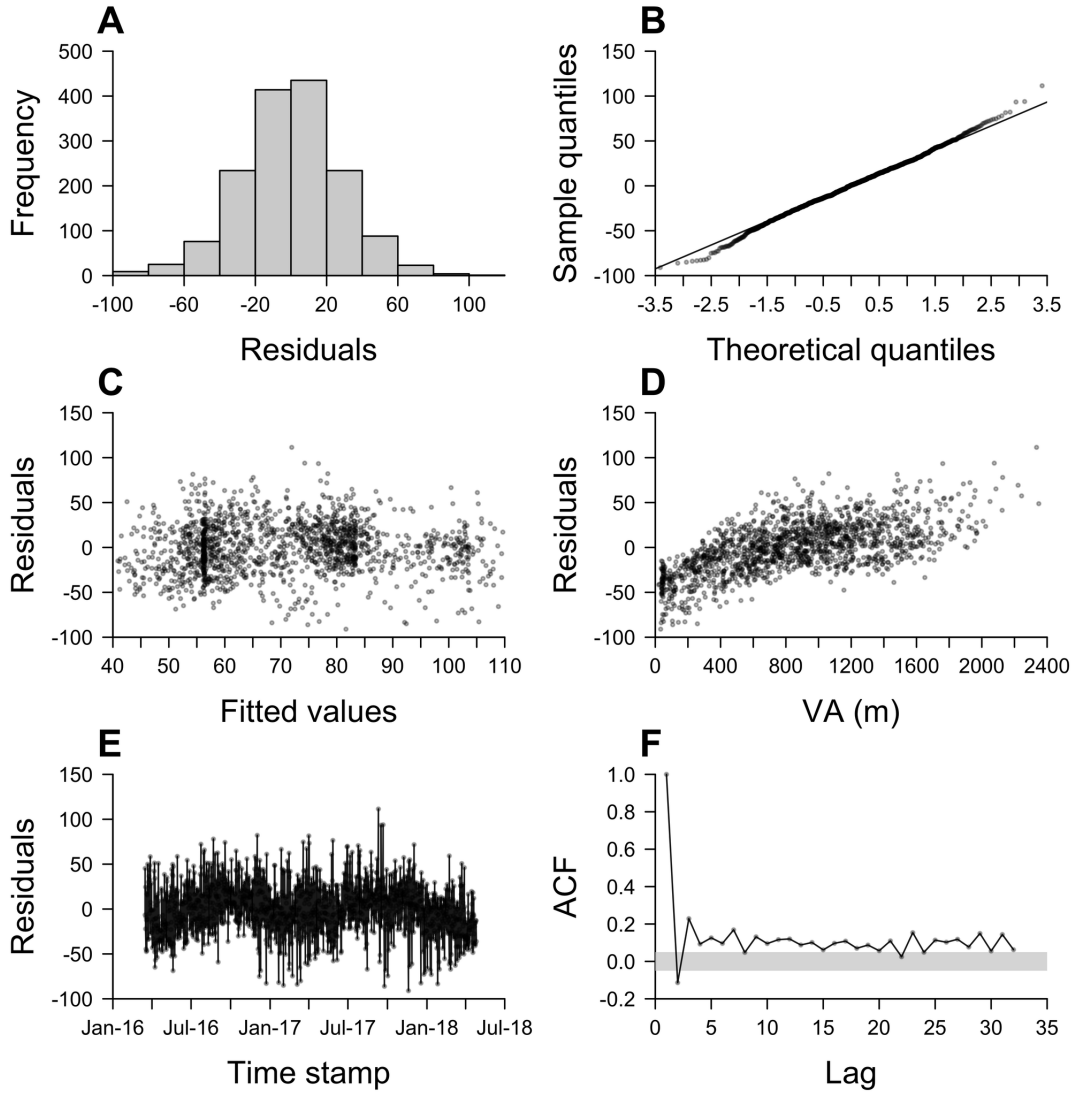

Figure S10. Standard residual diagnostic plots from the additive model of total absolute vertical activity per hour (VA) in relation to environmental cycles for female 1547. A, a histogram of residuals; **B**, a quantile-quantile plot; **C**, residuals versus fitted values; **D**, residuals versus depth; **E**, residuals versus time stamp; and **F**, the autocorrelation function (ACF) of residuals, with the 95 % confidence intervals for an uncorrelated series of white noise delineated by the grey envelope. In all cases, standardised residuals that are approximately uncorrelated under the correct model are shown.

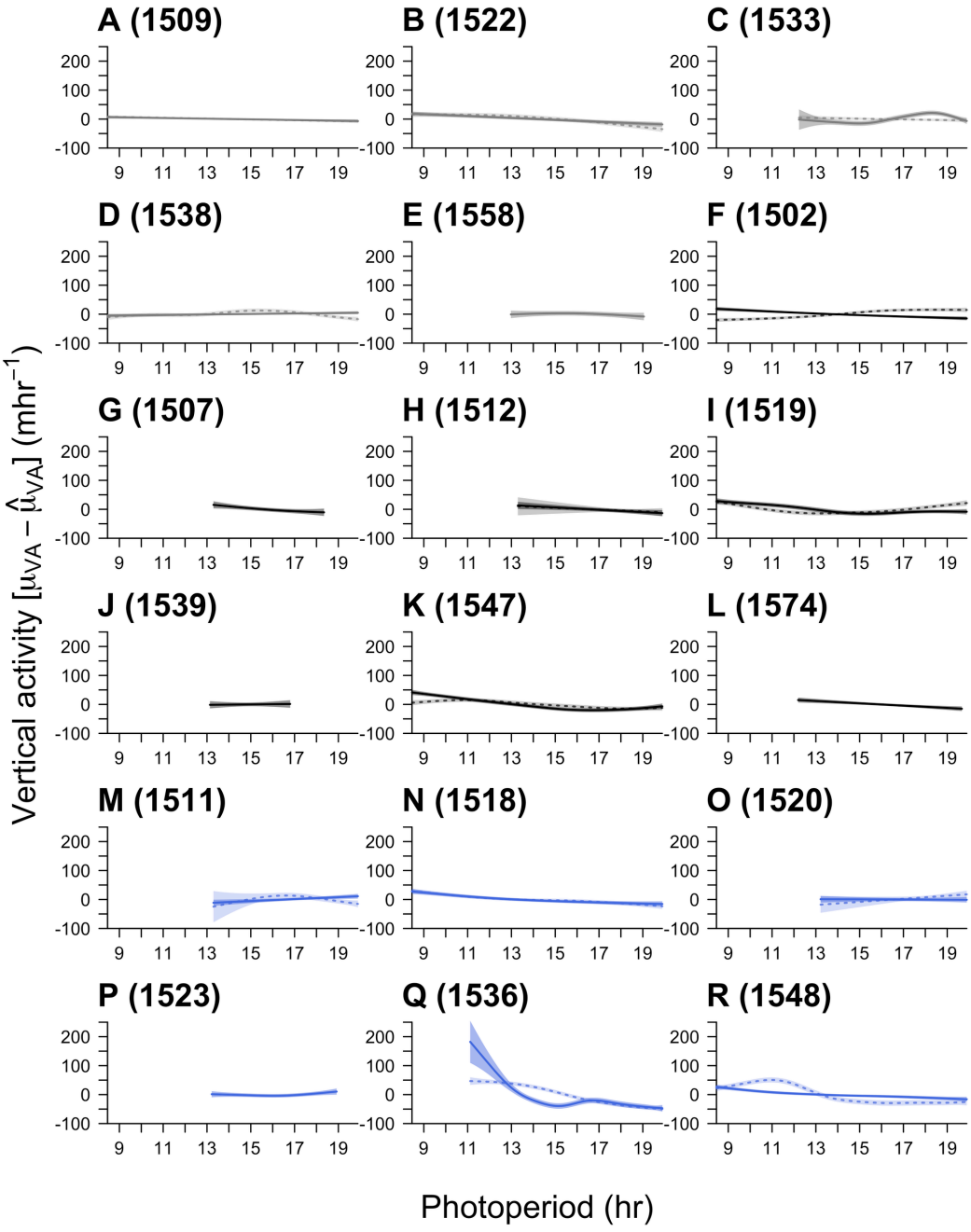

Figure S11. Predictions of the change in total absolute vertical activity per hour (VA) with photoperiod (lengthening and shortening) across all individuals. Each panel shows the expected VA (μ_{VA}), centred by the mean ($\hat{\mu}_{VA}$) and surrounded by 95 % pointwise confident bands, for a single individual, with individuals coloured by population group (immature females, light grey [**A–E**]; mature females, dark grey [**F–L**]; mature males, blue [**M–R**]). Predictions are shown for diel phase = 'day' and lunar phase = 0π radians and photoperiod direction = 'lengthening' (solid line and envelope) and, for individuals with sufficient data, photoperiod direction = 'shortening' (lighter dotted line and envelope).

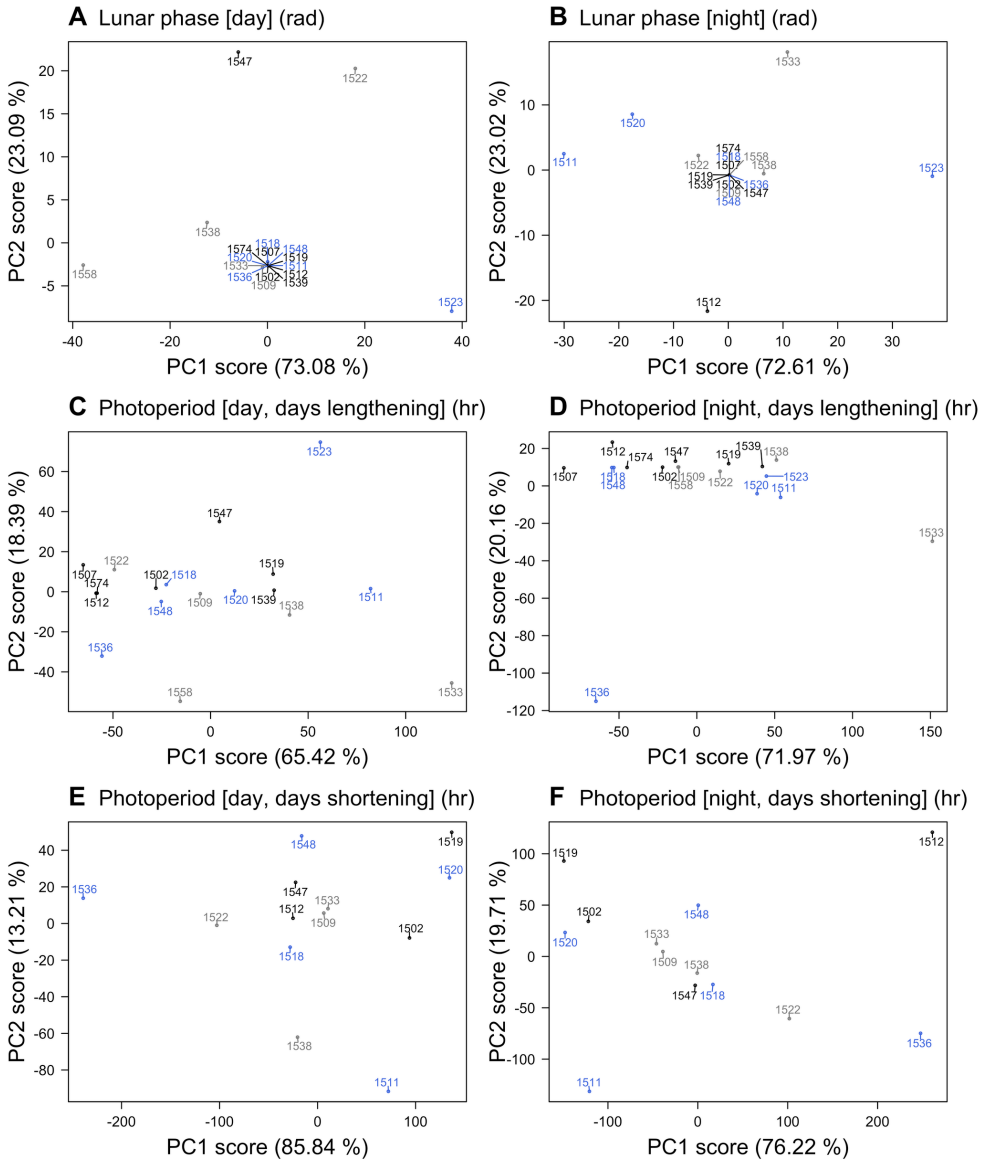

Figure S12. Functional principal component (PC) scores from predictions of the change in total absolute vertical activity per hour (VA) with environmental cycles across all individuals. Each panel shows the first two PC scores from FPCA of the predicted change in each individual's VA, centred by its mean VA, given the following effects during the day (left) or night (right): **A–B**, the effect of lunar phase during (**A**) the day and (**B**) the night; **C–D**, the effect of photoperiod, when the day length is increasing, during (**C**) the day and (**D**) the night; and **E–F**, the effect of photoperiod when the day length is shortening, during (**E**) the day and (**F**) the night. In each case, PCs are estimated from a B-spline reconstruction of the (centred) predicted change in VA with the change in each variable, while holding other variables constant at the following values: diel phase = 'day'; lunar phase = 0π radians; and photoperiod = 13.22 hours. Predictions are shown for 18 individuals except in panels **E–F**, for which sufficient data were only available for 13 individuals. Note that some FPCA scores are derived from predictions extrapolated by a limited amount beyond the range of observed values for some individuals. Scores should be interpretated as a single realisation of FPCA conducted for predicted values and do not represent statistical uncertainty.

Chapter Five

Behavioural responses to catch-and-release angling

Abstract

1. Catch-and-release angling is widespread, but the impacts of this practice for captured individuals are understudied, especially among elasmobranchs. Studies on sub-lethal behavioural impacts are particularly sparse, despite their importance for the interpretation of biologging data and for assessments of species' tolerance to capture.
2. In this chapter, the behavioural responses of flapper skate (*Dipturus intermedius*) to catch-and-release angling were described for the first time, using archival (depth and temperature) observations for 21 tag deployment/retrieval events and five recreational angling events that occurred during tagged individuals' time at liberty from charter vessels off the west coast of Scotland in 2016–17.
3. During capture (8–50 minutes), the changes in depth and temperature experienced by individuals typically exceeded natural variability. Post-release, behavioural change was apparent from visual inspection, regression and functional data analysis of the time series. Immediately following release, movements into deeper water and short periods of low vertical activity (usually 1–2 hours in duration) were common. However, overall, average vertical activity was typically around 38 % higher in the 12 hours following release than in undisturbed activity. A small number of individuals (n = 3, 14 %) exhibited irregular post-release behaviour in the form of rapid, transient re-ascents towards the surface following release.
4. Collectively, the evidence for limited, short-term behavioural changes suggests that flapper skate behaviour is relatively resilient to catch-and-release angling from charter vessels, but

irregular post-release behaviour in 14 % of individuals is sufficiently notable to indicate that further research is required on the impacts of this practice.

5. This chapter clearly demonstrates the value of biologging data and behavioural analyses for examining the impacts of disturbance and separating 'disturbed' and 'undisturbed' behaviours in studies of animal movement.

Keywords

activity, angling, behaviour, biologging, catch-and-release, disturbance

1. Introduction

Catch-and-release angling is widespread (Cooke and Schramm, 2007). This activity can have substantial socioeconomic, conservation and scientific benefits, including the contribution of information on population ecology (Arlinghaus and Cooke, 2009). However, these benefits can come with conservation concerns (Cooke et al., 2014). While these have been studied extensively for teleosts, the impacts of catch-and-release angling on elasmobranchs have received less attention (Arlinghaus et al., 2007; Gallagher et al., 2017; Musyl and Gilman, 2019).

The impacts of capture on individual elasmobranchs (namely, sharks) have been examined principally from physical, physiological and behavioural perspectives. These impacts may be sub-lethal, cumulative and/or lethal over short or long timeframes. Physical damage caused by hooks is often the most obvious (Brownscombe et al., 2017). Physiological impacts, such as metabolic acidosis, have also been documented (Brill et al., 2008; Mohan et al., 2020; Weber et al., 2020). However, less attention has been paid to behavioural responses (Gallagher et al., 2017), despite their potential influence on the interpretation of biologging data (Hoolihan et al., 2011) and their utility as indicators of species' tolerance to capture (Guida et al., 2017; Mohan et al., 2020; Whitney et al., 2021).

To date, most research on the behavioural responses of elasmobranchs to capture has been conducted in commercial fisheries settings and focused on specific behavioural metrics, such as

reflex impairment indices or behavioural release scores, that indicate release condition and survival prospects (Hyatt et al., 2016; Ellis et al., 2017). Studies in recreational catch-and-release angling settings that have examined behaviour have also tended to focus on specific indicators of survival (Heberer et al., 2010; Danylchuk et al., 2014; Sepulveda et al., 2015; Mohan et al., 2020; Weber et al., 2020). Meanwhile, few studies have examined behaviour *per se* during angling or post-release (Hoolihan et al., 2011; Whitney et al., 2016, 2017). Furthermore, existing research has focused almost exclusively on sharks, while the behavioural responses of batoids such as skate (Rajidae) to catch-and-release angling remain unstudied.

One technology that can be used to examine behaviour in relation to capture via hook and line is depth sensors such as archival tags. These principally collect high-resolution data on vertical movement (i.e. depth use and vertical activity), from which metrics describing behavioural responses during and following capture have been developed in several settings (Hoolihan et al., 2011; Guida et al., 2016, 2017; Whitney et al., 2016). During capture, fight time is a key variable that can be defined from depth observations. Fight time is underpinned by the static force required to pull an animal to the surface (which depends on body size and shape), but it is also affected by resistance from hooked individuals, alongside other variables (Gallagher et al., 2016). Consequently, statistical modelling of fight time can indicate the conditions that affect individuals' propensity to resist capture (alongside the importance of other variables). For example, fight time may be longer at particular times of day or year in association with the effects of environmental variables, such as temperature and dissolved oxygen levels, on physiological performance (Lear et al., 2019). Prior experience may also influence the response to capture, as demonstrated for other forms of disturbance (Jordan et al., 2013). These possibilities are important because empirical studies show that fight time is a consistent correlate of physiological indicators of stress (Danylchuk et al., 2014; Gallagher et al., 2014; French et al., 2015; Whitney et al., 2017). Consequently, models of fight time can indicate the circumstances under which individuals may be more or less susceptible to capture-related impacts, even in the absence of physiological parameters. During capture, the rate and magnitude of the changes that individuals experience in depth or environmental conditions, such as temperature, relative to the experiences of undisturbed individuals, are also indicative of the potential impacts of catch-and-release, since particularly rapid ascents and temperature change may exacerbate anaerobic exertion, cause thermal shock or

induce barotrauma (Garcia et al., 2015; Cook et al., 2019). For example, evidence for systemic gas embolism following capture from deep-sea trawls has been documented in sleeper sharks (*Somniosus rostratus*), suggesting that in some circumstances elasmobranchs may be vulnerable to barotrauma, despite the lack of internal air spaces (Garcia et al., 2015).

Post-release, depth observations can reveal changes in movement, such as reduced or elevated vertical activity, that reflect behavioural changes, including switches between resting and more active behaviours (Hoolihan et al., 2011; Danylchuk et al., 2014; Rogers et al., 2017). Similarly, unusual movements, such as prolonged use of a constant depth or erratic changes in depth, may indicate irregular post-release behaviours (IPRBs), such as depth-holding, hyperactive or escape behaviour (Hoolihan et al., 2011). For benthic or demersal species in bathymetrically heterogeneous environments, these responses may be closely related to overall activity levels and patterns of space use, and collectively they can provide an indicator of the extent to which individuals are disturbed by capture (Chapter Six; Whitney et al., 2016). However, current research suggests that behavioural responses to capture are often individual-, species- and environment-specific, which challenges *a priori* predictions for the impacts of catch-and-release on unstudied species.

The flapper skate (*Dipturus intermedius*) is a large, benthic, Critically Endangered elasmobranch that is prized by recreational anglers (Chapters One–Two; Neat et al., 2015; Ellis et al., 2021). Once widespread, this species was extirpated from parts of its former range (Brander, 1981), but it remains locally abundant in an area off the west coast of Scotland where recreational angling and tagging underpinned the designation of the Loch Sunart to the Sound of Jura Marine Protected Area (LStSJ MPA) for its conservation (Neat et al., 2015). However, the responses of skate to catch-and-release angling in this area remain poorly studied.

The possible responses of flapper skate to catch-and-release angling can be exhibited in four primary stages. In the contact phase (1), skate bite the bait and then typically dig into the sediment, forming a seal which only breaks after a period (typically less than 10 minutes in duration) of tension from a rod and line. In the ascent phase (2), skate are pulled to the surface. Some fish make strong downwards movements, overcoming the ratchet on the line, during this phase. In the surface

phase (3), individuals are brought onto angling vessels (or the shore) before release. Post-release (4), information is restricted to angler mark-recapture records from tagging and photo-identification (Neat et al., 2015; Benjamins et al., 2018; Skatespotter, 2021). In the most recent report of recapture records for the west coast of Scotland, 40 % of individuals (n = 631) are identified as having been recaptured at least once (Skatespotter, 2021). Evidence for numerous, repeated captures is also recorded for specific individuals, with one individual having been recaptured 22 times. However, while this research shows that individuals can survive catch-and-release angling (at least in some circumstances), the short-term, sub-lethal impacts of capture, including on behaviour, remain unknown (Chapter One).

The aim of this chapter is to investigate the behavioural responses of flapper skate to catch-and-release angling, and their potential implications for our understanding of the wider impacts of this practice, using biologging data from archival tags. There are two objectives:

A. **The capture experience**—to quantify fight time, its drivers and the change in depth and temperature that individuals experience during angling as metrics of the potential stress induced by this practice.
B. **Post-release movements**—to examine individual movement patterns, systematic changes in depth use and vertical activity, and IPRB as indicators of post-release behavioural change.

2. Methods

2.1. Study site

The LStSJ MPA is situated on the west coast of Scotland in complex bathymetric environment that includes shallow (< 50 m) platforms alongside glacially over-deepened basins and channels up to 290 m in depth (Figure 1) (Howe et al., 2014). Most recorded angling (post 2016) occurs from a small number (2–3) of charter vessels in three areas over relatively deep (> 100 m) water (Figure S1) (Chapters Two–Three). Water temperature varies seasonally from a minimum of approximately 6 °C in March to a maximum of 16 °C in September, with the surface waters

warming by 1–2 °C more than the layers below in summer (Chapter Two). Seasonal variation in air temperature is greater, typically extending from -2 °C in winter to 22 °C in summer.

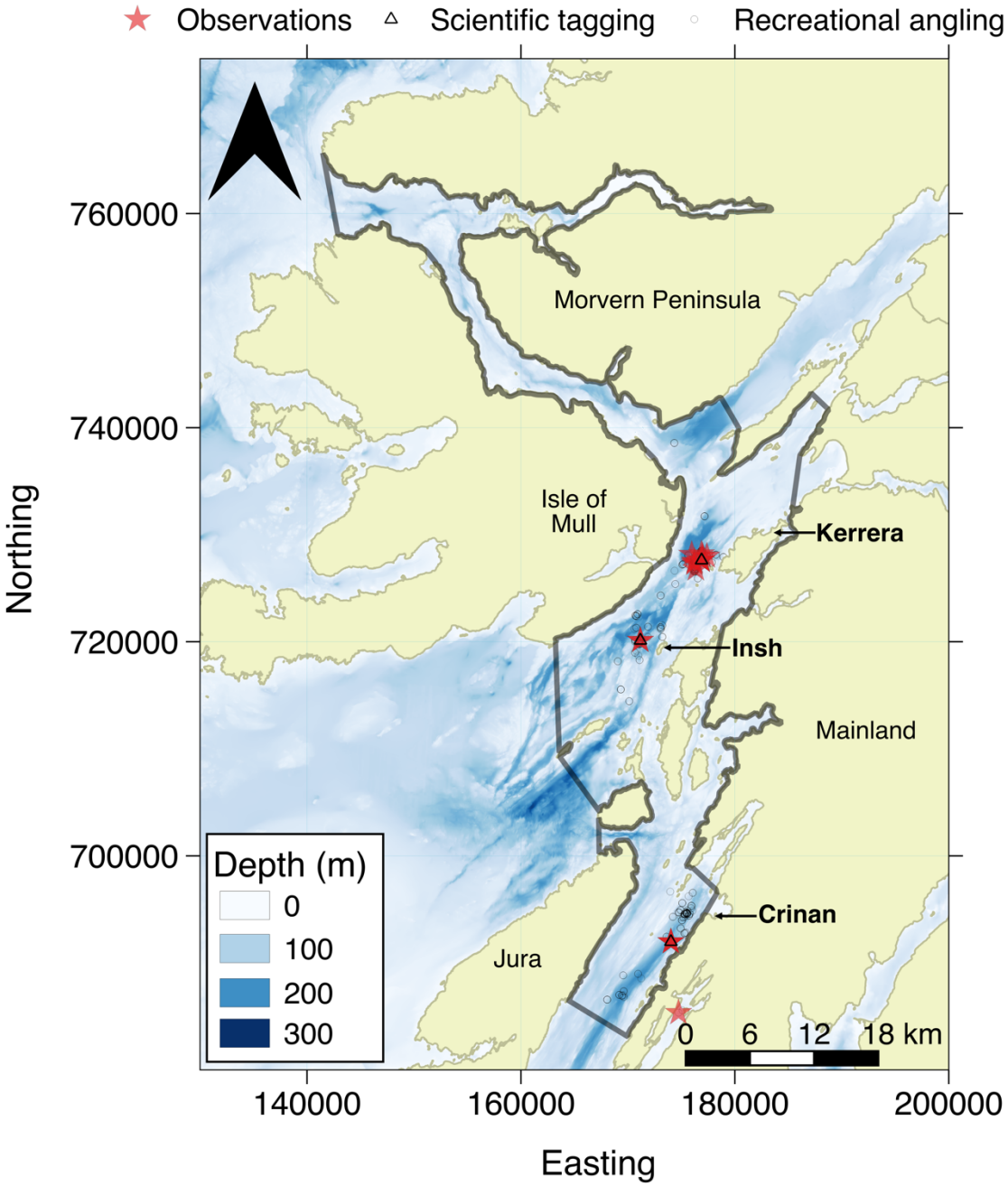

Figure 1. The study site and catch-and-release records. The grey envelope marks the Marine Protected Area. The three main angling sites (Kerrera, Insh and Crinan) are noted in bold. Points mark recreational angling and scientific tagging events recorded in the mark-recapture (n = 1,166) and Movement Ecology of Flapper Skate archival (Star Oddi milli-TD) tagging (n = 45) databases, as described in Chapter Three. Stars mark capture events associated with archival data used in this chapter for which locational data were also recorded (including n = 21 tag deployment events, n = 2/5 recreational angling events that occurred during individuals' time at liberty and n = 7/21 tag retrieval events).

The bathymetry is shown at mixed 5 m and one arc-second resolution, with high-resolution data from Howe et al. (2014) shown where available and lower resolution data from Digimap shown elsewhere (Chapter Two). Background Ordnance Survey map © Crown copyright and database rights [2019] Ordnance Survey (100025252).

2.2. Tagging

In the MPA, 45 individuals were caught and tagged with Star Oddi milli-TD archival tags in March 2016–April 2017 as part of research conducted by the Movement Ecology of Flapper Skate project (Chapter Two). Captured individuals were sexed and the total length (snout tip to tail tip) and disc width (wing tip to wing tip) were measured (Chapter Two). Maturation status (immature, mature) was later inferred using a model for maturation status with total length (Chapter Two). In all cases, one state was considerably more likely than the other: for all 'immature' individuals, the probability of being immature given their total length was 1.00; for all 'mature' individuals, the probability of being mature was ≥ 0.98. After measurement, individuals were tagged with archival tags, programmed to record depth and temperature every two minutes, and released (Chapter Two). During their time at liberty, individuals could be caught and released by recreational anglers. Data were retrieved from individuals that were recaptured and had their tags removed, either by recreational anglers or as part of ongoing monitoring. In this chapter, these data were used opportunistically to investigate the capture process and behavioural responses to catch-and-release.

2.3. Catch-and-release events

Three sources of information on the capture process and the behavioural responses of flapper skate to catch-and-release angling were identified within retrieved time series: tag deployment events; recreational catch-and-release angling events that occurred during individuals' time at liberty; and tag retrieval events (Figure S2). For recreational catch-and-release events that occurred during individuals' time at liberty, only confirmed events, recorded in a mark-recapture database maintained by NatureScot, Marine Scotland Science and the Scottish Association for Marine Science (Chapter Two), were incorporated in analyses. However, all near-surface (≤ 5 m) movements in individuals' depth time series were inspected visually for evidence of unrecorded capture events.

2.4. The capture experience

Retrieved data were analysed in R, version 4.0.2, using the prettyGraphics, stats and fda packages (Lavender, 2020a; R Core Team, 2020; Ramsay et al., 2020). The capture process was investigated using data around recreational angling events that occurred during individuals' time at liberty and immediately preceding tag retrieval (Figure S2). For each event, the start time was defined as the time of last depth observation preceding the capture ascent and the surface time as the time of the first observation at the surface. Fight time was estimated from the difference between the start and surface times as an indicator of the potential stress induced by capture. To investigate putative drivers of capture fights, fight time was considered in relation to sex ('M', 'F'), body 'size' (specifically, dorsal surface area, m^2), the number of previous captures ('n'), the time (days) since the last capture ('gap') and the angle of the sun above the horizon (°), temperature (°C) and depth (m) at the onset of each capture event, while accounting for the effects of the tide with a metric of the rate of change in tidal elevation, using a generalised linear model of the form:

$$fight_i \sim N(\mu_i, \sigma^2) \quad (1)$$

$$\log(\mu_i) = \alpha + \beta_1 sex_{M_i} + \beta_2 size_i + \beta_3 tide_i + \beta_4 size_i tide_i + \beta_5 n_i + \beta_6 gap_i + \beta_7 sun_i + \beta_8 temperature_i + \beta_9 depth_i$$

where sex_M defines males, i indexes capture events and other terms are as defined above (see Appendix §1.1). It is recognised that other variables, such as angler experience and environmental conditions, may affect fight time, but in this chapter these additional possibilities could not be directly investigated (see Appendix §1.1). For recreational events, following capture fights, handling time was estimated as the difference between the surface and release time, with the latter defined as the time of the last depth observation preceding the rapid descent phase that followed individual release (Figure S2).

During capture, the total changes in depth and temperature that each individual experienced were compared to the distribution of changes in the rest of each individual's time series as additional indicators of the potential impacts of capture. The 'rest of each individual's time series' was defined to exclude all observations from two hours before capture events until 12 hours post-release: this ensured that analyses were comparable across all individuals and that any time spent on the hook pre-ascent or within the 'post-release' period considered in subsequent analyses (see

below) was excluded. Outside of capture events, both (a) the change in depth and temperature between sequential observations and (b) the total, sustained change in depth and temperature over successive time bins equal in duration to the capture duration were examined, since it was not clear *a priori* whether sequential or sustained changes would reflect the true extent of the changes experienced under normal conditions.

2.5. Post-release movements

Observations immediately following tag deployment and recreational angling events that occurred during individuals' time at liberty (Figure S2) were used to investigate short-term post-release vertical movement patterns as indicators of behaviour. 'Short-term' was defined as 12-hours post-release. This window of time was chosen because it was expected that, if capture affects post-release behaviour, at least some signatures of behavioural change would be exhibited shortly following release while, over longer periods, any changes may be masked by natural variability. This definition also permitted investigation of post-release behaviour across all sampled individuals. For each capture event, observed time series before and/or immediately post-release were visualised to identify patterns in depth use or vertical activity (the difference between sequential depth observations: Chapter Four) potentially attributable to capture—especially descent into deeper water, low vertical activity and erratic movement—reflective of behavioural change.

2.6. Average changes in depth and vertical activity

To quantify systematic changes in depth use and vertical activity, post-release time series were compared against 'undisturbed' time series samples drawn from the rest of each individual's time series. Each 'undisturbed' sample was drawn such that it began at the same time of day as the capture event and lasted for the same duration as the post-release period under consideration (12 hours). Time series were sampled at random according to a uniform distribution. In this way, 50 % of the total number of available, non-overlapping 12-hour samples (up to a maximum of 100 samples) was drawn for each individual. (The actual number depended on the length of available data, which differed among individuals due to variation in their time at liberty.) For each sample,

the first four observations were excluded to focus on the movements of skate once they had returned to the seabed.

Given substantial variability in vertical movements, the mean depth, the mean absolute vertical activity and the duration of 'minimal' (≤ 0.5 m) absolute vertical activity from each 12-hour sample were identified as response variables indicative of average movement patterns. To determine whether or not capture affected these variables, and how responses differed among life-history categories, each response was modelled in a generalised linear modelling framework in relation to a three-way interaction between a factor ('sample') distinguishing post-release ('PR') and 'undisturbed' time series, sex and body size (specifically total length). Following the model for fight time, temperature was included as a metric of seasonality. Each model took the form:

$$y_i \sim f(\mu_i) \tag{2}$$

$$\begin{aligned} log(\mu_i) = \alpha + \ & \beta_1 sample_{PR_i} + \beta_2 sex_{M_i} + \ \beta_3 size_i + \beta_4 temperature_i \\ & + \beta_5 sample_{PR_i} sex_{M_i} + \beta_6 sample_{PR_i} size_i + \beta_7 sex_{M_i} size_i \\ & + \beta_8 sample_{_{PR_i}} sex_{M_i} size_i \end{aligned}$$

where y denotes the response variable, f represents the Gaussian distribution for the mean depth and absolute vertical activity and the Gamma distribution for the duration of minimal absolute vertical activity, $sample_{PR}$ denotes post-release samples and other terms are as defined previously (see Appendix §1.2).

2.7. Irregular post-release behaviour

Post-release and 'undisturbed' samples were compared qualitatively and using functional principal component analysis (FPCA) to identify IPRB. FPCA is a type of functional data analysis that represents each time series as a smooth function and then applies FPCA to the set of smooths (Chapter Four; Ullah and Finch, 2013; Wang et al., 2016). The outcome is a series of harmonics (one for each principal component) that describes the variation among the smooths and a corresponding set of scores for each smooth that maps it onto the harmonics. Distinct time series have mappings that differ substantially from other time series and appear as isolated points on score plots.

FPCA was implemented separately for each individual, since the number of post-release and 'undisturbed' time series varied among individuals and behaviour unusual for one individual might not be unusual for another, using the fda package (Ramsay et al., 2020). For each individual, FPCA was implemented for (a) the depth time series and (b) the absolute vertical activity time series. For these analyses, post-release and 'undisturbed' depth and absolute vertical activity time series were represented as smooths using a B-spline basis with 25 or 100 basis functions respectively. FPCA was applied to these smooths and the resultant harmonics and scores for the post-release time series relative to those for the 'undisturbed' time series were visually inspected for evidence of distinctness (see Appendix §1.3).

3. Results

3.1. Capture events

Archival tags were successfully retrieved from 21 individuals (46 %) following deployment periods of 3–772 (median = 164) days (Table S1, Chapters Two and Four). Five recreational catch-and-release events were recorded during individuals' time at liberty (Table S1, Chapter Two). All events occurred from charter angling vessels. Visual inspection of near-surface movements suggested that two unrecorded catch-and-release events may also have occurred (Figure S3). Across all confirmed capture events (n = 26), fight time ranged from 8–50 (median = 18) minutes while recreational handling time (n = 5) ranged from 4–6 (median = 4) minutes (Table S1). In the model of fight time, there was indicative evidence that capture fights were longer for larger individuals caught in cooler, deeper water (Figure 2, Tables S1–S2). However, none of the terms in the model were statistically significant at the 0.05 level (Table S2). Nonetheless, the model explained 60 % of the deviance and residual diagnostics were reasonable.

During capture fights, changes in depth and temperature generally exceeded naturally observed variation (Figure S4, Table S1). While sequential changes in depth were generally small outside of capture events, and only exceeded 100 m on 14 occasions, capture ascent distances varied between 80–178 (median = 145) m. Likewise, the distribution of sequential changes in temperature (-3.61–2.46, median = 0.00 °C) was generally smaller than the change during capture fights (-

0.24–14.77, median = 0.14 °C). For the recreational angling events that occurred during individuals' time at liberty, the additional temperature change during handling varied from -0.57–5.26 (median = 1.05) °C. However, overall, individuals only experienced temperatures that exceeded the maximum bottom temperature (16.00 °C) expected in the study site (Chapter Two) on 2/26 occasions (Table S1).

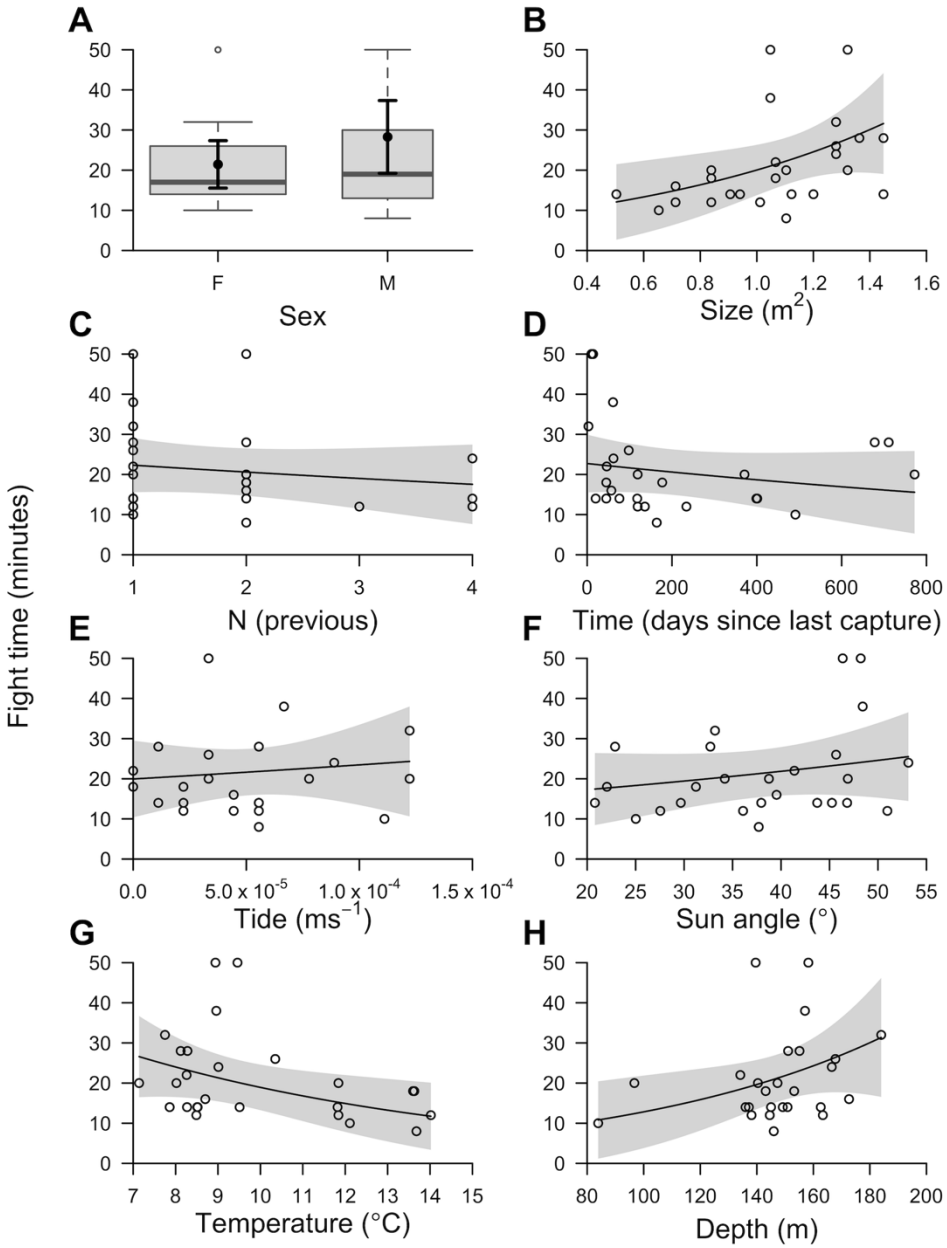

Figure 2. The drivers of fight time during catch-and-release angling. Each panel shows the relationship between fight time and one of the following variables: **A,** sex; **B**, body size (dorsal surface area); **C**, the number of previous capture events; **D**, the number of days since the last capture event; **E**, the strength of the tide; **F**, the sun angle above the horizon; **G**, the water temperature; and **H**, the depth. In **A**, boxplot width is proportional to the number of capture

events of females (n = 18) and males (n = 8). The lower, middle and upper whiskers in grey represent the 25th, 50th and 75th percentiles respectively. The black points and surrounding lines mark the mean ± 95 % confidence intervals. In **B–H**, the black lines and grey envelopes mark predictions and 95 % confidence intervals. Predictions are shown based on a generalised linear model of fight time, with other variables held at their median values.

3.2. Post-release movement patterns

A total of 26 post-release time series were identified from 21 tag deployment events and five recreational catch-and-release events that occurred during individuals' time at liberty (Table S1). Following release, in all cases individuals rapidly descended into deeper water (Figures 3–4). In 13 cases, individuals exhibited a short hiatus in their descent (e.g., Figure 4H), usually lasting less than half an hour and in some cases resembling a small 'bounce' in the depth time series (e.g., Figure 4N), before continuing to descend more gradually into deeper (150–200 m) water over a period of one or more hours (labelled '1' in Figure 4). Following descent, in 15 cases individuals exhibited very low vertical activity at depths around 150 or 200 m for periods of time lasting from less than hour (e.g., Figure 4B), to around two hours (e.g., Figure 4C), to more than 10 hours (e.g., Figure 4R) (labelled '2'). The onset of this low vertical activity phase typically occurred within three hours post-release, but it did not become apparent until eight hours post-release for individual 1552 (Figure 4S). In seven time series with relatively short-lived initial resting phases, the phase repeated after a few hours (e.g., Figure 4C) (labelled '3'). In contrast, more erratic movements (rather than a clear period of low vertical activity) were exhibited in 11 cases (e.g., Figure 4E) (labelled '4').

Shortly following descent, three individuals also undertook distinct, rapid, short-lived re-ascents into very shallow (< 25 m) water. These movements were exhibited by a mature male (1523: Figure 3C) following recreational capture in May 2016 and a mature female (1507: Figure 4B) and an immature female (1558: Figure 4T) following tag deployment in March 2016. All events followed one (1523) to four (1507) previous (recorded) captures and occurred within 46–76 days of the last capture in relatively cool water (8.72–10.13 °C) (Table S1).

The mature male (1523) was one of only five individuals with pre-capture and post-capture time series and the only such individual to exhibit such distinctive post-release movements. During

capture, the fight time (38 minutes) for this individual exceeded (by ≥ 16 minutes) that for the other four individuals, but the temperature change experienced during capture was small (0.27 °C) (Table S1). Following release and descent, the individual re-ascended, by 99 (112 to 13) m, over a period of 1.97 hours (an average speed of 0.014 ms^{-1}). This compares with a depth range of 63–209 m and an average ascent speed over equivalent time windows of 0.000–0.016 ms^{-1} during the rest of the individual's time at liberty. Re-ascent was followed by a second descent resembling a series of 'bounce dives' into progressively deeper water (Figure 3C).

In the mature female (1507), a short period of very low vertical activity preceded a re-ascent of 152 (163–11) m in 0.56 hours. Both the depth attained and the ascent speed (0.743 ms^{-1}) exceeded naturally observed variation between 27–224 m and 0.000–0.053 ms^{-1} respectively. This movement was followed by rapid descent and then a more gradual re-ascent over a period of hours (Figure 4B). After a more prolonged period of low vertical activity, individual 1518 undertook a similarly rapid ascent, but did not move into such shallow water, remaining around 50 m following ascent (Figure 4F). The other individuals that exhibited near-stationary vertical activity for a period of time post-release similarly all ascended rapidly at the end of this phase, but less substantially (by less than 100 m).

For the immature female (1558), the descent-re-ascent-re-descent movement was much smaller (Figure 4T). The individual ascended by 97 (118–21) m over 1.30 hours (an average speed of 0.020 ms^{-1}), with the depth and speed of ascent at the upper end of that experienced over the rest of its time at liberty (24–219 m and 0–0.030 ms^{-1} respectively). Following ascent, the individual descended slightly but remained in water less than 60 m deep over the following 12 hours before descending back to greater depths.

Over subsequent hours, individual movements were highly variable, including periods of low and high vertical activity in both deep (> 150 m) and shallow (< 50 m) water (Figures 3–4). However, 11 recently tagged individuals and one individual released by recreational anglers showed a clear pattern of moving shallower with the onset of night (e.g., Figures 3B and 4A).

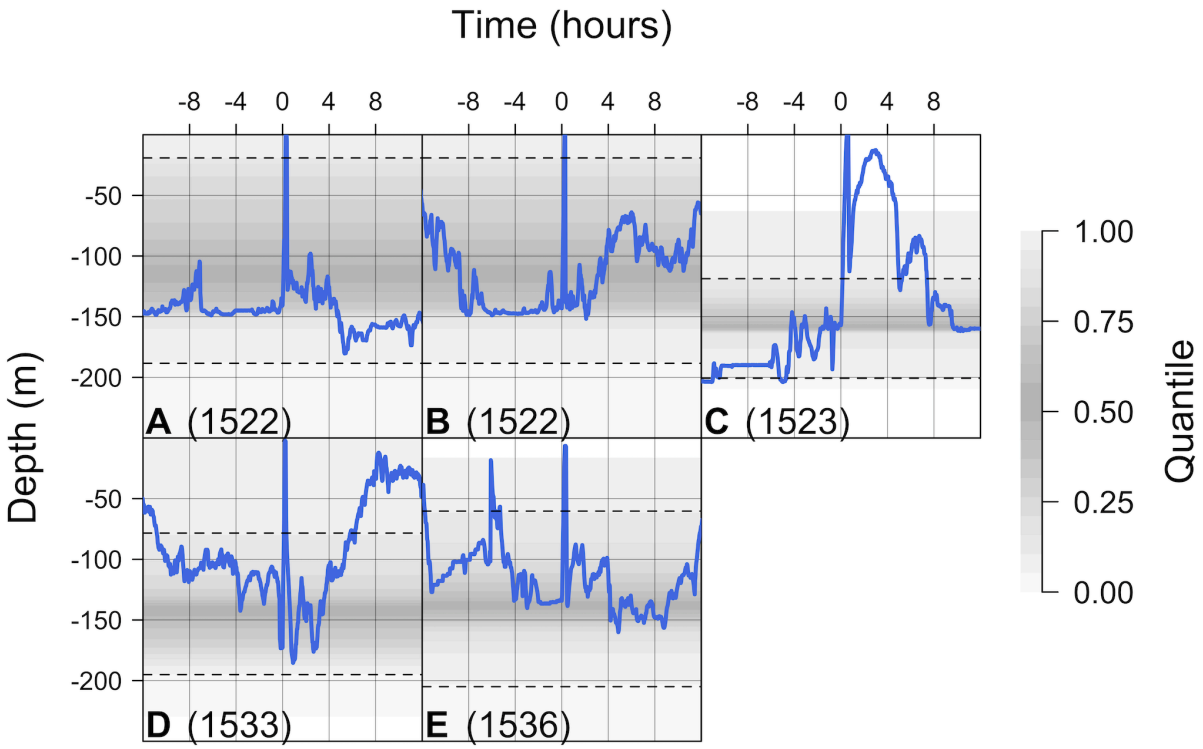

Figure 3. Depth time series around recreational catch-and-release events that occurred during individuals' time at liberty. Each panel shows the observed time series (in blue) around a capture event for a specific individual. The background shading marks the quantiles of observed variation in depth based on the rest of each individual's time series, with quantiles near the middle of the distribution shaded more darkly than quantiles towards the edge of the distribution. The dashed lines mark the 25th and 75th quantiles respectively. Depth observations beyond these lines are considerably shallower or deeper than average, while depth observations beyond the shading are more extreme than observed outside of capture event(s).

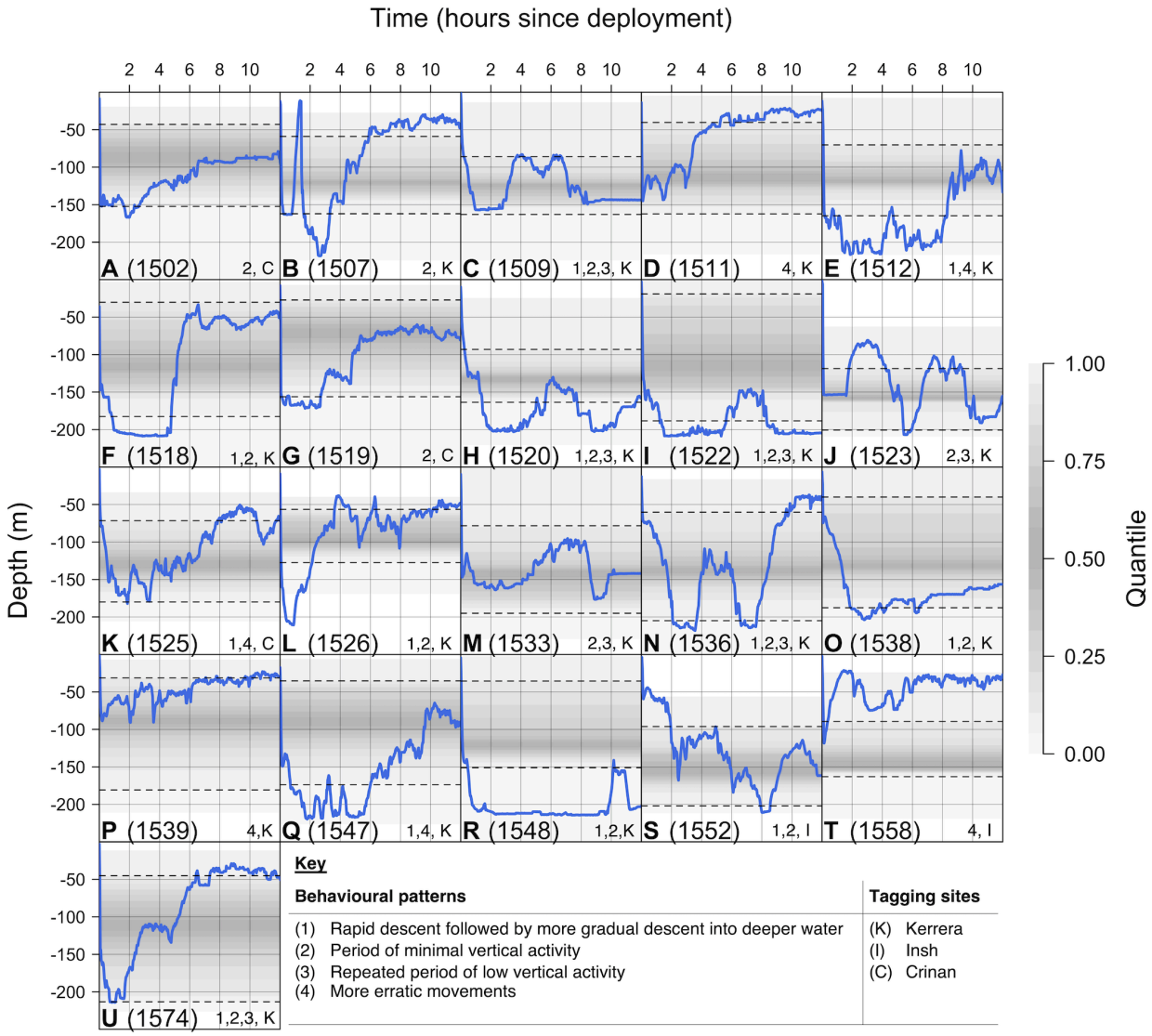

Figure 4. Depth time series following tag deployment. Each panel shows the observed time series (in blue) for a specific individual. The background shading marks the quantiles of observed variation in depth based on the rest of each individual's time series, with quantiles near the middle of the distribution shaded more darkly than quantiles towards the edge of the distribution. The dashed lines mark the 25th and 75th quantiles respectively. Depth observations beyond these lines are considerably shallower or deeper than average, while depth observations beyond the shading are more extreme than observed outside of capture event(s). Numbers and letters mark distinct patterns and tagging locations, respectively.

3.3. Average changes in depth and vertical activity

Average depth use was associated with sex and total length in 'undisturbed' samples but there was no evidence that post-release samples differed (Figure 5A–B, Table S3). Similarly, mean absolute vertical activity was associated with sex, length and temperature in 'undisturbed' samples, with mean absolute vertical activity noticeably higher for larger individuals in particular. However, these relationships differed post-release (Figure 5C–D, Table S3). The smaller males (1536 and 1520) were more active post-release (Figure 5C). For instance, for individual 1536 the expected mean absolute vertical activity in 'undisturbed' samples (1.28 [1.18–1.40 (95 % confidence intervals)]) significantly increased post-release (2.57 [1.54–4.31] m). While a small difference numerically (in line with the two-minute resolution of observations), these estimates imply that vertical activity on average doubled post-release. However, this difference was less apparent for the three larger males, probably due to individual variation rather than an effect of length (given the small number of males and the length range). In females, mean absolute vertical activity was higher post-release across all sampled lengths (135–218 cm). Taking a female (e.g., 1525) with the median length (201 cm) as an example, the expected mean absolute vertical activity in 'undisturbed' samples (1.69 [1.63–1.91]) increased by approximately 38 % post-release (2.34 [1.74–2.87] m). Accordingly, compared to 'undisturbed' time series, the duration of minimal absolute vertical activity was shorter post-release for the smaller males (43.60 [24.75–76.83] versus 114.59 [107.87–121.70] minutes for individual 1536) and across all sampled sizes of females (50.66 [40.44–63.66] versus 85.91 [83.46–88.44] minutes for a median-sized female) (Figure 5E–F, Table S3). Taken together, across all individuals, the expected mean absolute vertical activity was -13–101 (median = 38) % higher and the duration of minimal absolute vertical activity -8–62 (median = 42) % lower than in undisturbed activity. These models only explained 10–14 % of the variability, but residual diagnostics were acceptable.

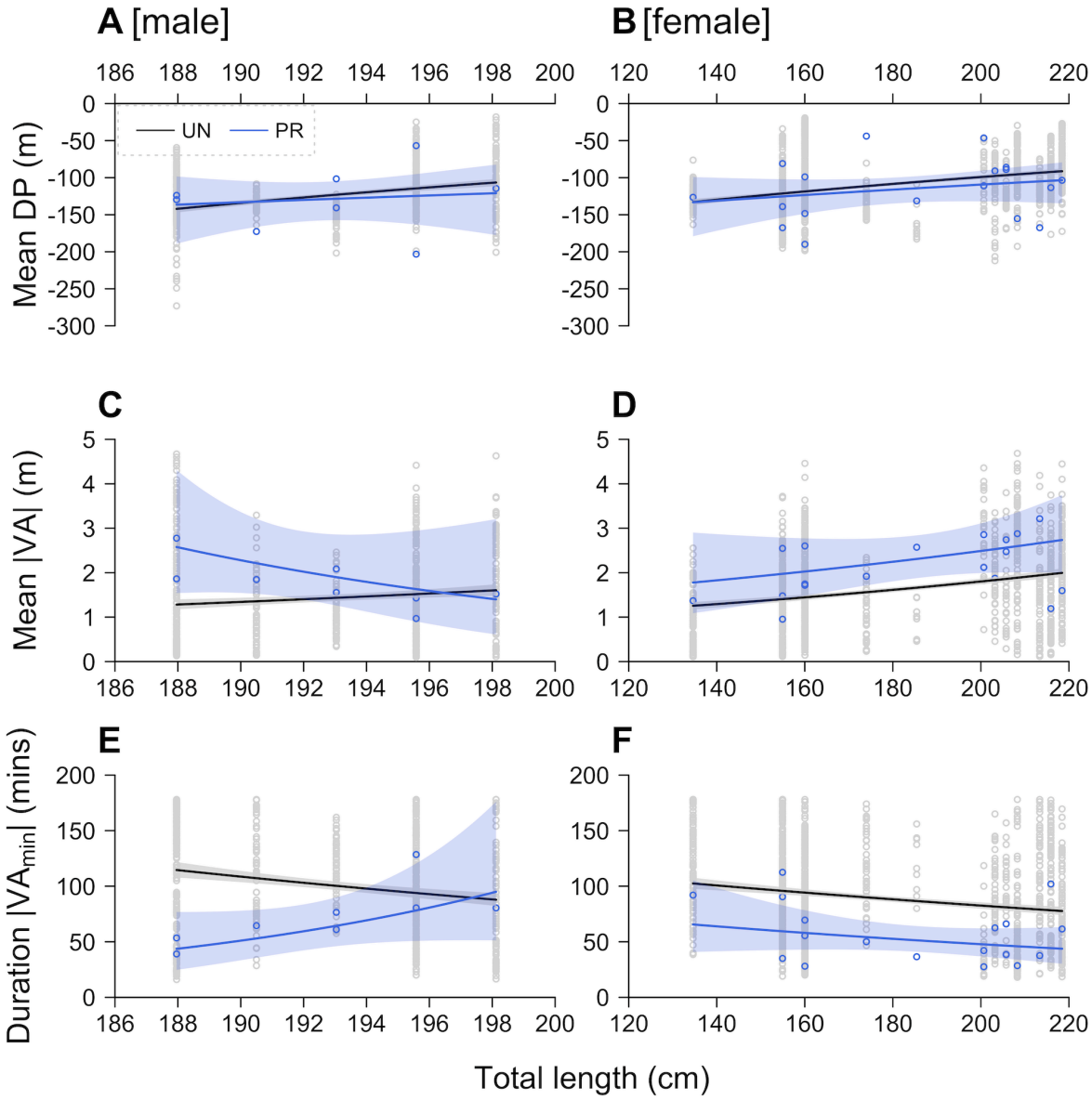

Figure 5. Predictions of the mean depth (A–B), mean absolute vertical activity (C–D) and the duration of 'minimal' (≤ 0.5 m) absolute vertical activity (E–F) for males (left-hand side: A, C, E) and females (right-hand side: B, D, F) in 'undisturbed' (UN) and 'post-release' (PR) 12-hour samples with total length. Points mark observations and the lines and surrounding envelopes mark model predictions and 95 % confidence intervals. In all panels, temperature is held at the mean (scaled) value.

3.4. Irregular post-release behaviour

Qualitative examination of movement time series did not indicate IPRB, with similar patterns apparent in both 'undisturbed' and 'post-release' time series (Figure S5, Chapter Four). For instance, in 'undisturbed' samples there was evidence for periods of minimal vertical activity lasting for hours or days as well as low vertical activity over more prolonged periods (Figure S5A). 'Undisturbed' time series also exhibited occasional periods of very high vertical activity (Figure S5B–C). A tendency for movement into shallower water at night was also common among sampled individuals, demonstrating that these movements were not unique to post-release periods (Figure S5D).

In line with the results from qualitative examination, FPCA suggested that most 'undisturbed' and 'post-release' time series were similar in structure (Figure 6). For most individuals, 'undisturbed' and 'post-release' samples clustered together, despite substantial variability (e.g., Figure 6A). Even for individuals with moderately extreme principal component (PC) scores (e.g., Figure 6H), there was limited separation of post-release and 'undisturbed' time series along the PCs.

However, there was evidence for IPRB from distinct post-release PC scores for three individuals (1523, 1507 and 1558). For these individuals, distinct PC scores were driven by rapid movement into shallow (< 25 m) water, a pattern which appeared to be irregular (Figure S6). There was weaker evidence for IPRB in five other cases (1518, 1525, 1526, 1552 and 1512) but the differences between 'undisturbed' and post-release scores were not as strong. For example, individual 1518 also rapidly re-ascended into shallow water post-release (Figure 4F) and this movement was associated with slightly higher PC scores from the depth time series (Figures 6F and S6D). Distinct PC scores for individuals 1525, 1526 and 1552 were suggestive of IPRB, but these were derived from comparison against a small number (< 10) of 'undisturbed' samples.

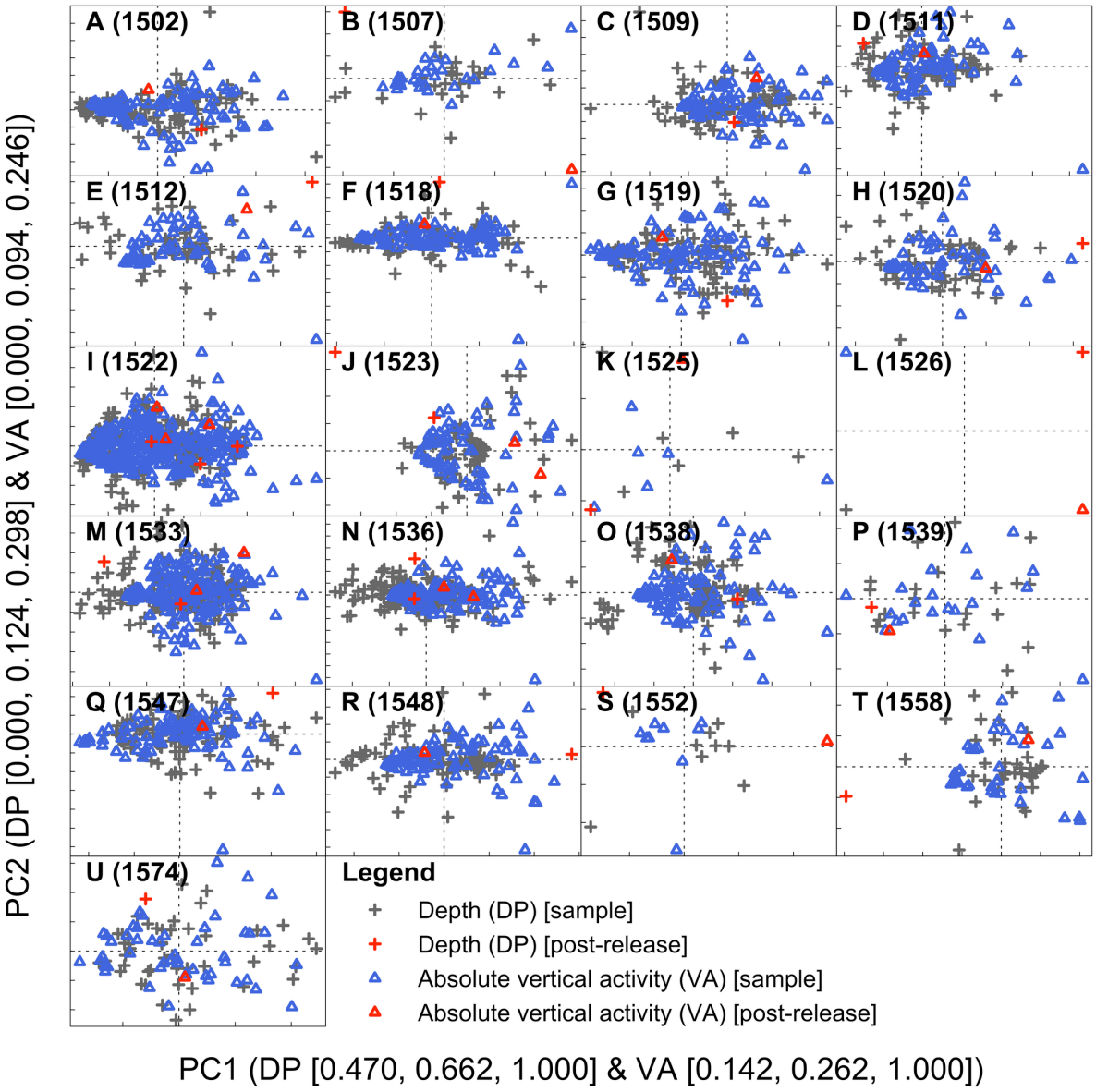

Figure 6. Functional principal component analysis (FPCA) scores for post-release and 'undisturbed' depth and absolute vertical activity time series samples. Following the order of Figure 4, each panel shows the scores for a specific individual from FPCA of the (i) depth and (ii) absolute vertical activity time series, with 'undisturbed' samples shown in grey and blue, respectively, and post-release time series (following tag deployment and recreational angling, if applicable) shown in red. Note that the number of 'undisturbed' samples varies among individuals due to variation in individuals' time at liberty. All scores are centred and scaled to facilitate comparisons. The dashed horizonal and vertical lines mark adjusted scores on principal component 1 (PC1) and principal component 2 (PC2) of zero. Tick marks (bottom and left for each panel) are spaced one unit apart. The relative placement of scores for different samples indicates distinctness. The proportion of the variability explained by FPCA of the depth (DP) and absolute vertical activity (VA) time series for PC1 and PC2 [minimum, median, maximum] across all individuals is provided in the axis labels.

4. Discussion

This is the first study on the impacts of catch-and-release angling on flapper skate and one of only a handful on elasmobranchs (and the only study on a skate species) to examine behaviour (Hoolihan et al., 2011; Whitney et al., 2016, 2017). Following the contact phase, there is indicative evidence that fight time was associated with size, temperature and depth. During capture, the changes that individuals experienced in depth and temperature were extreme in the context of natural variability. For most individuals (n = 15, 71 %), tag deployment was followed by a short period (typically 1–2 hours in duration) of minimal vertical activity that resembles recovery behaviour, as observed following capture and handling in other elasmobranchs (Hoolihan et al., 2011; Danylchuk et al., 2014; Raoult et al., 2019), but overall vertical activity was typically higher in the 12-hours post-release. There was limited evidence for IPRB, which suggests that in general flapper skate is behaviourally resilient to catch-and-release angling from charter vessels. However, short-lived IPRB was documented in three individuals, which is consistent with observations of more erratic or active post-release behaviour in other species following capture by recreational and commercial gear (Hoolihan et al., 2011; Whitney et al., 2021). These results demonstrate the multifaceted value of biologging data and how they can be used opportunistically to address knowledge gaps in data-poor systems.

Among elasmobranchs, fight time is a major driver of the impacts of catch-and-release, with documented impacts on physiology (Danylchuk et al., 2014; French et al., 2015; Whitney et al., 2017) and survival (Heberer et al., 2010; Sepulveda et al., 2015) principally attributable to injury and/or exhaustive exercise. While studies on rajids are lacking, the estimates for fight time for flapper skate (8–50 minutes) are broadly comparable with those for other large elasmobranchs targeted by anglers, such as common thresher sharks (*Alopias vulpinus*) (Heberer et al., 2010; Sepulveda et al., 2015), notwithstanding substantial differences in biology and capture context. In the model of fight time for flapper skate, there was indicative evidence that fight times were higher for larger individuals, as observed by anglers and in other settings, which suggests that larger individuals may be more susceptible to capture-related impacts (Danylchuk et al., 2014). Similarly, graphical analysis supported the hypothesis that fight times are longer for individuals caught in cooler, deeper water. However, in line with the limited availability of data, unsurprisingly these

terms were not statistically significant and further data are required to clarify their effects. In contrast, there was no evidence that fight times were substantially longer for males compared to females, in relation to recent capture history or at particular times of day.

Collectively, the results from the model of fight time suggest that a large portion of variation in fight time is attributable to unmeasured variables, potentially including environmental conditions (such as dissolved oxygen levels), angler variables (such as gear) and individual characteristics (such as energy levels). For instance, dissolved oxygen levels underpin aerobic activity and are likely to influence individual responses during capture (Musyl and Gilman, 2019). In this study, the effects of dissolved oxygen levels are likely to correlate with temperature, but the shape and strength of this relationship in the study site, and its effects on capture responses, warrant further investigation, as noted elsewhere (Musyl and Gilman, 2019). Other environmental conditions, such as seabed sediment type, suspended sediment loads and localised variation in current speeds not captured by the rate of change in tidal elevation metric used in this chapter, may also be important. In other settings, angler variables such as gear have been shown to influence fight time (Mullen et al., 2020) and post-release outcomes such as survival (Mohan et al., 2020). In this study, gear was standardised for tag deployment, but the gear used by recreational anglers to capture individuals during their time at liberty and in association with tag retrieval events may have differed and these differences may explain some residual variability. However, it is worth noting that there are clear gear guidelines in the study site and most recorded recreational angling occurs from a small number (2–3) of charter vessels, where standard gear is available. Thus, while angler effects on capture responses warrant further investigation, it may be that other variables, such as skate energy levels, are important too. In many taxa, there is also accumulating evidence that personality affects responses to novel situations (Chapter One; Roche et al., 2016). In a study on Port Jackson sharks (*Heterodontus portusjacksoni*), bolder individuals were more responsive to a stress-inducing stimulus than shyer individuals (Byrnes and Brown, 2016). This raises the intriguing possibility that flapper skate may have distinct personalities that affect capture responses. Taken together, the results demonstrate that a targeted scientific data collection programme is required to understand fully the drivers of fight time in flapper skate. In particular, future sampling should prioritise the collection of data using standardised gear across a more representative range of body sizes, temperatures and depths (Chapter Seven). Direct measurements of fight time, in situ environmental

conditions (such as current speeds) and physiological parameters of the muscular activity induced by capture would greatly support this research (Chapter Seven).

During capture, the changes that individuals experienced in depth and temperature were relatively extreme given the distribution of natural variation. While these changes could not be related to post-release outcomes for most individuals in this study, evidence from other species suggests that extreme changes in depth and temperature have the potential to impact skate. For example, in sleeper sharks, decompression-like gas bubbles were documented following capture by commercial trawlers in waters 600–800 m deep (Garcia et al., 2015). While catch-and-release angling for flapper skate differs from commercial trawling for sleeper sharks, this suggests that rapid ascents can affect elasmobranchs and that the impacts of rapid capture-induced ascents in flapper skate warrant further investigation. Elevated water temperatures can also influence the impacts of catch-and-release angling (Danylchuk et al., 2014). It is notable that the maximum temperature experienced by a flapper skate (1519) during capture (22.89 °C) was 44 % higher than the typical maximum water temperature in the area (16.00 °C), but the consequences of exposure to elevated temperatures remain uncertain (Chapter Seven).

Following catch-and-release angling, there was evidence for altered post-release movement patterns and behaviour. Progressive descents into deeper water are probably partly attributable to the bathymetric landscape, particularly off Kerrera where the deep channel over which most angling occurred deepens towards the west of the study site. However, individuals may have also sought refuge in deeper water, with similar movements documented in other species following capture by recreational and commercial gear (Hoolihan et al., 2011; Rogers et al., 2017). Particularly in summer, deeper water may provide a suitable resting location in which cooler temperatures and/or shelter from currents facilitate recovery from exhaustive exercise. Indeed, following tagging and descent, 67 % of individuals exhibited a period of minimal vertical activity that is suggestive of ‘reorientation’, resting or recovery behaviour, like that observed in other species (Hoolihan et al., 2011; Danylchuk et al., 2014). However, low vertical activity around angling marks could also result from rapid horizontal movement along the bottom of the long, deep channels found in these locations. Hence, the development of modelling methods for the reconstruction of movements over the seabed alongside the collection of additional

(accelerometry) data would help to clarify the links between these movements and behaviour, and the ways in which movements are shaped by the local environment (Chapters Six–Seven; Gleiss et al., 2017). Despite short-lived periods of low vertical activity post-release, overall average vertical activity in the 12-hours post-release increased. Post-release elevations in vertical activity or 'hyperactivity' have been documented in other elasmobranchs (Hoolihan et al., 2011) and teleosts (Cooke and Philipp, 2004). The causes for this remain unclear, but physiological changes, such as elevated adrenaline, and post-recovery 'escape' behaviour are possibilities.

However, there was limited evidence for IPRB. This result suggests that flapper skate are generally behaviourally resilient to catch-and-release angling conducted from charter vessels in the LStSJ MPA. This suggestion is consistent with repeated captures of individual skate by anglers (Chapter Three; Benjamins et al., 2018; Skatespotter, 2021) and the condition of rajids caught in commercial fisheries, although the capture experience between hooks and nets differs (Little, 1995; Benoît et al., 2010). This resilience may reflect skate biology, angling practices and the study design. Biologically, elasmobranchs with buccal-pump ventilation are generally thought to be relatively resilient to capture (Cook et al., 2019). The adoption of best-practice angling guidelines, such as the use of barbless hooks, may also have minimised capture-related impacts (Skomal, 2007). Aspects of this study's design may have further contributed towards the apparent resilience of skate. Importantly, only catch-and-release angling from charter vessels was considered, which may be less impactful than shore-based angling in situations where skate are pulled over the substrate for substantial distances. Additionally, archival time series only permit examination of a small number of movement metrics based on depth use and vertical activity which, in turn, only directly reflect behavioural responses to capture (Whitney et al., 2016). A related limitation is the small sample of capture events. This translates into a limited sample of the conditions which might worsen capture-induced stress, including ontogeny, environmental variables, such as temperature, and angling mishaps, such as hooking damage or retention (Cook et al., 2019). For example, despite best practices, individuals are occasionally deep hooked and, in these situations, hooks can be difficult to recover and may be left in skate (Chapter Two). An additional consideration is that archival data may positively bias inferred resilience because they can only be retrieved from individuals that have survived multiple capture events. However, the recapture rate in this study

(46 %), in line with the rate documented across all individuals identified in the area (Skatespotter, 2021), suggests that survivability for many skate is high following angling.

Nevertheless, there was evidence for IPRB in at least three skate. This took the form of rapid re-ascents towards the surface. Few studies are available against which to compare this behaviour and its causes are unclear. Some teleosts show qualitatively similar patterns following catch-and-release. For example, Pacific cod (*Gadus macrocephalus*) often undertake a rapid 'escape' dive before re-ascending and then descending once more through a series of 'bounce' dives which progressively weaken over a period of days (Nichol and Chilton, 2006). In cod, this behaviour is attributable to the rupture, subsequent repair and refilling of swim bladder. While elasmobranchs lack a swim bladder, their buoyancy is sensitive to pressure changes and similar movements following capture of a leafscale gulper shark (*Centrophorus squamosus*) by a commercial longline (Rodríguez-Cabello and Sánchez, 2017) suggest that rapid ascents might contribute to a loss of equilibrium. In other elasmobranchs, reports of aberrant behaviour are generally associated with extreme external trauma (Kabasakal, 2010; Rodríguez-Cabello and Sánchez, 2017), but this is unlikely to apply for angled flapper skate. However, this suggests that skate may be more sensitive to capture than previously assumed in some circumstances.

Given limited pre-capture data, there are few obvious factors that might have increased the vulnerability of the individuals that exhibited IPRB to capture-related impacts. Among the five individuals with pre-capture data, it is notable that the individual that exhibited IPRB (1523) had the longest fight time (38 minutes), given the influence of fight time on capture-related impacts in other species (Danylchuk et al., 2014; Sepulveda et al., 2015). Additionally, all individuals that exhibited IPRB had relatively recent capture records (within 46–76 days), though the number of previous captures varied from one (1523) to four (1507). In terms of individual characteristics, IPRB was documented in both sex and maturity categories. Furthermore, IPRB was documented in spring in relatively cool water (8.72–10.13 °C) and the temperature change that the individual with data (1523) experienced during capture was small (0.27 °C), contrary to the hypothesis that capture resilience might be lower in late summer. There are insufficient data to determine whether the prevalence of IPRB differed between recreational catch-and-release angling events that occurred during individuals' time at liberty (0.20) and post-tagging (0.14), but preliminary

estimates suggest this is not the case. Other aspects of the capture process, such as hooking location, may have affected IPRB but the data required to evaluate these were unavailable.

While IPRB was uncommon, from a conservation perspective it is potentially concerning. Rapid ascents are likely to be energetically costly for skate. On top of the exertion of capture, such ascents may have implications for activities such as foraging (Skomal, 2007). Rapid ascents may also induce barotrauma or worsen symptoms caused by the initial capture process. If a loss of equilibrium underlies rapid ascents, they may reflect increased predation risks for smaller skate, as shown for other taxa (Cooke and Philipp, 2004). Disruption to mating, which is thought to occur in spring when catch-and-release angling is most frequent (Chapter Three), may occur too. Taken together, the main message of these results is that flapper skate is typically behaviourally resilient to catch-and-release angling from charter vessels in the LStSJ MPA, but observed post-release behavioural changes inferred from archival data, especially IPRB, are sufficiently notable to indicate that further research is required into the cumulative individual and population-level impacts of this practice. This is essential for accurate population estimates and successful conservation (Chapter Seven; Neat et al., 2015).

Appendices

1. Supporting methods

1.1. The capture experience

A generalised linear modelling framework was used to identify the drivers of variation in fight time and thus the conditions in which skate may be more or less susceptible to capture-related impacts. Fight time was considered in relation to the following variables:

- **Sex.** Sex (male, M; female, F) was included in the model as a factor.
- **Body size.** Skate dorsal surface area (m^2) was included in the model as a metric of body size and as part of a term to account for the intertwined effects of body shape and tidal flows. For this analysis, individual surface area was approximated by treating each individual's disc width (cm) as the diagonal of a square, with area (m^2) given as $½(disc\ width/100)^2$. This metric is a pragmatic option in the absence of detailed morphometric data and is likely to represent surface area reasonably well, despite ignoring the influence of the tail and individual variation in body shape. The expectation was that larger skate should have longer fight times. Yet since skate are typically caught in the mouth and thus pulled up in a vertical position during capture (Chapter Two), the influence of body size was expected to be greater for larger skate in line with the strength of tidal flows. For this reason, body size was included via an interaction with the tidal term in the model (see below).
- **Recent capture history.** The number of capture events prior to each capture event and the number of days since the last recorded capture event were taken as metrics of recent capture history. Capture events were sourced from the mark-recapture database maintained by NatureScot, Marine Scotland Science and the Scottish Association for Marine Science (Chapter Two).
- **Capture depth.** The depth (m) at the onset of each capture event was included to control for the depth at which skate were captured.
- **Tidal phase.** The rate of change in tidal elevation (ms^{-1}) at the onset of each capture event was included as a metric for the strength of the tidal force pulling captured individuals

away from a vessel. Rates of change were derived from the differences between sequential tidal elevation (m) values, resolved every 15 minutes at Oban and linearly interpolated to two-minute intervals, sourced from POLTIPS.3 tidal prediction software. The influence of this metric was expected to be proportional to individual surface area and thus included via an interaction with body size in the model (see above). The metric is a pragmatic option, given the absence of locations for 9/26 captures (see Table S1), and supported by recent work (Chapter Two). However, the metric is unavoidably imperfect, given the complex interactions between currents, bathymetry and depth in the study site (Aleynik et al., 2016).

- **Light levels and biological time of day.** Sun angle above the horizon (°) at the onset of each capture event was included as a metric of 'light levels' or 'biological time of day' designed to capture putative diel changes in vertical activity levels (Chapter Four). As for tidal information, given the absence of capture locations, sun angles were calculated for Oban. The suncalc package was used for calculations (Thieurmel and Elmarhraoui, 2019).
- **Temperature and time of year.** Temperature (°C), as recorded by archival tags at the onset of each capture event, was included to capture variation in thermal performance and/or associated seasonality in vertical activity levels.

It is recognised that many other variables may affect fight time, including environmental conditions such as dissolved oxygen levels, alongside 'angler variables', such as gear, experience and energy levels (Mullen et al., 2020). In this chapter, the data required to include these variables in the model were unavailable and their effects remain important avenues for future research. Nevertheless, it is anticipated that dissolved oxygen levels are likely to correlate with bottom temperatures and the influence of angler variables may be limited by the availability of standard gear onboard charter vessels. Furthermore, skate angling is generally driven by the pull on the line from the bottom, rather than the top: when the pull from the skate eases, skate can be pulled up by the angler, with the line taking up the slack; when the pull from the skate increases, the line and the angler simply hold the tension. During this time, skate that fight strongly tend to overcome the ratchet on the line, irrespective of the angler at the other end. It is only when the line temporarily relaxes again that the skate can be reeled in by the angler.

Based on these considerations, fight time (`fight`) was modelled in relation to sex (`sex`), skate surface area (`size`) and the rate of change in tidal elevation (`tide`), the number of capture events prior to each capture (`n`), the time (days) elapsed since the last capture event (`gap`) and the sun angle (`sun`), temperature (`temperature`) and the depth (`depth`) at the start of each event. Prior to model fitting, rates of change in tidal elevation were centred (by minusing the mean) and scaled (by dividing by the standard deviation) to facilitate convergence. All captures were assumed to be independent, since only four individuals were caught more than once. Models were fitted using the `glm` function in the `R` `stats` package, as shown below:

```
# Load stats package
library(stats)
# Fit the model
mod <- glm(fight ~
             sex +
             size * tide +
             n +
             gap +
             sun +
             temperature +
             depth,
           data = captures,
           family = gaussian(link = "log")
           )
```

where `sex` is a factor that distinguishes males and females and other variables are as previously defined. `captures` refers to a dataset with one row for each capture event and one column for each variable.

1.2. Average changes in depth and vertical activity

To quantify the average changes in depth and vertical activity between post-release and 'undisturbed' samples and the drivers of variation in individuals' responses to capture, the mean depth (`depth_mean`), the mean absolute vertical activity (`va_abs_mean`) and the duration of

minimal absolute vertical activity (`va_abs_min_duration`) were considered as response variables in generalised linear models.

Each variable was modelled in relation to a factor distinguishing post-release and 'undisturbed' samples (`sample`), sex, body size (total length, `size`) and the mean temperature across each 12-hour sample, calculated from the archival tag record (`temperature`). Total length and temperature were centred and scaled before model fitting to facilitate convergence. Since 17/21 individuals were uniquely defined by their total length, individual was not included as a random effect despite the incorporation of multiple samples per individual. Models were fitted as shown below:

```
# Load stats package
library(stats)
# Fit mean depth model
mod_depth_mean <-
  glm(depth_mean ~ sample * sex * size + temperature,
      data = dat_avg,
      family = gaussian(link = "log")
  )
# Fit mean, absolute vertical activity model
mod_va_abs_mean <-
  glm(va_abs_mean ~ sample * sex * size + temperature,
      data = dat_avg,
      family = gaussian(link = "log")
  )
# Fit duration of minimal, absolute vertical activity model
mod_va_abs_min_duration <-
  glm(va_abs_min_duration ~ sample * sex * size + temperature,
      data = dat_avg,
      family = Gamma(link = "log")
  )
```

where all variables are as previously defined. `dat_avg` is a dataframe, with one row for each time series sample and one column for each variable.

1.3. Irregular post-release behaviour

Functional data analysis (FDA), specifically functional principal component analysis (FPCA), was used to identify irregular post-release behaviour (IPRB) from depth and vertical activity time series according to the protocol shown below for an example individual:

```
#### Define observations
# For each individual, the post-release depth and vertical activity
# ... time series and the accompanying 'undisturbed' samples were
# ... formatted as matrices, with one column for each time series and
# ... one row for each time step. For each variable,
# ... FPCA was then performed on the corresponding matrix, as illustrated
# ... below for an example matrix named 'mat'.

#### Make B-splines
# 25 basis functions were used for short depth time series.
# 100 basis function were used for absolute vertical activity time series.
# This number of basis functions was sufficient to capture the
# ... main features of observed time series reasonably. However,
# ... the overall results were robust to 5-fold
# ... changes in the number of basis functions.
# In this example, we apply FPCA to a matrix for the depth time series
n_basis    <- 25
rng        <- 1:nrow(mat)
bs_splines <- fda::create.bspline.basis(range(rng), n_basis)

#### Create a functional data object using the matrix and B-spline basis
fda_df <- fda::Data2fd(mat, argvals = rng, basisobj = bs_splines)

#### Compare smooths and observations
# Extract necessary objects
fdobj  <- fda_df
y      <- rng
```

```
Lfdobj <- fda::int2Lfd(0)
fdmat  <- fda::eval.fd(y, fdobj, Lfdobj)
# Plot first time series and smooth as an example
plot(y, fdmat[, 1], col = "red")
lines(y, mat[, 1])

#### Implement FPCA
pcs_1 <- fda::pca.fd(fda_df)
```

2. Supporting tables

Table S1. A summary of capture events. For each individual (Tag ID), the following variables are shown: body size (estimated dorsal surface area); the event type (capture during [D] individuals' time at liberty by recreational anglers or the final [F] capture immediately preceding tag retrieval); the location if known (Kerrera, K; Loch Sween, LS); the date (year-month-day); the time since the last capture; the start ([1]), surface ([2]), release ([3]), fight ([F]) and handling ([H]) time (if applicable); the start rate of change in tidal elevation; the start depth; the start, surface and release temperature (if applicable); and the number of previous (recorded) captures. Locations were recorded for two recreational angling events and seven tag retrieval events. However, the capture location recorded for 1536 (Loch Sween*) is inconsistent with the depth time series around capture for that individual given that the maximum depth for the area reported by the Loch Sween Possible Nature Conservation Marine Protected Area Data Confidence Assessment is 40 m (Chapter Two; Scottish Natural Heritage, 2013). Data are sorted by Tag ID and capture date.

Tag ID	Size (m^2)	Event	Site	Date	Time [since last capture] (days)	Time [1]	Time [2]	Time [3]	Time [F]	Time [H]	Tide [1] (m/s)	Depth [1] (m)	T [1] (°C)	T [2] (°C)	T [3] (°C)	N (previous)
1502	1.36	F	-	19-02-26	678	10:36	11:04	-	28	-	1.11×10^{-5}	155.11	8.28	18.08	-	2
1507	1.28	F	-	16-05-18	62	11:21	11:45	-	24	-	8.89×10^{-5}	166.52	9.01	9.47	-	4
1509	0.50	F	K	17-04-20	399	10:39	10:53	-	14	-	2.22×10^{-5}	150.87	8.52	8.72	-	1
1511	1.10	F	K	16-08-28	164	13:39	13:47	-	8	-	5.56×10^{-5}	146.00	13.68	13.62	-	2
1512	1.45	F	-	16-07-13	118	14:19	14:33	-	14	-	5.56×10^{-5}	162.62	11.82	12.23	-	4
1518	1.10	F	K	17-03-22	371	11:30	11:50	-	20	-	3.33×10^{-5}	96.69	8.02	7.81	-	1
1519	1.45	F	-	19-03-31	711	13:40	14:08	-	28	-	5.56×10^{-5}	151.08	8.12	22.89	-	1
1520	1.01	F	-	16-07-13	119	13:22	13:34	-	12	-	2.22×10^{-5}	138.14	11.84	11.84	-	1
1522	0.84	D	-	16-07-13	119	15:12	15:28	15:32	20	4	7.78×10^{-5}	140.39	11.84	11.80	12.85	1
1522	0.84	D	K	16-08-27	45	14:46	15:00	15:04	18	4	2.22×10^{-5}	143.14	13.63	13.57	14.38	2
1522	0.84	F	K	17-04-18	234	14:08	14:20	-	12	-	5.56×10^{-5}	144.58	8.49	8.56	-	3
1523	1.05	D	-	16-05-16	61	09:56	10:28	10:34	38	6	6.67×10^{-5}	157.04	8.96	9.23	10.45	1
1523	1.05	F	-	16-05-26	10	13:56	14:46	-	50	-	3.33×10^{-5}	158.23	9.46	11.10	-	2
1525	1.32	F	-	17-05-03	14	10:46	11:36	-	50	-	3.33×10^{-5}	139.59	8.94	8.94	-	1

Tag ID	Size (m^2)	Event	Site	Date	Time [since last capture] (days)	Time [1]	Time [2]	Time [3]	Time [F]	Time [H]	Tide [1] (m/s)	Depth [1] (m)	T [1] (°C)	T [2] (°C)	T [3] (°C)	N (previous)
1526	1.28	F	-	16-03-19	3	11:54	12:26	-	32	-	1.22×10^{-4}	184.00	7.75	7.82	-	1
1533	0.71	D	-	16-05-10	57	14:29	14:41	14:45	16	4	4.44×10^{-5}	172.63	8.70	8.73	13.99	2
1533	0.71	F	K	16-10-08	136	11:21	11:33	-	12	-	4.44×10^{-5}	163.36	14.02	13.78	-	4
1536	1.07	D	LS*	16-04-29	46	09:26	09:42	09:48	22	6	0.00	134.17	8.26	8.22	7.65	1
1536	1.07	F	K	16-10-23	177	11:18	11:36	-	18	-	0.00	153.21	13.60	13.42	-	2
1538	0.65	F	-	17-07-19	491	16:48	16:58	-	10	-	1.11×10^{-4}	83.90	12.11	13.65	-	1
1539	1.20	F	-	16-04-29	45	10:40	10:54	-	14	-	5.56×10^{-5}	136.01	8.27	8.47	-	1
1547	1.32	F	-	18-04-26	772	11:16	11:36	-	20	-	1.22×10^{-4}	147.33	7.14	9.20	-	2
1548	1.12	F	K	17-04-21	401	13:58	14:12	-	14	-	1.11×10^{-5}	137.20	8.51	9.04	-	1
1552	0.94	F	-	16-04-02	20	15:40	15:54	-	14	-	5.56×10^{-5}	149.18	7.86	7.86	-	2
1558	0.91	F	-	16-05-28	76	16:10	16:24	-	14	-	2.22×10^{-5}	145.03	9.51	10.13	-	2
1574	1.28	F	-	16-06-09	98	14:18	14:44	-	26	-	3.33×10^{-5}	167.80	10.35	13.39	-	1

Table S2. Coefficient estimates from a generalised linear model of fight time. Coefficients were estimated from 26 capture events of 21 individuals. The model explained 59.691 % of the deviance. For each term, the estimate, standard error, *t*-value and *p*-value are shown.

Term	Estimate	SE	*t*-value	*p*-value
(Intercept)	1.326	1.254	1.057	0.306
Size	0.900	0.552	1.629	0.123
Tide	1.179	0.768	1.536	0.144
Size: Tide	-1.054	0.645	-1.634	0.122
Sex (male)	0.277	0.221	1.257	0.227
Number of previous captures	-0.080	0.105	-0.762	0.457
Number of days since last capture event	0.000	0.001	-0.972	0.345
Sun angle	0.012	0.012	0.970	0.346
Temperature	-0.119	0.068	-1.744	0.100
Depth	0.011	0.006	1.689	0.111

Table S3. Coefficient estimates from generalised linear models of the mean depth, the mean absolute vertical activity and the duration of minimal (≤ 0.5 m) absolute vertical activity in 12-hour post-release periods versus corresponding 'undisturbed' samples. Coefficients were estimated from 1,844 observations, including 26 capture events and 1,818 'undisturbed' samples. The models explained 14.459, 11.104 and 9.524 % of the deviance, respectively. For each term, the estimate, standard error, *t*-value and *p*-value are shown.

Term	**Model and estimates**											
	Mean depth (DP, m)				**Mean absolute vertical activity (|VA|, m)**				**Duration minimal absolute vertical activity ($\|VA_{min}\|$, mins)**			
	Estimate	***SE***	***t-value***	***p-value***	***Estimate***	***SE***	***t-value***	***p-value***	***Estimate***	***SE***	***t-value***	***p-value***
(Intercept)	4.675	0.011	439.240	0.000	0.491	0.017	29.455	0.000	5.165	0.014	367.617	0.000
Sample (post-release)	0.072	0.077	0.933	0.351	0.330	0.110	3.008	0.003	-0.520	0.115	-4.533	0.000
Sex (male)	0.440	0.034	12.874	0.000	-0.366	0.079	-4.640	0.000	0.416	0.057	7.278	0.000
Total length (scaled)	-0.110	0.009	-12.349	0.000	0.135	0.014	9.833	0.000	-0.081	0.012	-6.788	0.000
Temperature (scaled)	-0.010	0.008	-1.364	0.173	0.122	0.013	9.281	0.000	-0.116	0.011	-10.221	0.000
Sample (post-release): sex (male)	-0.206	0.324	-0.635	0.526	0.828	0.548	1.512	0.131	-1.022	0.551	-1.856	0.064
Sample (post-release): total length (scaled)	0.036	0.071	0.504	0.614	-0.009	0.103	-0.092	0.927	-0.037	0.107	-0.350	0.726
Sex (male): total length (scaled)	-0.586	0.078	-7.506	0.000	0.404	0.162	2.494	0.013	-0.560	0.123	-4.546	0.000
Sample type (post-release): sex (male): total length (scaled)	0.369	0.728	0.508	0.612	-2.002	1.378	-1.452	0.147	2.555	1.212	2.108	0.035

3. Supporting figures

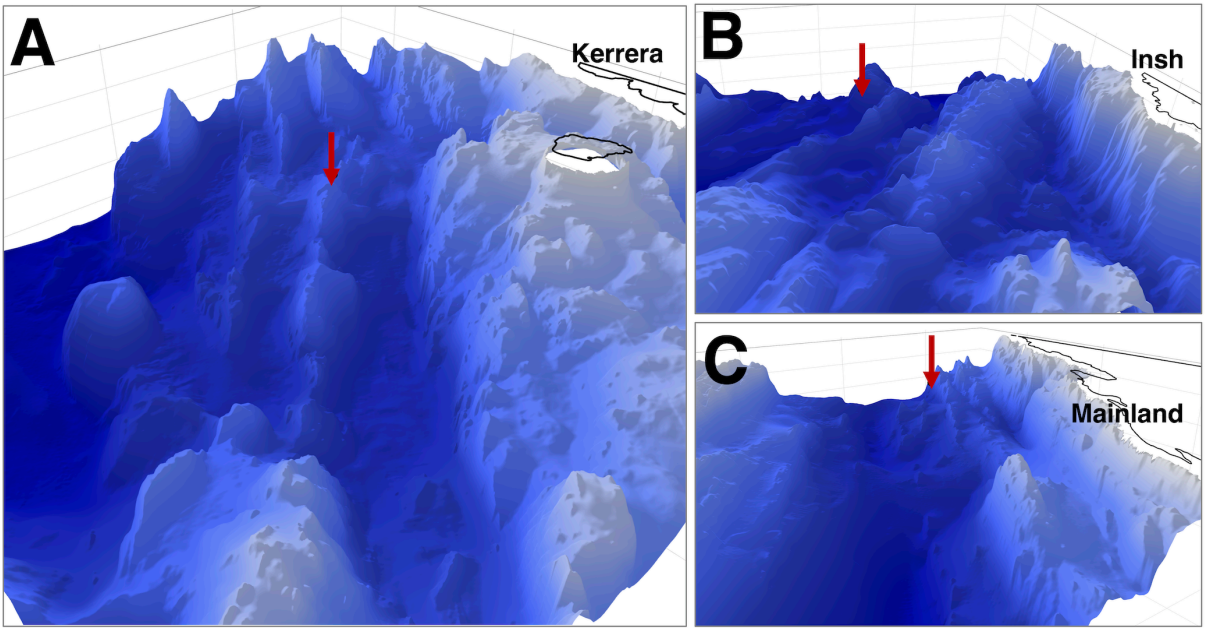

Figure S1. The bathymetry around angling marks. Each panel shows the shape of the bathymetry in an approximately 2000 m area around an angling mark (marked by the red arrow) at (**A**) Kerrera, (**B**) Insh and (**C**) Crinan. Maps are orientated to show the bathymetric structure at each site and thus lie in only approximately a North–South orientation. Bathymetry data were sourced from Howe et al. (2014). Coastline data were sourced from Digimap. Digimap data © Crown copyright and database rights [2019] Ordnance Survey (100025252).

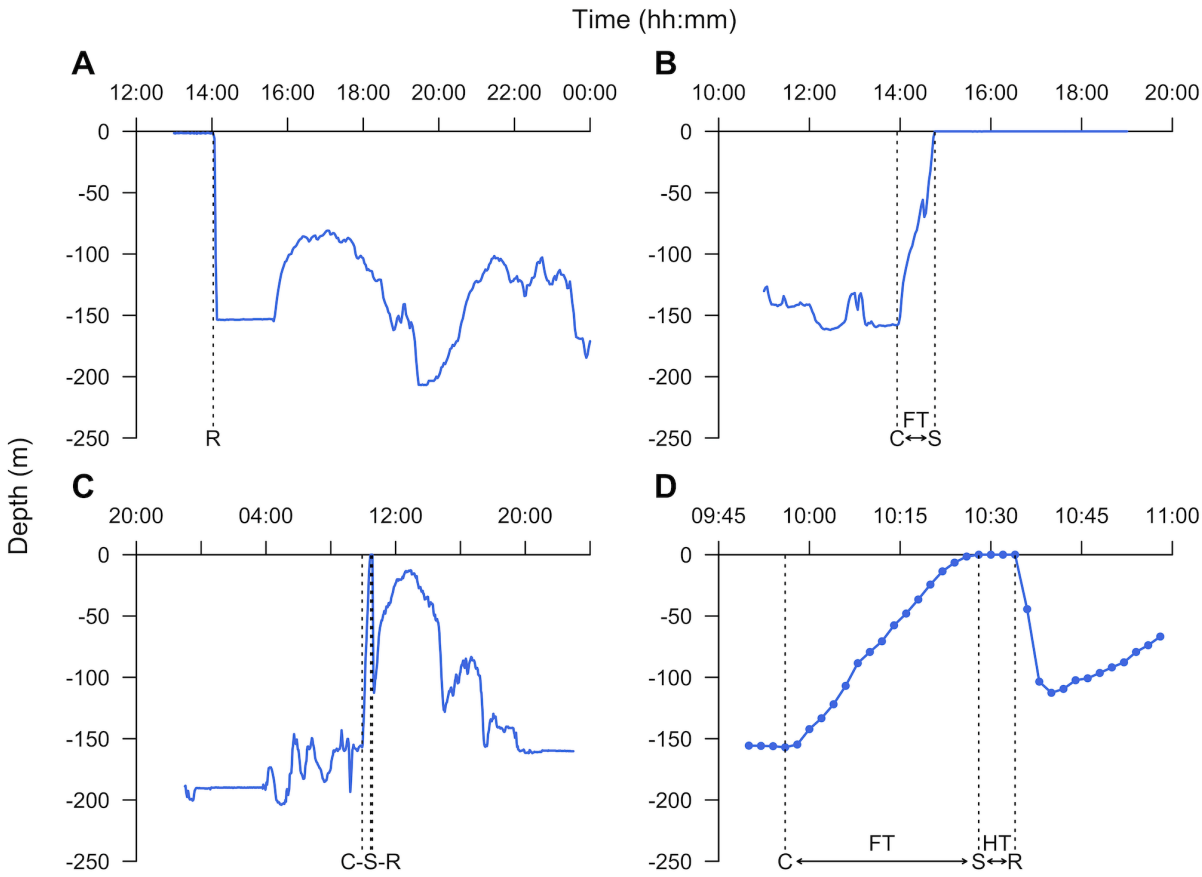

Figure S2. The characterisation of catch-and-release events. Each panel shows an individual's depth time series around a catch and/or release event: **A**, a tag deployment event; **B**, a tag retrieval event; and **C–D**, a catch-and-release event during the individual's time at liberty, in outline in **C**, where it is clearly visible on the recorded day of capture as a spike in the depth time series, and in detail in **D**. Tag deployment events (**A**) provide information on post-release behaviour; tag retrieval events (**B**) provide information on the capture process; and catch-and-release events during individuals' time at liberty (**C–D**) provide information on both. Event times were defined using the depth time series. The capture time (C) was defined as the time of the last depth observation preceding the capture ascent; the surface time (S) as the time of the first observation at the surface; and the release time (R) as the time of the last observation preceding the post-release descent. Fight time (FT) was defined as S – C. Note that this is likely to be an underestimate of the true fight time, since hooked individuals—especially large individuals—tend to dig into the sediment when hooked and only ascend after a period of tension from a rod and line. For recreational catch-and-release events that occurred during individual's time at liberty (**C–D**), handling time (HT) was defined as R – S.

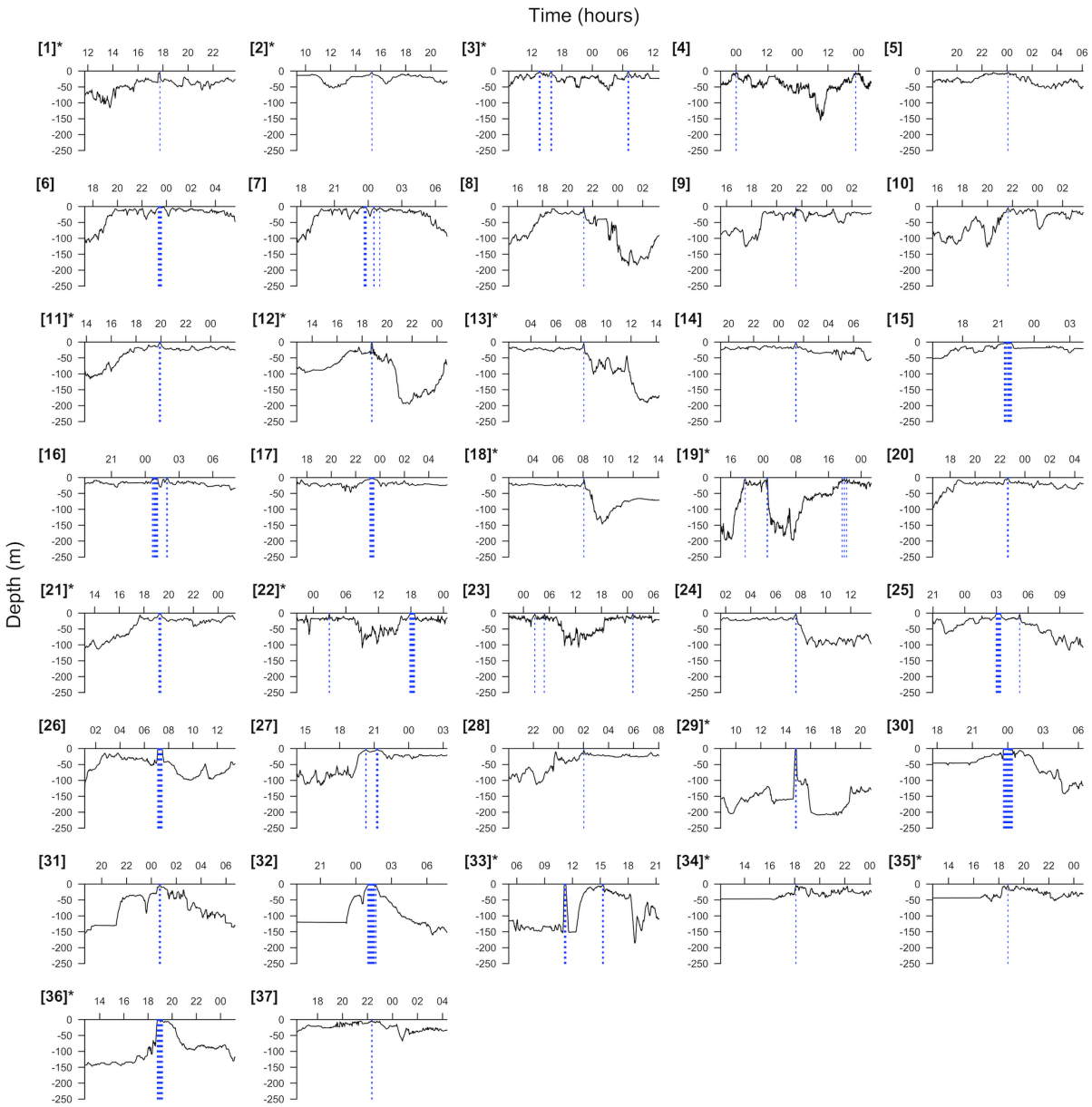

Figure S3. Near-surface movements of tagged individuals during their time at liberty. Each panel (n = 37) shows the depth time series around a period of near-surface movement when the depth was shallower than 5 m. These movements represent potential unrecorded capture events resulting from recreational angling. Asterisks highlight near-surface movements that occurred between 0800 and 2000 hours (n = 15), which are more likely to have been capture events. Of these, the depths at which individuals were caught and the shape of the depth time series are consistent with changes observed during known capture events from vessels around angling marks (Figure 3) in two cases: [29] (individual 1533 on 2016-05-25) and [33] (individual 1538 on 2016-06-25). In both cases, rapid ascent from approximately 150 m, followed by a short-lived period at the surface, rapid descent and a period of low vertical activity match patterns observed around known capture events. For event 33, subsequent rapid ascent also resembles the irregular post-release behaviour observed following known capture events for some individuals. There are two other cases ([19] and [36]) in which relatively rapid ascents preceded a period of daytime near-surface water use, but the longer durations in near-surface water suggest that these movements did

not result from capture from vessels. Other periods of near-surface movement do not resemble recorded catch-and-release events. Taken together, the paucity of evidence for unrecorded capture events suggests that they are rare and their influence on analyses of the capture process and the behavioural impacts of catch-and-release is likely to have been minimal (especially in the context of the rest of each individual's time series). However, it is possible that some daytime near-surface movements result from shore-based angling, which is likely to leave different signatures in the depth time series from vessel-based angling.

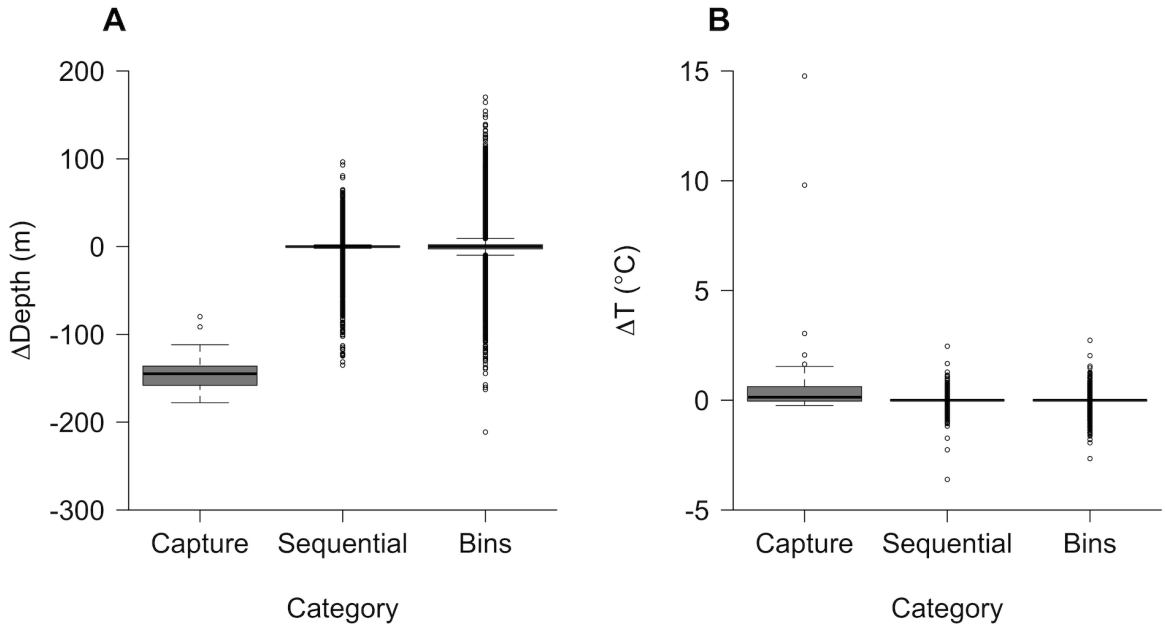

Figure S4. The changes in (A) depth and (B) temperature during capture fights relative to sequential or sustained changes in the rest of individuals' time series. Sequential changes are between consecutive observations. Sustained changes are the total change in each bin in the rest of individuals' time series of comparable size to the duration of capture events.

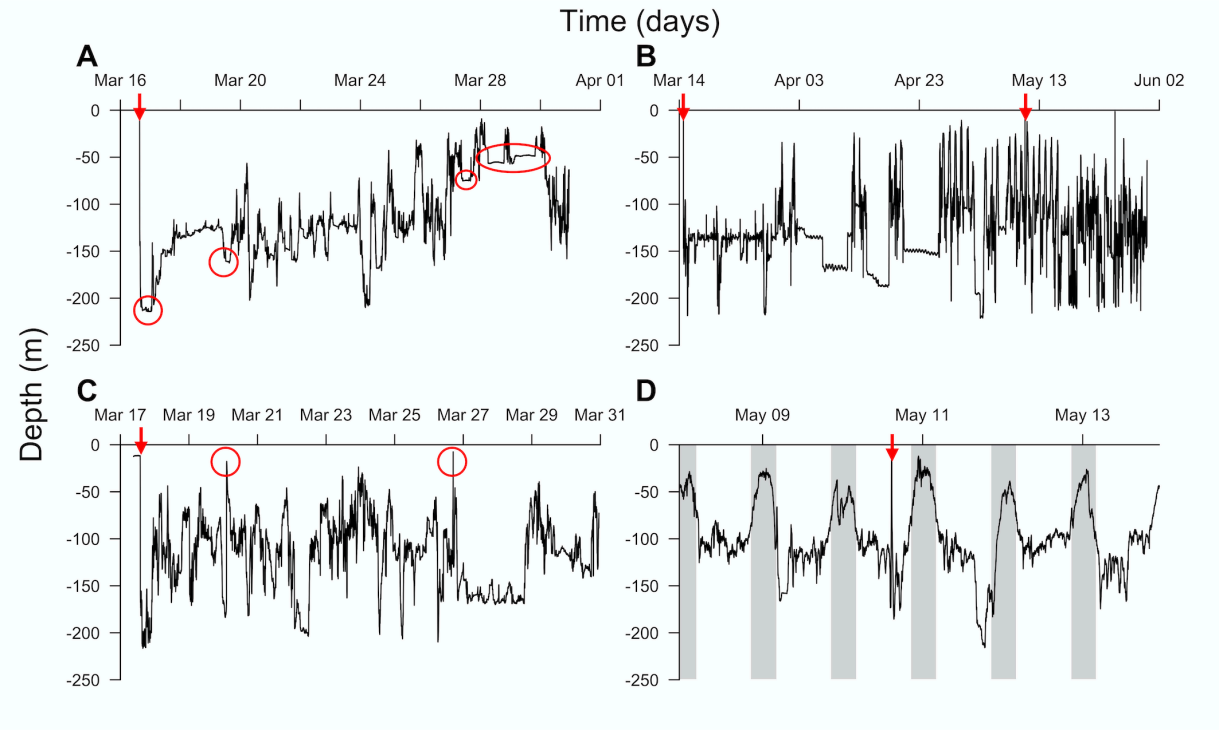

Figure S5. Example longer term depth time series spanning capture events and 'undisturbed' time series. Each panel shows a sample of depth time series for individuals **A**, 1548; **B**, 1533; **C**, 1512; and **D**, 1533. Samples were chosen to represent a diversity of patterns. Arrows mark capture or release and circles highlight notable patterns. In **A**, low vertical activity immediately post-release (circled) is repeated at later dates, presumably reflecting 'undisturbed' activity. In **B**, highly variable movement patterns are apparent, including periods of low vertical activity and higher vertical activity. In **C**, high vertical activity beyond capture events is highlighted. In **D**, a pattern of diel vertical migration appears unperturbed by capture.

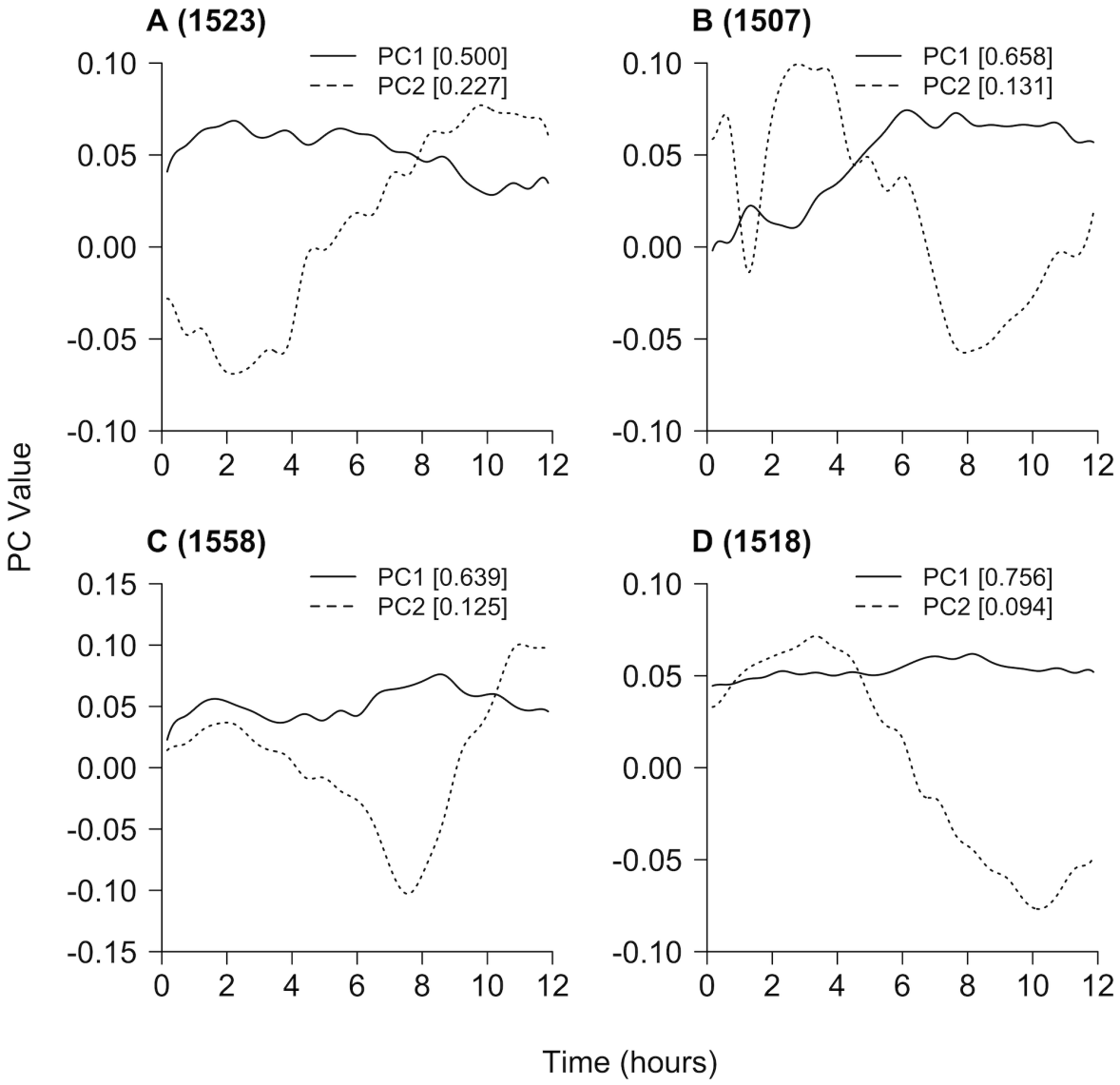

Figure S6. Functional principal component analysis (FPCA) harmonics for the depth time series. Each panel shows the first (solid line) and second (dashed line) harmonic from FPCA of the depth time series for a specific individual. These are the functions that explain the most variation among the post-release and 'undisturbed' sample time series. Time series with highly positive scores for a principal component (PC) are more similar to that function than time series with lower scores (near zero), while time series with highly negative scores are more similar to the reflection of that function around y = 0. In turn, higher PC values correspond with movement into deeper water. Thus, the post-release time series for individual 1523 following recreational angling with a highly negative score on PC2 (Figure 6J) is well described by the mirror image of the second harmonic, reflecting the rapid re-ascent of this individual into shallower water following release (Figure 3C).

Chapter Six

A semi-stochastic modelling framework for passive acoustic telemetry

Abstract

1. Passive acoustic telemetry is widely used to study the movements of aquatic animals. However, a holistic, mechanistic modelling framework that permits the reconstruction of fine-scale movements and emergent patterns of space use from discrete detections at receivers remains lacking.
2. This chapter introduces a semi-stochastic modelling framework that recapitulates the movement and detection processes that generate detections to reconstruct fine-scale movements and patterns of space use. This framework is supported by a new family of algorithms designed specifically for the kinds of detection and depth time series commonly collected during passive acoustic telemetry studies and can be flexibly extended to incorporate other types of data. Using simulation, applications of the framework are illustrated and algorithm utility is evaluated in different settings. As a case study, movement data collected from the Critically Endangered flapper skate (*Dipturus intermedius*) in Scotland are analysed.
3. The results show that the methods can be used to reconstruct fine-scale movement paths, patterns of space use and support analyses of habitat preferences. For reconstructing patterns of space use, simulations show that the methods are consistently more instructive than the most widely used alternative approach (the mean-position algorithm), particularly in clustered receiver arrays. For flapper skate, the reconstruction of movements reveals responses to disturbance, fine-scale spatial partitioning and patterns of space use with significant implications for marine management.
4. This framework represents a widely applicable methodological advance with applications to studies of pelagic, demersal and benthic species across multiple spatiotemporal scales.

Keywords
aquatic ecology, biotelemetry, centre of activity, particle filtering, passive acoustic telemetry utilisation distribution

1. Introduction

Animal movement has a pivotal influence on ecosystem structure and function (Chapter One; Riotte-Lambert and Matthiopoulos, 2020; Nathan et al., 2022). Within selected areas, movement can reflect habitat preferences (Mercker et al., 2021), species' interactions, such as foraging (Sims et al., 2008), and responses to disturbance (Doherty et al., 2021). Across species' distributions, movement underpins migration (Fudickar et al., 2021), redistribution (Pecl et al., 2017) and large-scale patterns of space use, with profound conservation implications (Hays et al., 2019).

Advances in biotelemetry have revealed movement trajectories in unprecedented detail (Chapter One; Nathan et al., 2022). Satellite tracking has been a major development. In aquatic environments, this technology has been exploited to study a wide range of taxa (Hussey et al., 2015). Yet for many species, satellite tracking is limited by the time individuals spend at the surface and alternative tracking technologies are used. For example, at large spatial scales (typically over hundreds of kilometres), global location sensors have been coupled with latent-variable modelling to reconstruct the movements of pelagic and demersal species (Block et al., 2005; Pedersen et al., 2008). Meanwhile, at fine spatial scales (typically over hundreds of metres), acoustic positioning systems have been used to estimate the positions of tagged animals and reconstruct movements via multilateration (Orrell and Hussey, 2022). However, at intermediate spatial scales (typically over tens of kilometres), there remains a gap in our ability to track aquatic species. At this scale, passive acoustic telemetry systems are widely deployed (Matley et al., 2022). These generally comprise static arrays of receivers with non-overlapping detection ranges that record individual-specific detections of tagged animals within range. Yet while detections can indicate broad-scale features of movement, such as occupancy, the lack of information in detection gaps challenges the reconstruction of movements and patterns of space use.

Four main approaches have been developed to reconstruct movements or patterns of space use from detections (Chapter One). The first approach simply maps detections (Chapter Three). The second (and most common) approach estimates 'centres of activity' (COAs), usually as weighted averages of the locations at which detections were recorded over consecutive time intervals (the mean-position algorithm) (Simpfendorfer et al., 2002). COAs are translated into maps of space use via smoothing techniques such as kernel utilisation distribution (KUD) estimation (Udyawer et al., 2018). Network analysis is a third approach which treats acoustic receivers as nodes on a network that are connected by edges defined by sequential detections (Lea et al., 2016). However, these approaches do not represent the processes that generate detections, including movement and the detection process. Consequently, the underlying movements remain unresolved and maps of space use may be substantially influenced by array design. Building on this limitation, latent-variable models represent a fourth approach (Pedersen and Weng, 2013; Winton et al., 2018; Hostetter and Royle, 2020). These models treat individual locations as latent variables that are linked, via movement and observation models, to detections. Yet existing latent-variable models cannot easily incorporate ancillary information on location, such as depth observations, that is often collected alongside detections. The incorporation of movement barriers, such as coastline, also currently requires bespoke Bayesian model-fitting algorithms that are computationally intensive.

Recently, a fifth 'semi-stochastic' approach has been developed with the potential to address these shortcomings. This approach generates movement path(s) that are consistent with the observations. In its 'refined-shortest paths' implementation, one path (the shortest) is generated between the receivers that recorded sequential detections and used to fit a dynamic Brownian bridge movement model that incorporates path uncertainty with movement away from receivers (Niella et al., 2020). The 'synthetic path' method extends this approach, simulating multiple least-cost paths to map space use (Aspillaga et al., 2019). Yet while this method offers promise for capturing mechanistically the movement and detection processes that generate detections, a general modelling framework for achieving this goal remains lacking (Chapter One).

The aim of this chapter is to establish a holistic semi-stochastic modelling framework for detections that can incorporate observations, the observation process and properties of movement. The framework splits the inference process into two stages. In the first stage, each source of observations is used to establish the set of locations in which a tagged individual

could have been located through time. The 'acoustic-container' (AC) branch of algorithms is introduced for capturing the information provided by detection and depth observations in this stage, but other types of data could be combined in the same way. In the second stage, a particle filtering (PF) process is used to incorporate movement. Alongside the central framework, the coupling of the AC-branch and PF-branch algorithms collectively represents a new family of algorithms for inferring movement paths and patterns of space use that is termed the 'flapper family', following its motivation by research on the Critically Endangered flapper skate (*Dipturus intermedius*) (Chapters Three–Five). To support the application of these algorithms, the flapper R package is introduced. With this foundation, three subsequent objectives are addressed:

A. **Illustration—**using simulation, algorithm applications are illustrated.
B. **Evaluation—**using simulation, algorithm utility in different settings is examined.
C. **Demonstration—**using flapper skate data, real-world applications for reconstructing fine-scale movements, patterns of space use and in analyses of habitat preferences are demonstrated.

2. Methods

2.1. Conceptual overview

The framework advanced here recognises two sources of information on movement trajectories in passive acoustic telemetry systems. Information on location is the first: at any one time, detections (alongside other observations) restrict our uncertainty in an animal's possible location. Information on movement is the second: at any one time, given a previous location, movement limitations restrict our uncertainty in possible future locations. This distinction translates into a two-stage modelling framework. The first stage reconstructs the set of locations in which a tagged individual could have been located through time, given available data, using an AC-branch algorithm. The second stage uses movement restrictions to connect sequential locations, using a PF-branch algorithm.

The chapter introduces three AC-branch algorithms and three corresponding PF-branch algorithms. The first-stage AC algorithm is the backbone of the framework, capturing the information provided by passive acoustic telemetry to define the set of possible locations of an individual through time. In an extension for depth observations, the depth-contour (DC)

algorithm is introduced and the AC and DC algorithms are combined via the ACDC algorithm. For each AC-branch algorithm, its corresponding PF-branch counterpart (the ACPF, DCPF and ACDCPF algorithms) is identified. Collectively, these are termed the 'flapper algorithms' (Table 1). In this chapter, these algorithms are considered in discretised form with locations represented on a uniform grid and the coordinates of cell i's midpoint are denoted by $\boldsymbol{s}^i$.

Table 1. The flapper algorithms. The family comprises three AC-branch algorithms and three corresponding PF-branch algorithms. Together, the AC and ACPF algorithms provide a framework for the semi-stochastic modelling of passive acoustic telemetry data and the DC, DCPF, ACDC and ACDCPF algorithms represent modifications/extensions of this framework that incorporate depth observations.

AC branch	PF branch
AC	ACPF
DC	DCPF
ACDC	ACDCPF

2.2. Acoustic-container algorithm

The AC algorithm is designed to capture the information provided by detections (Figure S1). The crux is that detections anchor our knowledge of an individual's location around receivers, while in the gaps between detections our uncertainty in the individual's location expands away from the receiver that recorded the previous detection while shrinking towards the receiver that recorded the next detection, in line with the individual's movement capabilities. The dynamics of this process are captured by the expansion, contraction and intersection of areas termed 'acoustic containers' that define the set of possible locations of an individual according to receiver(s). Here, for simplicity, these dynamics are described for a simple array with non-overlapping receivers; in the Appendix §1.1, this description is generalised.

Let us consider a sequence of time steps, indexed by t, along which detections of a tagged individual, indexed by t_{acc}, are recorded at regular or irregular intervals (Figure S1). For each pair of detections, let us consider the individual's location from (A) the perspective of the receiver at which it was just detected (or its previous location) and (B) the receiver at which it was next detected. At the moment of the first detection ($t = 1$ and $t_{acc} = 1$), from perspective A, the individual must be within the receiver's maximum detection range (γ), excluding any

inhospitable habitats (U), in an area termed the 'detection container'. If we denote a disk centred (in generic terms) at location $\boldsymbol{x}$ with radius R by $D(\boldsymbol{x}, R)$, then at the moment of first detection the set of locations within which the individual must be located from perspective A (i.e., the container C_A) is given by

$$C_{A,t=1} = D\left(\boldsymbol{r}^{k}_{t_{acc}=1}, \gamma\right) - U, \quad (1)$$

where $\boldsymbol{r}$ is a matrix of receiver coordinates and $\boldsymbol{r}^{k}_{t_{acc}=1}$ denotes the location of the receiver (k) that detected the individual at $t_{acc} = 1$. From perspective B, at $t = 1$ the set of possible locations spans a wider area, in line with the time between detections and the individual's mobility, according to the equation:

$$C_{B,t=1} = D\left(\boldsymbol{r}^{l}_{t_{acc}=2}, \gamma + \Delta(t_{acc} = 1, t_{acc} = 2)\right) - U, \quad (2)$$

where γ is assumed to remain constant and $\Delta(T_1, T_2)$ is a function that defines the maximum distance the individual could move in the time between any two time indices (generically labelled T_1 and T_2). This function is defined as:

$$\Delta(T_1, T_2) = mobility \times \left(\tau(T_2) - \tau(T_1)\right), \quad (3)$$

where $mobility$ is the maximum movement speed and $\tau(T)$ is a function that returns the 'clock' time at time index T. The intersection of C_A and C_B (C_I) defines the set of possible locations at $t = 1$:

$$C_{I,t=1} = C_{A,t=1} \cap C_{B,t=1}. \quad (4)$$

Within C_I, the probability of the individual being in any given location according to the AC algorithm, $\Pr(\boldsymbol{s}^i|AC)$, may vary given variation in detection probability (Figure S1). A standard detection probability model is a logistic model where the probability of a detection event at receiver k at time t ($E[k,t]$), given a transmission from $\boldsymbol{s}^i$, declines with the Euclidean distance ($|\cdot|$) between the two locations:

$$\Pr\left(E[k,t]\middle|\boldsymbol{s}^i\right) \sim logistic\left(\alpha - \beta\left|\boldsymbol{s}^i - \boldsymbol{r}^k\right|\right) = \frac{1}{1+e^{-(\alpha-\beta\times|\boldsymbol{s}^i-\boldsymbol{r}^k|)}}, \quad (5)$$

where α and β are parameters. In a simple array, this model implies that the probability of the individual being in location $\boldsymbol{s}^i$ given a detection at k declines with distance in the same way:

$$\Pr\left(\boldsymbol{s}^i\middle|E[k,t]\right) \sim logistic\left(\alpha - \beta \times \left|\boldsymbol{s}^i - \boldsymbol{r}^k\right|\right), \quad (6)$$

where $\sum_i \Pr\left(\boldsymbol{s}^i\middle|E[k,t]\right) = 1$ (see Appendix §1.1).

Moving forwards in time, we can consider a sequence of intermediate time steps before the next detection (Figure S1). During this time, from the perspective of the individual's previous location (A), the set of possible locations of the individual expands (in line with $mobility$)

because it could have moved away from its previous location. At time step $t+1$ the container $C_{A,t+1}$ will contain all locations ($\boldsymbol{z}$) at most a distance of $\Delta(t, t+1)$ beyond the previous container $C_{I,t}$:

$$C_{A,t+1} = \{\boldsymbol{z}^i \text{ such that } |\boldsymbol{z}^i - \boldsymbol{p}| \leq \Delta(t, t+1) \text{ for any } \boldsymbol{p} \in C_{I,t}\} - U, \quad (7)$$

where $\boldsymbol{p}$ represents all locations in $C_{I,t}$. Meanwhile, from perspective B, the set of possible locations shrinks, as the individual must have been located within the detection container of that receiver by the time of the next detection:

$$C_{B,t+1} = D(\boldsymbol{r}^l_{t_{acc}=2}, \gamma + \Delta(t+1, t_{acc} = 2) - U. \quad (8)$$

At each time step, the intersection of the two containers defines the set of possible locations of the individual:

$$C_{I,t+1} = C_{A,t+1} \cap C_{B,t+1}. \quad (9)$$

During this time, the probability of the individual being at location $\boldsymbol{s}^i$ in C_I, given the absence of a detection at k ($E^c[k,t]$), increases with distance from receivers:

$$\Pr(\boldsymbol{s}^i | E^c[k,t]) \sim 1 - logistic(\alpha - \beta \times |\boldsymbol{s}^i - \boldsymbol{r}^k|), \quad (10)$$

where $\sum_i \Pr(\boldsymbol{s}^i | E^c[k,t]) = 1$ (see Appendix 1.1).

Collectively, these dynamics recognise that as time passes between detections the individual could have moved away from the receiver that recorded the previous detection but only at a rate and in a direction that fits with the receiver that recorded the next detection. Thus, when the individual is detected again, the set of possible locations collapses to the detection container around the relevant receiver (and its intersection with previous and future containers) (Figure S1).

The result is a set of surfaces that describe the individual's set of possible locations though time. Their sum (over the number of time steps) defines a utilisation distribution that describes the expected proportion of time steps spent in each location. The key innovation of this framework is the mechanistic perspective that exploits information both within and between detections, through the incorporation of detection probability, movement barriers and mobility, and the flexibility with which it can incorporate additional information (see §2.3–5).

2.3. Depth-contour algorithm

The DC algorithm captures the information provided by depth observations (Figure S2). In general terms, this algorithm represents the probability of a tagged animal being in a location ($\boldsymbol{s}^i$) at time t according to a depth-error model (f) that depends on the bathymetric depth in that location $\left(bathy(\boldsymbol{s}_t^i)\right)$ and the observed depth ($depth_t$):

$$\Pr\left(\boldsymbol{s}^i|depth_t\right) = f\left(bathy(\boldsymbol{s}_t^i), depth_t\right). \tag{11}$$

For example, we could consider all locations in which the bathymetric depth is deeper than a lower limit and shallower than an upper limit, given two depth-error functions (ε_{lower} and ε_{upper}), as possible locations of the individual:

$$\Pr\left(\boldsymbol{s}^i\middle|DC\right) = \Pr\left(\boldsymbol{s}^i|depth_t\right) \sim \begin{cases} a & \text{if } depth_t + \varepsilon_{lower}(depth_t) \leq bathy(\boldsymbol{s}_t^i) \leq depth_t + \varepsilon_{upper}(depth_t) \\ 0 & \text{otherwise} \end{cases} \tag{12}$$

where a is a positive constant that defines possible locations of the individual, chosen such that $\sum_i \Pr\left(\boldsymbol{s}^i\middle|DC\right) = 1$. This model is suitable for both benthic and pelagic species and permits depth-dependent measurement errors. As for the AC algorithm, the result is a set of surfaces that describe the expected proportion of time steps spent in each $\boldsymbol{s}^i$ and the extent to which an area captures an animal's depth preferences (i.e., habitat representation). It also provides a means to incorporate depth within the AC algorithm (see §2.4).

2.4. Acoustic-container depth-contour algorithm

The ACDC algorithm integrates the AC and DC algorithms (Figure S3). At each time step, the AC algorithm defines the containers of the individual's possible location and within these the DC algorithm defines possible locations. At each step, the probability of each location is the (normalised) product of the probabilities derived from each algorithm:

$$\Pr\left(\boldsymbol{s}^i|ACDC\right) \sim \Pr\left(\boldsymbol{s}^i|AC\right) \times \Pr(\boldsymbol{s}^i|DC). \tag{13}$$

2.5. Particle filtering algorithms

AC-branch algorithms can be extended via a PF process that incorporates a movement model to refine the set of possible locations of a tagged individual through time (Figure S4). Coupled with the AC, DC and ACDC algorithms, the combined workflow forms the ACPF, DCPF and ACDCPF algorithms (Table 1).

PF proceeds as follows. At the first time step, q locations ('particles') are sampled (with replacement) from the set of possible locations, according to 'background' location probabilities from an AC-branch algorithm; i.e., $\Pr(\boldsymbol{s}_{t=1}^{i}|\psi)$ where $\psi \in \{AC, DC, ACDC\}$. For each particle, movement probabilities to surrounding locations are assigned from a pre-defined movement model. In general, movement probabilities may depend on properties of the route between two locations ($\boldsymbol{s}_t^i$ and $\boldsymbol{s}_{t+1}^j$) and temporal variables (b):

$$\Pr\left(\boldsymbol{s}_{t+1}^{j} \middle|\, \boldsymbol{s}_t^i\right) = g(\boldsymbol{s}_t^i, \boldsymbol{s}_{t+1}^j; b_t), \tag{14}$$

where g is some function. For example, we could consider a model in which movement probabilities decline logistically with Euclidean or shortest distances between locations, with the rate of decline dependent on pre-defined behavioural states ($b \in \{0,1\}$), such as:

$$\Pr\left(\boldsymbol{s}_{t+1}^{j} \middle|\, \boldsymbol{s}_t^i\right) = \begin{cases} logistic\left(\alpha_1 - \beta_1 \times h(\boldsymbol{s}^i, \boldsymbol{s}^j)\right) & \text{if } b = 0 \\ logistic\left(\alpha_2 - \beta_2 \times h(\boldsymbol{s}^i, \boldsymbol{s}^j)\right) & \text{otherwise} \end{cases} \tag{15}$$

where $h\left(\boldsymbol{s}^i, \boldsymbol{s}^j\right)$ is a measure of the distance between $\boldsymbol{s}^i$ and $\boldsymbol{s}^j$. For each particle, location probabilities from an AC-branch algorithm for the next time step are updated with these movement probabilities:

$$\Pr\left(\boldsymbol{s}_{t+1}^{j} \middle|\, \psi, \boldsymbol{s}_t^i\right) \sim \Pr\left(\boldsymbol{s}_{t+1}^{j}|\psi\right) \times \Pr\left(\boldsymbol{s}_{t+1}^{j} \middle|\, \boldsymbol{s}_t^i\right). \tag{16}$$

At subsequent time steps, this process repeats, with q new locations ('particles') sampled according to their probability, given the set of possible locations and previously sampled particles. The result is a time series of particle samples that are consistent with the data and model parameters.

2.6. Particle processing

Particles require processing before they can be used to build maps of space use (see §2.7) and reconstruct movement paths (see §2.8). Particle processing is achieved via the two-step particle-processing algorithm (Figure S5):

A. Pairing. For each pair of time steps, the (sub)set of particle pairs between which movement may have occurred is identified from the movement probabilities between each pair of particles. This step is not strictly necessary, but it provides an opportunity to recalculate movement probabilities using more expensive algorithms (for instance those dependent on shortest distances) and to identify new routes between sampled particles for each pair of time steps (see Appendix §1.2).

B. Connecting. The subset of particles that connect into continuous paths from the start to the end of the time series is identified, with any particle samples that led to 'dead-ends' (when the set of possible locations, given the movement model, did not overlap with the set of locations in which the individual must have been located) dropped.

2.7. Mapping

Processed particle samples can be used to generate maps of space use (i.e., utilisation distributions). For mapping, two approaches are suggested (Figure S5). The first approach is based on a metric termed proportion-of-use (POU) that represents the expected proportion of time steps spent in each grid cell and is directly derived from particle samples via a two-step process:

A. Normalisation. At each time step, particle probabilities are normalised such that one unique record for each location is retained and probabilities sum to one. Let the N distinct particles at time t be denoted by $\boldsymbol{\sigma}_t^j$ where $j \in \{1, \dots, N\}$. Distinct particles may be multiple copies of the same location or different locations (i.e., the same or different $\boldsymbol{s}^i$). For each $\boldsymbol{s}^i$, the probability of being in that location at time t is the normalised sum of the probabilities from each copy of that location (i.e., all j where $\boldsymbol{\sigma}^j = \boldsymbol{s}^i$), as described by the equation:

$$\Pr(\boldsymbol{s}_t^i) = \frac{\sum_{\{j:\boldsymbol{\sigma}_t^j = \boldsymbol{s}_t^i\}} \Pr(\boldsymbol{\sigma}_t^j)}{\sum_{k=1}^{N} \Pr(\boldsymbol{\sigma}_t^k)}. \quad (17)$$

This step accounts for both particle probabilities and the number of copies of each location and ensures that the number of time steps during which a location was sampled (rather than the total number of copies) drives its influence on resultant maps.

A. Mapping. For each location, assuming that time steps are regularly spaced in time, POU is calculated as the sum of the number of time steps that the location was sampled, weighted by the associated probabilities of each sample, over the number of time steps (n_t):

$$\Pr(\boldsymbol{s}^i) = \frac{\sum_t \Pr(\boldsymbol{s}_t^i)}{n_t}. \quad (18)$$

The second approach applies smoothing to POU maps via kernel utilisation distribution (KUD) estimation. This process brushes over pixel-level variation to illustrate broad patterns and

facilitates comparison of the flapper algorithms with alternative methods, which are widely represented using KUDs. The approach can be described in four steps:

A. Gridding. The first step is to define a grid over which to implement KUD estimation. In some circumstances, the POU grid may be appropriate, but in others the POU grid may need to be downscaled, with POU scores aggregated across grid cells and renormalised, to cope with the computational demands of KUD estimation.

B. Sampling. The second step is to define a set of locations for KUD estimation. Sampling locations from the (re-)gridded POU map, with replacement, in line with their probability, is suggested. The aim is to generate an expanded sample of locations such that the number of copies of each location is approximately proportional to its POU score; for many applications, a sample of 100 times the number of locations with non-zero POU scores should be sufficiently large for this (and in practice a smaller number may suffice).

C. KUD estimation. The expanded sample of locations is used to fit a standard KUD (or another model). This process effectively treats each observation as a 'relocation' and accounts for POU scores through variation in the number of copies of each location.

D. Renormalisation. For KUDs, it is common to implement estimation across the study site using the reference bandwidth estimator. In coastal areas, a post-hoc correction that masks any predictions on land and renormalises the KUD is then used to restrict the boundaries of KUDs to aquatic habitats (although other options have been developed) (Benhamou and Cornélis, 2010).

2.8. Path reconstruction

Processed particle samples can be used to reconstruct movement paths via the path-reconstruction algorithm (Figure S5). This comprises three main stages:

A. Chaining. Connected particle pairs are successively linked into longer chains (i.e., movement paths) using a stepwise approach, with all the particles from time t paired against all connected particles from time $t + 1$, which are in turn paired against connected particles from time $t + 2$, and so on. In many circumstances, the set of particles contains a vast number of possible movement paths, so it is necessary to restrict the number of copies of each location retained at each time step (i.e., the number

of routes to that location) and/or the maximum number of paths, for instance by randomly sampling a specified number of possible paths for retention at each time step.

C. **Path processing** (optional). For the set of assembled paths, path processing can be implemented. This step provides another opportunity to recalculate particle probabilities using more expensive algorithms (see Appendix §1.2).

D. **Ranking** (optional). The relative plausibility of each path can be calculated from the sum of the log probabilities of each location along the path (as defined from AC-branch location probabilities and the movement model) and used to rank paths.

2.9. Simulation

For this chapter, the flapper algorithms were illustrated, evaluated and applied using simulated and real-world data in R (R Core Team, 2020) via the flapper package (Lavender, 2020b) (Figure S6, Table S1) (see Appendix §1.2). To illustrate algorithms and to evaluate their utility in different settings, a simulation approach was used (see Appendix §1.3). A 4 x 4 km^2 area and 12 simulated array designs were considered (Table S2) (see Appendix §1.3.1.1). The movements of a benthic animal were simulated from a discrete-time random walk model, with the individual taking a 'step' up to 500 m in length every two minutes, over 500 time steps (see Appendix §1.3.1.2). At each step, detections were simulated at receivers given a logistic detection probability model in which detection probability declined to zero by 300 m away from receivers (see Appendix §1.3.1.3). Using open-access bathymetry data, depths were simulated at each step from a depth-error model (see Appendix §1.3.1.4). The result was a set of detection and depth 'observations' per array. Using these data, two analyses (named S1–2 in Table S1) were implemented.

For illustration purposes, the first analysis considered one of the simulated arrays and the associated observations (S1). Starting with the AC branch, the DC algorithm was applied to the simulated depths to demonstrate its utility for examining habitat representation, using the bathymetry data and depth-error model used to simulate the data (see Appendix §1.3.2). The AC and ACDC algorithms were applied to the detection and depth datasets in the same way to examine the possible extent of movements (see Appendix §1.3.2). Using the outputs of the AC-branch algorithms and the movement model used to simulate the data, PF was applied. The DCPF algorithm was used to reconstruct possible 'post-release' movements over the first 30

time steps and the ACPF and ACDCPF algorithms were used to reconstruct patterns of space use across the whole time series (see Appendix §1.3.2).

Following illustration, algorithm utility for reconstructing patterns of space use was evaluated under the different array designs (S2) (see Appendix §1.3.3). For this analysis, POU and KUD representations of the simulated data versus those reconstructed by the mean-position algorithm (a point of reference) and the ACPF and ACDCPF algorithms were qualitatively compared.

2.10. Case study

Real-world algorithm applications were demonstrated using detection and depth data from flapper skate (Figures S7–10, Table S1) (see Appendix §1.4). For these analyses, the 'study site' centred on a region in the Loch Sunart to the Sound of Jura Marine Protected Area (MPA) where data were collected (Figure S7) (see Appendix §1.4.1.1). Within this area, four analyses were implemented to investigate habitat representation (A1), reconstruct patterns of space use (A2), examine post-release movements (A3) and explore fine-scale spatial partitioning (A4). For the analyses that incorporated depth (A1–4), a depth-error model was used that accounted for tag error, tidal range, bathymetry error and limited movements off the seabed (see Appendix §1.4.1.2). For the analyses incorporating detections (A2 and A4), a logistic detection probability model around receivers, with detection probability declining to 0 by 750 m away from receivers, was assumed (see Appendix §1.4.1.3). For the analyses incorporating movement (A2–4), mobility was defined as 500 m in two minutes, with movement probabilities declining dramatically beyond 250 m following a logistic model, especially during periods of minimal vertical activity that may reflect resting behaviour (see Appendix §1.4.1.4). This model was based on an analysis of movement speeds estimated from acoustic and archival data (see Appendix §1.4.1.4). For analyses based on PF (A2–4), 1,000 particles were sampled at each time step. Euclidean distances were used during particle sampling but shortest distances were used for particle/path processing (see Appendix §1.4.2–4).

For analyses A1–2, the movements of a selected individual (540) were considered over a one-month period for which frequent detections and depth observations collected every two minutes were available (Chapter Three) (Figure S8). In analysis A1, the DC algorithm was applied to the depth observations to examine the extent to which exploited depths were represented within

the study site (see Appendix §1.4.2). In analysis A2, the mean-position, ACPF and ACDCPF algorithms were used to reconstruct patterns of space use, quantify residency and investigate sediment preferences (see Appendix §1.4.2). In analysis A3, the DCPF algorithm was applied to reconstruct the movements of two individuals (1507 and 1558) suggested to exhibit irregular post-release behaviour (IPRB), in the form of rapid re-ascents towards the surface, following catch-and-release angling (Figure S9) (see Appendix §1.4.3). In analysis A4, the ACDCPF algorithm was applied to reconstruct the movements of two other individuals (542 and 560) during a period of cooccurring detections to examine fine-scale spatial partitioning (Figure S10) (see Appendix §1.4.4).

3. Results

3.1. Simulations

Flapper algorithms can be applied to examine habitat representation, reconstruct movement paths and map space use (Figure 1, Table S3). In the simulated data analysed for illustrative purposes (Figure 1A–B), the DC algorithm indicated the extent to which exploited depths were represented in the study site, highlighting areas at shallow (~50 m) and intermediate (~150 m) depths that coincided with exploited depths most frequently (Figure 1C). The AC algorithm highlighted peaks in POU around specific receivers (in line with the concentrating effect of detections on location probabilities) but also suggested a core range alongside the possibility of wider movements in detection gaps (Figure 1D). In the ACDC algorithm, the combination of detections with depth observations algorithm highlighted a narrower region within which movements must have concentrated (Figure 1E).

PF-branch algorithms develop the AC-branch algorithms to reconstruct possible movement paths and refine maps of space use (Figure 1F–L). The DCPF algorithm reconstructed multiple ‘post-release’ movement paths (Figure 1F). Over the whole time series, the ACPF and ACDCPF algorithms revealed further paths consistent with the data (Figure 1G–H). Early in the time series, when detections were most frequent, the illustrated and simulated paths overlapped most heavily. This was especially true for the ACDCPF-derived path, for which initial particle samples were restricted to the deep-water area within which the individual was initially located. However, the reconstructed paths spread out over time, in line with the limited

geographic restrictions on the individual's possible locations in detection gaps in a relatively homogenous bathymetric landscape.

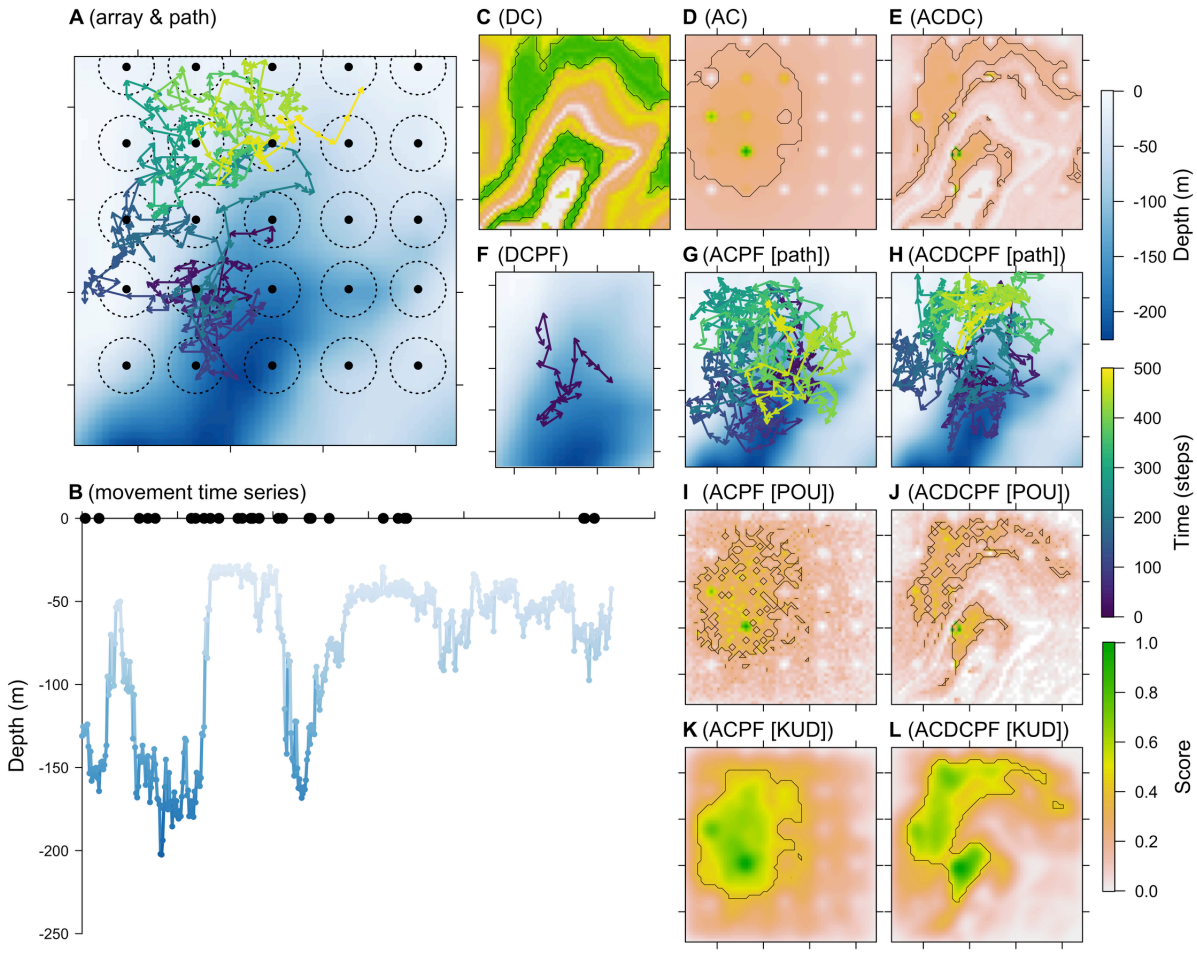

Figure 1. Illustrations of the flapper algorithms. A–B show the simulated data for which algorithms are illustrated. **A** shows the simulated array, including the bathymetry (blue), acoustic receivers (points), detection containers (dotted circles) and a movement path (arrows). **B** shows detections (black) and depths (blue) arising from the simulated path. **C–L** show the results from flapper algorithms applied to these 'observations'. **C–E** show DC, AC and ACDC scores. **F–H** exemplify reconstructed movement paths from the DCPF, ACPF and ACDCPF algorithms. The shorter path in **F** corresponds with the shorter time interval over which the DCPF algorithm was implemented and is shown on a zoomed-in bathymetry surface. **I–L** exemplify the use of particles to reconstruct maps of space use in terms of POU (**I–J**) and KUD scores (**K–L**). All scores are scaled to a maximum value of one for comparison. Lines mark 50 % contours.

Beyond movement paths, particle samples from the ACPF and the ACDCPF algorithms revealed emergent patterns of space use via POU maps and KUDs (Figure 1I–L). POU maps are detailed but pixelated (Figure 1I–J) while KUDs smooth pixel-level variation to illustrate broad patterns (Figure 1K–L). For the ACPF algorithm, POU concentrated at specific receivers. Wider patterns broadly corresponded with the simulated path, though movements beyond the boundaries of the simulated path allowed by the 'observations' mean that reconstructed patterns are broader than those for the simulated path. For the ACDCPF algorithm, reconstructed patterns also encapsulated the simulated path but departed from the shape of simulated patterns as a result of the influence of the depth 'observations' and the shape of the bathymetry: while the simulated individual mainly exploited shallow-water habitats in the west, the 'observations' are also consistent with the exploitation of areas further east where these depth contours trace the edges of the deeper, central basin.

Across simulated arrays, the utility of the ACPF and ACDCPF algorithms for reconstructing patterns of space use varied but often compared favourably with the mean-position algorithm (Figures 2 and S11–12, Table S4). For all algorithms, performance was higher in arrays with more and regularly arranged receivers. For the array with 25 regularly arranged receivers, the mean-position algorithm captured the true pattern reasonably well (Figure 2). The ACPF algorithm suggested a similar—but more diffuse—pattern, indicating potential movements to more distant parts of the study site. The ACDCPF algorithm represented the true pattern most effectively, but also highlighted areas that could have been—but were not—exploited. For random or clustered arrays with similar numbers of receivers, algorithm performance was poorer. In these circumstances, the mean-position algorithm tended to generate few COA estimates that concentrated around receivers and do not capture the extent of simulated movements or the pattern of space use. For the ACPF and ACDCPF algorithms, detections at receivers similarly concentrated location probabilities, but the incorporation of movement in the gaps between detections resulted in less concentrated patterns that more effectively captured the extent of simulated movements. Of these two algorithms, the ACDCPF algorithm generally suggested more precise maps that better represent the simulated patterns, but also appeared to highlight locations that were not—but could have been—exploited.

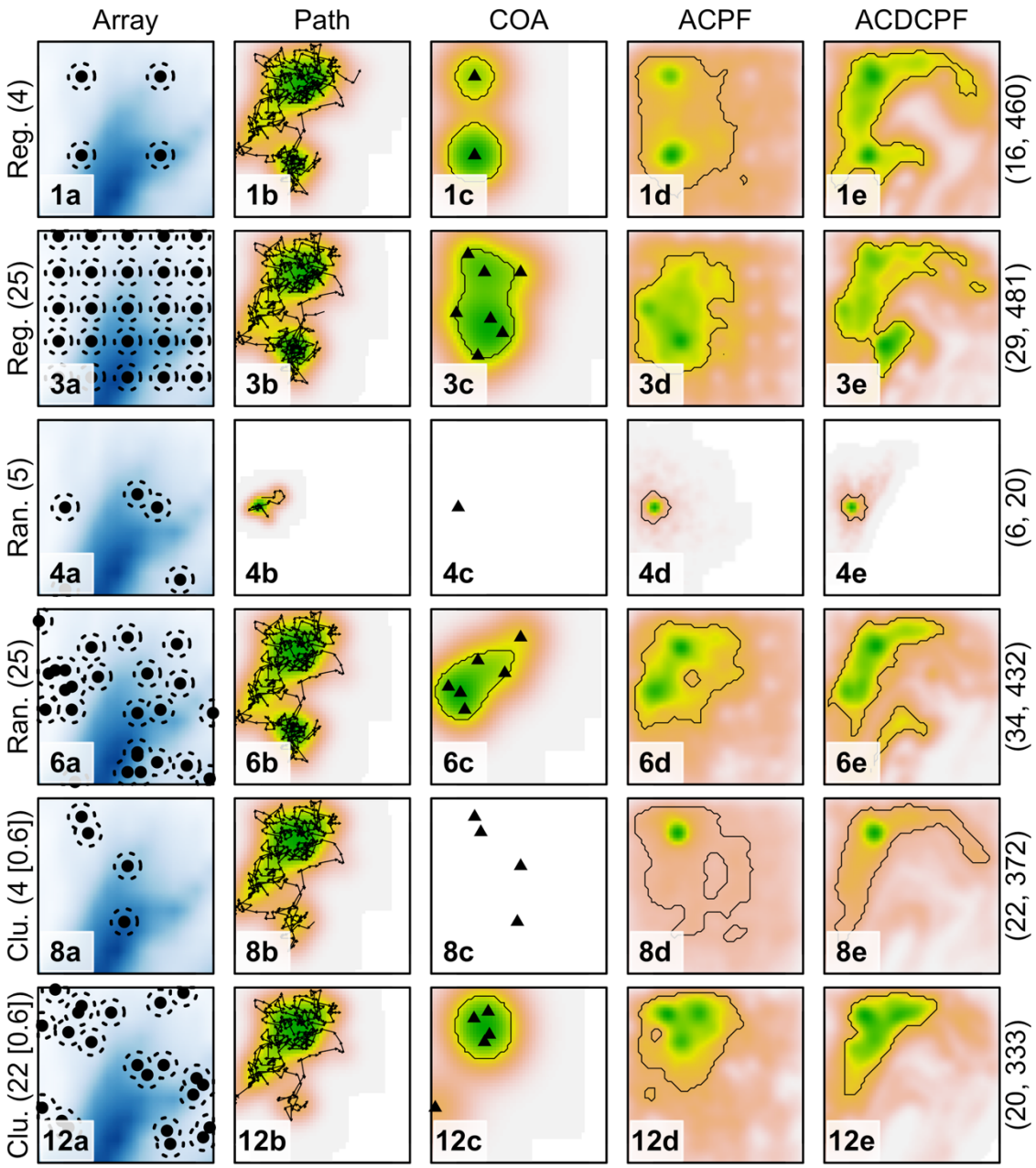

Figure 2. Simulation-based evaluation of the flapper algorithms for reconstructing patterns of space use. For each array (row), the array (a) is shown and numbered following Table S2 alongside reconstructed patterns of space use (b–e). Illustrated arrays comprise regular, random or clustered receiver arrangements with a small (~5) or large (~25) number of receivers and a clustering parameter ([0.6] if applicable), as denoted on the left-hand side. The number of detection and depth 'observations' per array is given in brackets on right-hand side. The blue background shows the bathymetry (following Figure 1). For each array, the portion of the simulated path between the first and last detections (b) is shown; while the underlying path was the same for all simulations (Figure 1A), there are differences in illustrated paths due to differing detection data from each array. KUDs from COAs (triangles) (c) and the ACPF (d) and ACDCPF (e) algorithms are also shown for simulations that generated sufficient numbers of 'observations', following Figure 1. Lines mark 50 % contours.

3.2. Case study

Applied to flapper skate datasets, the flapper algorithms indicated patterns of space use, possible habitat preferences and fine-scale movements (Figures 3 and S13). The application of the DC algorithm indicated that all parts of the study site could have been used over the time window examined (Figure 3A, Table S5). However, there are specific areas, away from the coast but throughout the study site, in which bathymetric depths overlapped more often with observed depths. They represent habitats potentially favoured on the basis of their depth (for the selected time series).

Moving beyond the DC algorithm, patterns of space use reconstructed from the mean-position, ACPF and ACDCPF algorithms differed substantially (Figures 3B–D and S13, Tables S5–6). The mean-position algorithm's KUD broadly corresponded with a map of detection days while the ACPF and ACDCPF algorithms suggested more diffuse patterns of space use that illustrate the extent of possible movements away from receivers (Figures 3C–D and S13). Importantly, both flapper algorithms demonstrated that the individual could have remained in the study site throughout the study period, despite detection gaps lasting up to 43.70 hours. Indeed, the ACDCPF algorithm suggested relatively restricted movements within deep-water channels during this time (Figures 3D and S7). Assuming this result broadly applies to the flapper skate analysed in this thesis, estimates for the minimum time that tagged individuals spent in the area increase from 1–256 (median = 34) to 2–324 (median = 42) days (Chapter Three).

Differences in reconstructed patterns of space use have implications for analyses of home ranges and habitat preferences (Figure 3E). According to the COA algorithm, the prevalence of muddy sand within the individual's core range substantially exceeded background levels. However, the ACPF and ACDCPF algorithms suggested that this result is an artefact of COAs' localised distribution; accounting for possible movements beyond receivers indicated that the prevalence of muddy sand is only marginally higher than expected.

Alongside patterns of space use, the DCPF and ACDCPF algorithm applications revealed fine-scale movements (Figure 3F–H). The application of the DCPF algorithm to two individuals that exhibited IPRB shows that the rapid post-release ascents of these individuals are consistent with benthic/demersal behaviour, despite the ascent rate (Figure 3F–G, Table S5). Meanwhile,

during a period of overlapping detections for individuals 542 and 560, the application of the ACDCPF algorithm suggested fine-scale spatial partitioning (Figure 3H, Table S5).

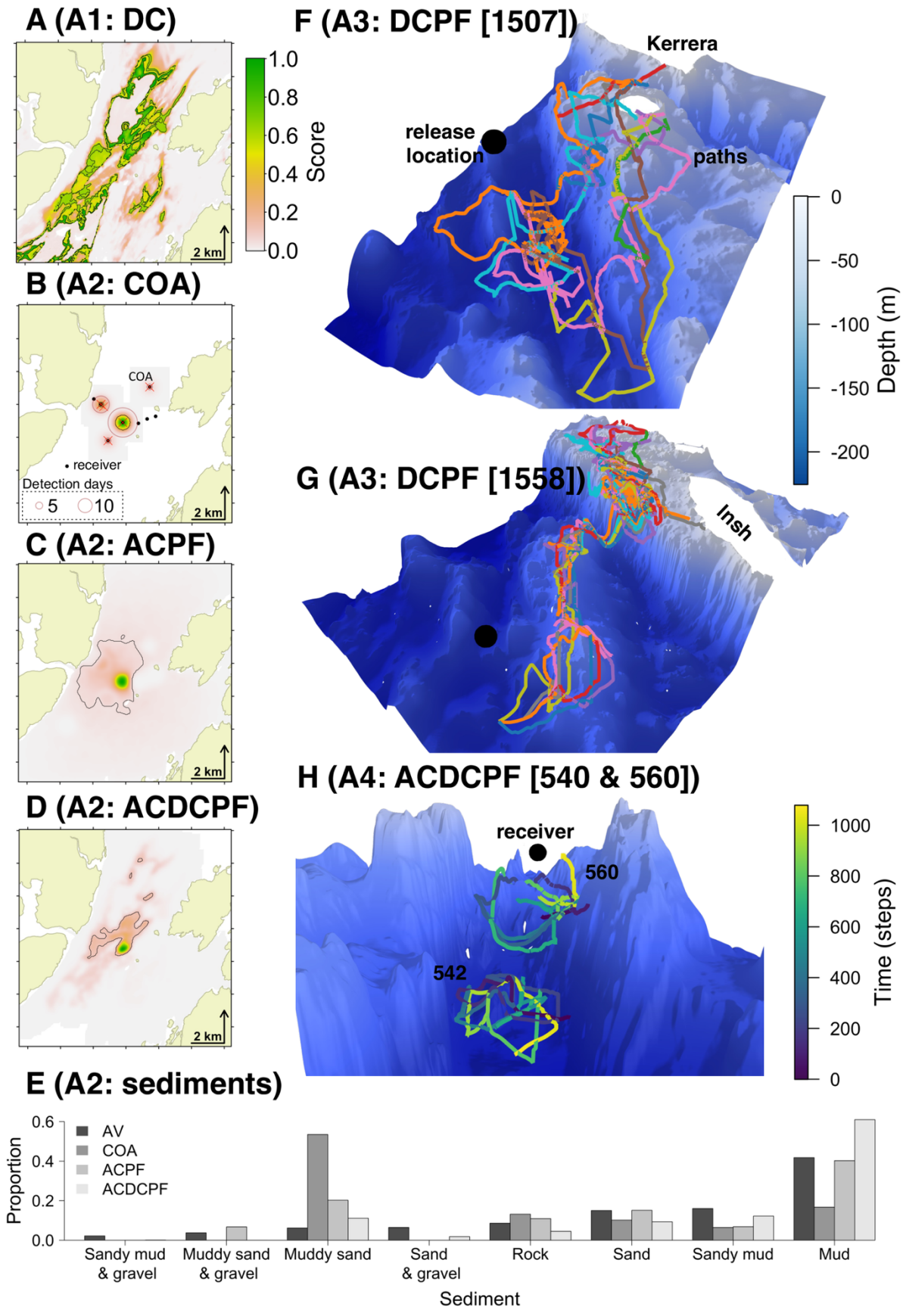

Figure 3. Applications of the flapper algorithms illustrating habitat representation (A), space use (B–D), habitat preferences (E) and movement paths (F–H) for selected flapper skate (overleaf). A–D show reconstructed patterns of space use from the DC, mean-position, ACPF and ACDCPF algorithms, with POU (**A**) or KUD (**B–D**) scores scaled to a maximum value of one for comparison. Lines mark core ranges (50 % contours). **E** shows the implications of reconstructed patterns for an analysis of sediment preferences comparing the 'background' proportion of each sediment type available (AV) in the study site versus the core range inferred from each algorithm. **F–H** show reconstructed movement paths. **F–G** show the ten most likely post-release movement paths reconstructed by the DCPF algorithm. **H** shows the most likely movement paths reconstructed by the ACDCPF algorithm for two individuals during a period of overlapping detections at one receiver. For all paths (**F–H**), shortest paths are drawn between sequential locations. Bathymetry and coastline data were sourced from Howe et al. (2014) and Digimap. Digimap data © Crown copyright and database rights [2019] Ordnance Survey (100025252).

4. Discussion

This chapter provides a holistic framework and a new family of algorithms for the semi-stochastic modelling of passive acoustic telemetry data. Important developments include the exploitation of detection gaps alongside detections, the flexibility to incorporate diverse movement datasets and the comprehensive recapitulation of the movement and detection processes that generate observations. The methods encapsulated by this framework provide a means to reconstruct fine-scale movements and investigate their drivers, examine emergent patterns of space use and infer habitat preferences for both benthic and pelagic species. For reconstructing patterns of space use, the methods compare favourably with the mean-position algorithm, producing maps that more effectively illustrate the distribution of possible movements (particularly in clustered receiver arrays) and provide a means to quantify residency through detection gaps. For flapper skate, the illustrative applications extend research on movement (Chapters Three–Four), depth use (Thorburn et al., 2021) and disturbance responses (Chapter Five), revealing for the first time movements following disturbance and fine-scale spatial partitioning. For the selected individual, the results strengthen the evidence for localised movements in the MPA, supporting the view that spatial management can contribute towards flapper skate conservation (Chapter Three; Siskey et al., 2019). For mobile aquatic species more broadly, the analyses highlight the potential for this line of research to support the implementation of conservation measures such as MPAs.

The framework in this chapter extends existing semi-stochastic approaches, especially Aspillaga et al.'s (2019) 'synthetic path' methodology. A key innovation is the separate

representation of locational and movement information. This two-step framework provides a flexible means to combine datasets in the reconstruction of possible locations (the AC branch) and their linkage into movement paths (the PF branch). In the AC branch, at the moment of detection, the detection probability calculations presented here permit any array design, including designs with overlapping receivers. At subsequent time steps, the approach can utilise information in detection gaps or consider sequential detections (as in the 'synthetic path' methodology). The representation of detection gaps is a significant development because it permits a fuller exploration of possible movements than permitted under the assumption that individuals follow least-cost paths between detection containers. In situations with ancillary data, this approach also facilitates the reconstruction of movements at temporal resolutions limited by ancillary data rather than detections, which are often sparser. The PF branch provides a flexible means to integrate movement probabilities into this process. During PF, current routines can incorporate movement probabilities based on Euclidean or shortest distances, alongside time-specific variables, such as behavioural state, informed by ancillary data. The shortest-path routines themselves also improve upon those implemented elsewhere (Aspillaga et al., 2019; Niella et al., 2020) due to the exploitation of effective approximations and efficient C++ routines (Larmet, 2019).

These developments provide opportunities to reconstruct fine-scale movement paths, improved maps of space use and support analyses of habitat preferences. For reconstructing maps of space use, simulations illustrate that the mean-position and flapper algorithms fall at opposite ends of a precision/bias spectrum. In the mean-position algorithm, COAs are estimated from receiver locations, which means that maps of space use are relatively precise but can be biased by receiver locations. The flapper algorithms are also influenced by the concentrating effect of detections on location probabilities, but the incorporation of movement reduces the restrictive influence of array design, generating more diffuse maps. For reconstructing patterns of space use, the implications of this difference depend on array design. In regular, high-coverage arrays, simulations suggest that both approaches can be instructive, though residency during detection gaps can only be estimated from the latter. In contrast, in clustered arrays, since COAs only capture movement around receivers, particle-based maps of the distribution of possible movements can better encapsulate the full extent of movement. The distribution of possible movements may be wider and shaped differently from the true movement path, but it is more useful for prediction (the bias–variance trade off). In sparse arrays, neither approach is informative.

The main challenge for applications of the framework advanced here is the data required on detection probability and movement. As in any modelling framework, misspecification of these variables may mislead inferences. However, algorithm sensitivity to misspecification is likely to vary with array design and movement properties. While a comprehensive sensitivity study would be worthwhile, it is anticipated that algorithm outputs will often be robust to the detection probability model since simple distance-dependent models are widely applicable and low-coverage receiver arrays are common (Kessel et al., 2014). However, outputs may be more sensitive to the movement model: if movement capacity is underestimated, convergence failures or overly concentrated patterns of space use may result; if capacity is overestimated, reconstructed movements may be too extensive. Hence, it is suggested that passive acoustic telemetry studies adopt integrated tagging programmes to support inference (Hussey et al., 2015).

Computational requirements also challenge applications of the framework. While AC-branch algorithms are deterministic, often 'perfectly' parallelisable and relatively fast, particle sampling is generally slower because samples at each time step are contingent upon previous samples. Consequently, for big datasets, focusing on periods of relatively frequent detections, thinning and/or reducing the temporal resolution of the analysis may be required. Given the accumulation of passive acoustic telemetry data (Matley et al., 2022), detailed evaluation of the consequences of these choices, alongside further computational optimisation, would be beneficial.

For the case-study species, the illustrative analyses indicate responses to catch-and-release angling, fine-scale partitioning and localised patterns of space use. The post-release analyses demonstrate that the rapid ascents of two individuals suggested to exhibit IPRB are consistent with movement over the seabed, despite their irregularity. These analyses represent the first step in understanding responses to capture and how they are shaped by the local environment (Chapter Five). For the two individuals with cooccurring detections, the analyses suggest fine-scale spatial partitioning rather than close-knit interactions. This demonstrates that multiple individuals may inhabit a similar (< 0.5 km^2) area at the same time while behaving differently, as previously suggested (Chapter Three). The analyses of space use suggest that localised movements may continue over longer timescales, with continuous residency of individual 540 in a 13 x 13 km area over one month fully consistent with the data. While this result does not

preclude movements further afield, it strengthens the evidence that residency in the study site may continue through detection gaps (Chapter Three). During residency in the MPA, the analysis of habitat preferences points towards the exploitation of multiple benthic habitats, in concordance with recent work (Thorburn et al., 2021).

The limiting factor for the case-study analyses is the lack of information on movement speeds. While this chapter develops methods for inferring mobility from detection and depth data, high-resolution activity data would support the expansion of the analyses. Building on studies of depth use (Thorburn et al., 2021), the DC algorithm should refine population-level maps of depth representation. The AC and ACDC algorithms should highlight locations in the MPA unexploited by tagged individuals and the PF algorithms should enable a detailed examination of fine-scale movements, population-level patterns of space use, residency and habitat preferences. This information is critical in the design of MPAs for mobile species (MacKeracher et al., 2019).

Continued methodological development will support applications of the framework advanced here. On the technical side, further computational optimisation is desirable. For reconstructing patterns of space use, investigations into the impacts of data processing, sensitivity analyses and evaluation of the merits of existing methods would support the use of available approaches in different settings. The flapper algorithms may also offer unexplored opportunities to optimise tag and array deployment programmes, through simulation-based comparisons of alternative options. Nevertheless, exploration of alternative frameworks, such as ant-colony optimisation algorithms (Mullen et al., 2009), remains worthwhile. However, all approaches are limited by available data and there is no panacea to the reconstruction of movements over long detection gaps. Thus, coupled development of tagging and array deployment programmes alongside analytical approaches is crucial for continued progress.

Appendices

1. Supporting methods

1.1. Detection probability

The importance of detection probability. In the acoustic-container (AC) algorithm, information on detection probability reduces our uncertainty in the possible locations of an individual by upweighting areas in which an individual is more likely to be located and downweighting others (Figure S1). However, the precise translation of a model for detection probability into location probabilities at any one time depends on whether or not the individual was detected at that moment in time and the array design.

Scenario (A): location probability at the moment of detection in an array with non-overlapping receivers. When an individual is detected in a simple array with non-overlapping receivers, we can translate a standard detection probability model describing the probability of a detection event at receiver k (located at $\boldsymbol{r}^k$) at time t ($E[k,t]$) given a transmission from location $\boldsymbol{s}^i$ into a location probability model describing the probability of a detected individual being in $\boldsymbol{s}^i$ given the detection event. These two quantities are related via Bayes Theorem, such that

$$\Pr\left(\boldsymbol{s}^i \middle| E[k,t]\right) = \Pr\left(E[k,t] \middle| \boldsymbol{s}^i\right) \frac{\Pr\left(\boldsymbol{s}^i\right)}{\Pr\left(E[k,t]\right)}. \quad \text{(S1)}$$

In practice, the unconditional probability of the individual being in a given location, i.e., $\Pr\left(\boldsymbol{s}^i\right)$, and the unconditional probability of a detection, i.e., $\Pr(E[k,t])$, are unknown. However, under the assumption that the ratio $\frac{\Pr\left(\boldsymbol{s}^i\right)}{\Pr(E[k,t])}$ is constant, we can translate a model for $\Pr\left(E[k,t] \middle| \boldsymbol{s}^i\right)$, such as a logistic model, into a model for $\Pr\left(\boldsymbol{s}^i \middle| E[k,t]\right)$ via:

$$\Pr\left(\boldsymbol{s}^i \middle| E[k,t]\right) \sim \Pr\left(E[k,t] \middle| \boldsymbol{s}^i\right) \sim logistic\left(\alpha - \beta \times \left|\boldsymbol{s}^i - \boldsymbol{r}^k\right|\right). \quad \text{(S2)}$$

Scenario (B): location probability in the gaps between detections in an array with non-overlapping receivers. In the gaps between detections, detection probability also influences our uncertainty in the possible locations of an individual. The absence of a detection at receiver k at time t is denoted as the complement of a detection event, i.e., $E^c[k,t]$. Given a standard

logistic detection probability model, we can relate the desired quantity $\Pr(\boldsymbol{s}^i|E^c[k,t])$ to $\Pr(E^c[k,t]|\boldsymbol{s}^i) = 1 - \Pr(E[k,t]|\boldsymbol{s}^i)$ via Bayes Theorem:

$$\begin{aligned}\Pr(\boldsymbol{s}^i|E^c[k,t]) &= \Pr(E^c[k,t]|\boldsymbol{s}^i)\frac{\Pr(\boldsymbol{s}^i)}{\Pr(E^c[k,t])} \\ &= \left(1 - \Pr(E[k,t]|\boldsymbol{s}^i)\right)\frac{\Pr(\boldsymbol{s}^i)}{\Pr(E^c[k,t])}.\end{aligned} \tag{S3}$$

As above, by assuming the ratio of $\Pr(\boldsymbol{s}^i)$ to $\Pr(E^c[k,t])$ is constant, $\Pr(\boldsymbol{s}^i|E^c[k,t])$ is defined as:

$$\Pr(\boldsymbol{s}^i|E^c[k,t]) \sim 1 - \Pr(E[k,t]|\boldsymbol{s}^i) \sim 1 - logistic(\alpha - \beta \times |\boldsymbol{s}^i - \boldsymbol{r}^k|) \tag{S4}$$

This model increases the probability of possible locations (within an acoustic container) that are further away from receivers in the gaps between detections.

Scenario (C): location probability at the moment of detection in an array with overlapping receivers. In an array with overlapping receivers, the detection or lack of detection at effectively the same time at receivers with overlapping detection containers provides further information on the location of the individual. (The definition of 'effectively' is context specific but depends on the accuracy with which the clocks of different receivers are synchronised and the resolution of the analysis.)

Building on the framework defined above, in general terms, at the moment of detection, the probability of an individual being in location $\boldsymbol{s}^i$ is proportional to the product of the detection probability from that location at all the receivers at which the individual was detected, which up-weights areas that intersect between receivers that recorded detections, multiplied by the product of not being detected at any of the operational receivers at which it was not detected. Suppose that out of M operational receivers, the individual was detected by receivers $k = 1,2,\dots,m$ at locations $\boldsymbol{r}^1, \boldsymbol{r}^2, \dots, \boldsymbol{r}^m$ but not detected by receivers $l = m+1, m+2, \dots, M$, at locations $\boldsymbol{r}^{m+1}, \boldsymbol{r}^{m+2}, \dots, \boldsymbol{r}^M$. Then the combined probability of an individual being in $\boldsymbol{s}^i$ is given by:

$$\begin{aligned}&\Pr(\boldsymbol{s}^i|E[(1,2,\dots,m),t], E^c[(m+1,m+2,\dots,M),t]) \\ &\quad = \prod_{k=1,2,\dots,m} \Pr(\boldsymbol{s}^i|E[k,t]) \times \prod_{l=m+1,m+2,\dots,M} \Pr(\boldsymbol{s}^i|E^c[l,t]).\end{aligned} \tag{S5}$$

Scenario (D): location probability in the gaps between detections in an array with overlapping receivers. In arrays with overlapping receivers, given a lack of detections, locations within areas surveyed by fewer receivers are more likely (all else being equal) than locations surveyed by more receivers. In general, the probability of an individual being in any given location in the acoustic container ($C_{I,t}$) is the product of the probabilities given the absence of detection at each receiver:

$$\Pr\left(\boldsymbol{s}^i \middle| E^c[(1,2,\dots M),t]\right) = \prod_k \Pr\left(\boldsymbol{s}^i \middle| E^c[k,t]\right) \quad \text{(S6)}$$

where k includes all operational receivers. This equation is a limit case of Equation S5 when no detections are recorded.

$\Pr\left(\boldsymbol{s}^i|AC\right)$ denotes all of the ways in which detection events are incorporated in the AC algorithm. This notation generalises the description in Equations S5 and S6 for the probability of an individual being in a selected location given the detection data (detection, non-detection) at each operational receiver. For all scenarios, $\Pr\left(\boldsymbol{s}^i|AC\right)$ is normalised such that $\sum_i \Pr\left(\boldsymbol{s}^i|AC\right) = 1$.

1.2. The flapper package

The flapper package was developed to implement the flapper algorithms (Figure S6). Current routines are fully documented elsewhere (Lavender, 2020b). Of specific relevance to this chapter is the way that distances are incorporated into the AC-branch and PF-branch algorithms. All AC-branch algorithm implementations (`ac`, `dc` and `acdc`) currently enforce Euclidean distances. The implementation of PF (`pf`) currently supports movement models that depend on the Euclidean or shortest distance between locations and time-specific variables, such as behavioural state. For PF, movement models based on Euclidean distances, for which the 'fast-Euclidean distances method' can be exploited, are preferable. The key feature of this method is that at each time step it considers all particles simultaneously; for all particles, a single distance surface is calculated that represents distances from the nearest particles and this is translated, via the movement model (and accounting for temporal variables, such as behavioural state), into a single surface that describes movement probabilities. In situations in which shortest distances need to be integrated into the analysis, current routines provide three options:

A. **Shortest-distances sampling.** Shortest distances can be implemented during PF. This option is slowest, and thus not used here, but simplifies particle/path processing.
B. **Particle processing.** Shortest distances can be incorporated via the particle-processing algorithm (see §2.6). Under this approach, particles are sampled using the fast-Euclidean distances method (via `pf`) and then processed (via `pf_simplify`). During the first particle-processing stage ('pairing': see §2.6), movement probabilities between particle pairs are recalculated using shortest distances. This approach is typically faster than option A because shortest distances only need to be calculated between sampled particle pairs. Additional approximations can also be implemented by `pf_simplify` to restrict further the number of calculations that are required (see Appendix §1.4.2). This approach is adopted for analyses A1–2 in this chapter (see Appendix §1.4.2) because it provides means to incorporate shortest distances into particle samples without the need to assemble paths (option C, below).
C. **Path processing.** Shortest distances can be incorporated during path processing. Under this approach, particles are sampled via `pf` and processed via `pf_simplify` on the basis of Euclidean distances. For the set of reconstructed paths, shortest paths are then interpolated between successive locations along each path and used to update movement probabilities via the movement model; paths with any connections assigned a probability of zero (i.e., when the shortest distance, unlike the Euclidean distance, exceeds $mobility$) can be dropped. For analyses of movement paths, this approach is often fastest because shortest distances are only calculated for the subset of locations represented by reconstructed paths. This approach is adopted for analyses A3–4 in this chapter (see Appendix §1.4.3–4).

1.3. Simulations

1.3.1. Simulation parameters

1.3.1.1. Array designs

To illustrate applications of the flapper algorithms and to evaluate their utility in different settings, a variety of array designs were simulated in a small, rectangular area (without any barriers to movement) (Table S2). Three arrangements of receivers were considered: regular,

random and clustered. For each arrangement, arrays comprising small, medium and large numbers of receivers (M = 5, 15 and 25, respectively) were simulated. For clustered arrays, arrays with a low and high degree of clustering, with the number of clusters equal to 0.6 and 0.4 of the number of receivers respectively, were simulated.

1.3.1.2. Movement model

Within the simulated area, the movement path of a tagged animal was simulated according to a standard discrete-time, continuous-space, random walk model based on step lengths and turning angles, for 500 time steps, with time steps conceptualised as two-minutes in duration. The simulation began with a randomly sampled location. At each subsequent time step, a step of length d_t was simulated from a discrete distribution of lengths $d_t \in \{0.00000, 0.05005, \ldots, 500.00000\}$ with probability

$$\Pr(d_t) = \frac{logistic(7.5 - 0.025 \times d_t)}{\sum_i logistic(7.5 - 0.025 \times d_i)}, \quad \text{(S7)}$$

where $d_1, d_2, \ldots, d_{9991}$ are the possible values of d_t and $\Pr(d_t)$ declines logistically with step length. The individual's heading (α_t) was sampled from wrapped normal distribution as $\alpha_t \sim WN(0,1)$. Given a location at time t of $\boldsymbol{z}_t = (x_t, y_t)$, the location at the next time step was generated by

$$\boldsymbol{z}_{t+1} = (x_{t+1}, y_{t+1}) = (x_t + d_t \cos \alpha_t, y_t + d_t \sin \alpha_t). \quad \text{(S8)}$$

This approach was implemented in an iterative fashion to ensure simulated locations were within the boundaries of the study site. To facilitate comparisons between simulated and reconstructed movements, receiver locations and the simulated movement path were re-expressed on a 75 x 75 m grid across which analyses are implemented (see Appendix §1.3.2–3). This resolution reflects a compromise between a low-resolution grid, which is computationally more tractable for multiple simulations, and a high-resolution grid, which resolves detection and movement probabilities with higher resolution.

1.3.1.3. Detections

At each step (t) along the path, detections (0, 1) were simulated at each receiver (indexed by k) as a Bernoulli random variable (denoted $\rho[k, t]$). The probability of detection at receiver k was uniquely determined for each t and declined with distance between the receiver's location

on the grid ($\boldsymbol{r}^k$) and the individual's location on the grid ($\boldsymbol{s}^i$) according to a simple logistic model:

$$\rho[k,t] \sim \text{Bernoulli}\left(\Pr\left(E[k,t]\middle|\boldsymbol{s}_t^i\right)\right)$$
$$\Pr\left(E[k,t]\middle|\boldsymbol{s}_t^i\right) = \begin{cases} logistic\left(3 - 0.03 \times |\boldsymbol{s}^i - \boldsymbol{r}^k|\right) & \text{if } |\boldsymbol{s}^i - \boldsymbol{r}^k| \leq 300 \\ 0 & \text{otherwise.} \end{cases} \quad \text{(S9)}$$

1.3.1.4. Depths

Using open-access 257 x 463 m bathymetry data from the General Bathymetric Chart of the Oceans (GEBCO), resampled to a resolution of 75 x 75 m, depth (m) observations were simulated by imagining that the animal was on or near the seabed at each time step. To simulate depths, a value was sampled at each time step from a uniform distribution according to the equation:

$$depth_t \sim U(bathy(\boldsymbol{s}_t^i) - 5, bathy(\boldsymbol{s}_t^i) + 5) \quad \text{(S10)}$$

where $bathy(\boldsymbol{s}_t^i)$ defines the depth of the GEBCO bathymetry grid in the individual's location on the grid at time t ($\boldsymbol{s}_t^i$).

1.3.2. Algorithm illustration

Approach. To illustrate applications of the flapper algorithms, one of the simulated array designs (ID 3) was taken as an example (Table S2). Each algorithm was then applied to the simulated time series across the 75 x 75 m grid and the resultant maps and movement paths were visualised.

AC-branch algorithms. Starting with the AC-branch algorithms, the DC algorithm was implemented using the simulated depth time series, the resampled bathymetry data and the depth-error model used in the simulation (Equation S10). The AC and ACDC algorithms were implemented for a time step duration of two minutes, using acoustic and archival time series (if applicable), the detection probability model and a relaxed $mobility$ parameter (575 m per two minutes) to account for the effect of grid resolution. For each AC-branch algorithm (DC, AC, and ACDC), the main results of this process were a time series of maps that describe the set of locations in which the individual could have been located at each time step, given the

observations and model parameters, alongside an overall map that describes expected proportion of time steps spent in each grid cell.

PF-branch algorithms. AC-branch maps were refined using PF. For each PF algorithm (DCPF, ACPF and ACDCPF), the outputs of the corresponding AC-branch algorithm were used alongside a modified movement model that accounted for the effect of grid resolution,

$$\Pr\left(\boldsymbol{s}_{t+1}^{j} \middle| \boldsymbol{s}_{t}^{i}\right) = \begin{cases} logistic\left(7.5 - 0.025 \times |\boldsymbol{s}^{j} - \boldsymbol{s}^{i}|\right) & \text{if } |\boldsymbol{s}^{j} - \boldsymbol{s}^{i}| < 575 \\ 0 & \text{otherwise,} \end{cases} \quad \text{(S11)}$$

to sample 100 particles at each time step, as follows:

A. **DCPF.** For the DCPF algorithm, the initial sample of particles was biased by the origin, mimicking real-world settings in which individuals are caught and then released with tags attached in recorded locations. Using Euclidean distances and the movement model described above (Equation S11), the DCPF algorithm was implemented for the first 30-time steps, which represents a realistic time window over which this algorithm can be usefully applied, given the absence of strong geographic restrictions on the individual's possible location through time in most settings.
B. **ACPF and ACDCPF.** For the ACPF and ACDCPF algorithms, PF was implemented for all time steps between the first and last detection, mimicking the way in which acoustic data are used in real-world settings.

Movement paths. The outputs of each PF-branch algorithm comprised a time series of particle samples that capture possible movements over the seascape. For each algorithm, movement paths represented by captured particles were reconstructed via the path-reconstruction algorithm (see §2.8) and simulated and reconstructed paths on the bathymetry were compared visually.

Space use. For the ACPF and ACDCPF algorithms, the patterns of space use exhibited by the simulated path were compared to reconstructed patterns via POU maps and KUDs:

A. **POU-based comparisons.** POU maps were generated for (a) the simulated path versus (b) processed particle samples from the ACPF and ACDCPF algorithms. For the simulated path, POU was simply calculated as the number of time steps during which the simulated individual was located in each grid cell, over the total number of time

steps. For the processed particle samples, POU was calculated following Equation 18 (see §2.6).

B. **KUD-based comparisons.** For the KUD-based comparisons, a KUD was estimated for (a) the simulated path versus (b) particle samples. For the simulated path, the locations at each step of the path were used to estimate the KUD. For the flapper algorithms, locations were resampled from each POU map in line with their probability for KUD estimation (steps B–C in Appendix §1.3.2). In both cases, the reference bandwidth estimator was used to facilitate comparisons. Given the selected array design, with 25 regularly arranged receivers, and the close correspondence between the parameters used to simulate and reconstruct movements, in this illustrative exercise the expectation was that the reconstructed patterns of space use should contain the simulated path. However, given gaps between receivers, it was not expected the simulated and reconstructed patterns would match perfectly, since the algorithms can also reveal areas that were not—but could have been—exploited (given the 'observations').

1.3.3. Algorithm evaluation

Approach. For the 12 simulated array designs, the utility of the mean-position, ACPF and ACDCPF algorithms for reconstructing the patterns of space use exhibited by the simulated path was evaluated. In this analysis, for each array design, the portion of the simulated path that occurred between the first and last detections (i.e., the time period over which detection time series can be used to reconstruct movements) was considered. For this portion of the simulated path, POU was calculated and a KUD was estimated, as described previously (see Appendix §1.3.2). These maps for the simulated path were compared against equivalent maps derived from the mean-position, ACPF and ACDCPF algorithms.

Mean-position algorithm. For the mean-position algorithm, a three-stage process was used to calculate COAs and then KUDs.

A. **Time interval selection.** For each detection time series, a time interval (two hours) for the calculation of COAs was selected using the standard methods proposed by Simpfendorfer, Heupel & Hueter (2002).
B. **COA estimation.** For each interval with sufficient data, COAs were estimated.
C. **KUD estimation.** For all array designs for which at least five COAs could be calculated, a KUD was estimated.

Flapper algorithms. For the ACPF and ACDCPF algorithms, POU was calculated across the area and a KUD was estimated as described previously (see Appendix §1.3.2).

Qualitative evaluation. For each array design, POU maps and KUDs for the simulated data were visually compared against the corresponding maps derived from the mean-position, ACPF and ACDCPF algorithms to evaluate the utility of each algorithm in different settings.

Expectations. In regular, high-coverage arrays, the expectation for this analysis was that all methods should effectively encapsulate simulated patterns; in more clustered, low-coverage arrays, all methods were expected to perform less well, but the mean-position estimates were expected to be more strongly biased by the locations of receivers than the flapper algorithms.

1.4. Case study

1.4.1. Case-study parameters

1.4.1.1. Study site

The flapper algorithms were applied to acoustic and archival data collected by the Movement Ecology of Flapper Skate (MEFS) project from flapper skate in 2016–17 (Chapters Two–Three). For these analyses, the 'study site' centred on a region within the Loch Sunart to the Sound of Jura Marine Protected Area where acoustic and archival tagging took place and acoustic receivers were deployed by the MEFS project (Figure S7). Within this region, the analyses were focused in an area that approximately corresponds to the 'southern receiver array' in Chapter Three and is described by 1:10,000 scale coastline data from Digimap and 5 x 5 m bathymetry data from Howe et al. (2014) (Figure S7). However, for each analysis (A1–4), the boundaries of the 'study site' were tuned to minimise memory and computational requirements (Figure S7).

1.4.1.2. Depth-error model

For the analyses that incorporated depth time series, four sources of uncertainty were addressed:

A. **Tag accuracy**—the accuracy of deployed Star Oddi milli-TD archival tags (± 4.77 m).
B. **Tidal variability**—the maximum tidal range predicted by the West Coast of Scotland Coastal Modelling System (Aleynik et al., 2016) for the study site (± 2.5 m).
C. **The bathymetry error**—a bathymetry error term $\left(\sqrt{0.500^2 + (0.013 \times depth)^2}\right)$ based on industry standards set by the International Hydrographic Organisation for the maximum allowable vertical uncertainty for Order 1a surveys, as conducted by Howe et al. (2014) (International Hydrographic Organization, 2020).
D. **Demersal movements**—an additional term designed to capture potential movements off the seabed (+ 5 m).

In line with these uncertainties, for any observed $depth$, the individual's location on the bathymetry grid was restricted to locations between a lower (shallow) and an upper (deep) depth limit, as defined by the equations:

$$\varepsilon_{lower}(depth_t) = -\left(4.770 + 2.500 + \sqrt{0.500^2 + (0.013 \times depth_t)^2} + 5.000\right) \quad \text{(S12)}$$

$$\varepsilon_{upper}(depth_t) = 4.770 + 2.500 + \sqrt{0.500^2 + (0.013 \times depth_t)^2}\,. \quad \text{(S13)}$$

1.4.1.3. Detection probability

For the analyses incorporating acoustic data, following previous analyses of drift-testing data for the MEFS array (Klöcker, 2019), a simple logistic detection probability model was assumed, with the probability of a detection event (given a transmission from some location $\boldsymbol{s}^i$) declining from ~0.97 near receivers to ~0.50 by 425 m away from receivers and 0.00 by 750 m away from receivers. This model took the form:

$$\Pr\left(E[k,t]|\boldsymbol{s}^i\right) = \begin{cases} logistic\left(4.00 - 0.01 \times |\boldsymbol{r}^k - \boldsymbol{s}^i|\right) & \text{if } |\boldsymbol{r}^k - \boldsymbol{s}^i| < 750 \\ 0 & \text{otherwise.} \end{cases} \quad \text{(S14)}$$

This model qualitatively reproduces the main properties of detection probability curves identified by previous research (Klöcker, 2019) and fits with the maximum observed detection range (708 m) for the MEFS array (Chapter Two). It is recognised that there are additional

drivers of detection probability, but distance is typically the most influential and the most widely applicable, especially given the limitations of available data (Klöcker, 2019).

1.4.1.4. Movement parameters

Data. For analyses incorporating mobility or movement, estimates of skate movement speeds were derived from acoustic (n = 205,323 observations) and archival (n = 3,908,294) time series for all individuals with acoustic (n = 33) and archival (n = 21) data (Chapter Two). All available data were used for this analysis because only a subset of the data for each individual was expected to meet the criteria required to estimate movement speeds.

Acoustic analysis. Using the acoustic time series, speeds were calculated for movements that occurred between receivers with non-overlapping detection containers that recorded sequential detections that exceeded the maximum acoustic transmission interval (90 s). For any given pair of receivers, if we denote $\boldsymbol{r}^i$ as the location of the receiver that recorded a detection at time step $t_{acc} = t$ and $\boldsymbol{r}^j$ as the location of the receiver that recorded the next detection at time step $t_{acc} = t + 1$ then the movement speed (ms^{-1}) between these two receivers was approximated as

$$speed = \frac{h\left(\boldsymbol{r}^i, \boldsymbol{r}^j\right)}{|\tau(t_{acc} = t) - \tau(t_{acc} = t + 1)|} \quad \text{(S15)}$$

where $\tau(\cdot)$ is the 'clock function' and $h\left(\boldsymbol{r}^i, \boldsymbol{r}^j\right)$ is a distance metric. For this analysis, two distance metrics were considered:

A. **Euclidean distances**—the linear distance between the nearest edges of receiver detection containers (assuming a detection container of 750 m as specified in Equation S14), denoted $|\cdot|$.
B. **Shortest distances**—the distance of the shortest (least-cost) path between the nearest edges of receiver detection containers, assuming movement over a one arc-second bathymetry layer sourced from Digimap, resampled to 50 x 50 m resolution, denoted $h_{LCP}(\cdot,\cdot)$. (High-resolution data from Howe et al. (2014) do not span all areas with receivers at which detections were recorded.)

The result was two speed estimates (one for each distance variable) per movement. On many occasions, individuals probably took indirect routes between receivers so these estimates were

expected to be uninformative; however, given relatively close proximity among receivers, sometimes individuals may have moved directly between receivers and therefore the faster speed estimates were expected to indicate likely movement speeds.

Archival analysis. To complement the acoustic analysis, vertical movement speeds between sequential depth observations were also examined.

Estimates. The acoustic analyses (n = 641 observations) indicated maximum movement speeds of 272.53 and 281.59 m per two-minutes for Euclidean and shortest distances respectively. The archival analyses (n = 3,908,294) indicated maximum vertical movement speeds of 135.03 m per two-minutes.

Assumptions. Based on these analyses, a mobility of up to 500 m in a two-minute period was assumed but a model was specified in which movement probabilities declined dramatically beyond 250 m. This model was refined by considering two putative behavioural states: a 'resting' state (mode 0), for which movement was more limited, and an active state (mode 1), for which movement was less limited. Following previous research (Chapter Five), 'mode 0' time steps were defined as those when the absolute vertical activity was ≤ 0.5 m (an indicator of resting behaviour) and 'mode 1' time steps were defined as those when the absolute vertical activity > 0.5 m. Based on these considerations, for each time step, if the distance between two locations was less than 500 m, the probability of movement between those locations was defined as follows:

$$\Pr\left(\boldsymbol{s}_{t+1}^{j}|\boldsymbol{s}_{t}^{i}\right) = \begin{cases} logistic\left(7.5 - 0.50 \times h(\boldsymbol{s}_{t+1}^{j}, \boldsymbol{s}_{t}^{i})\right) & \text{if } mode\ 0 \\ logistic(7.5 - 0.05\ \times h(\boldsymbol{s}_{t+1}^{j}, \boldsymbol{s}_{t}^{i})) & \text{if } mode\ 1. \end{cases} \quad \text{(S16)}$$

During PF, for computational efficiency, it was defined that $h\left(\boldsymbol{s}_{t+1}^{j}, \boldsymbol{s}_{t}^{i}\right) = \left|\boldsymbol{s}_{t+1}^{j} - \boldsymbol{s}_{t}^{i}\right|$ and $\Pr\left(\boldsymbol{s}_{t+1}^{j}|\boldsymbol{s}_{t}^{i}\right) \leq 0.001 \equiv 0.001$. In contrast, if $h(\boldsymbol{s}_{t+1}^{j}, \boldsymbol{s}_{t}^{i})$ exceeded 500 m, $\Pr\left(\boldsymbol{s}_{t+1}^{j}|\boldsymbol{s}_{t}^{i}\right) = 0$. During particle processing, h was updated with a function that approximated h_{LCP} or h_{LCP} specifically, depending on the computational requirements of the analysis (see Appendix §1.4.2–4).

This formulation recognised that most movements are probably slower than 250 m in a two-minute period, given the results of the above analyses. This formulation also recognised that movements are likely to be much more restricted during resting, but since minimal vertical

activity is not a guarantee of resting, larger movements during 'mode 0' time steps were permitted. Indeed, while most movements are likely to be less than 250 m, given that available data provide imperfect indicators of movement speed, for both modes faster movements up to 500 m per two minutes, for instance in association with tidal flows, were permitted.

1.4.2. Analyses A1–2

Data. In the first two analyses, habitat representation (A1) and patterns of space use (A2) were examined using acoustic and/or archival data for a selected individual (540) over a one-month period from September–October 2016 (Figure S8). For these analyses, the 'study site' was defined as the area within a 5 km^2 buffer around the receivers at which the selected individual (540) was detected. Within this area, the selected observations were processed, expressing both time series at a resolution of two-minutes and thinning the acoustic time series to exclude any duplicate detections at the same receiver in each two-minute period, to ensure alignment and minimise computational requirements. Processed data were then analysed to examine habitat representation (A1) and space use (A2).

Analysis A1. For analysis (A1), the DCPF algorithm was applied to the depth observations, using the high-resolution bathymetry data (see Appendix §1.4.1.1) and the depth-error model (see Appendix §1.4.1.2) described above. A POU map was generated to explore habitat representation as the sum of the surfaces from each time step, over the number of time steps.

Analysis A2—the mean-position algorithm. For analyses of space use (A2), for the mean-position algorithm, a time interval of 48 hours was considered, based on the considerations described previously (see Appendix §1.3.3). For each time interval with detections, COAs were calculated. To translate COAs into a KUD, a 25 x 25 m grid was used to improve computation time. The KUD was estimated across this grid using the reference bandwidth estimator, the land was masked and the KUD renormalised.

Analysis A2—the flapper algorithms. For the ACPF and ACDCPF algorithms, the parameters previously described were used to sample q = 1000 particles at each time step. A complication with this analysis, unlike the simulations described above (see Appendix §1.3), was the need to account for the effects of the bathymetry on movement probabilities for a benthic animal. This was achieved by sampling particles using the fast-Euclidean distances

method for PF but re-calculating distances and movement probabilities among the set of sampled particles during particle processing using (approximated) shortest distances (option B: see Appendix §1.2). Since there were 1,000 x 1,000 possible particle pairs at each time step (and 21,159 time steps for this analysis) two approaches were implemented to minimise the time required for distance calculations during particle processing:

A. Mobility threshold. At each time step, Euclidean distances were calculated between particle pairs and only those pairs for which the Euclidean distance was less than $mobility$ were retained for subsequent calculations.

B. Shortest-distances approximation.

Concept. A statistical model, generated from a randomised sampling procedure, was used to predict shortest distances (h_{LCP}) between each pair of particles based on the Euclidean distance of the transect connecting each pair of particles and whether or not that transect crossed a barrier (i.e., the coastline). This approach avoided the need to implement computationally expensive shortest-distance algorithms repeatedly during particle processing.

Sampling procedure. To generate a model for h_{LCP}, a four-step randomised sampling procedure was used:

I. **Sampling.** From the study site (excluding land), 200,000 locations were sampled at random.
II. **Euclidean distances.** For each pairwise combination of locations, the Euclidean distance between them was calculated.
III. **Subsampling.** For all of the location pairs for which the Euclidean distance was within $mobility$, a maximum of 1,000,000 pairs were selected at random (to reduce the time taken for subsequent calculations).
IV. **Calculations.** For each subsampled location pair, it was identified whether or not the Euclidean transect connecting the locations crossed a barrier and Euclidean and shortest distances were calculated. Given the scale of this exercise, shortest distances were calculated by the Dijkstra algorithm via the flapper package (Lavender, 2020b) using efficient C++ routines provided by

Larmet (2019), rather than the routines typically used in the ecological literature (Aspillaga et al., 2019; Niella et al., 2020).

Model fitting. Using the data generated by the randomised sampling procedure, the minimum distance of transects that crossed barriers was calculated and a statistical model was fitted for the shortest distance depending on the Euclidean distance and whether or not each transect crossed a barrier. This model took the form:

$$h_{LCP}(\boldsymbol{s}_t^{\boldsymbol{i}}, \boldsymbol{s}_t^{\boldsymbol{j}}) \sim N\left(E_{LCP}(\boldsymbol{s}_t^{\boldsymbol{i}}, \boldsymbol{s}_t^{\boldsymbol{j}}), \sigma^2\right)$$
$$E_{LCP}(\boldsymbol{s}_t^{\boldsymbol{i}}, \boldsymbol{s}_t^{\boldsymbol{j}}) = \beta_1 \phi_{0_t} \left|\boldsymbol{s}_t^{\boldsymbol{j}} - \boldsymbol{s}_t^{\boldsymbol{i}}\right| + \beta_2 \phi_{1_t} |\boldsymbol{s}_{\boldsymbol{t+1}}^{\boldsymbol{j}} - \boldsymbol{s}_t^{\boldsymbol{i}}| \quad \text{(S17)}$$

where $\boldsymbol{s}^{\boldsymbol{i}}$ and $\boldsymbol{s}^{\boldsymbol{j}}$ in this case represent the start and end coordinates of each transect (t); $E_{LCP}\left(\boldsymbol{s}_t^{\boldsymbol{i}}, \boldsymbol{s}_t^{\boldsymbol{j}}\right)$ represents the expected distance of the shortest path; ϕ_0 is an integer that defines whether (0) or not (1) each transect crossed the barrier; ϕ_1 is a switched version of the same interger that describes whether (1) or not (0) each transect crossed the barrier; and β_1 and β_2 are parameters.

Results. The results of this process were as follows:

I. **Transect distance.** For the segments that crossed a barrier (n = 1,066), the shortest transect measured 99 m long in Euclidean distance, but 95 % of transects that crossed a barrier exceeded a Euclidean distance of 265 m.
II. **Model for $\boldsymbol{h_{LCP}}$.** Based on the data from all transects for which Euclidean and shortest distances could be calculated (n = 999,905), $\beta_1 = 1.065 \pm 0.000$ standard error and $\beta_2 = 1.173 \pm 0.001$ standard error respectively. This model described 99.909 % of the variation.

Distance calculations. Based on these study site-specific results, during particle processing, $h\left(\boldsymbol{s}^i, \boldsymbol{s}^j\right)$ was defined as $E_{LCP}\left(\boldsymbol{s}^i, \boldsymbol{s}^j\right) = 1.065\phi_0\left|\boldsymbol{s}^i - \boldsymbol{s}^j\right| + 1.173\phi_1\left|\boldsymbol{s}^i - \boldsymbol{s}^j\right|$. To improve the implementation speed of this model, the assumption was made that any transect shorter than 265 m in Euclidean distance would not overlap with a barrier and only barrier overlaps for longer transects were checked.

Analysis A2—Qualitative comparison of maps of space use from the mean-position and flapper algorithms. Following particle processing, for each algorithm, POU was mapped as described previously and smoothed using KUD estimation (see Appendix §1.3.3). For the latter

process, POU scores were aggregated across the 25 x 25 m grid used for COA KUD estimation via the arithmetic mean and then locations were sampled from this surface in line with their renormalised POU scores for KUD estimation, as described previously (see Appendix §1.3.3). The maps derived from each algorithm were qualitatively compared.

Analysis A2—Implications of reconstructed patterns of space use in an analysis of habitat preferences. Using the KUDs from each algorithm, the consequences of differences between the algorithms were illustrated for a simple analysis of core ranges and habitat preferences. For this analysis, following convention the 'core range' was defined as the smallest region containing 50 % of the volume of the KUD. For each algorithm, the proportion of each sediment type found in the core range was compared against the 'background' proportions for the study site, using published sediment maps (Howe et al., 2014; Boswarva et al., 2018). With an accurate map of space use, if the skate exhibits strong preferences for a specific sediment type, the expectation is that the relative availability of this sediment type in the core range may exceed background levels.

Analysis A2—Implications of reconstructed patterns of space use for residency. Using the results of the ACDCPF algorithm, the implications of reconstructed patterns for residency were considered. If the individual was resident in the study site over the analysed period, the expectation is that the ACDCPF algorithm should reveal patterns of space use—accounting for movement in the gaps between detections—that are entirely localised within this area. In this scenario, we can explore how the 'known time spent in the study site' changes under the assumption that other individuals tagged by the MEFS project remained in the study site during detection gaps up to the duration of those exhibited by the 'resident' individual. For example, in an earlier study of 33 tagged flapper skate, known time spent in the MEFS array, measured as the number of days on which individuals were detected (i.e., 'detection days') ranged from 1–256 (median = 34) days (Chapter Three). If the data for the selected individual are consistent with residency in the study site over gaps up to x days in duration, this implies a potential factor $\sim x$ increase upon previously documented values for time (days) spent in the area. The result is a preliminary indication of the extent to which estimates of time spent in the area may be sensitive to short detection gaps and an illustration of the potential value of the flapper algorithms, which can account for these, to support future analyses of residency in sample-wide studies.

1.4.3. Analysis A3

Data. In the third analysis (A3), the application of the DCPF algorithm to reconstruct movement paths following catch-and-release angling was illustrated. This analysis focussed on two individuals (1507 and 1558) for which previous research has indicated irregular post-release behaviour (IPRB), in the form of rapid re-ascents towards the surface following release, to examine the extent to which irregular movements were consistent with benthic movement or indicative of pelagic behaviour (Chapter Five).

Data processing. Following catch-and-release angling, both individuals rapidly descended to the seabed before resting or moving elsewhere (Figure S9) (Chapter Five). For the reconstruction of movement paths, depth observations were considered following the return of each individual to the seabed until 80 minutes post-release (i.e., the time period over which IPRB was most apparent) (Chapter Five). The 'start time' from which movement paths were reconstructed was defined as the time of the first depth observation proceeding the rapid post-release descent after which the change in depth stabilised or reversed, based on qualitative inspection of the depth time series (Figure S9). Thus, the eighth and fifth post-release observations represented the start of the post-release time series for individual 1507 and 1558 respectively. For each time series, the 'study site' within which subsequent movements were reconstructed was defined as the area within 5 km of the release location. It is recognised that individuals could have moved beyond the selected area during this time period, given the $mobility$ parameter (500 m per two minutes), but considering a smaller area facilitated the identification of the most plausible movement paths and reduced wall time.

DCPF. Within the study site, for each individual, the assumption was made that the initial location (at the start of the post-release time series) must have been within 1,000 m of the release location. As for the study site as a whole, while this limit is more restrictive than permitted under the selected $mobility$ parameter, given the time (10–16 minutes) between release and the start time of each analysis, it was expected to encapsulate the most likely starting locations. Within this limit, starting locations (particles) were sampled from the set of possible locations (i.e., those within the appropriate depth range) in line with the probabilities defined by the movement model given above (Equation S16). Thus, possible locations closer to the release location were more likely to be sampled than locations further away. For subsequent time steps, particles were sampled with replacement according to the same

movement model but within a $mobility$ restriction of 500 m rather than 1,000 m (in line with the regular two-minute interval between sequential observations).

Path assembly and processing. For computational efficiency, particles were sampled and paths were reconstructed on the basis of Euclidean distances, following the protocol laid out for the simulated data (see Appendix §1.3.2). Unlike analysis A2, the effects of the bathymetry on movement probabilities were accounted for in this analysis following (rather than during) particle processing, by post-processing reconstructed paths (option C: see Appendix §1.2), in two steps:

A. **Interpolation.** For each path, shortest paths were interpolated between sequential locations and location probabilities were recalculated using shortest distances (via the movement model).
B. **Filtration.** Any paths with shortest distances exceeding 1,000 m (for the first time step) or 500 m (for later time steps) were excluded from the set of reconstructed paths: these paths are not admissible under $mobility$.

Analysis. For each individual, the resultant set of paths was ranked by their log probability (see §2.8) and the ten most likely paths were visualised in relation to the bathymetry.

1.4.4. Analysis A4

Data. In the fourth analysis, the ACDCPF algorithm was applied to reconstruct fine-scale movement paths for individuals exhibiting overlapping detection patterns. For this analysis, the pair of individuals (542 and 560) for which detections most frequently cooccurred at receivers (Chapter Three) was considered. More specifically, an illustrative 52-minute period (12:28–13:20 hours on 22nd May 2016) during which time cooccurrences were most frequent was modelled. As for analyses A1–2, during this time acoustic and archival time series were considered at the same (two-minute) resolution. Only unique detections within each two-minute interval were considered. Over the selected time period, both individuals were detected in almost every interval at a single receiver and the longest gap between detections was only four minutes (Figure S10). Based on these data, the 'study site' was defined as the area within a 2,750 m buffer of the receiver at which detections were recorded, which captures the limits of both individuals' possible movements during time period under investigation.

PF, path assembly and processing. For each two-minute window, plausible movement paths of each individual were reconstructed by sampling possible locations using the ACDCPF algorithm with the fast-Euclidean distances method and the parameters defined previously (see Appendix §1.4.1). As for analysis A3, 1,000 movement paths were reconstructed from particle samples using Euclidean distances, shortest paths between sequential locations were interpolated and the subset of paths for which all movements were ≤ 500 m in distance were isolated, before the most likely reconstructed path for each individual was visualised over the bathymetric landscape.

1.5. R code

For all simulations, R code is available from https://github.com/edwardlavender/flapper_sim. For all case-study analyses, R code is available from https://github.com/edwardlavender/flapper_appl.

2. Supporting tables

Table S1. An overview of simulations and case-study analyses. For each scenario (simulation or case study), for each analysis, the identifier and objective are provided, alongside a list of the algorithms implemented, the data used and the references for those data. For all analyses, acoustic data comprised detections at receivers and archival data comprised depth (m) observations sampled at a resolution of two-minutes.

Scenario	ID	Objective	Algorithm	Data	Fig	Source
Simulation	S1	Illustrate 'flapper' algorithms	DC	Simulated acoustic and/or archival data from array 3 (Table S2)	1	Simulation
			AC			
			ACDC			
			DCPF			
			ACPF			
			ACDCPF			
	S2	Evaluate algorithm utility for reconstructing patterns of space use	Mean-position	Simulated acoustic and/or archival data from arrays 1–12 (Table S2)	2, S11–12	
			ACPF			
			ACDCPF			
Case study	A1	Investigate depth habitat representation	DC	Acoustic and/or archival data for individual 540 for a one-month period from 2016-09-29 13:00–2016-10-28 22:16	S8	Chapter Three
	A2	Reconstruct maps of space use	Mean-position			
			ACPF			
			ACDCPF			
	A3	Examine post-release movement paths	DCPF	Archival data for two individuals (1507 and 1558) following archival tag deployment on 2016-03-17 14:37 off Kerrera and 2016-03-13 14:18 off Insh, respectively, from 8–80 and 5–80 minutes following release	S9	Chapter Five
	A4	Explore fine-scale spatial partitioning	ACDCPF	Acoustic and archival data for two individuals (542 and 560) that shared the highest proportion of detections during a 52-minute period (12:28–13:20 on 2016-05-22) when shared detections were most frequent	S10	Chapter Three

Table S2. A summary of simulated array designs. For each array design (ID), the number of receivers, the arrangement, the proportion and number of clusters (if applicable), and the areal coverage of detection containers is shown. Note small differences between the number of simulated (5, 15 or 25) and realised receivers for some array designs due to the constraints imposed by receiver arrangements.

ID	Arrangement	Receivers (No.)	Clusters (Pr)	Clusters (No.)	Coverage (km^2)	Coverage (%)
1	Regular	4	-	-	1.11	6.95
2	Regular	16	-	-	4.00	25.00
3	Regular	25	-	-	6.60	41.27
4	Random	5	-	-	1.32	8.23
5	Random	14	-	-	3.40	21.26
6	Random	25	-	-	5.27	32.94
7	Clustered	4	0.4	2	1.11	6.95
8	Clustered	4	0.6	3	1.05	6.59
9	Clustered	15	0.4	6	2.95	18.47
10	Clustered	15	0.6	9	3.58	22.35
11	Clustered	22	0.4	10	4.43	27.68
12	Clustered	22	0.6	15	4.65	29.08

Table S3. Example applications and challenges for flapper algorithms.

Branch	Algorithm	Applications	Challenges
AC	DC	• Examine habitat (depth) representation (e.g., the extent to which utilised depths are represented within a particular location, such as a Marine Protected Area); • Identify unexploited locations; • Support the reconstruction of movement paths and patterns of space use via PF;	• Prolonged gaps in detections in low-coverage arrays are limiting (as for other methods) in the absence of additional information, because during this time the containers of an individual's location can grow to span the entire study site. For mapping, this can give rise to a 'hotspot' pattern, with elevated scores around receivers relative to surrounding areas, as seen in Figures 1–3 and S11–13;
	AC		
	ACDC		
PF	DCPF	• Examine fine-scale movement paths, including in relation to the bathymetry; • Examine post-disturbance movements, for instance following catch-and-release angling; • Examine cooccurring movements and/or social interactions; • Reconstruct improved maps of space use; • Estimate the time spent in an area (i.e., residency indices), accounting for movement in the gaps between detections; • Support analyses of habitat preferences; • Inform tagging and array deployment programmes (e.g., quantification of the relative contribution of acoustic and archival data to maps of space use under different array designs);	• Prolonged gaps in detections can remain problematic, as described above; • Data are required on detection ranges (and ideally detection probability) as well as mobility limits (and ideally movement probabilities); • Wall time can be substantial, especially in large areas represented by high-resolution grids and for long time series; • Convergence issues are possible, especially if model assumptions are uncertain, so multiple iterations of the algorithms may be required as assumptions are revised;
	ACPF		
	ACDCPF		

Table S4. Wall times for simulations. For each array ID, the duration (minutes) of AC- and PF-branch algorithms is shown. AC-branch algorithms were implemented on a single core. PF algorithms were implemented using the fast-Euclidean distances method and 100 particles. While these times are indicative for the simulations shown, wall times are contingent on many factors, such as the size and resolution of the grid, the volume of data, algorithm parameters and computational specifications. Furthermore, for PF algorithms, the wall times of subsequent steps, such as particle processing, mapping and path reconstruction, while limited here, can be substantial, particularly when large numbers of particles are involved (see Tables S5–6). All times were tracked on a MacBook Pro (with a 2.2 GHz 6-Core Intel Core i7 processor and 32 GB 2400 MHz DDR4 memory).

ID	Flapper algorithm					
	DC	AC	ACDC	DCPF	ACPF	ACDCPF
1	-	0.50	0.59	-	3.35	3.75
2	-	0.52	0.93	-	3.73	3.95
3	0.07	0.54	0.64	0.02	3.87	4.09
4	-	0.02	0.02	-	0.18	0.15
5	-	0.44	0.52	-	2.99	3.20
6	-	0.48	0.56	-	3.44	3.47
7	-	0.35	0.41	-	2.38	2.53
8	-	0.41	0.47	-	2.62	2.88
9	-	0.47	0.56	-	3.12	3.41
10	-	0.34	0.43	-	2.60	2.64
11	-	0.29	0.34	-	1.95	1.99
12	-	0.36	0.42	-	2.55	2.70

Table S5. Wall times for case-study analyses. For each analysis (A1–4), for each individual, the number of time steps analysed (N[step]) and the wall time (minutes) for the AC-branch algorithm (T[AC]), the PF-branch algorithm (T[PF]), particle processing (T[PP]), path reconstruction (T[PR]), shortest-paths interpolation (T[PI)]) and overall (T[O]) are shown. Numbers in brackets indicate the number of socket (SK) or fork (FK) clusters utilised for parallelisable operations. For analysis A2, the mean-position algorithm was also implemented; wall time for this algorithm was negligible. For this analysis, following particle processing, POU maps and KUDs were also created (see Table S6). Note that the number of time steps and the size of the study site differed between analyses, but all PF steps comprised 1,000 particles and in all path-based analyses 1,000 paths were built. All times were tracked on a MacBook Pro (as in Table S4) running an 8 TB Western Digital USB 3.0 Desktop Hard Drive.

ID	Algorithm	Individual	N[step]	T[AC]	T[PF]	T[PP]	T[PR]	T[PI]	T[O]
A1	DC	540	21,159	228.11 (1)	-	-	-	-	228.11
A2	ACPF			509.52 (4_{SK})	2,383.69	320.72 (10_{FK})	-	-	3,213.93
	ACDCPF			481.34 (4_{SK})	2,364.36	638.11 (10_{FK})	-	-	3,483.81
A3	DCPF	1507	33	0.24 (1)	17.02	0.36 (4_{SK})		2.82	20.44
		1558	36	0.25 (1)	16.85	0.39 (4_{SK})		3.05	20.54
A4	ACDCPF	542	27	0.27 (1)	20.93	0.83		1.63	23.66
		560	27	0.26 (1)	18.74	0.42		1.88	21.30

Table S6. Wall times for particle mapping in case-study analysis A2. For each algorithm, the number of samples (N[samples]) analysed and the wall time (minutes) required to estimate POU maps (T[POU]) and KUDs (T[KUD]) is shown. POU maps were estimated across a 5 x 5 m grid; KUDs were estimated across a 25 x 25 m grid and resampled to 5 x 5 m resolution. All times were tracked as in Table S5.

ID	Algorithm	N[samples]	T[POU]	T[KUD]
A2	ACPF	26,320,200	1.34	685.96
	ACDCPF	17,512,600	0.63	411.45

3. Supporting figures

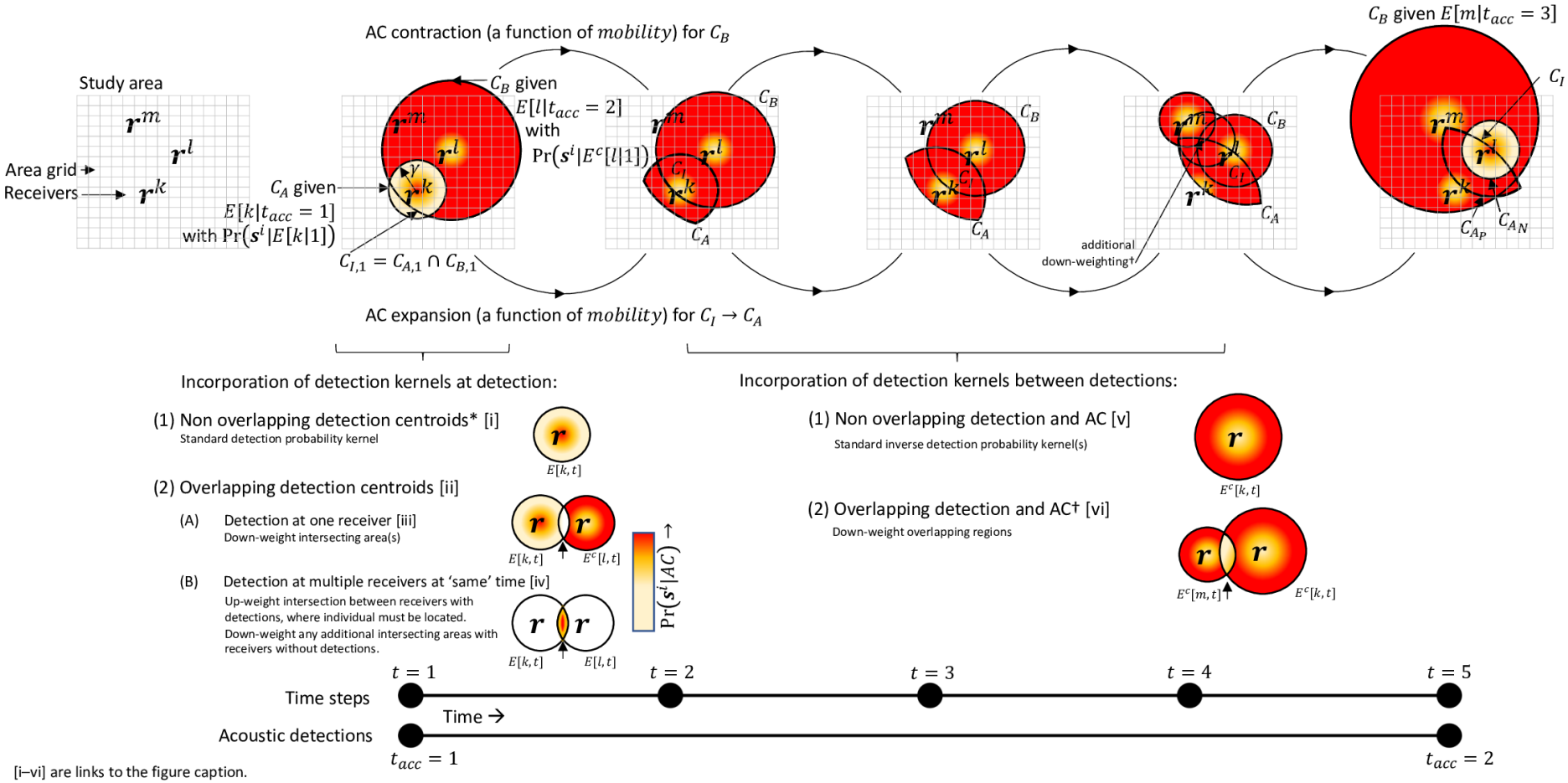

[i–vi] are links to the figure caption.

Figure S1. The acoustic-container (AC) algorithm (overleaf). This algorithm uses acoustic detections to infer the possible locations of an acoustically tagged animal within an area over time. In discretised form, the algorithm represents the study site as a grid, with cells indexed by i and the coordinates of each cell's mid-point denoted by $\boldsymbol{s}^i$. Detections at receivers on the grid may occur irregularly in time (at time steps indexed by t_{acc}), but we can think of them as occurring along a sequence of time steps (indexed by t), as shown at the base of the figure. At each time step, the AC algorithm considers the set of possible locations for the detected individual from the perspective of (A) its previous location and (B) its future location. The regions(s) within which the individual must be located according to receiver(s) are termed 'acoustic containers'.

A hypothetical area with three receivers (k, l and m) at locations $\boldsymbol{r}^k$, $\boldsymbol{r}^l$ and $\boldsymbol{r}^m$ is shown, with the first detection event at receiver k ($E[k, t_{acc} = 1]$), the second at l ($E[l, t_{acc} = 2]$) and the third at m ($E[m, t_{acc} = 3]$). At the moment of first detection, perspective A is provided by the receiver(s) at which the individual is detected at that moment and perspective B depends on the receiver(s) at which the individual is next detected. In the example shown, when the individual is detected at receiver k, from perspective A detection probability implies that the individual must be within finite radius of that receiver dependent on the detection range (γ), in an area termed the 'detection container' (labelled C_A). This is a specific type of acoustic container that defines the region within which an individual must be located at the moment of detection according to the receiver(s) at which it was detected. Within this container, for the simple array shown in which receiver k's detection container does not overlap with that for any other receiver, a surface (the detection kernel) that describes the probability of being each grid cell given the detection at receiver k, $\Pr(\boldsymbol{s}^i|E[k, t])$, can be assigned via a model of detection probability. For example, typically locations nearer to a receiver, given a detection, are more likely (red) than locations further away (yellow to white) [i]. In an array in which the detection container of the receiver that recorded a detection overlaps with that for other receiver(s), the presence or absence of detections at those receivers refines this probability surface [ii]. If the individual is only detected at one receiver, then it follows that the individual must be within the detection container of that receiver, but the probability that it is in the overlapping region is reduced, given it was not detected at the other receiver(s) [iii]. In contrast, if the individual is detected at multiple receivers at effectively the same time (given receiver clock synchronisation), then the individual must be within the intersecting region between the receivers that recorded detections [iv], with the probability of locations in any additional intersecting areas with detection containers of receivers that did not record detections reduced, given the absence of detections at those receivers. These multifarious dynamics emerge from a single mathematical description for the probability of being in each grid cell given detection/non-detection at each operational receiver and the information encapsulated in the AC algorithm, i.e., $\Pr(\boldsymbol{s}^i|AC)$ (see Appendix §1.1). Still at the moment of detection but moving from perspective A to B, the perspective of the receiver at which the individual is next detected, the acoustic container that defines set of possible locations is wider, in line with the time between detections and the mobility of the animal. Within this container, according to receiver l, the probability of the individual being in location $\boldsymbol{s}^i$ is lower nearer the receiver (white to yellow) and highest beyond the receiver's detection container (red), given the complement (absence) of a detection event at receiver l, i.e., $E^c[l, t_{acc} = 1]$. The intersection of these two containers (C_I) describes, for $t = 1$, the set of possible locations for the individual. In the example shown, the detection containers of receivers k and l do not overlap, so within container C_I, $\Pr(\boldsymbol{s}^i|AC)$ depends entirely on receiver k's detection kernel.

Moving forwards in time along the intermediate time steps before the next detection, the expansion, contraction and intersection of acoustic containers describe how the set of possible locations changes. Consider the step from $t = 1$ to $t = 2$. From (A) the perspective of the individual's previous location (within C_I), the set of possible locations expands—because the individual could have moved beyond C_I—in line with a $mobility$ parameter that controls the distance an individual could move in the time between intermediate time steps. In the figure, this is shown by the expansion of container C_I at $t = 1$ into container C_A at $t = 2$. Meanwhile, from the perspective of the receiver at which the individual was next detected (B), the set of possible locations shrinks, as a function of $mobility$, as the individual must have been located within the detection container of that receiver by the time of the detection. The intersection of the two containers defines the set of possible locations for the individual (C_I). This process repeats for subsequent time steps, with the container of the individual's previous location (C_I) expanding in line with the animal's $mobility$ into C_A, which intersects with the contracting container C_B. During this time, in a simple array with non-overlapping detection containers, grid cell probabilities, given the absence of detection, are derived from inverse detection probability kernels [v]. In the sample shown, this means that locations near to receivers are less likely (yellow) than those further away. In an array with non-overlapping receivers, cell probabilities that fall within the detection containers of any receivers are reduced (given the absence of detections) [vi].

These dynamics recognise that as time passes between detections the individual could have moved away from the receiver(s) at which it was last detected but only at a rate and in a direction that fits with the receiver(s) at which the individual was next detected. Thus, when the individual is detected again (labelled $t_{acc} = 2$ here), the set of possible locations for the individual collapses to the intersection between the expanded set given the previous location (C_{A_P}), the detection container for receiver at which it is detected now (C_{A_N}) and the container for the next receiver (C_B) (and any other intersecting receivers that influence the probability surface). The end result of this process is a set of surfaces, one per time step, that describe the probability that the individual could have been in each grid cell according to the algorithm.

This representation makes two assumptions: (a) the detections and intermediate time steps perfectly align and (b) containers expand and contract at a constant rate. These assumptions are not integral to the algorithm but they are convenient. In the current application of the algorithm, these assumptions are currently enforced, though they can be relaxed via PF (see Figure S4).

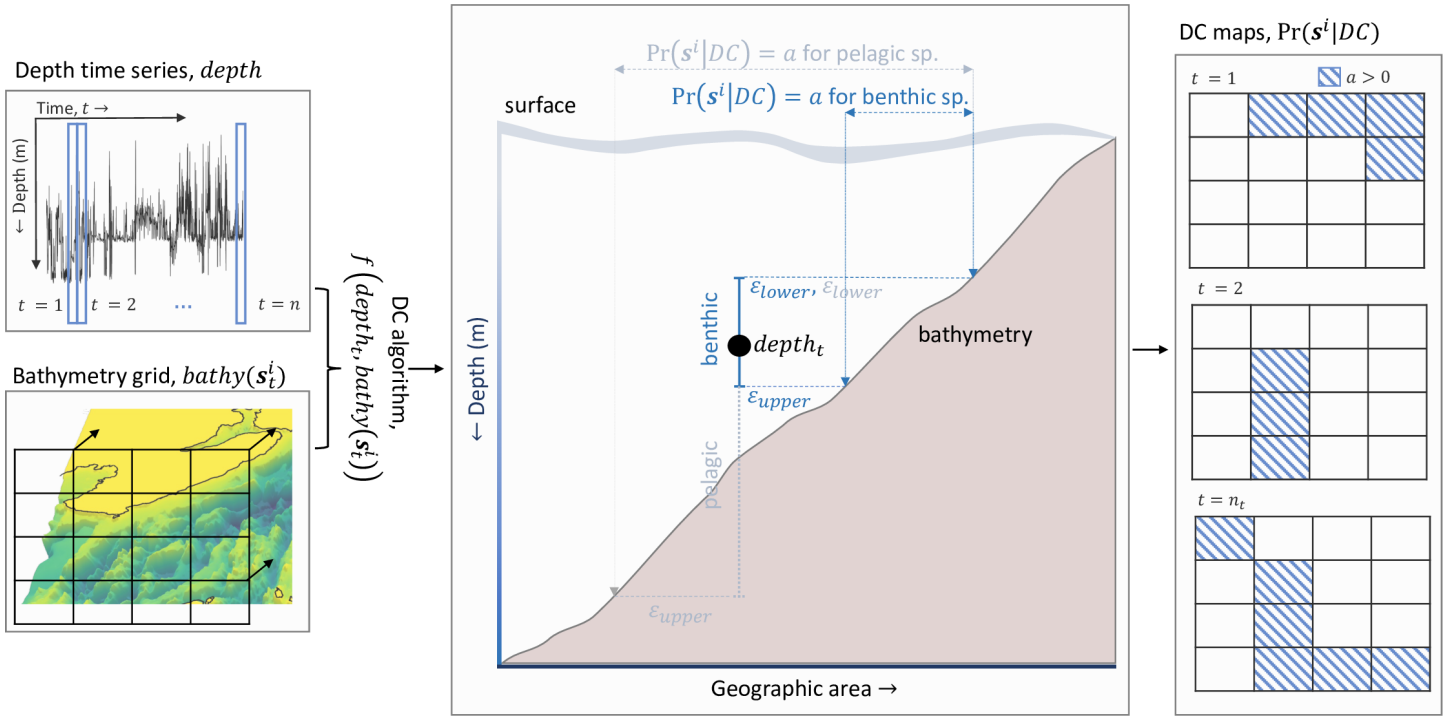

Figure S2. The depth-contour (DC) algorithm. This algorithm relates one-dimensional depth time series (labelled $depth$ in the top-left) to a two-dimensional bathymetry grid (labelled $bathy$ in the bottom-left, with the coordinates of each grid cell denoted by $\boldsymbol{s}^i$) via a depth-error model (labelled $f(\cdot,\cdot)$) to determine the set of possible locations on the grid for an individual through time (t), as shown on the right. In the example shown, observed and bathymetric depths are linked via a depth-error model in which the probability of any given location on the grid, $\Pr(\boldsymbol{s}^i|DC)$, depends on the overlap between the observed depth (± a shallow depth error [ϵ_{lower}] and a deep depth error [ϵ_{upper}]) and the bathymetric depth. This model is appropriate for both benthic/demersal species (which remain close to the seabed and thus must occupy an area where the seabed depth is close to the observed depth) and pelagic species (which range at most from the seabed to the surface and must occupy an area where the depth of the seabed is at least as deep as the observed depth). Admissible locations are defined by a positive constant, a, as indicated by the hatching on the right-hand side. Illustrated depth time series were sourced from a study of flapper skate (*Dipturus intermedius*) (Chapter Three). Illustrated bathymetry and coastline data refer to an area in the Loch Sunart to the Sound of Jura Marine Protected Area (off west Scotland) and were sourced from Howe et al. (2014) and Digimap (see Figure S7). Digimap data © Crown copyright and database rights [2019] Ordnance Survey (100025252).

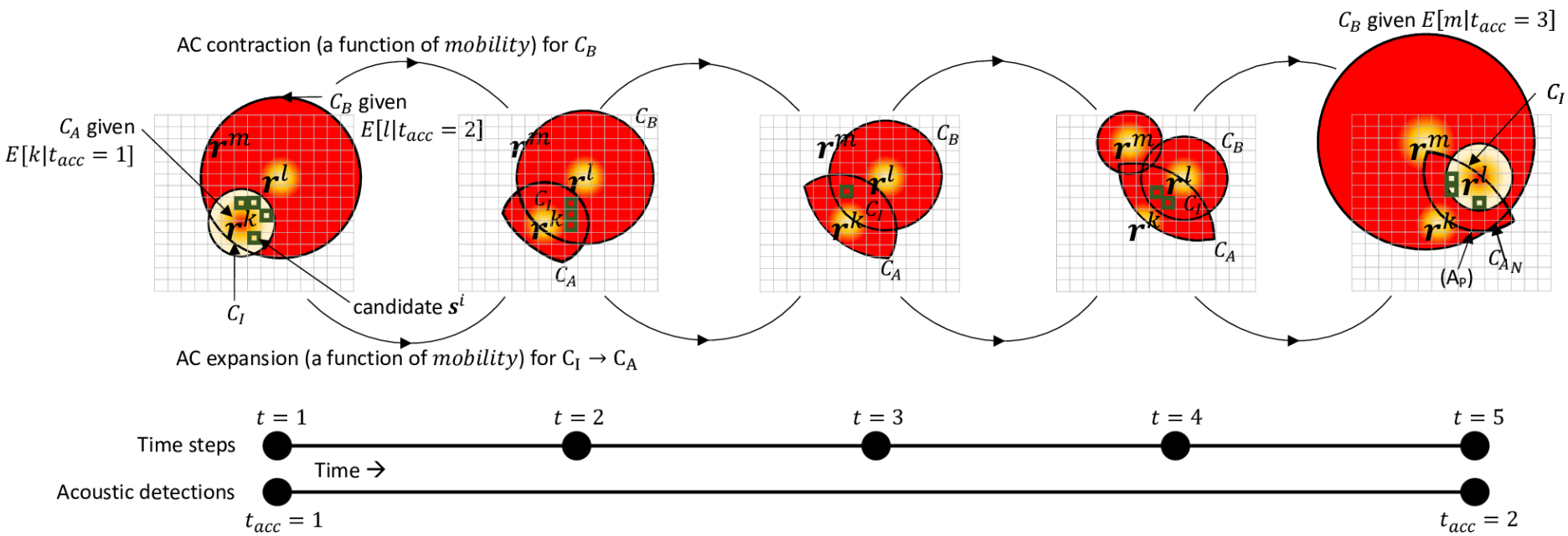

Figure S3. The acoustic-container depth-contour (ACDC) algorithm. This algorithm extends the AC algorithm (see Figure S1) to incorporate depth observations via the DC algorithm (see Figure S2). At each time step, the AC algorithm defines the containers of the individual's possible location, as illustrated in Figure S1. Within these containers, the DC algorithm refines the possible locations of the individual, highlighting the subset of locations (labelled 'candidate $\boldsymbol{s}^i$' and marked by the green rectangles) that meet depth constraints, as illustrated in Figure S2.

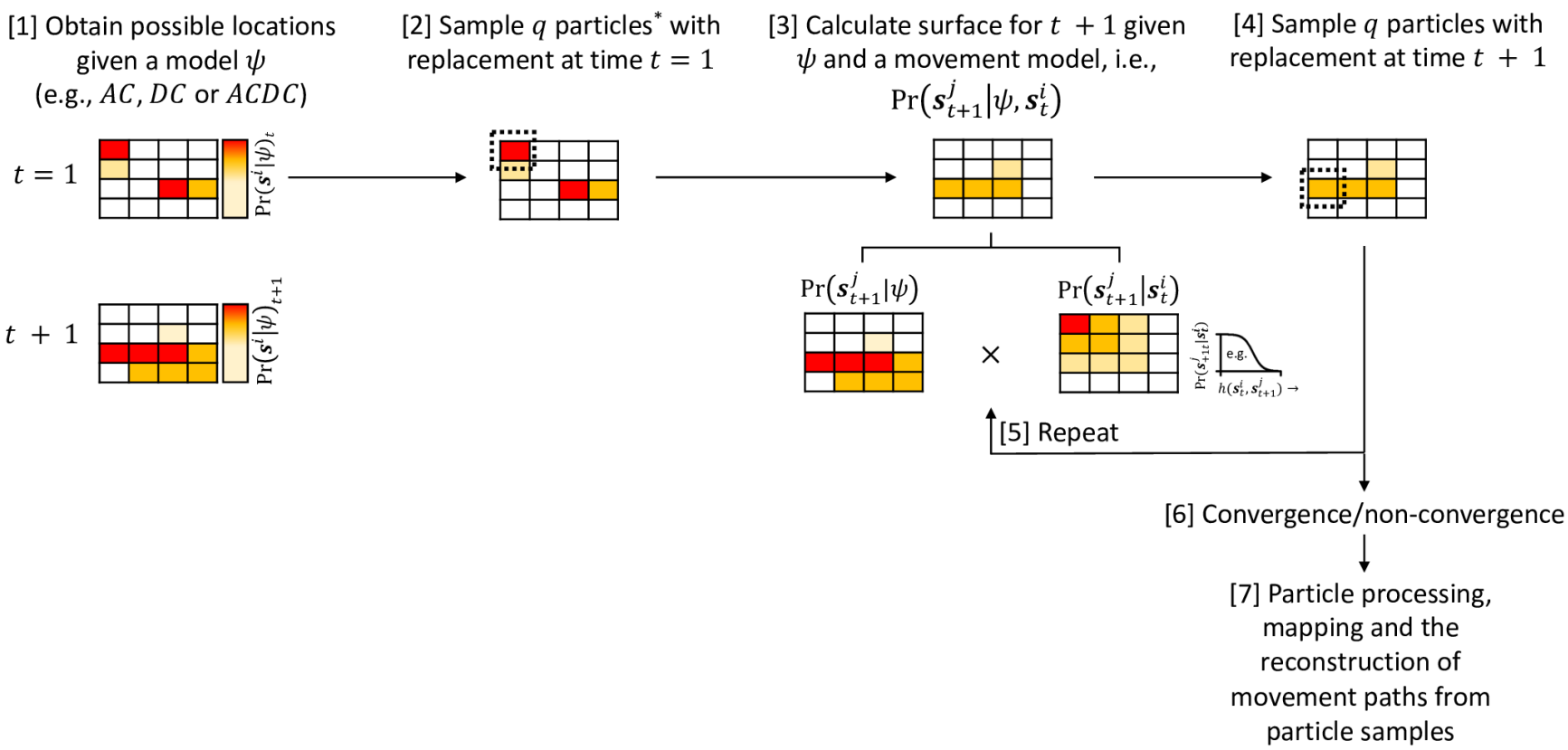

*Only one particle shown for simplicity.

Figure S4. The particle filtering (PF) routine (overleaf). This routine provides a flexible means to extend AC-branch algorithms via the incorporation of a movement model for the reconstruction of movement paths and emergent patterns of space use. The starting point (step [1]) is a set of surfaces that describe the probability that a tagged individual is in any given location on the grid ($\boldsymbol{s}^i$) from an AC-branch algorithm (ψ) through time (i.e., $\Pr(\boldsymbol{s}_t^i|\psi)$, see Figures S1–3). In the example shown, the possible locations of the individual are shown for two time steps ($t = 1$ and $t + 1$), with more likely locations shown in orange–red. Beginning with $t = 1$, the PF routine samples q grid cells ('particles') with replacement, according to $\Pr(\boldsymbol{s}_t^i|\psi)$ (step [2]). In the example shown, the enclosed particle is sampled. For the selected particles, a movement model is used to predict where the individual could have moved to at the next time step, i.e., $\Pr(\boldsymbol{s}_{t+1}^j|\boldsymbol{s}_t^i)$. A simple, time-independent example is a logistic model in which the probability of movement from one location to another declines with a distance metric, denoted $h(\boldsymbol{s}_t^i, \boldsymbol{s}_{1+1}^j)$, as illustrated. This results in location probabilities that decline with distance from the selected particles, as indicated for $\Pr(\boldsymbol{s}_{t+1}^j|\boldsymbol{s}_t^i)$ by the red–white colour gradient away from the sampled location. This set of possible locations into which the individual could move the next time step, given the previously sampled particle(s), is combined with the set of locations in which the individual must have been at the next time step, according to ψ, resulting in an updated probability surface in which cell probabilities depend on both ψ and the movement model (step [4]). The whole process can then be repeated, by sampling q particles from the surface at time $t + 1$, predicting plausible locations from these for time $t + 2$ and filtering these by ψ at time $t + 2$ (step [5]). This process continues until (a) the end of the time series (i.e., convergence) or (b) the algorithm reaches a time step at which the set of locations into which the individual could move, given previously sampled particles, does not overlap with the set of locations within which the individual must have been, given ψ (i.e., non-convergence). If the algorithm converges, the outcome is a set of particle samples that describe possible locations of the individual through time, accounting for ψ and the movement model, though these may include 'dead-ends' (see Figure S5). Particle samples can be processed and used to reconstruct movement paths, by linking sequential particle samples, and maps of space use (step [7]) (see Figure S5). If the algorithm fails to converge, this implies that either too few particles have been sampled to explore the set of possibilities effectively or one or more assumptions in the AC-branch algorithm or the movement model been violated; for example, the movement capability of the animal may exceed expectations (at the selected grid resolution).

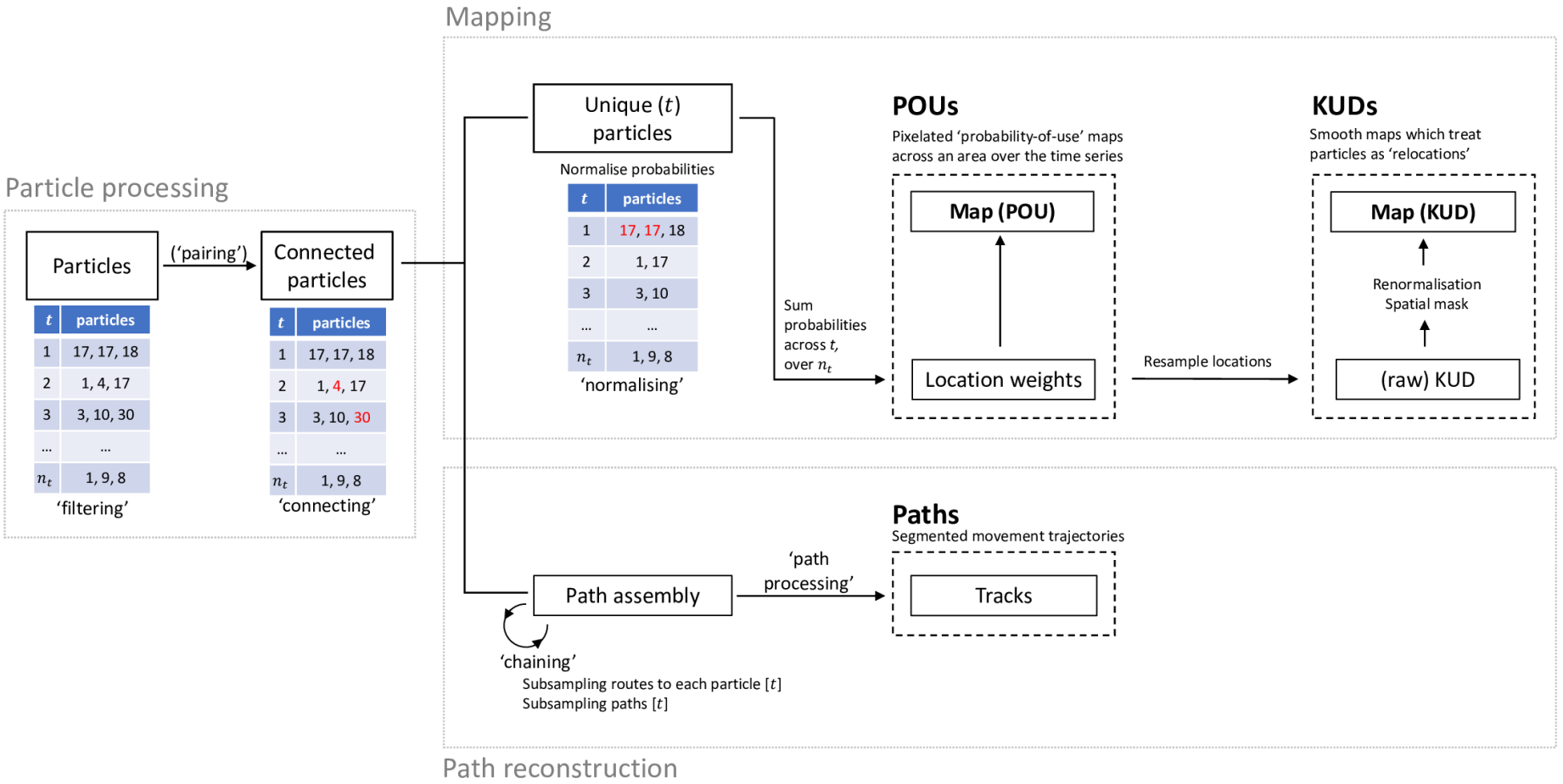
Mapping
Particle processing
Particles
('pairing')
Connected particles
t
particles
1
17, 17, 18
2
1, 4, 17
3
3, 10, 30
...
...
n_t
1, 9, 8
'filtering'
'connecting'
Unique (t) particles
Normalise probabilities
1, 17
3, 10
1, 9, 8
'normalising'
Sum probabilities across t, over n_t
POUs
Pixelated 'probability-of-use' maps across an area over the time series
Map (POU)
Location weights
Resample locations
KUDs
Smooth maps which treat particles as 'relocations'
Map (KUD)
Renormalisation
Spatial mask
(raw) KUD
Paths
Segmented movement trajectories
'path processing'
Path assembly
Tracks
'chaining'
Subsampling routes to each particle [t]
Subsampling paths [t]
Path reconstruction

Figure S5. From particles to maps of space use and movement paths (overleaf). The outcome of PF (the 'filtering' stage) is a time series of particle samples for each time step ($t = 1, 2, 3, \ldots, n_t$) (left-hand side). This requires processing before further analysis. The first processing step (the 'pairing' stage) identifies the (sub)set of particle pairs between which movement may have occurred given the movement probabilities connecting each pair of particles. The second processing step (the 'connecting' stage) filters 'dead-ends' (particles that did not lead to future particles) from the sample so that only the particles that connect into contiguous paths from the start to the end of the time series (given the movement model) remain. In the example table, particles '4' and '30' at time steps two and three are highlighted as hypothetical 'dead-ends' that are dropped. Connected particles can then be used to map the expected proportion of time spent in different areas (i.e., space use [top]) or to reconstruct paths (bottom). If connected particles are used directly for mapping, the next step (the 'normalising' stage) is to normalise particle probabilities at each time step such that at each time step only one record of each location is retained and the probabilities across all locations sum to one. In the example table, particle '17' has been sampled twice at $t = 1$; following normalisation, only one copy of the corresponding location is retained. This set of locations can be used to build two types of maps ('mapping'). The first type maps the sum of location probabilities across the time series over the total number of time steps (i.e., POU) across an area. The second type treats locations with positive POU scores (or an expanded sample of these) as 'relocations' for KUD estimation. In areas with barriers to movement, the KUD may be processed with a spatial mask and renormalised before mapping. Connected particle samples can also be linked into movement paths via 'chaining' (bottom). In situations where the number of admissible connections between sequential particle samples (given the movement model) is vast, subsampling either the routes to each particle or a selection of paths at each time step in this stage may be necessary, given finite vector memory. The set of reconstructed paths can then be processed ('path processing') and analysed.

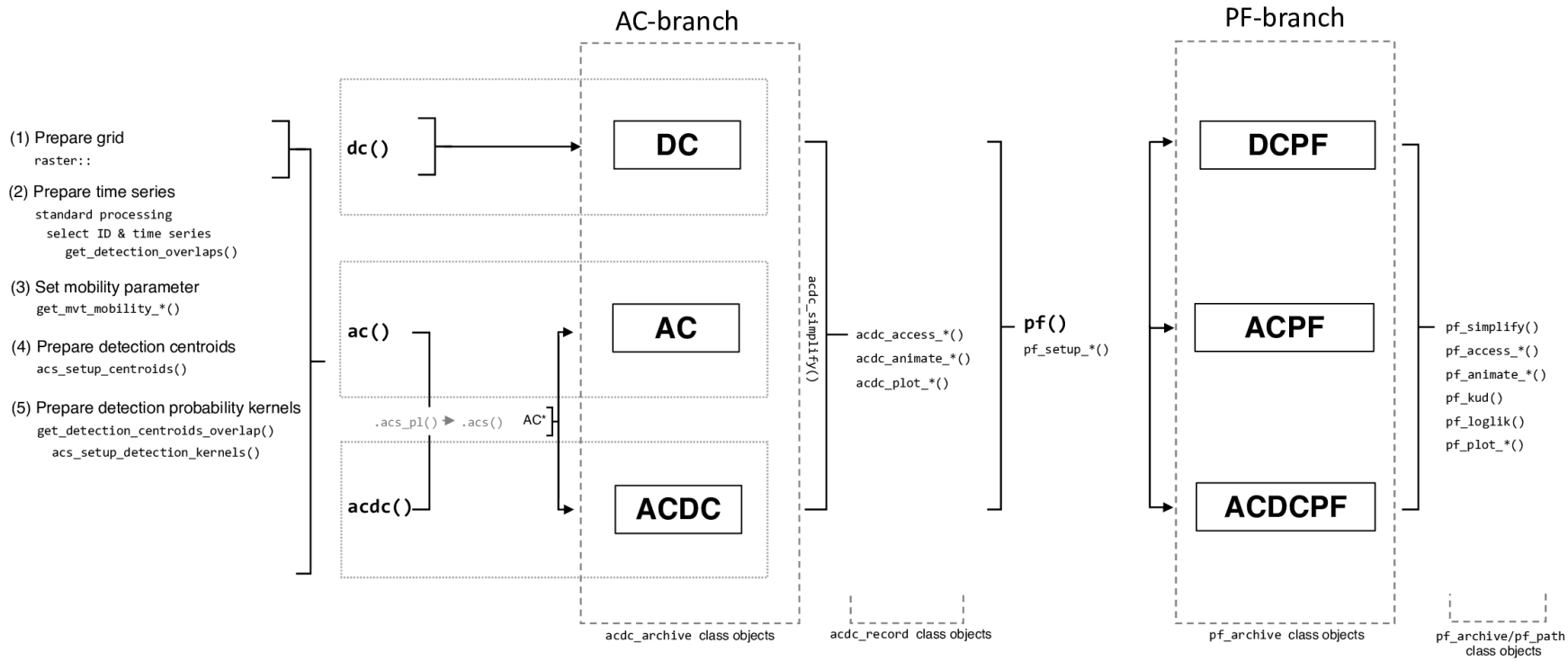

Figure S6. A schematic of the flapper algorithms as implemented by the flapper R package (version 0.1.0). Within this package, for all algorithms, prior to analysis a raster grid over which the algorithms are implemented needs to be defined, using standard `raster` routines. For the AC* algorithms, the detection time series, containers and kernels require preparation, a process facilitated by `acs_setup_*()` functions. AC-branch algorithms (i.e. DC, AC and ACDC) are implemented via `dc()`, `ac()` and `acdc()`. Under-the-hood, `ac()` and `acdc()` call `.acs_pl()` and ultimately `.acs()`. The three AC-branch functions each return an `acdc_archive` class object that can be simplified via `acdc_simplify()` into an `acdc_record` class object. This provides a record of an individual's possible locations through time, according to an AC-branch algorithm. Additional `acdc_*()` functions support the examination and visualisation of `acdc_record` objects. For each AC-branch algorithm, the corresponding PF algorithms (DCPF, ACPF and ACDCPF) are implemented via `pf()` and associated helper functions. `pf()` returns an `pf_archive` object, which is essentially a time series of particle samples. Particle samples can be processed via `pf_simplify()` into a streamlined `pf_archive` class object (comprising processed particle samples) or a `pf_path` class object (comprising movement paths). Additional `pf_*()` functions support the examination and visualisation of these objects.

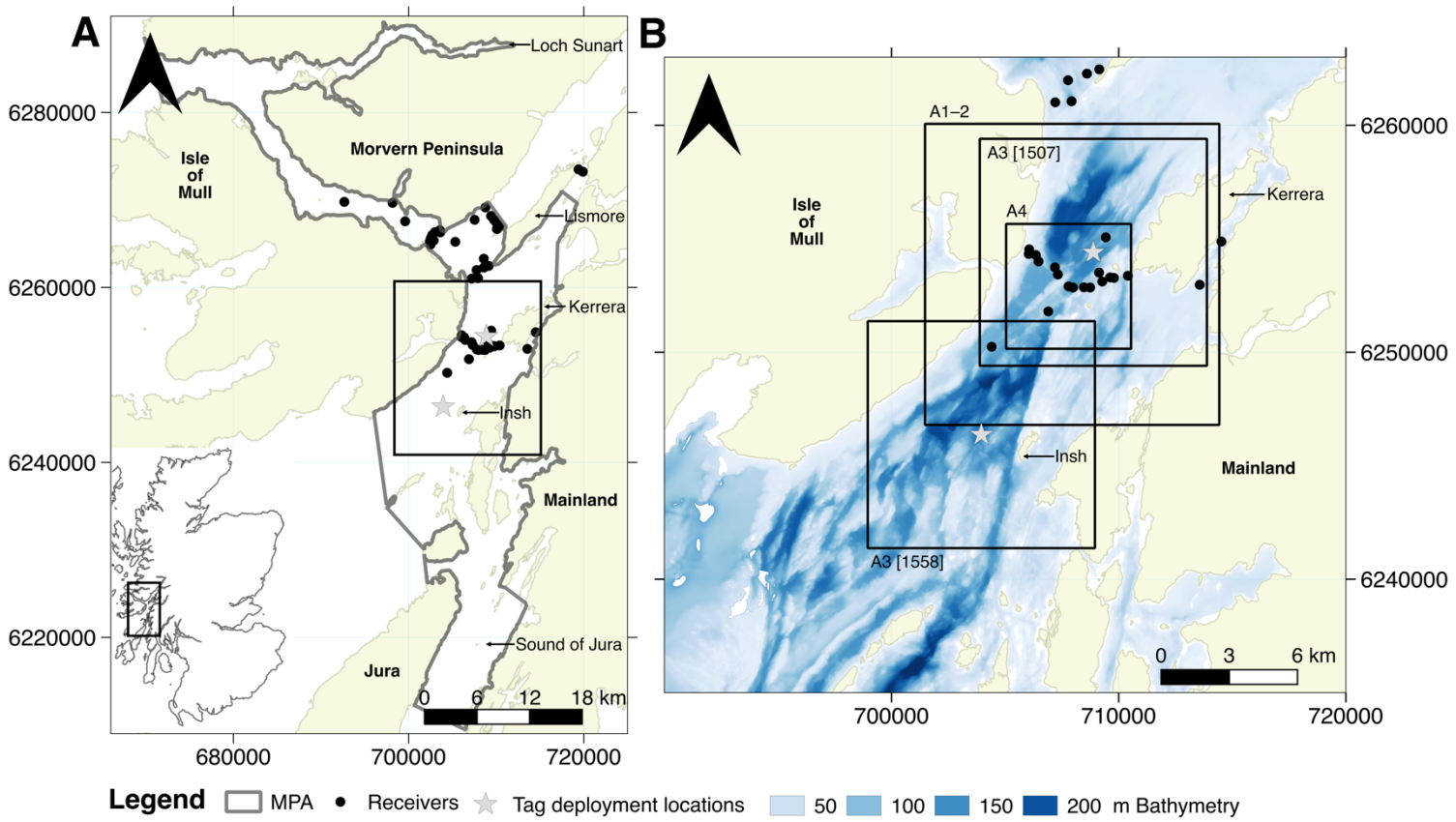

Figure S7. The case-study site. A shows the location of the study site within Scotland (inset) and within the Loch Sunart to the Sound of Jura Marine Protected Area (main figure). Acoustic receivers deployed within this area are shown, with the case-study region of focus enclosed. In **B**, the precise study site for each case-study analysis (A1–4) is shown, along with acoustic receivers, the bathymetry and the tagging locations for analysed individuals. Five analysed individuals (540, 1507, 542 and 560) were tagged off Kerrera and the remaining individual (1558) was tagged off Insh. Bathymetry data were sourced from Howe et al. (2014) and coastline data were sourced from Digimap. Digimap data © Crown copyright and database rights [2019] Ordnance Survey (100025252). The coordinate reference system is the Universal Transverse Mercator projection (Zone 29), as used for algorithm implementation.

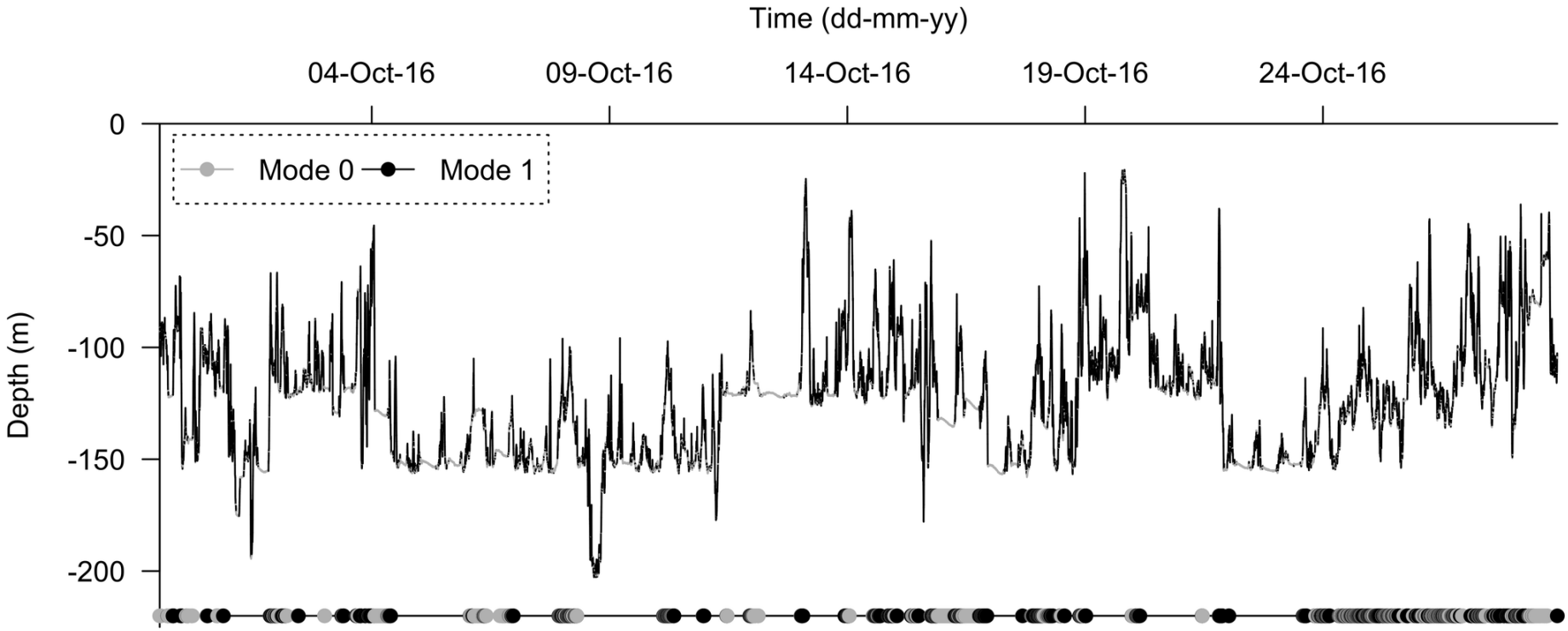

Figure S8. Case-study acoustic and archival time series from a selected individual (540) used to reconstruct patterns of space use via the DC, mean-position, ACPF and ACDCPF algorithms (analyses A1–2). The main panel shows the individual's depth time series over a one-month period (29th September–28th October 2016), distinguishing 'mode 0' movements (in grey), when the absolute vertical activity was ≤ 0.5 m (i.e., putative 'resting' behaviour used to restrict movement) and 'mode 1' movements (in black), when absolute vertical activity > 0.5 m. Points mark acoustic detections at receivers. Note that both acoustic and archival time series are expressed at a resolution of two-minutes, with acoustic time series thinned to exclude any duplicate detections at the same receiver in each two-minute period. Over the time period shown, detections occurred at four receivers.

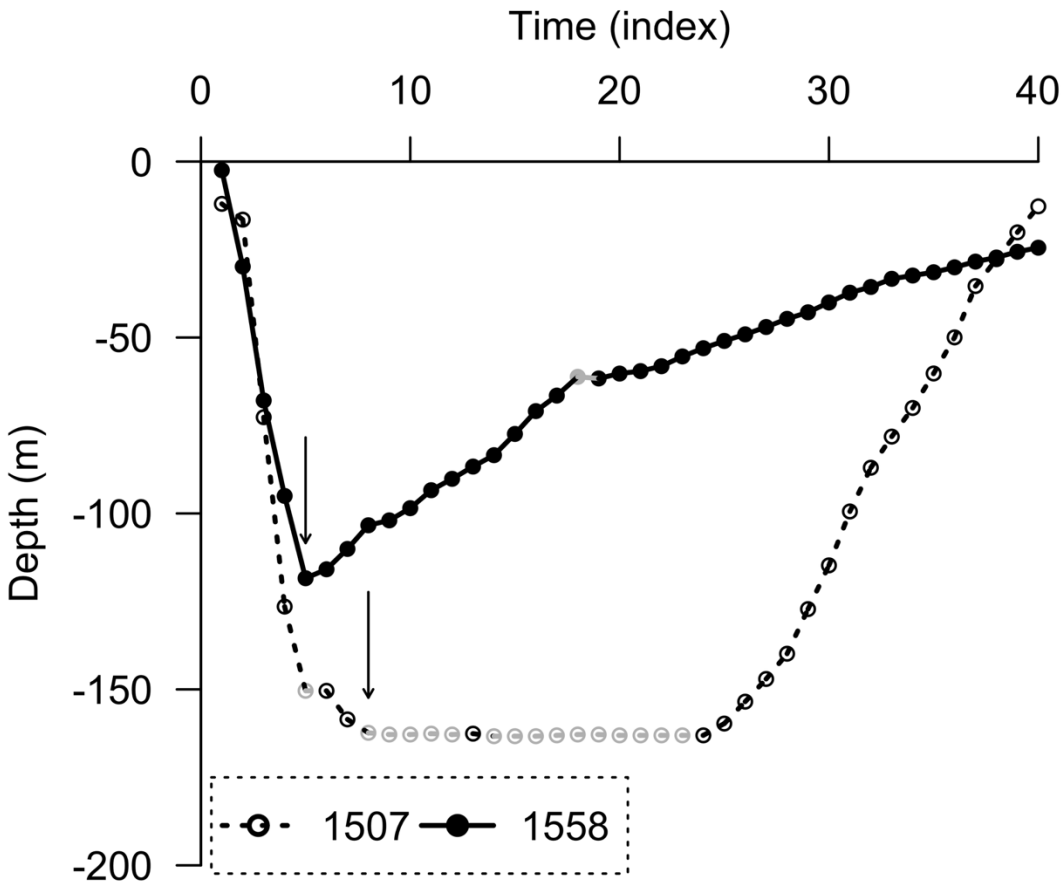

Figure S9. Case-study depth time series used to reconstruct post-release movement paths (analysis A3). The depth time series for individual 1507 following tag deployment off Kerrera on 2016-03-17 14:37:00 is shown by the dotted line and the time series for individual 1558 following tag deployment off Insh on 2016-03-13 14:18:00 is shown by the continuous line. Points mark observations. Grey and black colours distinguish mode 0 and 1 movements (i.e., putative 'resting' and 'non-resting' behaviour), used to influence the movement probabilities, as in Figure S8. Following rapid post-release descents, arrows mark the time step at which each individual was inferred to have returned to the seabed, and thus the 'start' of the time period over which post-release movement paths were reconstructed. Both time series are shown over a period of 40 time steps (80 minutes), during which time both individuals rapidly descended following release and then re-ascended towards the surface, a movement that appears irregular (Chapter Five).

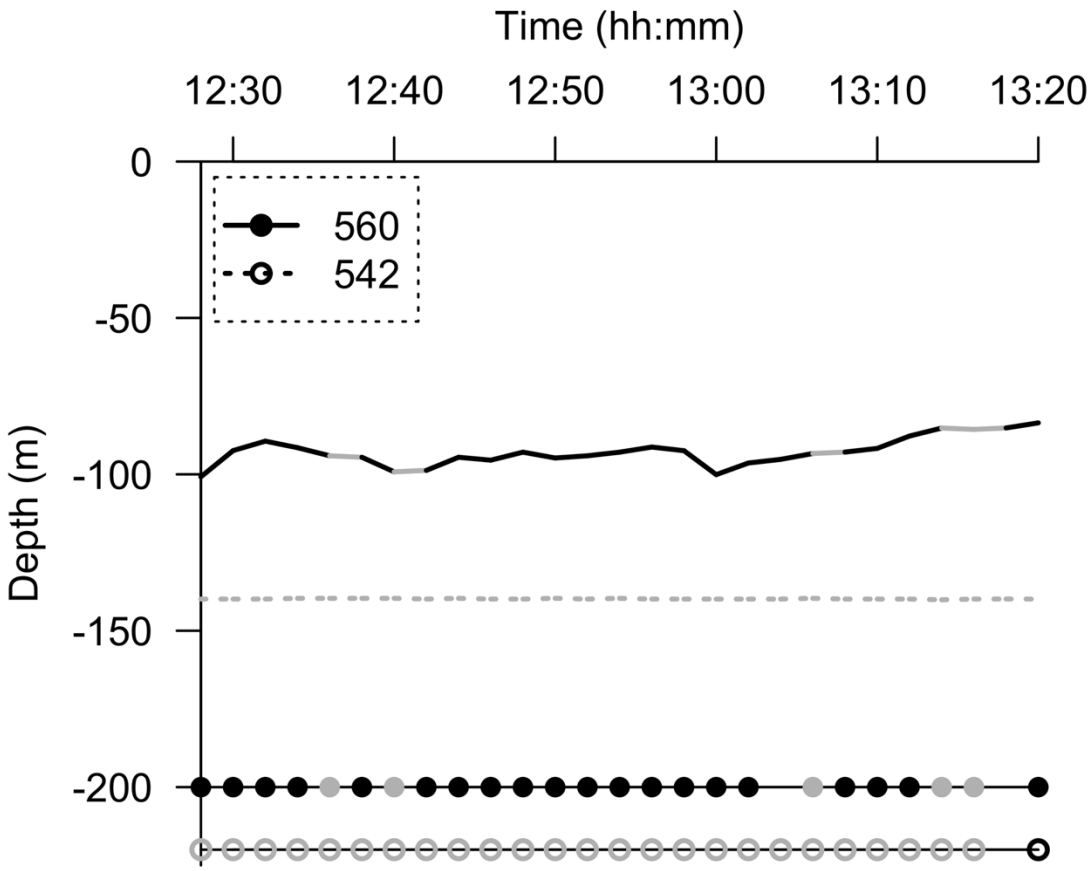

Figure S10. Example cooccurring acoustic and archival time series for a pair of individuals (542 and 560: analysis A4). For each individual, lines show the depth time series and points mark detections. Grey and black colours distinguish mode 0 and 1 movements (i.e., putative 'resting' and 'non-resting' behaviour), used to influence the movement probabilities, as in Figure S8. Note that both acoustic and archival time series are expressed at a resolution of two-minutes, with acoustic time series thinned to exclude any duplicate detections at the same receiver in each two-minute period. Over the 52-minute time period shown (12:28:00–13:20:00 on 2016-05-22), all detections occurred at a single receiver.

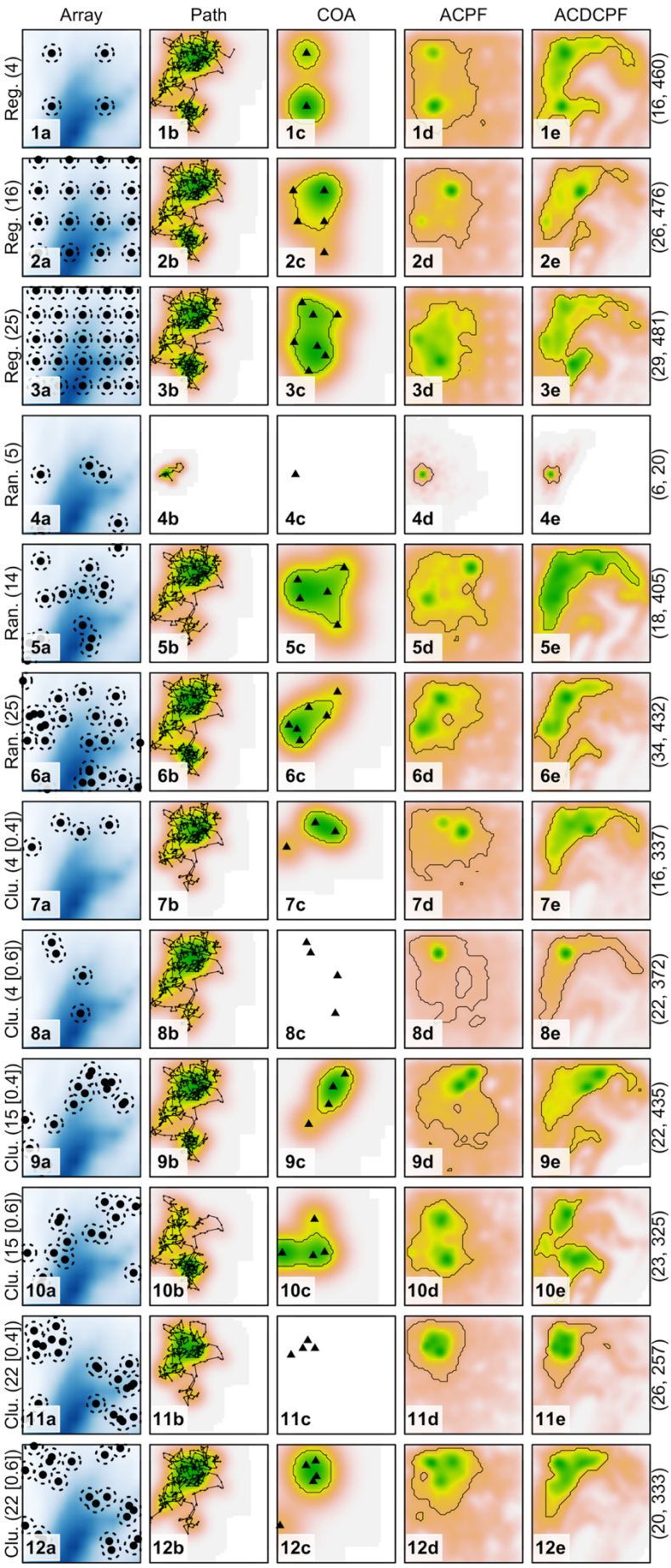
Array
Path
COA
ACPF
ACDCPF
Reg. (4)
1a
1b
1c
1d
1e
(16, 460)
Reg. (16)
2a
2b
2c
2d
2e
(26, 476)
Reg. (25)
3a
3b
3c
3d
3e
(29, 481)
Ran. (5)
4a
4b
4c
4d
4e
(6, 20)
Ran. (14)
5a
5b
5c
5d
5e
(18, 405)
Ran. (25)
6a
6b
6c
6d
6e
(34, 432)
Clu. (4 [0.4])
7a
7b
7c
7d
7e
(16, 337)
Clu. (4 [0.6])
8a
8b
8c
8d
8e
(22, 372)
Clu. (15 [0.4])
9a
9b
9c
9d
9e
(22, 435)
Clu. (15 [0.6])
10a
10b
10c
10d
10e
(23, 325)
Clu. (22 [0.4])
11a
11b
11c
11d
11e
(26, 257)
Clu. (22 [0.6])
12a
12b
12c
12d
12e
(20, 333)

Figure S11. Evaluation of the flapper algorithms for all simulated array designs according to KUDs (simulation S2; overleaf). Following Figure 2, for each row, the array design (Table S2) is shown (a) alongside reconstructed patterns of space use (b–e). The array designs comprise regular, random or clustered receiver arrangements with a small (~5), medium (~15) or large (~25) number of receivers and a low or high degree of clustering ([0.6 or 0.4] if applicable), as denoted on the left-hand-side. The number of acoustic and archival 'observations' for each array is given in brackets on right hand-side. The blue background shows the bathymetry (following Figure 1). For each array, the portion of the simulated path between the first and last detections (b) is shown. KUDs from COAs (in triangles) (c) and the ACPF (d) and ACDCPF (e) algorithms are also shown for simulations that generated sufficient numbers of 'observations', following the colour scheme in Figure 1. Lines mark 50 % contours. Across the simulated array designs, there are clear differences between the mean-position and flapper algorithms:

A. **The mean-position algorithm.** In the higher coverage arrays with regularly arranged receivers (e.g., **3a**), the mean-position algorithm effectively reconstructs the patterns exhibited by the simulated path (**3c** versus **3b**). However, in the lower coverage, clustered arrays (e.g., **10a**), reconstructed patterns do not effectively capture the extent of movements or relative use across the area (**10c** versus **10b**). These patterns reflect the absence of movement from the mean-position algorithm, which is entirely dependent on detections at receivers.

B. **The ACPF algorithm.** The ACPF algorithm also tends to perform more effectively in higher coverage arrays with regularly arranged receivers than lower coverage, clustered arrays (e.g., **3d** versus **10d**). In high coverage arrays, the incorporation of movement can lead to more diffuse patterns of space use that resemble the specific simulated path less effectively than those from the mean-position algorithm (e.g., **3d** versus **3c**). However, they are more useful for prediction on account of the bias–variance trade off (see (3)). In lower coverage arrays, as for the mean-position algorithm, 'hotspots' tend to emerge around receivers. These 'hotspots' result from the concentrating effect of detections on location probabilities, while in the gaps between detections location probabilities spread out thinly across a wider area and carry less weight. (This effect is even more apparent in AC-branch algorithms, as shown in Figure 3D–E.) However, the possibility for movement away from these areas in the gaps between detections can result in maps that encapsulate the distribution spanned by the simulated path more effectively than those from the mean-position algorithm (e.g., **10d** versus **10c**) and which can be used to quantify residency in an area, despite detection gaps.

C. **The ACDCPF algorithm.** The ACDCPF algorithm produces more refined maps that are less influenced by array design as a result of the restrictions posed by the depth-error model (e.g., **3e** versus **3d**). However, in simulation–model comparisons, in arrays with gaps (as shown here), the incorporation of depth observations in the ACDCPF algorithm can lead to the emergence of 'hotpots' that are not exhibited by simulated paths but which are consistent with observations, as apparent in the north east of the simulated area in most ACDCPF maps. While this complicates the interpretation of simulation–model comparisons—because differences between simulated and reconstructed patterns do not necessarily indicate poor performance and are in fact expected—in real-world settings this feature of the ACDCPF algorithm is highly desirable because locations that *could* have been used by a selected individual, given the data, may be as important to other individuals as the locations that *were* used by the selected individual. In other words, by reconstructing the distribution of possible movements, the flapper algorithms are expected to have higher predictive power than an algorithm that could accurately recapitulate the one true movement path (the bias–variance trade-off).

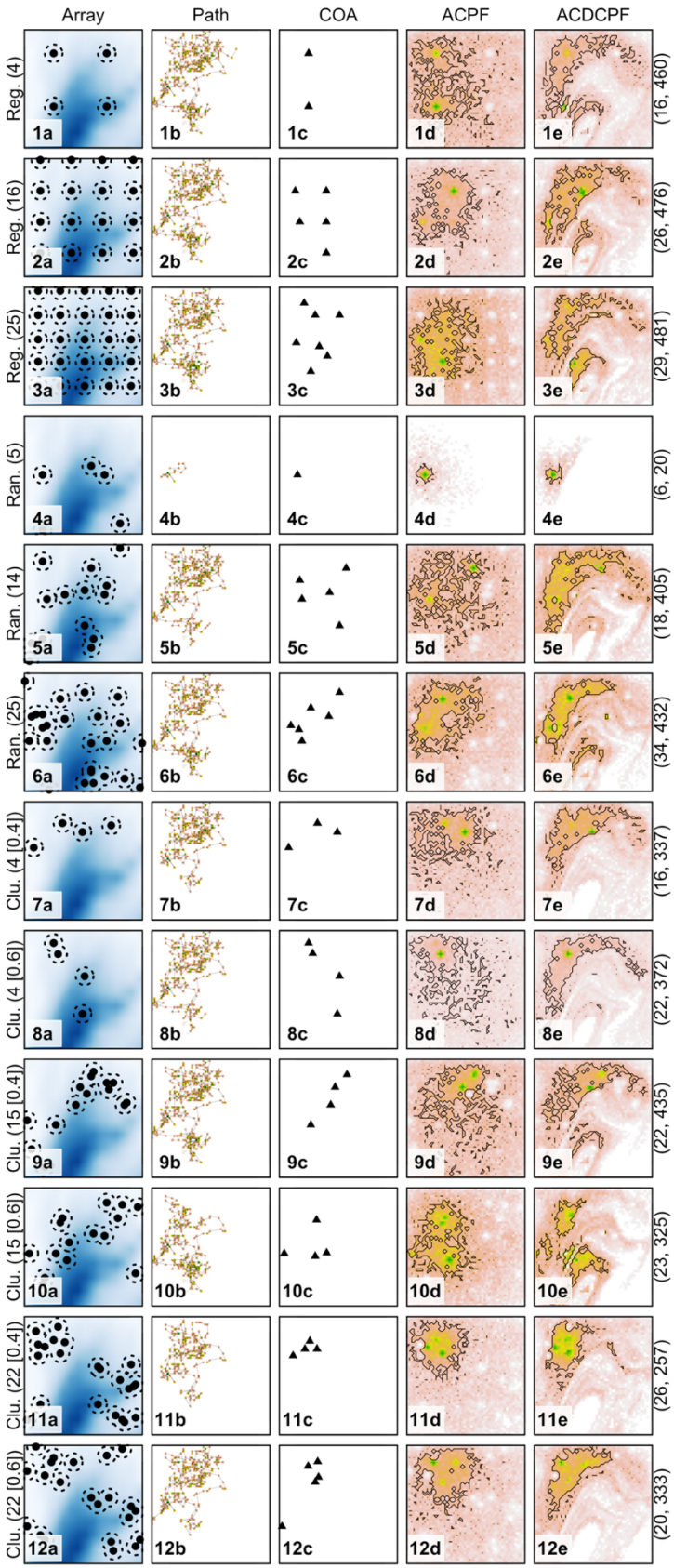

Figure S12. Evaluation of the flapper algorithms for all simulated array designs according to POU maps (simulation S2). Following Figure 2 and S11 for each row, the array design (Table S2) is shown (a) alongside reconstructed patterns of space use (b–e). For each array, the portion of the simulated path between the first and last detections (b) and the associated POU scores are shown. Compared to KUDs (Figure S11), POU maps are more pixelated but they can provide a more refined picture of uncertainty and the influence of array design on reconstructed patterns (see Figures S11 and S13).

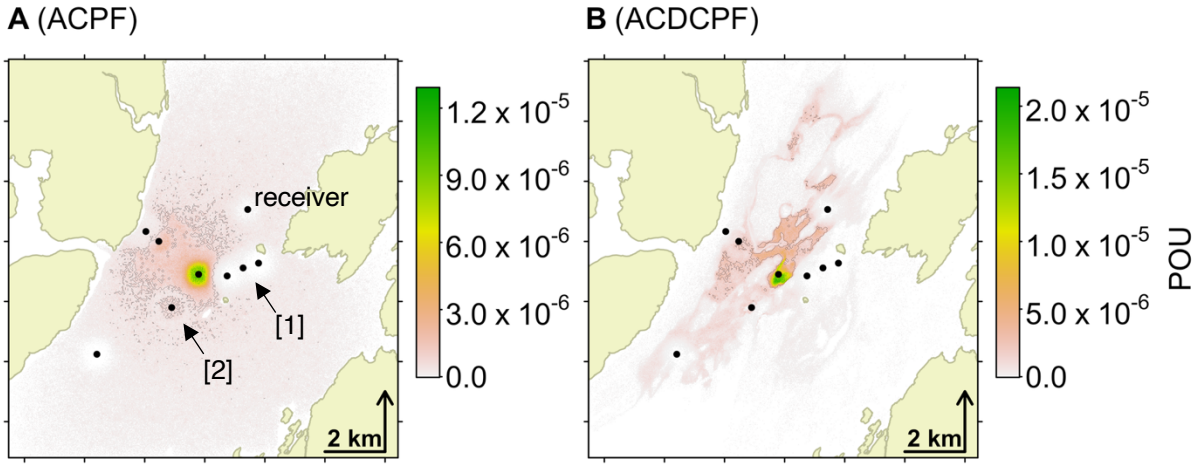

Figure S13. POU maps from the (A) ACPF and (B) ACDCPF algorithms for the selected individual (540) over a one-month period (analysis A2). The POU maps are similar to the KUD maps presented earlier (Figure 3C–D), but faster to estimate (see Table S6) and more refined. As a result, they provide opportunities to examine patterns in more detail and check for artefacts of the array design and/or model parameters in reconstructed patterns. In **A**, two such artefacts are visible. [1] One artefact of the array design is the contrast between areas around the receivers that recorded few detections, where there is a dearth of particle samples, and the surrounding areas. This pattern emerges from the simple fact that movements close to receivers that recorded few detections must have been rare (given the absence of detections), while movements further afield (in areas in which detection probability is low) must have been more common. In these surrounding areas between receivers, particles spread out more freely because there is little information to restrict uncertainty beyond detection containers. Thus, while the ACPF algorithm can be less sensitive to receiver locations than the mean-position algorithm, the influence of receivers on uncertainty is still inevitably realised in maps of space use in arrays with substantial detection and receiver gaps (see also Figures S11–12, Table S3). [2] A second pattern that emerges from the combined influence of the array design and the specific model parameters that underpin map **A** is the presence of a circular band around particular receivers, approximately 500 m from their locations, with a dearth of particle samples. This pattern emerges around isolated receivers from the antagonistic influence of detection probability when the individual was versus was not detected and the movement model, which permits the individual to 'step' from areas close to a receiver, when it is detected, to near the edge of the receiver's detection container, when it is not detected. This is an example of a situation where smoothing or additional data can be useful. In **B**, the integration of depth observations prevents the emergence of these patterns by restricting particle sampling to specific areas that meet the constraints of the depth-error model. For both panels, area coordinates are shown in Figure S7. Coastline data were sourced from Digimap. Digimap data © Crown copyright and database rights [2019] Ordnance Survey (100025252).

Chapter Seven

Discussion

Abstract

1. Over the last two decades, elasmobranchs have come to be recognised as one of the most threatened vertebrate taxa. During this time, research on the movement ecology of sharks has burgeoned, yet studies on skate (Rajidae) have remained comparatively sparse.
2. In Scotland, recent research on the movements of flapper skate (*Dipturus intermedius*) in relation to the Loch Sunart to the Sound of Jura Marine Protected Area (MPA), as laid out in this thesis, has developed our understanding of flapper skate movement, the evidence base required to support conservation and the suite of modelling techniques available to the movement ecology community. Following this progress, a review of recent developments, knowledge gaps and future priorities for research on flapper skate and within the field of movement ecology more broadly is a timely way to close this thesis.
3. This chapter reviews progress in our understanding of the movement ecology of flapper skate, its conservation implications and the wider significance of methodological modelling developments inspired by this research. Knowledge gaps in flapper skate ecology and conservation, both within the MPA and the wider conservation context in Scotland, are identified to guide future research. Within the field of movement ecology as a whole, opportunities for continued development of modelling techniques motivated by recent research and the wider lessons of this work are highlighted.
4. Key findings include the prevalence of residential behaviour in flapper skate, depth-specific periodic behaviours, behavioural resilience following angling and the benefits of new modelling techniques, especially a semi-stochastic modelling framework for passive acoustic telemetry data. Important avenues for future research include the ecological drivers of movement, the implications of movement for population recovery within MPAs and the contribution MPAs can make to skate conservation more broadly.

5. This discussion demonstrates the substantial contributions that studies of animal movement can make to ecology and conservation, both through the generation of species-specific insights and the stimulation of widely applicable methodological advances.

Keywords
conservation, ecology, elasmobranch, marine protected area, modelling, movement

1. Introduction

The pressures on Earth's ecosystems have increased dramatically in recent decades (Díaz et al., 2019). In marine environments, overfishing, destructive fishing practices and other anthropogenic stressors have decimated populations of marine species (Jackson et al., 2001; Halpern et al., 2008). Large, mobile species have experienced the greatest declines and their loss from marine food webs is associated with a pervasive pattern of trophic downgrading (Estes et al., 2011; McCauley et al., 2015). Elasmobranchs have been impacted particularly heavily, becoming one of the most threatened vertebrate taxa (Dulvy et al., 2014; Pacoureau et al., 2021). Only one third of elasmobranch species are considered 'safe' and one quarter are threatened with extinction (Dulvy et al., 2014). As a result, there is a pressing need to understand the exposure of these species to stressors and develop conservation solutions.

For mobile species, movement is a key influence on exposure to stressors and the efficacy of conservation measures (Fraser et al., 2018; Hays et al., 2019). In recent decades, research on the movement ecology of elasmobranchs has grown markedly, but most studies have focused on the movements of sharks, while batoids, especially skate (Rajidae), remain comparatively understudied (Papastamatiou and Lowe, 2012; Flowers et al., 2016; Siskey et al., 2019). Against this backdrop, the Critically Endangered flapper skate (*Dipturus intermedius*) has emerged in recent years as focus for research in association with the Movement Ecology of Flapper Skate (MEFS) project (Chapters Two–Six; Thorburn et al., 2021). Building on earlier work (Little, 1995, 1997; Wearmouth and Sims, 2009; Pinto and Spezia, 2016; Pinto et al., 2016), this project aimed to investigate the movements of flapper skate in relation to the Loch Sunart to the Sound of Jura Marine Protected Area (LStSJ MPA) in Scotland (Chapter One). As part of the project, a passive acoustic telemetry array was deployed within the MPA and skate were tagged with acoustic and archival tags between 2016–17 to study movement (Chapters One–Two).

The acoustic and archival data collected between 2016–17 established the basis for this thesis on flapper skate movement and conservation. Previous chapters investigated the spatiotemporal scale of movement and time spent within MPA boundaries (Chapter Three), depth-specific periodic behaviour (Chapter Four), responses to disturbance (Chapter Five), fine-scale movements over the seabed and emergent patterns of space use (Chapter Six). At the same time, this work highlighted convenient modelling workflows (Chapter One), brought underutilised modelling techniques to the attention of the movement ecology community (Chapters Four and Five) and inspired research into new modelling techniques (Chapters Two and Six). Following this progress, there is a need to consolidate recent insights, identify remaining knowledge gaps and prioritise future actions.

The aim of this final chapter is to review recent research on the movement ecology of flapper skate and point the way for future work. The key findings of previous chapters are reviewed from the perspectives of ecology, conservation and modelling. The significance of this work for flapper skate and for the field of movement ecology more broadly is discussed. Remaining knowledge gaps are identified and evaluated to establish priorities for future research, and the wider lessons of this work are considered.

2. Recent developments

2.1. Developments for ecology

The first important development in this thesis is an improved understanding of the spatial scale of flapper skate movements with respect to the LStSJ MPA. Building on early work indicating site affinity to the region (Little, 1995, 1997; Wearmouth and Sims, 2009; Neat et al., 2015), the study of the MEFS passive acoustic telemetry array estimated that 24–52 % of individuals may be resident in the study site over monthly and seasonal timescales (Chapter Three). During this time, phases of regular detections at a subset of receivers termed the ‘southern receiver array’ indicated periods of highly localised movements across an area less than 15 km^2, though there was no evidence for close-knit associations among individuals in this area (Chapters Three and Six). This result is the first step in understanding flapper skate resource requirements and the carrying capacity of the MPA. The prevalence of localised movements adds to the emerging evidence that rajids may exhibit prolonged periods of residency (Hunter et al., 2005b;

Morel et al., 2013; Sousa et al., 2019), as documented in other elasmobranch groups, such as tropical coral reef-associated sharks (Chapman et al., 2015; Flowers et al., 2016).

Although the drivers of localised movement remain unclear, local conditions are likely to influence the scale of residency in line with resource requirements and habitat preferences (Schlaff et al., 2014). Within the LStSJ MPA, it is clear that resource availability is sufficiently high to meet the requirements of resident flapper skate. In concordance with diet studies on common skate (*D. batis*) (Steven, 1947; Wheeler, 1969) and common blue skate (*D. batis*) (Brown-Vuillemin et al., 2020) and variation in vertical movements (Chapter Four), preliminary analyses of putative sediment preferences indicate the exploitation of a variety of sediments, which are likely to support different prey (Chapter Six). For example, Norway lobster (*Nephrops norvegicus*), which skate in the MPA are known to consume (Thorburn et al., 2021), are generally associated with muddy sediments (Johnson et al., 2013) whereas sandeels (*Ammodytes spp.*) prefer gravelly sand (Wright et al., 2000). In places such as the MPA where a variety of prey are found in a relatively small area (741 km^2), the flexibility of skate to exploit different prey may contribute towards localised movements. A preference for deeper water and the avoidance of shallow, inshore areas adjacent to freshwater sources (i.e., habitat restriction) may also contribute towards the localised scale of residency in this area (Chapter Three).

More broadly, it may be significant that among other temperate elasmobranchs residency is more commonly associated with deep-water species (Chapman et al., 2015). This pattern suggests an influence of environmental stability on movement and community structure, in line with research in other systems (Riotte-Lambert and Matthiopoulos, 2020). In the literature on animal migration, it is widely recognised that the balance between the costs and benefits of movement is influenced by environmental conditions (Fudickar et al., 2021). The potential costs of movement can be substantial and in stable environments with adequate food supply and/or few higher predators, there may be few reasons to leave an area. Meanwhile, in seasonally fluctuating environments, long-range movements can facilitate the exploitation of short windows of opportunity for key life-history events, such as breeding, despite unfavourable conditions at other times of year (Fudickar et al., 2021). However, notwithstanding the intuitive appeal of this explanation, evidence for seasonal movements in both deep-sea and tropical terrestrial environments cautions against premature

characterisations of environmental stability and its effects on movement (Jahn et al., 2020; Milligan et al., 2020).

For flapper skate, a competing explanation for residency within the LStSJ MPA is the influence of historical and contemporary fishing pressure. While flapper skate were fished to near extinction beyond the boundaries of the (now) MPA, the rugged bathymetry of this region is likely to have limited the exposure of skate in this area to fisheries (Neat et al., 2015). In the intervening years, the prevalence of residency may have increased as a result of experience or strong selection for residential behaviour (Parsons et al., 2010). Given the importance of connectivity for population ecology (Drake et al., 2021), the role of these factors on movement in skate deserves further attention.

While residential behaviour is a common feature of studied flapper skate, the evidence for variability in movement patterns among individuals has also been strengthened by this thesis (Chapters Three–Five). Analyses of detection and archival time series indicated site fidelity and transiency (with respect to receivers), with seasonal and more irregular gaps in detections as well as movements into water depths that exceed those found in the MPA (Chapter Three). A considerable difference in detection patterns of males versus females indicates that sex is an important driver of this variation, with males spending less time around receivers on average. This pattern fits with the historical view that males migrate offshore over the summer months while at least some females remain in inshore areas (Little, 1997; Neat et al., 2015). Genetic studies have shown that male-biased dispersal is relatively common in elasmobranchs and explanations for this bias are often linked to competitive ability and reproductive requirements (including the need to avoid inbreeding) (Phillips et al., 2021b), but their applicability to flapper skate remains unknown. There also remains substantial inter-individual variability in movement patterns, with some males exhibiting longer periods of residency around receivers than others and some females spending rather less time around receivers. These kinds of individual differences are widely documented and there is no shortage of proposed explanations (Shaw, 2020). In the literature on partial migration, for instance, variation in individuals' physiological tolerances to environmental variation, competitive ability, predation vulnerability and trophic ecology have all been proposed as causes of differences in migratory strategies (Chapman et al., 2011, 2012). A challenge for future research is to move beyond descriptive studies and hypothesis development towards explanatory studies and hypothesis

testing (Papastamatiou and Lowe, 2012), as illustrated by recent work (Andrzejaczek et al., 2019; Lawson et al., 2019).

For benthic species, patterns of space use emerge from movement over the seabed (Chapter Fours and Six). Work on the vertical movements of flapper skate has revealed periods of low and high vertical activity, depth-specific periodic behaviours and cyclical trends that may help to explain localised movements and individuals' activities within exploited areas (Chapter Four). Switches between periods of low and high vertical activity over daily and monthly timescales point towards behavioural changes that are probably tied to activities such as foraging. For example, low vertical activity may reflect ambush predation, resting following recent activity or recovery following disturbance (Chapters Four and Five). These activities may contribute towards localised patterns of space use. Meanwhile, high vertical activity may reflect more active behaviours, including the pursuit of demersal or pelagic prey (such as teleosts) that have been identified in the diets of multiple skate species (Orlov, 2003; Treloar et al., 2007; Brown-Vuillemin et al., 2020). In some individuals, periods of low and high vertical activity are connected by movements to and from a central depth that suggest central foraging or refuging behaviour (Humphries et al., 2017; Papastamatiou et al., 2018b). This possibility implies a spatiotemporal separation in the areas that are preferentially exploited for activities characterised by low vertical activity (such as resting, digestion or ambush predation) versus those characterised by higher vertical activity (such as active foraging), with individuals choosing to return to the same place between excursions. This may signify the presence of a cognitive map (Powell and Mitchell, 2012), competition or territorial behaviour (Papastamatiou et al., 2018a). While such links remain speculative, these results develop the evidence base that benthic species switch between low and high vertical activity levels and that behavioural switches may underlie variation in patterns of space use (Kawabe et al., 2004; Wearmouth and Sims, 2009; Humphries et al., 2017).

For flapper skate, there is also evidence for diel and seasonal cycles in vertical movement, with individuals typically remaining in deeper water for longer during the day in summer while undergoing more extensive and frequent diel vertical migrations (DVMs) in winter (Chapter Four). These cycles are likely tied to foraging through temporal changes in prey availability and the efficacy of different foraging approaches, as well as environmental conditions such as light levels (Schlaff et al., 2014). Despite uncertainty in the mechanistic drivers of these patterns, the prevalence of cyclical trends in vertical movements of flapper skate strengthens

the evidence that environmental cycles are associated with the movements of both pelagic and benthic species, building the platform for further work in this area (Wearmouth and Sims, 2009; Peklova et al., 2014; Humphries et al., 2017).

Beyond developing our understanding of the movements of individuals at liberty, this thesis has also shed light on behavioural responses to disturbance—namely, catch-and-release angling (Chapter Five). Analyses of movement time series showed that most skate initially respond to this disturbance by progressively descending into deeper water habitats, after which a period of low vertical activity is exhibited, in line with the hypothesis that these environments may be preferred areas for resting, recovery or prey (bait) digestion. However, among studied individuals this 'recovery' phase was relatively short-lived and generally followed by elevated vertical activity in the 12 hours following release. Evidence for irregular post-release behaviour was also documented in three individuals (14 %) in the form of rapid re-ascents towards the surface (Chapter Five). Subsequent reconstruction of post-release movements for two of these individuals with sufficient data showed that they were consistent with benthic behaviour—despite the rate of ascent—but their causes remain uncertain (Chapter Six). Following on from research on the vertical movements of skate (Chapter Four), disturbance by high light levels near the surface is one explanation for these patterns, but physiological disturbance and/or perturbed buoyancy are also possibilities (Chapter Five). Few studies are available on elasmobranchs with which to contextualise these results, but it is worth noting that similar patterns, including reduced activity, elevated activity and, in one case, re-ascent towards the surface following capture in commercial gear, have been documented (Hoolihan et al., 2011; Rodríguez-Cabello and Sánchez, 2017).

2.2. Developments for conservation

From a conservation perspective, the key finding of this thesis is the prevalence and scale of residency within the LStSJ MPA (Chapters Three and Six). Residency was documented in both immature and mature males and females and shown to extend from periods of several months to more than 15 months (Chapters Three and Six). Over longer time scales, the evidence for multi-annual site fidelity has also been strengthened (Chapter Three). These developments corroborate the case that LStSJ MPA is likely to confer repeated benefits to flapper skate over monthly and seasonal time scales year after year. Beyond the LStSJ MPA, this information will support the design and management of future MPAs. For example, the highly localised

movement patterns of some individuals suggest that even smaller MPAs could confer benefits to flapper skate. However, larger MPAs would be expected to cover a larger proportion of skate movements over longer timescales. Taken together with results from other skate species, this work suggests that studies on the movements of other rajids in relation to potential MPAs would be worthwhile (Hunter et al., 2005b; Morel et al., 2013; Sousa et al., 2019; Simpson et al., 2020).

Another important finding for conservation is that the vertical movements of tagged skate span the entire depth range of the MPA (Chapters Three and Four). Within this range, evidence for the importance of deep-water channels throughout the MPA has been strengthened, corroborating the conclusions of previous research conducted in the south of the MPA (Neat et al., 2015). Particularly in summer, tagged skate spent large amounts of time in deep-water channels, perhaps because they provide sheltered environments in which to rest, suitable foraging grounds or refugia from unfavourable surface conditions, such as high light levels (Chapter Four). These results are consistent with predictions from species distribution modelling (Pinto et al., 2016) and suggest that current management measures in the MPA, which protect the entire depth range, are appropriate (Thorburn et al., 2021). In the same way, future MPAs should cover a wide depth range, including areas of both shallow (< 50 m) and deep (> 200 m) water (Thorburn et al., 2021).

The vertical movements of skate have implications for their vulnerability as bycatch (Chapter Four). Work on other elasmobranchs has shown that vertical movements affect both exposure to fisheries (Bizzarro et al., 2014) and catchability (Bayse et al., 2016). Flapper skate are potentially exposed to fisheries across a depth range from the surface to at least 312 m, according to the work in this thesis on skate off the west coast of Scotland (Chapter Four), and up to 1,500 m according to a species-wide review (Ellis et al., 2021). However, the exposure and catchability of skate are likely to vary through time. Research on the use of tickler chains, which are deployed in front of trawls to startle resting fish into the net, has shown that their removal can substantially reduce skate bycatch (Kynoch et al., 2015). The efficacy of this measure is likely to depend on skate activity levels, being more effective when skate are resting on the seabed and less effective when they are more active, especially if they move into the water column to pursue prey, as suggested by dietary studies of large skate of other species (Orlov, 2003; Treloar et al., 2007; Brown-Vuillemin et al., 2020).

Alongside commercial fisheries, skate are exposed to recreational angling both within and beyond the LStSJ MPA (Chapter Five). The benefits of this practice for scientific research and conservation are clear but until recently its impacts on skate remained unstudied (Chapter Five). In line with current management, this thesis supports the hypothesis that skate are generally behaviourally resilient to catch-and-release angling: while skate appear to require a period of recovery following angling and exhibit elevated vertical activity thereafter, these changes are relatively short-lived. However, evidence for irregular post-release behaviour in three individuals suggests that catch-and-release angling may appreciably perturb individuals in some circumstances, and the physiological resilience of skate remains unknown (see §3.1–2). Taken together with research on other elasmobranchs (Gallagher et al., 2017), there is a clear need for further work on the impacts of this practice (see §3.2).

2.3. Developments for modelling

Recent developments have been supported by progress in data storage, processing and modelling. An important output from this thesis is the establishment of clear data processing protocols and quality-controlled datasets, which ensure that the movement data collected from flapper skate can continue to support research in years to come (Chapter Two). The publication of four widely applicable R packages (‘prettyGraphics’, ‘fvcom.tbx’, ‘Tools4ETS’ and ‘flapper’) for data processing and analysis, whose development was motivated by these data, should support this research (Chapter Two).

Newly developed methods provide expanded opportunities to exploit underutilised values of electronic tagging and tracking data. The development of a method for integrating acoustic and archival datasets from benthic species for the validation of hydrodynamic models is a notable step forward, not only because this extends the range of ‘animal oceanographers’ in aquatic environments but also because improved validation of hydrodynamic models can support movement ecology research (Harcourt et al., 2019). In the work reported here, this is apparent through analyses of the links between temperature and movement (Chapters Two and Three) but accurate hydrodynamic models also support many areas of related research, from particle tracking (Swearer et al., 2019) to geolocation (Braun et al., 2018).

This thesis has also highlighted the use of underutilised movement modelling techniques, alongside more widely used methods, in movement ecology research. Research on vertical

movement illustrated the combined use of generalised additive models (GAMs) and posterior simulation as a simple, effective and widely applicable modelling approach that recognises the importance of both individual- and group-level variation (Chapter Four). The same work brought functional data analysis (especially functional principal components analysis or FPCA) to the attention of movement researchers as an underutilised but powerful approach for examining structure and revealing clusters in time series data (Ullah and Finch, 2013; Wang et al., 2016). Importantly, in contrast to other clustering algorithms, such as k-means clustering (Gleiss et al., 2017), FPCA does not require an *a priori* definition of the number of clusters. In addition, FPCA provides a straightforward and widely applicable method for analysing the effects of disturbance (Chapter Five). This should support more refined consideration of the effects of capture and tagging throughout the field of movement ecology.

The most significant modelling developments in research inspired by flapper skate have been in the field of passive acoustic telemetry (Chapter Six). Simple detection indices are useful descriptors of the time spent around receivers, particularly when supported with modelling, but they provide very limited information on movement away from receivers (Chapter Three). Inferences from more sophisticated approaches, including the mean-position algorithm (Simpfendorfer et al., 2002), network analysis (Lea et al., 2016) and latent variable models (Pedersen and Weng, 2013; Winton et al., 2018; Hostetter and Royle, 2020), are typically constrained around receivers in the same way (Chapter Six). However, the earlier work in this thesis motivated the development of a comprehensive movement modelling framework that recapitulates the processes that give rise to detections to reconstruct movement paths and emergent patterns of space use, both during periods of detection and in the gaps between detections. Key attributes of this framework include the effective representation of array design, the exploitation of detections and detection gaps, the representation of movement and improved routines for integrating topography into analyses. The framework also has the flexibility to integrate discrete detections with other movement datasets and is supported by new modelling methods for archival time series. These developments provide exciting opportunities to reconstruct fine-scale movements and emergent patterns of space use, quantify residency, support analyses of habitat preferences and guide tagging and array deployment programmes in a wide range of settings (Chapter Six).

3. Future directions

3.1. Ecological research

Alongside new insights into skate ecology, conservation and movement modelling, this thesis has highlighted a number of knowledge gaps in each of these areas that would benefit from further research. From an ecological perspective, a key area of uncertainty remains regarding the spatiotemporal scales of movement in flapper skate and especially the extent to which tagged individuals remained resident in the MPA through detection gaps. This is a common area of uncertainty in passive acoustic telemetry studies that challenges inferences of the spatial scale of movements, since 'out-of-range' residency in a study site versus 'out-of-area' movements (e.g. dispersal) can produce the same detection patterns (CHapter Three; Bond et al., 2012; Kessel et al., 2014; Williamson et al., 2021). The expanded application of new methods for reconstructing movements will go some way to addressing this knowledge gap, especially for individuals for which detections were recorded relatively regularly (Chapter Six). For flapper skate, this would be supported by analyses of detection probability data collected by the MEFS project from sentinel tags. For individuals with sparser detection histories, refined latent variable models should facilitate the reconstruction of movement tracks over wider areas (Pinto et al., 2016). Continued recovery of archival tags deployed by the MEFS project will support these objectives, especially for males for which passive acoustic telemetry detections are sparser (Chapter Three). Together, these modelling approaches should provide a means to quantify the spatiotemporal scales of movement in flapper skate and the strategies exhibited by different individuals. Critically, this research can be conducted using data already collected by the MEFS project, though higher resolution information on activity levels and movement speeds would greatly support the reconstruction of movement paths (Chapter Six).

Developing our understanding of the drivers of movement, the ways in which movement is shaped by conditions across multiple spatiotemporal scales and the influence of these factors on the repeatability of movement patterns is more challenging (Papastamatiou and Lowe, 2012). This thesis has suggested potential roles for individual characteristics (such as sex), environmental conditions (including depth, salinity and light levels), ecological interactions (such as foraging) and anthropogenic activity (such as fishing) but links remain speculative. Improved understanding of skate biology (especially reproduction and foraging ecology) alongside continued monitoring is likely to be key to unlocking these knowledge gaps.

Historical captures of mating pairs of individuals in spring suggest that mating may be seasonal (Day, 1884), but timing, locations and individual interactions remain unclear (Chapter Three). This uncertainty limits understanding of the role of reproduction as a driver of movement and the interpretation of patterns, such co-occurring detections, that may be attributable to mating (Chapter Three). However, hormonal analyses of blood samples and ultrasound images of females collected through tagging programmes have the potential to refine our understanding of the timing and regularity of reproduction, which could unlock hidden patterns in movement time series. Recent evidence of egg-laying grounds off Skye and genetic samples from the area (NatureScot, 2021), limited evidence off Orkney (Phillips et al., 2021a) and further prospecting around Scotland also have the potential to clarify the movements of females in relation to reproduction and the implications of these movements for population connectivity.

Alongside reproduction, foraging is likely to be key to understanding the movements of flapper skate. Diet, foraging modes (such as ambush versus active hunting) and spatiotemporal changes in feeding activity (such as nocturnal foraging) may contribute towards residency (Chapter Three), influence vertical movements (Chapter Four) and shape responses to disturbance (Chapter Five). Foraging is also likely to influence interactions with fisheries and affect conservation (see §3.2). Information on foraging ecology is difficult to collect but there are four immediately feasible possibilities to develop previous analyses with respect to foraging behaviour and to capitalise upon existing infrastructure to collect new data. First, it would be instructive to extend preliminary analyses of sediment use to examine evidence for preferences and differences over time, space and among individuals (Chapter Six). Second, high-resolution depth time series and reconstructed paths could be analysed using behavioural modelling techniques, such as Markov switching autoregressive models, and in relation to theoretical optimal foraging models to identify periods of possible foraging (Sims et al., 2008; Pinto and Spezia, 2016). For example, theory predicts that predators with limited knowledge of prey distribution should exhibit Lévy walk-like movements to maximise prey-encounter rates and empirical studies have shown that these movements are widely exhibited by marine predators (Sims et al., 2008; Reynolds, 2018), although results are debated (Pyke, 2015; Patterson et al., 2016). Third, there are significant opportunities to collect diet data from recreational angling. Flapper skate caught from charter vessels sometimes regurgitate prey upon capture and this information could be collected through citizen-science projects using mobile phone applications of the kind currently in development for skate and in other systems (Merrifield et al., 2019). Fourth, opportunities to sample flapper skate captured on scientific surveys, such as

the Scottish West Coast and Irish Groundfish Surveys (Stokes et al., 2014), should be exploited. Tissue samples, gastric lavage, DNA analysis of faecal matter and stomach contents, and dissection of dead specimens could be used to study diets, as in other elasmobranchs (Barnett et al., 2010; Shiffman et al., 2012).

While existing options to improve our understanding of flapper skate foraging ecology should be explored, it would be beneficial to extend this research with targeted surveys and tagging. Expanding benthic habitat maps across the whole LStSJ MPA would support analyses of sediment preferences (Chapter Six; Boswarva et al., 2018) and habitat conservation (see §3.2). Benthic sampling of sediments (from photography, grabs or cores) and prey surveys in areas in which flapper skate are known to occur would help to ground-truth relationships between sediments and prey and enable analyses of spatiotemporal variation in prey availability. Further capture and tagging programmes would support this research, providing a platform to collect dietary data and to test hypotheses of the links between movements (such as DVM) and foraging, alongside tag deployment. Sonar tags provide direct information on predation (Lawson et al., 2015), but remain to be tested on skate. Even limited tag deployments may reveal foraging patterns that unlock information in existing datasets. For example, once signatures of foraging can be identified, their manifestations in existing data could be used to reconstruct time spent foraging and support the quantification of energy budgets.

Understanding the ways in which skate respond to disturbances, such as catch-and-release angling, also requires further research (Chapter Five). Key ecological knowledge gaps remain regarding the influence of environmental conditions on capture responses, the physiological changes that skate experience during capture and their role in explaining post-release movements. Studies on other elasmobranchs have shown that physiological changes, such as elevated lactate levels, can take from less than three hours to more than 12 hours to return to baseline levels following exhaustive exercise (Skomal, 2007). This kind of physiological research on flapper skate would provide a means to measure the extent to which individuals are stressed by capture and predict the implications of physiological recovery for movement, for instance through the ‘recovery’ period commonly exhibited following release. The collection of *in situ* environmental data and the deployment of accelerometers, which provide more detailed information on movement, would support this research (Whitney et al., 2016) as well as management (see §3.2).

An important knowledge gap with repercussions for the interpretation of flapper skate movements across the board concerns the extent to which flapper skate are truly benthic animals or exhibit periods of pelagic behaviour. While the weight of evidence from morphology, diet and fisheries strongly supports the assertion that flapper skate are predominately benthic (Wearmouth and Sims, 2009), the presence of demersal and pelagic teleosts in the stomachs of other skate, including large common blue skate (Brown-Vuillemin et al., 2020), indicates the potential for demersal and pelagic movements. This knowledge gap has significant ramifications for flapper skate movement ecology and management, underpinning the links between horizontal and vertical movement, the ways in which movement is shaped by the local environment, the role of environmental conditions, the interpretation of diet data and interactions with fisheries (see §3.2). Hence, a key objective for future ecological research should be to quantify the movements of flapper skate in relation to the seabed via the deployment of accelerometers and sonar tags (Chapter Four).

Another issue that surrounds this discussion is the extent to which the skate analysed in this thesis are representative of skate more broadly in the LStSJ MPA and beyond. The lack of data on small (< 1 m long) skate is a major knowledge gap. In flapper skate and other elasmobranchs, there is evidence for ontogenetic shifts in movement patterns, often in relation to foraging and predation risk (Grubbs, 2010; Thorburn et al., 2021). Studies on common blue skate and other species have indicated ontogenetic shifts in diets, with small, benthic invertebrates typically predominating in the stomachs of small skate while teleosts become increasingly prevalent in the stomachs of larger skate (Orlov, 2003; Treloar et al., 2007; Brown-Vuillemin et al., 2020). These differences in diet imply that movement patterns in larger skate may not be representative of those exhibited by smaller skate. Among the skate studied in this thesis, there are potential biases associated with capture technique too. For example, the use of baited lines may promote the capture of hungrier individuals that are poorer foragers. Studies on fish and seabirds have also highlighted animal personality as a driver of catchability, dispersal and migration (Mittelbach et al., 2014; Patrick and Weimerskirch, 2014). These links can be reversed, with capture inducing personality changes that have subsequent repercussions for movement (Monk et al., 2021). While poorly studied in elasmobranchs, there is evidence that sharks have personalities that affect the way they respond to the environment, which suggests that such links are plausible (Jacoby et al., 2014; Byrnes and Brown, 2016). For flapper skate, this work has implications not only for the extent to which angled flapper skate are representative of the wider population but also the influence of commercial fishing pressure

on skate movement, the extent to which movements in the LStSJ are representative of other areas and the validity of estimates of population abundance. Ultimately, these issues and many others (such as the influence of environmental stability on movement) can only be addressed by expanding studies of flapper skate movement into other areas and exploiting a variety of capture and tracking techniques. Given the broad ramifications of these links for studies across the field of movement ecology, further work in this area would be worthwhile (Shaw, 2020).

From a broader perspective, questions remain over the ecological consequences of movement in flapper skate. As a fundamental part of animal life, movement has repercussions that transcend ecological disciplines, influencing intra- and inter-specific interactions as well as population-, community- and ecosystem-level properties, such as food-web structure (Riotte-Lambert and Matthiopoulos, 2020; Shaw, 2020). For example, trophic cascades have been widely documented following changes in the abundance of elasmobranchs (Ferretti et al., 2010; Barrios-O'Neill et al., 2017). Recent dietary work on common blue skate suggest that large flapper skate are likely to act as top predators (Brown-Vuillemin et al., 2020). This research indicates that both localised movements and partial migration have the potential to influence skate prey population dynamics, alongside other ecological processes. These potential interactions are stimulating avenues for future research.

Beyond movement ecology, it is worth noting that many aspects of the biology of flapper skate remain unclear, including vital life-history parameters (Régnier et al., 2021). As for other Critically Endangered elasmobranchs (Heupel and Simpfendorfer, 2010), exploiting opportunities to collect these data—especially from specimens caught as bycatch on scientific surveys—will support improved understanding of flapper skate movements and conservation.

3.2. Conservation research

Ecological knowledge gaps have significant implications for conservation. Despite recent research, the conservation benefits of the LStSJ MPA remain partially uncertain, in large part as a result of uncertainty over the time individuals spend in the MPA and their exposure to threats such as fisheries, both within and beyond the MPA (Chapman et al., 2015; MacKeracher et al., 2019). In terms of the time that tagged individuals spent in the MPA, there are two key questions for conservation. The first is the extent to which localised movements continued in the gaps between detections. The second is the extent to which residency continued over larger

areas (beyond the receiver array) and longer time frames (beyond the duration of the study). As noted previously, further analyses of existing data will support quantification of residency within the MPA, but these would be greatly supported by new data on skate activity budgets and movement speeds (Chapter Six). For reconstructing movements, an expanded receiver array with fewer gaps between receivers is also highly desirable. However, the costs of this intervention have to be weighed against the need to address other knowledge gaps underpinning MPA efficacy and the conservation of flapper skate in Scotland more broadly.

Within the MPA, the potential exposure of skate to possible stressors, such as fisheries, aquaculture and electromagnetic cables, remains a key knowledge gap with significant implications for the population-level benefits of the LStSJ MPA (Chapter Three). In areas swept by fisheries, options to address this knowledge gap are difficult and expensive but include an expansion of the acoustic array during the 'closed' season, robotic surveys and fisheries observers. For aquaculture and electromagnetic cables, in situ observational studies alongside experimental studies on other species of skate (Brown et al., 1987; Dempster et al., 2005; Hutchison et al., 2018a) would support understanding of their influence on flapper skate.

The conservation implications of catch-and-release angling also require further research (Chapter Five). While skate can clearly survive multiple captures (Chapter Three), an essential conservation knowledge gap remains regarding the cumulative and population-level impacts of both shore-based and vessel-based angling (Chapter Five). There are substantial opportunities to expand the information gleaned from recreational angling on capture fights, hook retention, bait swallowing, bait regurgitation and egg abortion through mobile phone technology (Merrifield et al., 2019). Ideally, these data should be coupled with *in situ* environmental data, physical and physiological data on the impacts of capture and post-release movement studies (Gallagher et al., 2017). This information would shed light on the morbidity resulting from angling, recovery periods and the extent to which the impacts of repeated captures accumulate and influence survival and fecundity. This work is the only way to mitigate the impacts of angling whilst enhancing the positive socio-economic benefits that it can have for communities and as a monitoring tool for conservation (Gallagher et al., 2017).

Beyond the MPA, skate are likely to experience multiple stressors, including fisheries (Chapter Four; Bendall et al., 2017), marine pollution (Parton et al., 2019; Tiktak et al., 2020) and climate change (Heath et al., 2012; Wheeler et al., 2020). Research on the ecological drivers

of skate movement, including foraging and reproduction, and their influence on interactions between skate and stressors (through exposure and sensitivity) is needed to guide mitigation strategies, such as temporal fisheries restrictions and/or enhanced protections in important habitats (Siskey et al., 2019). A related priority is an improved understanding of how technical modifications can be used to reduce skate bycatch (Molina and Cooke, 2012; Kynoch et al., 2015). The use of specimens that are caught during scientific surveys and killed during this process should be maximised as part of this research (Heupel and Simpfendorfer, 2010; Hammerschlag and Sulikowski, 2011). Beyond diet studies, these have the potential to support research on the effects of capture (Benoît et al., 2010; Ellis et al., 2017), the influence of marine pollutants (Parton et al., 2019; Tiktak et al., 2020) and life history (Heupel and Simpfendorfer, 2010; Hammerschlag and Sulikowski, 2011).

Given the historical and contemporary exposure of flapper skate on the west coast of Scotland to threats both within and beyond the LStSJ MPA, the extent to which fisheries restrictions in this MPA will support population recovery is a critical knowledge gap (Chapter Three). It is widely recognised that the time individuals spend in an MPA (alongside other factors) underpins its efficacy (Chapman et al., 2015; MacKeracher et al., 2019). However, three broad categories of MPAs with different implications for population recovery have emerged in the conservation literature. ‘Paper parks’ provide protection in theory but not in practice, either due to a lack of protective measures or non-compliance (Pieraccini et al., 2017; Bender, 2018). ‘Safeguarding MPAs’ focus on protection for unexploited areas, helping to prevent future degradation but not fostering recovery (O’Leary et al., 2018; Kuempel et al., 2019). Many Nature Conservation MPAs and Special Areas of Conservation in Scotland largely fall into this category, focusing on ‘natural refugia’ where historical fishing pressure has been limited (Langton et al., 2020). In contrast, ‘rebuilding MPAs’ actively reduce pressures in managed areas, compensating for stressors experienced elsewhere and providing hope for population and ecosystem recovery (Duarte et al., 2020). In the LStSJ MPA, it is likely that the rugged terrain has supported natural refugia that have helped to maintain skate presence, but the implementation of management measures that reduce trawling and dredging in specific areas suggest that this MPA has the potential to contribute towards ‘rebuilding’. However, while movement data can support the establishment of rebuilding MPAs such as the LStSJ MPA, ultimately individual-based population models and continuous monitoring are required to estimate their population-level benefits and guide improved MPA design (Dwyer et al., 2020).

Beyond the LStSJ MPA, the movements of flapper skate and their implications for wider population recovery remain uncertain (Chapter Three). Future research should focus on the identification of other areas that support key life history stages (NatureScot, 2021; Phillips et al., 2021a) and/or high local abundance, movements within these areas and connectivity between sites. This work will be supported by continued recovery of archival tags and tidal geolocation, genetic sampling and new tag deployment programmes. In other areas where recreational angling for flapper skate occurs, including the Moray Firth, Orkney and the North Channel off Northern Ireland, exploratory deployments of pop-up satellite archival tags—which do not require skate to be recaptured—would be particularly helpful for developing our understanding of broad-scale movements and guiding future sampling (Chapter One).

As other possible MPAs for flapper skate are identified (NatureScot, 2021), an evaluation of the long-term contribution of MPAs to flapper skate conservation will become increasingly important. MPAs may only benefit certain types of individuals and, by definition, are focused in specific areas. In particular, MPAs are likely to benefit 'resident' individuals more than 'transient' individuals. If spatial protection increases the prevalence of residency, this difference may have implications for the contribution of MPAs to the conservation of genetically viable populations over longer time scales (Parsons et al., 2010). Even as the MPA network for flapper skate is expanded, the reliance of flapper skate on a variety of components in marine ecosystems and continued exposure of flapper skate to stressors beyond MPA boundaries mean that feature-based MPAs are not a panacea for conservation (Hopkins et al., 2016; Solandt et al., 2020). Moving forward, an ecosystem-based management approach is required (McLeod et al., 2005; Solandt et al., 2020).

3.3. Modelling research

Improvements in modelling will support continued research into the ecology and conservation of flapper skate, alongside other mobile species. Modelling animal movement data remains challenging due to the complex statistical properties of high-resolution time series (Chapter One). However, advances in flexible regression, time-series analysis, semi-stochastic modelling and other fields hold the promise of alleviating these challenges, strengthening the robustness of existing analyses and enhancing the value of movement datasets.

Building on GAMs of vertical movement (Chapter Four), there are opportunities to develop GAMs for location, scale and shape (GAMLSS) for movement time series. GAMLSS model the mean (location), variation (scale) and the shape of a distribution in a single framework (Rigby and Stasinopoulos, 2005). From a movement ecology perspective, this is significant because both the average movement and the variability in movement can change through time, for instance due to changes in behaviour (Pinto and Spezia, 2016). While relatively few ecological studies have employed GAMLSS to date (Hudson et al., 2010; Barbini et al., 2018; Secor et al., 2021), ongoing developments to integrate fast model-fitting routines and autocorrelation structures in GAMLSS have the potential to increase their applicability in movement ecology (D. Stasinopoulos, personal communication). In the same vein, continued developments in the applicability and accessibility of Markov switching autoregressive models for movement time series (Pinto and Spezia, 2016) should support coupled analyses of movement and behaviour, including in the context of disturbance (Chapters Four and Five).

In passive acoustic telemetry systems, continued development of the flapper movement modelling framework will support future research (Chapter Six). Technical developments that increase the flexibility with which movement can be modelled are particularly desirable. The incorporation of particle uncertainty in maps of space use is another important area for further development, with broad applications to other systems characterised by observational uncertainty (Kranstauber et al., 2012). These developments will be supported by continued improvements in memory use and computational efficiency. An improved understanding of the pros and cons of the flapper algorithms and how they compare to existing approaches in different settings would also help to guide their application. It is anticipated that there is substantial scope to apply the flapper algorithms to a wide range of benthic, demersal and pelagic species. In addition, untapped opportunities to couple these approaches with economic models for the evaluation of competing tag and array deployment programmes could make a substantial contribution towards the development of cost-effective and efficient array designs (Chapter Six).

Despite the prospects of the flapper movement modelling framework, progress in passive acoustic telemetry modelling will be supported by continued exploration of alternative approaches. For example, motif-discovery algorithms offer a wealth of opportunities to identify structure in movement time series (Torkamani and Lohweg, 2017). For benthic species, these algorithms could support the identification of repeated movement paths over the seabed, of the

kind expected from central place behaviours (Chapter Four). Other approaches such as ant-optimisation algorithms remain unexploited in the movement ecology literature but may provide a more efficient solution for the reconstruction of movement paths (Mullen et al., 2009). The integration of fine-scale movement models with latent variable models for global location sensors, such as archival tags, is the next step for this research. In the same way that nested hydrodynamic models resolve conditions in complex coastal habitats at high resolution while also capturing large-scale ocean properties (Aleynik et al., 2016), coupled frameworks in movement modelling would provide a means to reconstruct fine-scale movements during periods of residency in coastal habitats and reveal the connections between disparate habitats. Looking ahead, the ultimate goal for this research should be the integration of movement in individual-based models that simulate the dynamics of animal populations to study the eco-evolutionary processes that shape populations (Cornell et al., 2019).

3.4. Prioritisation

Given multiple knowledge gaps and limited financial and human capital, prioritisation of future research within the LStSJ MPA and in other regions is necessary (Table 1). There is a strong case to continue to maximise the value of existing data, including through baseline monitoring, further analysis, developments to existing infrastructure and targeted capture and tagging programmes. For conservation, detailed theoretical consideration of the spatiotemporal scale of monitoring in the LStSJ MPA that is required to evaluate survival and whether or not this is feasible should be undertaken (White, 2019; Lees et al., 2021). At the same time, further analyses of existing data, including reconstruction of movements, behavioural analyses of vertical movements and habitat preferences analysis will continue to contribute towards our understanding of flapper skate movement ecology and support the establishment of data collection programmes. Maintaining and developing existing infrastructure, including relationships with charter vessel skippers for recreational angling, software applications for data collection and existing scientific surveys, alongside targeted capture and tagging programmes, is essential, especially as part of pilot studies beyond the LStSJ MPA. As well as directly supporting the development and management of the MPA network, capture and tagging provide a platform for studying many aspects of skate biology (including reproduction, diet and responses to capture) that should be maximised. For tagging, integrative multi-sensor tags can be used to progress multiple areas of research. For example, accelerometers and sonar tags have the potential to provide information on post-release behaviour, activity levels and

behaviour, movement speeds, vertical movement in relation to the seabed and foraging, supporting analyses on responses to catch-and-release angling, residency, vertical movement and its drivers and the vulnerability of skate to bycatch. Looking ahead, a sustainable long-term monitoring plan for skate would greatly support continued improvements in our understanding of skate movement ecology and conservation, as highlighted in other settings (Clutton-Brock and Sheldon, 2010; Hughes et al., 2017; White, 2019). Integrating future research within the European Tracking Network would strengthen understanding of cross-border movements, data management, international collaboration and the value of research in the LStSJ MPA in a European context (Abecasis et al., 2018).

Initial indications of recovery among skate populations in the North Atlantic (including *Dipturus spp.*) provide an encouraging backdrop to this discussion (Rindorf et al., 2020). Yet given the lesson of history is that fisheries can decimate skate populations and management is vital (Brander, 1981), continued monitoring and research into contemporary trends in skate populations in the North Atlantic are essential. With understanding comes hope for the future.

Table 1. Knowledge gaps in the movements of flapper skate and their conservation implications. The table focuses on knowledge gaps that have emerged from work in this thesis. For each primary knowledge gap (bold), key subsidiary knowledge gaps and steps that need to be taken to address these are listed. Candidate priority actions from the perspective of conservation are given in *italics*. Prioritisation is based on the premise that the Loch Sunart to the Sound of Jura Marine Protected Area (LStSJ MPA) is likely to confer benefits to flapper skate, given recent studies (Chapter Three). Therefore, while consideration of the level of monitoring in this area that is required to measure population outcomes is essential, increased study of wider scale movements and the identification of other areas suitable for conservation are likely to make a more significant contribution to skate conservation than continued research in the LStSJ MPA. Actions that are imminently feasible (given previously collected data or opportunities to capitalise upon existing/developing infrastructure) and that fulfil multiple objectives are favoured as candidate priorities.

Knowledge gaps	**Future directions**
Spatiotemporal scale of movements & conservation benefits of the LStSJ MPA and MPAs more broadly	
• Residency in the MPA during detection gaps & exposure to threats within the MPA (fisheries, aquaculture, electromagnetic cables)	➢ Semi-stochastic modelling of existing acoustic and archival data, supported by detection probability models for available sentinel tag data and new data on movement speeds (Chapter Six) ➢ Expanded sampling, especially in areas beyond the MEFS project's 2016–17 receiver array, including in fished areas (e.g., via receiver deployments in the closed season, robotic surveys and fisheries observers); observational studies (e.g., around aquaculture cages); and experimental studies in other settings (e.g., to investigate to impacts of exposure to electromagnetic cables)
• Residency over longer time scales	➢ Continued monitoring in the MPA via passive acoustic telemetry and the recovery of archival tags, coupled with semi-stochastic modelling of acoustic and archival data as described above (Chapter Six)

Knowledge gaps	**Future directions**
• Residency over larger areas & exposure to threats beyond the MPA	➢ *Continued recovery of archival tags and tidal geolocation (latent-variable modelling) (Pinto et al., 2016)* ➢ Expanded monitoring throughout the MPA, via passive acoustic telemetry and archival tagging (ideally with pop-up satellite archival tags) for semi-stochastic (Chapter Six) and latent variable modelling (Pinto et al., 2016) ➢ *Investigations into exposure to fisheries and temporal changes in catchability (see 'the nature of movement'), technical modifications to minimise bycatch (Kynoch et al., 2015) and the use of captured specimens (including to examine the effects of capture and concentrations of marine pollutants)*
• Repeatability of movements in time and space	➢ Continued and expanded monitoring and movement reconstruction, as described above
• Population-level outcomes of the LStSJ MPA, including for population connectivity and growth	➢ *Theoretical consideration of the scale of monitoring required to measure survival in the MPA* ➢ Continued monitoring in the MPA using mark-recapture angling, passive acoustic telemetry and genetic sampling ➢ Development of individual-based population models
• Other areas used by flapper skate	➢ Continued recovery of archival tags and tidal geolocation, as described above (Pinto et al., 2016) ➢ Analysis of recreational angling across Scotland ➢ *Targeted capture and tagging (ideally using pop-up satellite tags), alongside genetic sampling, in areas in which skate are angled or known to occur*

Knowledge gaps	**Future directions**
Drivers of movement & basic skate requirements	
• The influence of the environment, including environmental stability	➢ Targeted capture and tagging (ideally using pop-up satellite tags) in other areas in which skate known to occur
• The influence of reproduction on movement (timing, locations and interactions)	➢ *Continued capture and tagging, including blood sampling for hormonal analyses and ultrasound imaging of females* ➢ *Identification and study of egg-laying grounds*
• The influence of foraging on movement (diets, foraging modes and spatiotemporal variation)	➢ Analyses of sediment preferences, using available data (Chapter Six) ➢ Behavioural analyses of vertical movements and reconstructed tracks, using available data ➢ *Collection of diet data from recreational angling (observations of regurgitation events) via mobile phone applications* ➢ *Collection of diet data from scientific surveys (especially gastric lavage, DNA analysis, tissue samples and dissection)* ➢ Targeted sediment and prey surveys ➢ Targeted capture and tagging programmes (including the collection of diet data via gastric lavage, DNA analysis, tissue samples and sonar tag deployments)

Knowledge gaps	**Future directions**
• The influence of historical and contemporary fishing on movement	➢ Targeted capture and tagging (ideally using pop-up satellite tags) in other areas in which skate known to occur
• The influence of scale	➢ Continued capture, tagging and analysis
Responses to disturbance, especially catch-and-release angling & the cumulative and population-level impacts of this practice	
• The capture experience	➢ *The collection of data from recreational anglers (including on hook retention, bait swallowing and regurgitation) via mobile phone applications*
• Physiological responses and their relationship to movement	➢ *Targeted capture and tagging programmes, including physiological sampling alongside the deployment of accelerometers and sonar tags*
The nature of movement & skate vulnerability to bycatch	
• The balance between benthic, demersal and pelagic movements	➢ Studies of skate diets, as described above ➢ Targeted capture and tagging programmes for the deployment of accelerometers and sonar tags

Knowledge gaps	Future directions
Representation of movements **& the application of insights from the LStSJ MPA to other areas for conservation**	
• Movements of juvenile skate	➢ Identify locations in which juvenile skate are captured, given evidence from recreational angling and bycatch ➢ *Capture and tagging of juveniles with modified gear (e.g., smaller baits)*
• The effects of capture technique and its implications	➢ Continued and expanded monitoring, as described above.
Ecological consequences of movement **& the development of an ecosystem-based management approach**	
• (E.g.) Relationships between flapper skate movement and prey abundance	➢ Coupled movement analyses with habitat and prey sampling

4. Wider themes and lessons

Species-specific studies—of the kind presented here and typical in the movement ecology literature—touch upon a wide range of theoretical and applied issues that have broad implications for the field of movement ecology at large. Key themes that emerge from this thesis include the relationship between movement and the environment, the role of modelling, the links between movement and conservation and the importance of scale. In each of these areas, there are lessons from research on flapper skate that shed light on future directions for the field of movement ecology.

One theme that transcends recent work on flapper skate is the relationship between the environment and movement. The environment can exert strong effects on animal movement and even before the collection of movement data an understanding of environmental conditions across an area can suggest potentially important drivers of variation, relevant scales and suitable metrics for modelling (Chapter Two). Movement studies can support this process, collecting environmental data in undersampled areas and contributing towards the development and validation of hydrodynamic models (Chapter Two). At the same time, movement can influence the physical environment in ways that subsequently affect movement (Riotte-Lambert and Matthiopoulos, 2020).

Yet, as evident from research on flapper skate, even extensive movement and environmental time series are insufficient when it comes to understanding the causes and consequences of animal movement. Technological developments in electronic tagging and tracking have led to tremendous progress (Hussey et al., 2015; Kays et al., 2015; Nathan et al., 2022), but for flapper skate and in the elasmobranch literature more broadly many studies have been principally descriptive and unable to address the ecological interactions that shape and are shaped by movement (Papastamatiou and Lowe, 2012). There is a risk of story-telling, of which other fields in biology have fallen foul (Gould and Lewontin, 1979; Padian, 2018). This has spurred calls for a hypothesis-driven and analytical approach to movement ecology (Papastamatiou and Lowe, 2012). Notwithstanding debates on the role of hypotheses in ecology and more broadly (Betts et al., 2021), it is clear that one goal for the next stage of movement ecology research should be not only to

describe movements and generate hypotheses but to test hypotheses on the causes and consequences of movement. As in conservation science (McLeod et al., 2005), this requires a shift in perspective from species-level to ecosystem-level thinking. Increasingly, more integrative sampling approaches that collect data not only on location and the environment but also energetics, foraging and other processes are leading the field in this direction (Andrzejaczek et al., 2019; Lawson et al., 2019). Alongside an improved understanding of animal movement, this research should extend the capacity of mobile aquatic animals as sources of data on both the abiotic and biotic components of aquatic ecosystems (Hazen et al., 2019).

At a time when the volume and complexity of movement data are expanding, the role of modelling in movement ecology research is also coming to the fore (Patterson et al., 2016; Williams et al., 2020). At the most basic level, models are simplified characterisations of a system (Jackson et al., 2000). Models may seek to describe, to explain or to predict and are variously conceptual or quantitative, mechanistic or data-driven, deterministic or stochastic, single-level or hierarchical—and often a combination of these properties (Jackson et al., 2000).

In the elasmobranch literature, early research often focused on descriptive models (Papastamatiou and Lowe, 2012). As research on the movements of flapper skate in this thesis has shown, these can provide a useful starting point for understanding a system (Chapter Three). 'Top-down' approaches summarise observations to infer underlying patterns. In the field of passive acoustic telemetry, for instance, residency indices, the mean-position algorithm and smoothing are widely used to summarise detections (Chapters Three and Six). In contrast, 'bottom-up' hierarchical models recapitulate the main processes that generate data to uncover patterns. Latent-variable and hybrid semi-stochastic models are examples. Both of these frameworks essentially simulate movements that are consistent with the observations, but the former achieves this within a formal statistical framework with *in situ* parameter estimation (e.g. Hostetter and Royle [2020]) while latter uses pre-defined parameters for simulation (e.g. Aspillaga et al. [2019]). At the time of writing, for passive acoustic telemetry data the semi-stochastic approach facilitates the integration of diverse data types and may improve computation time (Chapter Six). Amongst the diversity of modelling approaches, some authorities have pushed for the adoption of standardised modelling frameworks, such as the mean-position algorithm for passive acoustic telemetry data (Udyawer et

al., 2018). However, despite the benefits of standardisation for the integration of knowledge across multiple studies, as work on flapper skate has emphasised there is a need to investigate the strengths and weaknesses of approaches in different circumstances (Chapter Six). For the mean-position algorithm, clear limitations—especially in clustered receiver arrays—call into question its applicability in many settings (Chapter Six).

Following the reconstruction of movements, a subsequent use for models lies in the identification of patterns and their relation to potential drivers of movement. Many studies relate properties of movement to the environment via statistical models (Chapters Three and Four). These are predominately descriptive but can suggest potential drivers of movement, as illustrated by work on the vertical movements of flapper skate. As data and models become increasingly sophisticated, there is also growing interest in using statistical and machine learning approaches, such as motif-discovery algorithms, for data mining (Torkamani and Lohweg, 2017; Valletta et al., 2017). These approaches blur the boundaries between description and explanation and are likely to become increasingly prevalent, despite challenges for model validation. At the same time, rapid developments are evident in mechanistic models of animal movement. In the field of bioenergetics, for instance, developing models provide a means to quantify the energetic costs and benefits of different movement strategies, underpinning our understanding of the basis for movement decisions and the drivers of movement (Lawson et al., 2019). Looking ahead, divergences in modelling approaches are likely to fuel contemporary debates on 'hypothesis-driven' versus 'data-driven' science and the influence of 'big data' in ecology (Farley et al., 2018; Queiroz et al., 2019; Harry and Braccini, 2021; Nathan et al., 2022). These debates notwithstanding, a plurality of approaches is likely to be beneficial for continued progression in the field. All models have limitations and, as shown by research on flapper skate, different models can support research in different settings (Chapter Six).

The profound implications of movement for conservation are another key theme in work on flapper skate (Chapters Three–Six). Movement data support understanding of the time spent within protected areas (Chapter Three), exposure to stressors (Chapter Four) and responses to disturbance (Chapter Five). In addition, the collection of movement data provides a platform for supporting activities, such as dietary studies, that underpin effective conservation (Hammerschlag and

Sulikowski, 2011). Across the field of movement ecology, there is evidence that that these kinds of research can influence conservation planning (Fraser et al., 2018; Hays et al., 2019). However, work on flapper skate and other mobile species highlights that continued study is necessary to quantify the benefits of policy interventions for population recovery (Dwyer et al., 2020). At a time when mobile species across the globe are under unprecedented pressure, the conservation promise of movement ecology must be realised in full (Fraser et al., 2018; Hays et al., 2019).

Across ecology, modelling and conservation, the importance of scale is a unifying theme (Levin, 1992). Work on flapper skate has revealed movement patterns from diel to seasonal timescales (Chapters Three and Four) and how modelling 'stepwise' movements can elucidate emergent patterns of space use (Chapter Six). Research across disparate scales can have conservation implications from effective strategies for mitigating the impacts of disturbance (Chapter Five) to the design of MPAs (Chapters Three and Six). However, for flapper skate, as for the field of movement ecology as a whole, key questions remain over the scales at which to sample movement, the scales at which movement is influenced by the environment, the scales at which movement should be modelled and the scales that matter most for conservation. As electronic tagging and tracking technologies become ever more sophisticated and the ability to collect information at incredibly high resolutions over extended timeframes becomes increasingly feasible (Williams et al., 2020), issues of scale are likely to continue to remain a 'central problem' (Levin, 1992) for movement ecology research.

References

Abecasis, D., Horta e Costa, B., Afonso, P., Gonçalves, E. J., and Erzini, K. (2015). Early reserve effects linked to small home ranges of a commercial fish, *Diplodus sargus*, Sparidae. *Mar. Ecol. Prog. Ser.* 518, 255–266. doi:10.3354/meps11054.

Abecasis, D., Steckenreuter, A., Reubens, J., Aarestrup, K., Alós, J., Badalamenti, F., et al. (2018). A review of acoustic telemetry in Europe and the need for a regional aquatic telemetry network. *Anim. Biotelemetry* 6, 12. doi:10.1186/s40317-018-0156-0.

Ackerman, J. T., Kondratieff, M. C., Matern, S. A., and Cech, J. J. (2000). Tidal influence on spatial dynamics of leopard sharks, *Triakis semifasciata*, in Tomales Bay, California. *Environ. Biol. Fishes* 58, 33–43. doi:10.1023/A:1007657019696.

Aguzzi, J., and Sardà, F. (2008). A history of recent advancements on *Nephrops norvegicus* behavioral and physiological rhythms. *Rev. Fish Biol. Fish.* 18, 235–248. doi:10.1007/s11160-007-9071-9.

Aleynik, D., Dale, A. C., Porter, M., and Davidson, K. (2016). A high resolution hydrodynamic model system suitable for novel harmful algal bloom modelling in areas of complex coastline and topography. *Harmful Algae* 53, 102–117. doi:10.1016/j.hal.2015.11.012.

Andrews, K. S., Williams, G. D., Farrer, D., Tolimieri, N., Harvey, C. J., Bargmann, G., et al. (2009). Diel activity patterns of sixgill sharks, *Hexanchus griseus*: the ups and downs of an apex predator. *Anim. Behav.* 78, 525–536. doi:10.1016/j.anbehav.2009.05.027.

Andrzejaczek, S., Gleiss, A. C., Pattiaratchi, C. B., and Meekan, M. G. (2019). Patterns and drivers of vertical movements of the large fishes of the epipelagic. *Rev. Fish Biol. Fish.* 29, 335–354. doi:10.1007/s11160-019-09555-1.

Arlinghaus, R., and Cooke, S. J. (2009). "Recreational fisheries: socioeconomic importance, conservation issues and management challenges," in *Recreational Hunting, Conservation and Rural Livelihoods*, eds. B. Dickson, J. Hutton, and W. M. Adams (Oxford: Blackwell Publishing Ltd), 39–58. doi:10.1002/9781444303179.ch3.

Arlinghaus, R., Cooke, S. J., Lyman, J., Policansky, D., Schwab, A., Suski, C., et al. (2007).

Understanding the complexity of catch-and-release in recreational fishing: an integrative synthesis of global knowledge from historical, ethical, social, and biological perspectives. *Rev. Fish. Sci.* 15, 75–167. doi:10.1080/10641260601149432.

Arostegui, M. C., Gaube, P., Berumen, M. L., DiGiulian, A., Jones, B. H., Røstad, A., et al. (2020). Vertical movements of a pelagic thresher shark (*Alopias pelagicus*): insights into the species' physiological limitations and trophic ecology in the Red Sea. *Endanger. Species Res.* 43, 387–394. doi:10.3354/esr01079.

Aspillaga, E., Safi, K., Hereu, B., and Bartumeus, F. (2019). Modelling the three-dimensional space use of aquatic animals combining topography and Eulerian telemetry data. *Methods Ecol. Evol.* 10, 1551–1557. doi:10.1111/2041-210X.13232.

Bache-Jeffreys, M., de Moraes, B. L. C., Ball, R. E., Menezes, G., Pálsson, J., Pampoulie, C., et al. (2021). Resolving the spatial distributions of *Dipturus intermedius* and *Dipturus batis*—the two taxa formerly known as the 'common skate.' *Environ. Biol. Fishes* 104, 923–936. doi:10.1007/s10641-021-01122-7.

Barbini, S. A., Sabadin, D. E., and Lucifora, L. O. (2018). Comparative analysis of feeding habits and dietary niche breadth in skates: the importance of body size, snout length, and depth. *Rev. Fish Biol. Fish.* 28, 625–636. doi:10.1007/s11160-018-9522-5.

Barnett, A., Abrantes, K. G., Seymour, J., and Fitzpatrick, R. (2012). Residency and spatial use by reef sharks of an isolated seamount and its implications for conservation. *PLoS One* 7, e36574. doi:10.1371/journal.pone.0036574.

Barnett, A., Redd, K. S., Frusher, S. D., Stevens, J. D., and Semmens, J. M. (2010). Non-lethal method to obtain stomach samples from a large marine predator and the use of DNA analysis to improve dietary information. *J. Exp. Mar. Bio. Ecol.* 393, 188–192. doi:10.1016/j.jembe.2010.07.022.

Barrios-O'Neill, D., Bertolini, C., and Collins, P. C. (2017). Trophic cascades and the transient keystone concept. *Biol. Conserv.* 212, 191–195. doi:10.1016/j.biocon.2017.06.011.

Bates, A. E., Primack, R. B., Biggar, B. S., Bird, T. J., Clinton, M. E., Command, R. J., et al. (2021). Global COVID-19 lockdown highlights humans as both threats and custodians of the environment. *Biol. Conserv.* 263, 109175. doi:10.1016/j.biocon.2021.109175.

Baum, J. K., and Worm, B. (2009). Cascading top-down effects of changing oceanic predator abundances. *J. Anim. Ecol.* 78, 699–714. doi:10.1111/j.1365-2656.2009.01531.x.

Bayse, S. M., Pol, M. V, and He, P. (2016). Fish and squid behaviour at the mouth of a drop-chain trawl: factors contributing to capture or escape. *ICES J. Mar. Sci.* 73, 1545–1556. doi:10.1093/icesjms/fsw007.

Beath, K. (2021). robmixglm: Robust generalized linear models (GLM) using mixtures. R package version 1.2-1. Available at: https://cran.r-project.org/package=robmixglm.

Becker, S. L., Finn, J. T., Danylchuk, A. J., Pollock, C. G., Hillis-Starr, Z., Lundgren, I., et al. (2016). Influence of detection history and analytic tools on quantifying spatial ecology of a predatory fish in a marine protected area. *Mar. Ecol. Prog. Ser.* 562, 147–161. doi:10.3354/meps11962.

Bell, J., Lyle, J., Semmens, J., Awruch, C., Moreno, D., Currie, S., et al. (2016). Movement, habitat utilisation and population status of the endangered Maugean skate and implications for fishing and aquaculture operations in Macquarie Harbour. Fisheries Research and Development Corporation Project No. 2013/008. Hobart Available at: http://ecite.utas.edu.au/106905/1/2013-008-DLD.pdf.

Bendall, V. A., Jones, P., Nicholson, R., Hetherington, S. J., and Burt, G. (2017). Common skate survey annual report (ELECTRA MF6001: Work Package Task 1.4). Available at: http://randd.defra.gov.uk/Document.aspx?Document=14405_MF6001_CommonSkateSurvey_AnnualReport_2017.pdf.

Bender, M. (2018). As nature evolves, so too does MPA management need to evolve. *Biodiversity* 19, 131–136. doi:10.1080/14888386.2018.1479656.

Benhamou, S., and Cornélis, D. (2010). Incorporating movement behavior and barriers to improve kernel home range space use estimates. *J. Wildl. Manage.* 74, 1353–1360. doi:10.1111/j.1937-2817.2010.tb01257.x.

Benjamins, S., Cole, G., Naylor, A., Thorburn, J. A., and Dodd, J. (2021). First confirmed complete incubation of a flapper skate (*Dipturus intermedius*) egg in captivity. *J. Fish Biol.* 99, 1150–1154. doi:10.1111/jfb.14816.

Benjamins, S., Dodd, J., Thorburn, J., Milway, V. A., Campbell, R., and Bailey, D. M. (2018). Evaluating the potential of photo-identification as a monitoring tool for flapper skate (*Dipturus intermedius*). *Aquat. Conserv. Mar. Freshw. Ecosyst.* 28, 1360–1373. doi:10.1002/aqc.2937.

Benoît, H. P., Hurlbut, T., and Chassé, J. (2010). Assessing the factors influencing discard

mortality of demersal fishes using a semi-quantitative indicator of survival potential. *Fish. Res.* 106, 436–447. doi:10.1016/j.fishres.2010.09.018.

Betts, M. G., Hadley, A. S., Frey, D. W., Frey, S. J. K., Gannon, D., Harris, S. H., et al. (2021). When are hypotheses useful in ecology and evolution? *Ecol. Evol.* 11, 5762–5776. doi:10.1002/ece3.7365.

Bezerra, M. F., Lacerda, L. D., and Lai, C.-T. (2019). Trace metals and persistent organic pollutants contamination in batoids (Chondrichthyes: Batoidea): a systematic review. *Environ. Pollut.* 248, 684–695. doi:10.1016/j.envpol.2019.02.070.

Bianchi, D., and Mislan, K. A. S. (2016). Global patterns of diel vertical migration times and velocities from acoustic data. *Limnol. Oceanogr.* 61, 353–364. doi:10.1002/lno.10219.

Bird, C., Burt, G. J., Hampton, N., McCully Phillips, S. R., and Ellis, J. R. (2020). Fifty years of tagging skates (Rajidae): using mark-recapture data to evaluate stock units. *J. Mar. Biol. Assoc. United Kingdom* 100, 121–131. doi:10.1017/S0025315419000997.

Bizzarro, J. J., Broms, K. M., Logsdon, M. G., Ebert, D. A., Yoklavich, M. M., Kuhnz, L. A., et al. (2014). Spatial segregation in Eastern North Pacific skate assemblages. *PLoS One* 9, e109907. doi:10.1371/journal.pone.0109907.

Block, B. A., Teo, S. L. H., Walli, A., Boustany, A., Stokesbury, M. J. W., Farwell, C. J., et al. (2005). Electronic tagging and population structure of Atlantic bluefin tuna. *Nature* 434, 1121–1127. doi:10.1038/nature03463.

Bond, M. E., Babcock, E. A., Pikitch, E. K., Abercrombie, D. L., Lamb, N. F., and Chapman, D. D. (2012). Reef sharks exhibit site-fidelity and higher relative abundance in marine reserves on the Mesoamerican Barrier Reef. *PLoS One* 7, e32983–e32983. doi:10.1371/journal.pone.0032983.

Boswarva, K., Butters, A., Fox, C. J., Howe, J. A., and Narayanaswamy, B. (2018). Improving marine habitat mapping using high-resolution acoustic data; a predictive habitat map for the Firth of Lorn, Scotland. *Cont. Shelf Res.* 168, 39–47. doi:10.1016/j.csr.2018.09.005.

Boyd, C., Punt, A. E., Weimerskirch, H., and Bertrand, S. (2014). Movement models provide insights into variation in the foraging effort of central place foragers. *Ecol. Modell.* 286, 13–25. doi:10.1016/j.ecolmodel.2014.03.015.

Brander, K. (1981). Disappearance of common skate *Raia batis* from Irish Sea. *Nature* 290, 48–49. doi:10.1038/290048a0.

Braun, C. D., Galuardi, B., and Thorrold, S. R. (2018). HMMoce: An R package for improved geolocation of archival-tagged fishes using a hidden Markov method. *Methods Ecol. Evol.* 9, 1212–1220. doi:10.1111/2041-210X.12959.

Brill, R., Bushnell, P., Schroff, S., Seifert, R., and Galvin, M. (2008). Effects of anaerobic exercise accompanying catch-and-release fishing on blood-oxygen affinity of the sandbar shark (*Carcharhinus plumbeus*, Nardo). *J. Exp. Mar. Bio. Ecol.* 354, 132–143. doi:10.1016/j.jembe.2007.10.011.

Broman, K. W., and Woo, K. H. (2018). Data organization in spreadsheets. *Am. Stat.* 72, 2–10. doi:10.1080/00031305.2017.1375989.

Brost, B. M., Hooten, M. B., and Small, R. J. (2020). Model-based clustering reveals patterns in central place use of a marine top predator. *Ecosphere* 11, e03123. doi:10.1002/ecs2.3123.

Brown-Vuillemin, S., Barreau, T., Caraguel, J.-M., and Iglésias, S. P. (2020). Trophic ecology and ontogenetic diet shift of the blue skate (*Dipturus cf. flossada*). *J. Fish Biol.* 97, 515–526. doi:10.1111/jfb.14407.

Brown, J. R., Gowen, R. J., and McLusky, D. S. (1987). The effect of salmon farming on the benthos of a Scottish sea loch. *J. Exp. Mar. Bio. Ecol.* 109, 39–51. doi:10.1016/0022-0981(87)90184-5.

Brownscombe, J. W., Danylchuk, A. J., Chapman, J. M., Gutowsky, L. F. G., and Cooke, S. J. (2017). Best practices for catch-and-release recreational fisheries – angling tools and tactics. *Fish. Res.* 186, 693–705. doi:10.1016/j.fishres.2016.04.018.

Bürkner, P.-C. (2017). brms: An R package for Bayesian multilevel models using Stan. *J. Stat. Softw.* 80, 1–28. doi:10.18637/jss.v080.i01.

Bürkner, P.-C. (2018). Advanced Bayesian multilevel modeling with the R package brms. *R J.* 10, 395-411. doi:10.32614/RJ-2018-017.

Burt, W. H. (1943). Territoriality and home range concepts as applied to mammals. *J. Mammal.* 24, 346–352. doi:10.2307/1374834.

Byrnes, E. E., and Brown, C. (2016). Individual personality differences in Port Jackson sharks *Heterodontus portusjacksoni*. *J. Fish Biol.* 89, 1142–1157. doi:10.1111/jfb.12993.

Campbell, H. A., Hewitt, M., Watts, M. E., Peverell, S., and Franklin, C. E. (2012). Short- and long-term movement patterns in the freshwater whipray (*Himantura dalyensis*) determined by the signal processing of passive acoustic telemetry data. *Mar. Freshw. Res.* 63, 341–350.

doi:10.1071/MF11229.

Carey, F. G., Scharold, J. V, and Kalmijn, A. J. (1990). Movements of blue sharks (*Prionace glauca*) in depth and course. *Mar. Biol.* 106, 329–342. doi:10.1007/BF01344309.

Carlisle, A. B., and Starr, R. M. (2009). Habitat use, residency, and seasonal distribution of female leopard sharks *Triakis semifasciata* in Elkhorn Slough, California. *Mar. Ecol. Prog. Ser.* 380, 213–228. doi:10.3354/meps07907.

Carlisle, A. B., and Starr, R. M. (2010). Tidal movements of female leopard sharks (*Triakis semifasciata*) in Elkhorn Slough, California. *Environ. Biol. Fishes* 89, 31–45. doi:10.1007/s10641-010-9667-0.

Caruso, F., Hickmott, L., Warren, J. D., Segre, P., Chiang, G., Bahamonde, P., et al. (2020). Diel differences in blue whale (*Balaenoptera musculus*) dive behavior increase nighttime risk of ship strikes in northern Chilean Patagonia. *Integr. Zool.* 16, 594–611. doi:10.1111/1749-4877.12501.

Catania, K. C. (2005). Star-nosed moles. *Curr. Biol.* 15, R863–R864. doi:10.1016/j.cub.2005.10.030.

Chan, Y.-C., Tibbitts, T. L., Lok, T., Hassell, C. J., Peng, H.-B., Ma, Z., et al. (2019). Filling knowledge gaps in a threatened shorebird flyway through satellite tracking. *J. Appl. Ecol.* 56, 2305–2315. doi:10.1111/1365-2664.13474.

Chapman, B. B., Brönmark, C., Nilsson, J.-Å., and Hansson, L.-A. (2011). The ecology and evolution of partial migration. *Oikos* 120, 1764–1775. doi:10.1111/j.1600-0706.2011.20131.x.

Chapman, B. B., Hulthén, K., Brodersen, J., Nilsson, P. A., Skov, C., Hansson, L.-A., et al. (2012). Partial migration in fishes: causes and consequences. *J. Fish Biol.* 81, 456–478. doi:10.1111/j.1095-8649.2012.03342.x.

Chapman, D. D., Feldheim, K. A., Papastamatiou, Y. P., and Hueter, R. E. (2015). There and back again: a review of residency and return migrations in sharks, with implications for population structure and management. *Ann. Rev. Mar. Sci.* 7, 547–570. doi:10.1146/annurev-marine-010814-015730.

Chen, C., Liu, H., and Beardsley, R. (2003). An unstructured grid, finite-volume, three-dimensional, primitive equations ocean model: application to coastal ocean and estuaries. *J. Atmos. Ocean. Technol.* 20, 159–186. doi:10.1175/1520-

0426(2003)020<0159:AUGFVT>2.0.CO;2.

Clutton-Brock, T., and Sheldon, B. C. (2010). Individuals and populations: the role of long-term, individual-based studies of animals in ecology and evolutionary biology. *Trends Ecol. Evol.* 25, 562–573. doi:10.1016/j.tree.2010.08.002.

Coffey, D. M., Royer, M. A., Meyer, C. G., and Holland, K. N. (2020). Diel patterns in swimming behavior of a vertically migrating deepwater shark, the bluntnose sixgill (*Hexanchus griseus*). *PLoS One* 15, e0228253. doi:10.1371/journal.pone.0228253.

Collins, A. B., Heupel, M. R., and Motta, P. J. (2007). Residence and movement patterns of cownose rays *Rhinoptera bonasus* within a south-west Florida estuary. *J. Fish Biol.* 71, 1159–1178. doi:10.1111/j.1095-8649.2007.01590.x.

Cook, K. V, Reid, A. J., Patterson, D. A., Robinson, K. A., Chapman, J. M., Hinch, S. G., et al. (2019). A synthesis to understand responses to capture stressors among fish discarded from commercial fisheries and options for mitigating their severity. *Fish Fish.* 20, 25–43. doi:10.1111/faf.12322.

Cooke, S. J., Hogan, Z. S., Butcher, P. A., Stokesbury, M. J. W., Raghavan, R., Gallagher, A. J., et al. (2014). Angling for endangered fish: conservation problem or conservation action? *Fish Fish.* 17, 249–265. doi:10.1111/faf.12076.

Cooke, S. J., Lennox, R. J., Brownscombe, J. W., Iverson, S. J., Whoriskey, F. G., Millspaugh, J. J., et al. (2021). A case for restoring unity between biotelemetry and bio-logging to enhance animal tracking research. *FACETS* 6, 1260–1265. doi:10.1139/facets-2020-0112.

Cooke, S. J., and Philipp, D. P. (2004). Behavior and mortality of caught-and-released bonefish (*Albula* spp.) in Bahamian waters with implications for a sustainable recreational fishery. *Biol. Conserv.* 118, 599–607. doi:10.1016/j.biocon.2003.10.009.

Cooke, S. J., and Schramm, H. L. (2007). Catch-and-release science and its application to conservation and management of recreational fisheries. *Fish. Manag. Ecol.* 14, 73–79. doi:10.1111/j.1365-2400.2007.00527.x.

Corcoran, M. J., Wetherbee, B. M., Shivji, M. S., Potenski, M. D., Chapman, D. D., and Harvey, G. M. (2013). Supplemental feeding for ecotourism reverses diel activity and alters movement patterns and spatial distribution of the southern stingray, *Dasyatis americana*. *PLoS One* 8, e59235. doi:10.1371/journal.pone.0059235.

Cornell, S. J., Suprunenko, Y. F., Finkelshtein, D., Somervuo, P., and Ovaskainen, O. (2019). A

unified framework for analysis of individual-based models in ecology and beyond. *Nat. Commun.* 10, 4716. doi:10.1038/s41467-019-12172-y.

Cott, P. A., Guzzo, M. M., Chapelsky, A. J., Milne, S. W., and Blanchfield, P. J. (2015). Diel bank migration of Burbot (*Lota lota*). *Hydrobiologia* 757, 3–20. doi:10.1007/s10750-015-2257-6.

Cunha, J., Saraiva, J., and Visser, J. (2009). From spreadsheets to relational databases and back. *PEPM '09*, 179–188. doi:10.1145/1480945.1480972.

Dabrowski, T., Lyons, K., Berry, A., Cusack, C., and Nolan, G. D. (2014). An operational biogeochemical model of the North-East Atlantic: model description and skill assessment. *J. Mar. Syst.* 129, 350–367. doi:10.1016/j.jmarsys.2013.08.001.

Danylchuk, A. J., Suski, C. D., Mandelman, J. W., Murchie, K. J., Haak, C. R., Brooks, A. M. L., et al. (2014). Hooking injury, physiological status and short-term mortality of juvenile lemon sharks (*Negaprion bevirostris*) following catch-and-release recreational angling. *Conserv. Physiol.* 2, cot036. doi:10.1093/conphys/cot036.

Day, F. (1884). *The Fishes of Great Britain and Ireland*. London: Williams & Norgate.

Dempster, T., Fernández-Jover, D., Sánchez-Jérez, P., Tuya, F., Bayle-Sempere, J., Boyra, A., et al. (2005). Vertical variability of wild fish assemblages around sea-cage fish farms: implications for management. *Mar. Ecol. Prog. Ser.* 304, 15–29. doi:10.3354/meps304015.

Desforges, J.-P., Hall, A., McConnell, B., Rosing-Asvid, A., Barber, J. L., Brownlow, A., et al. (2018). Predicting global killer whale population collapse from PCB pollution. *Science* 361, 1373 LP – 1376. doi:10.1126/science.aat1953.

Díaz, S., Settele, J., Brondízio, E. S., Ngo, H. T., Agard, J., Arneth, A., et al. (2019). Pervasive human-driven decline of life on Earth points to the need for transformative change. *Science* 366, eaax3100. doi:10.1126/science.aax3100.

Doherty, T. S., Hays, G. C., and Driscoll, D. A. (2021). Human disturbance causes widespread disruption of animal movement. *Nat. Ecol. Evol.* 5, 513–519. doi:10.1038/s41559-020-01380-1.

Drake, J., Lambin, X., and Sutherland, C. (2021). The value of considering demographic contributions to connectivity: a review. *Ecography (Cop.).* 44, 1–18. doi:10.1111/ecog.05552.

Duarte, C. M., Agusti, S., Barbier, E., Britten, G. L., Castilla, J. C., Gattuso, J.-P., et al. (2020). Rebuilding marine life. *Nature* 580, 39–51. doi:10.1038/s41586-020-2146-7.

Dulvy, N. K., Fowler, S. L., Musick, J. A., Cavanagh, R. D., Kyne, P. M., Harrison, L. R., et al. (2014). Extinction risk and conservation of the world's sharks and rays. *eLife* 3, e00590. doi:10.7554/eLife.00590.

Dulvy, N. K., Metcalfe, J. D., Glanville, J., Pawson, M. G., and Reynolds, J. D. (2000). Fishery stability, local extinctions, and shifts in community structure in skates. *Conserv. Biol.* 14, 283–293. doi:10.1046/j.1523-1739.2000.98540.x.

Dulvy, N. K., Notarbartolo di Sciara, G., Serena, F., Tinti, F., Ungaro, N., C, M., et al. (2006). *Dipturus batis*. *IUCN Red List Threat. Species 2006 e.T39397A10198950.* doi:10.2305/IUCN.UK.2006.RLTS.T39397A10198950.en.

Dwyer, R. G., Krueck, N. C., Udyawer, V., Heupel, M. R., Chapman, D. D., Pratt, H. L., et al. (2020). Individual and population benefits of marine reserves for reef sharks. *Curr. Biol.* 30, 480–489. doi:10.1016/j.cub.2019.12.005.

Economakis, A. E., and Lobel, P. S. (1998). Aggregation behavior of the grey reef shark, *Carcharhinus amblyrhynchos*, at Johnston Atoll, Central Pacific Ocean. *Environ. Biol. Fishes* 51, 129–139. doi:10.1023/A:1007416813214.

Edgar, G. J., Stuart-Smith, R. D., Willis, T. J., Kininmonth, S., Baker, S. C., Banks, S., et al. (2014). Global conservation outcomes depend on marine protected areas with five key features. *Nature* 506. doi:10.1038/nature13022.

Ellis, J. R., Bendall, V. A., Hetherington, S. J., Silva, J. F., and McCully Phillips, S. R. (2015). National evaluation of populations of threatened and uncertain elasmobranchs (NEPTUNE) project report. Available at: http://sciencesearch.defra.gov.uk/Document.aspx?Document=13513_MB5201NEPTUNEFinalReportv1.4.pdf.

Ellis, J. R., McCully-Philipps, S. R., Sims, D., Walls, R. H. L., Cheok, J., Derrick, D., et al. (2021). *Dipturus intermedius*. *IUCN Red List Threat. Species 2021*, e.T18903491A68783461. doi:10.2305/IUCN.UK.2021-2.RLTS.T18903491A68783461.en.

Ellis, J. R., McCully Phillips, S. R., and Poisson, F. (2017). A review of capture and post-release mortality of elasmobranchs. *J. Fish Biol.* 90, 653–722. doi:10.1111/jfb.13197.

Estes, J. A., Terborgh, J., Brashares, J. S., Power, M. E., Berger, J., Bond, W. J., et al. (2011). Trophic downgrading of planet earth. *Science* 333, 301–306. doi:10.1126/science.1205106.

Farley, S. S., Dawson, A., Goring, S. J., and Williams, J. W. (2018). Situating ecology as a big-

data science: current advances, challenges, and solutions. *Bioscience* 68, 563–576. doi:10.1093/biosci/biy068.

Ferretti, F., Curnick, D., Liu, K., Romanov, E. V, and Block, B. A. (2018). Shark baselines and the conservation role of remote coral reef ecosystems. *Sci. Adv.* 4, eaaq0333. doi:10.1126/sciadv.aaq0333.

Ferretti, F., Worm, B., Britten, G. L., Heithaus, M. R., and Lotze, H. K. (2010). Patterns and ecosystem consequences of shark declines in the ocean. *Ecol. Lett.* 13, 1055–1071. doi:10.1111/j.1461-0248.2010.01489.x.

Flowers, K., Ajemian, M., Bassos-Hull, K., Feldheim, K. A., Hueter, R., Papastamatiou, Y. P., et al. (2016). A review of batoid philopatry, with implications for future research and population management. *Mar. Ecol. Prog. Ser.* 562, 251–261. doi:10.3354/meps11963.

Fouts, W. R., and Nelson, D. R. (1999). Prey capture by the Pacific Angel Shark, *Squatina californica*: visually mediated strikes and ambush-site characteristics. *Copeia* 1999, 304–312. doi:10.2307/1447476.

Frank, K. T., Petrie, B., Leggett, W. C., and Boyce, D. G. (2018). Exploitation drives an ontogenetic-like deepening in marine fish. *Proc. Natl. Acad. Sci.* 115, 6422–6427. doi:10.1073/pnas.1802096115.

Fraser, K. C., Davies, K. T. A., Davy, C. M., Ford, A. T., Flockhart, D. T. T., and Martins, E. G. (2018). Tracking the conservation promise of movement ecology. *Front. Ecol. Evol.* 6, 150. doi:10.3389/fevo.2018.00150.

French, R. P., Lyle, J., Tracey, S., Currie, S., and Semmens, J. M. (2015). High survivorship after catch-and-release fishing suggests physiological resilience in the endothermic shortfin mako shark (*Isurus oxyrinchus*). *Conserv. Physiol.* 3, cov044. doi:10.1093/conphys/cov044.

Froeschke, J., Stunz, G. W., and Wildhaber, L. M. (2010). Environmental influences on the occurrence of coastal sharks in estuarine waters. *Mar. Ecol. Prog. Ser.* 407, 279–292. doi:10.3354/meps08546.

Frost, M., Neat, F. C., Stirling, D., Bendall, V., Noble, L. R., and Jones, C. S. (2020). Distribution and thermal niche of the common skate species complex in the north-east Atlantic. *Mar. Ecol. Prog. Ser.* 656, 65–74. doi:10.3354/meps13545.

Fudickar, A. M., Jahn, A. E., and Ketterson, E. D. (2021). Animal migration: an overview of one of nature's great spectacles. *Annu. Rev. Ecol. Evol. Syst.* doi:10.1146/annurev-ecolsys-

012021-031035.

Gallagher, A. J., Hammerschlag, N., Danylchuk, A. J., and Cooke, S. J. (2017). Shark recreational fisheries: Status, challenges, and research needs. *Ambio* 46, 385–398. doi:10.1007/s13280-016-0856-8.

Gallagher, A. J., Serafy, J. E., Cooke, S. J., and Hammerschlag, N. (2014). Physiological stress response, reflex impairment, and survival of five sympatric shark species following experimental capture and release. *Mar. Ecol. Prog. Ser.* 496, 207–218. doi:10.3354/meps10490.

Gallagher, A. J., Staaterman, E. R., Cooke, S. J., and Hammerschlag, N. (2016). Behavioural responses to fisheries capture among sharks caught using experimental fishery gear. *Can. J. Fish. Aquat. Sci.* 74, 1–7. doi:10.1139/cjfas-2016-0165.

Gallego, A., Gibb, F. M., Tullet, D., and Wright, P. J. (2017). Bio-physical connectivity patterns of benthic marine species used in the designation of Scottish nature conservation marine protected areas. *ICES J. Mar. Sci.* 74, 1797–1811. doi:10.1093/icesjms/fsw174.

Garcia, D., Crespo, J. L., Guallart, J., García-Salinas, P., Jiménez, M., and Brodsky, M. (2015). *Systemic gas embolism in sharks. Evidence of decompression like lesions in by-caught little sleeper sharks Somniosus rostratus from deep sea trawls. Poster 19th Annual Scientific European Elasmobranch Association.* doi:10.13140/RG.2.1.4407.3685.

Gelsleichter, J., and Walker, C. (2010). "Pollutant exposure and effects in sharks and their relatives," in *Sharks and Their Relatives II*, 491–537. doi:10.1201/9781420080483-c12.

Gibson, R. N. (2003). Go with the flow: tidal migration in marine animals. *Hydrobiologica* 503, 153–161. doi:10.1023/B:HYDR.0000008488.33614.62.

Gille, S. T., Metzger, E. J., and Tokmakian, R. (2004). Seafloor topography and ocean circulation. *Oceanography* 17, 47–54. doi:10.5670/oceanog.2004.66.

Gilman, E., Chaloupka, M., Dagorn, L., Hall, M., Hobday, A., Musyl, M., et al. (2019). Robbing Peter to pay Paul: replacing unintended cross-taxa conflicts with intentional tradeoffs by moving from piecemeal to integrated fisheries bycatch management. *Rev. Fish Biol. Fish.* 29, 93–123. doi:10.1007/s11160-019-09547-1.

Gleiss, A. C., Morgan, D. L., Whitty, J. M., Keleher, J. J., Fossette, S., and Hays, G. C. (2017). Are vertical migrations driven by circadian behaviour? Decoupling of activity and depth use in a large riverine elasmobranch, the freshwater sawfish (*Pristis pristis*). *Hydrobiologia* 787,

181–191. doi:10.1007/s10750-016-2957-6.

Gleiss, A. C., Wright, S., Liebsch, N., Wilson, R. P., and Norman, B. (2013). Contrasting diel patterns in vertical movement and locomotor activity of whale sharks at Ningaloo Reef. *Mar. Biol.* 160, 2981–2992. doi:10.1007/s00227-013-2288-3.

Gorman, O. T., Yule, D. L., and Stockwell, J. D. (2012). Habitat use by fishes of Lake Superior. I. Diel patterns of habitat use in nearshore and offshore waters of the Apostle Islands region. *Aquat. Ecosyst. Health Manag.* 15, 333–354. doi:10.1080/14634988.2012.715972.

Gould, S. J., and Lewontin, R. C. (1979). The spandrels of San Marco and the Panglossian paradigm: a critique of the adaptationist programme. *Proc. R. Soc. B Biol. Sci.* 205, 581–598. doi:10.1098/rspb.1979.0086.

Graham, R. T., Roberts, C. M., and Smart, J. C. R. (2006). Diving behaviour of whale sharks in relation to a predictable food pulse. *J. R. Soc. Interface* 3, 109–116. doi:10.1098/rsif.2005.0082.

Greenway, E., Jones, K. S., and Cooke, G. M. (2016). Environmental enrichment in captive juvenile thornback rays, *Raja clavata* (Linnaeus 1758). *Appl. Anim. Behav. Sci.* 182, 86–93. doi:10.1016/j.applanim.2016.06.008.

Grohmann, C., Smith, M., and Riccomini, C. (2011). Multiscale analysis of topographic surface roughness in the Midland Valley, Scotland. *IEEE Trans. Geosci. Remote Sens.* 49, 1200–1213. doi:10.1109/TGRS.2010.2053546.

Grubbs, R. D. (2010). "Ontogenetic shifts in movement and habitat use," in *Sharks and Their Relatives II: Biodiversity, Adaptive Physiology and Conservation*, eds. J. C. Carrier, J. A. Musick, and M. R. Heithaus (Florida: CRC Press), 319–350.

Guida, L., Dapp, D. R., Huveneers, C. P. M., Walker, T. I., and Reina, R. D. (2017). Evaluating time-depth recorders as a tool to measure the behaviour of sharks captured on longlines. *J. Exp. Mar. Bio. Ecol.* 497, 120–126. doi:10.1016/j.jembe.2017.09.011.

Guida, L., Walker, T. I., and Reina, R. D. (2016). Temperature insensitivity and behavioural reduction of the physiological stress response to longline capture by the gummy shark, *Mustelus antarcticus*. *PLoS One* 11, e0148829. doi:10.1371/journal.pone.0148829.

Guttridge, T. L., Gruber, S. H., Franks, B. R., Kessel, S. T., Gledhill, K. S., Uphill, J., et al. (2012). Deep danger: intra-specific predation risk influences habitat use and aggregation formation of juvenile lemon sharks *Negaprion brevirostris*. *Mar. Ecol. Prog. Ser.* 445, 279–291.

doi:10.3354/meps09423.

Halpern, B. S., Walbridge, S., Selkoe, K. A., Kappel, C. V, Micheli, F., D'Agrosa, C., et al. (2008). A global map of human impact on marine ecosystems. *Science* 319, 948–952. doi:10.1126/science.1149345.

Hammerschlag, N., McDonnell, L. H., Rider, M. J., Street, G. M., Hazen, E. L., Natanson, L. J., et al. (2022). Ocean warming alters the distributional range, migratory timing, and spatial protections of an apex predator, the tiger shark (*Galeocerdo cuvier*). *Glob. Chang. Biol.*, 1–16. doi:10.1111/gcb.16045.

Hammerschlag, N., and Sulikowski, J. (2011). Killing for conservation: the need for alternatives to lethal sampling of apex predatory sharks. *Endanger. Species Res.* 14, 135–140. doi:10.3354/esr00354.

Hammond, P. S. (2009). "Mark–Recapture," in *Encyclopedia of Marine Mammals*, eds. W. F. Perrin, B. Würsig, and J. G. M. Thewissen (London: Academic Press), 705–709. doi:10.1016/B978-0-12-373553-9.00163-2.

Harcourt, R., Sequeira, A. M. M., Zhang, X., Roquet, F., Komatsu, K., Heupel, M., et al. (2019). Animal-borne telemetry: an integral component of the ocean observing toolkit. *Front. Mar. Sci.* 6, 326. doi:10.3389/fmars.2019.00326.

Harrison, P. M., Gutowsky, L. F. G., Martins, E. G., Patterson, D. A., Leake, A., Cooke, S. J., et al. (2013). Diel vertical migration of adult burbot: a dynamic trade-off among feeding opportunity, predation avoidance, and bioenergetic gain. *Can. J. Fish. Aquat. Sci.* 70, 1765–1774. doi:10.1139/cjfas-2013-0183.

Harry, A. V, and Braccini, J. M. (2021). Caution over the use of ecological big data for conservation. *Nature* 595, E17–E19. doi:10.1038/s41586-021-03463-w.

Hartman, K. L., Fernandez, M., Wittich, A., and Azevedo, J. M. N. (2015). Sex differences in residency patterns of Risso's dolphins (*Grampus griseus*) in the Azores: causes and management implications. *Mar. Mammal Sci.* 31, 1153–1167. doi:10.1111/mms.12209.

Hays, G. C. (2003). A review of the adaptive significance and ecosystem consequences of zooplankton diel vertical migrations. *Hydrobiologia* 503, 163–170. doi:10.1023/B:HYDR.0000008476.23617.b0.

Hays, G. C., Bailey, H., Bograd, S. J., Bowen, W. D., Campagna, C., Carmichael, R. H., et al. (2019). Translating marine animal tracking data into conservation policy and management.

Trends Ecol. Evol. 34, 459–473. doi:10.1016/j.tree.2019.01.009.

Hays, G. C., and Hawkes, L. A. (2018). Satellite tracking sea turtles: opportunities and challenges to address key questions. *Front. Mar. Sci.* 5, 432. doi:10.3389/fmars.2018.00432.

Hays, G. C., Rattray, A., and Esteban, N. (2020). Addressing tagging location bias to assess space use by marine animals. *J. Appl. Ecol.* 57, 1981–1987. doi:10.1111/1365-2664.13720.

Hazen, E. L., Abrahms, B., Brodie, S., Carroll, G., Jacox, M. G., Savoca, M. S., et al. (2019). Marine top predators as climate and ecosystem sentinels. *Front. Ecol. Environ.* 17, 565–574. doi:10.1002/fee.2125.

Heath, M. R., Neat, F. C., Pinnegar, J. K., Reid, D. G., Sims, D. W., and Wright, P. J. (2012). Review of climate change impacts on marine fish and shellfish around the UK and Ireland. *Aquat. Conserv. Mar. Freshw. Ecosyst.* 22, 337–367. doi:10.1002/aqc.2244.

Heberer, C., Aalbers, S. A., Bernal, D., Kohin, S., DiFiore, B., and Sepulveda, C. A. (2010). Insights into catch-and-release survivorship and stress-induced blood biochemistry of common thresher sharks (*Alopias vulpinus*) captured in the southern California recreational fishery. *Fish. Res.* 106, 495–500. doi:10.1016/j.fishres.2010.09.024.

Hedger, R. D., Martin, F., Dodson, J. J., Hatin, D., Caron, F., and Whoriskey, F. G. (2008). The optimized interpolation of fish positions and speeds in an array of fixed acoustic receivers. *ICES J. Mar. Sci.* 65, 1248–1259. doi:10.1093/icesjms/fsn109.

Hertel, A. G., Niemelä, P. T., Dingemanse, N. J., and Mueller, T. (2020). A guide for studying among-individual behavioral variation from movement data in the wild. *Mov. Ecol.* 8, 30. doi:10.1186/s40462-020-00216-8.

Heupel, M. R., Lédée, E. J. I., and Simpfendorfer, C. A. (2018). Telemetry reveals spatial separation of co-occurring reef sharks. *Mar. Ecol. Prog. Ser.* 589, 179–192. doi:10.3354/meps12423.

Heupel, M. R., Semmens, J. M., and Hobday, A. J. (2006). Automated acoustic tracking of aquatic animals: scales, design and deployment of listening station arrays. *Mar. Freshw. Res.* 57, 1–13. doi:10.1071/MF05091.

Heupel, M. R., and Simpfendorfer, C. A. (2008). Movement and distribution of young bull sharks *Carcharhinus leucas* in a variable estuarine environment. *Aquat. Biol.* 1, 277–289. doi:10.3354/AB00030.

Heupel, M. R., and Simpfendorfer, C. A. (2010). Science or slaughter: need for lethal sampling of

sharks. *Conserv. Biol.* 24, 1212–1218. doi:10.1111/j.1523-1739.2010.01491.x.

Hijmans, R. J. (2020). raster: Geographic data analysis and modeling. R package version 3.3-13. Available at: https://cran.r-project.org/package=raster.

Holbrook, C., Hayden, T., Binder, T., and Pye, J. (2020). glatos: A package for the Great Lakes Acoustic Telemetry Observation System. R package version 0.4.2. Available at: https://gitlab.oceantrack.org/GreatLakes/glatos.

Hoolihan, J. P., Luo, J., Abascal, F. J., Campana, S. E., De Metrio, G., Dewar, H., et al. (2011). Evaluating post-release behaviour modification in large pelagic fish deployed with pop-up satellite archival tags. *ICES J. Mar. Sci.* 68, 880–889. doi:10.1093/icesjms/fsr024.

Hopkins, C. R., Bailey, D. M., and Potts, T. (2016). Scotland's Marine Protected Area network: reviewing progress towards achieving commitments for marine conservation. *Mar. Policy* 71, 44–53. doi:10.1016/j.marpol.2016.05.015.

Horn, B. K. P. (1981). Hill shading and the reflectance map. *Proc. IEEE* 69, 14–47. doi:10.1109/PROC.1981.11918.

Hostetter, N. J., and Royle, J. A. (2020). Movement-assisted localization from acoustic telemetry data. *Mov. Ecol.* 8, 15. doi:10.1186/s40462-020-00199-6.

Howe, J. A., Anderton, R., Arosio, R., Dove, D., Bradwell, T., Crump, P., et al. (2014). The seabed geomorphology and geological structure of the Firth of Lorn, western Scotland, UK, as revealed by multibeam echo-sounder survey. *Earth Environ. Sci. Trans. R. Soc. Edinburgh* 105, 273–284. doi:10.1017/S1755691015000146.

Hudson, I. L., Kim, S. W., and Keatley, M. R. (2010). "Climatic influences on the flowering phenology of four eucalypts: a GAMLSS Approach," in *Phenological Research*, eds. I. L. Hudson and M. R. Keatley (Dordrecht: Springer Netherlands), 209–228. doi:10.1007/978-90-481-3335-2_10.

Hughes, B. B., Beas-Luna, R., Barner, A. K., Brewitt, K., Brumbaugh, D. R., Cerny-Chipman, E. B., et al. (2017). Long-term studies contribute disproportionately to ecology and policy. *Bioscience* 67, 271–281. doi:10.1093/biosci/biw185.

Humphries, N. E., Simpson, S. J., and Sims, D. W. (2017). Diel vertical migration and central place foraging in benthic predators. *Mar. Ecol. Prog. Ser.* 582, 163–180. doi:10.3354/meps12324.

Humphries, N. E., Simpson, S. J., Wearmouth, V. J., and Sims, D. W. (2016). Two's company,

three's a crowd: Fine-scale habitat partitioning by depth among sympatric species of marine mesopredator. *Mar. Ecol. Prog. Ser.* 561, 173–187. doi:10.3354/meps11937.

Hunter, E., Aldridge, J. N., Metcalfe, J. D., and Arnold, G. P. (2003). Geolocation of free-ranging fish on the European continental shelf as determined from environmental variables. *Mar. Biol.* 142, 601–609. doi:10.1007/s00227-002-0984-5.

Hunter, E., Berry, F., Buckley, A. A., Stewart, C., and Metcalfe, J. D. (2006). Seasonal migration of thornback rays and implications for closure management. *J. Appl. Ecol.* 43, 710–720. doi:10.1111/j.1365-2664.2006.01194.x.

Hunter, E., Buckley, A. A., Steward, C., and Metcalfe, J. D. (2005a). Repeated seasonal migration by a thornback ray in the southern North Sea. *J. Mar. Biol. Assoc. United Kingdom* 85, 1199–1200. doi:10.1017/S0025315405012300.

Hunter, E., Buckley, A. A., Stewart, C., and Metcalfe, J. D. (2005b). Migratory behaviour of the thornback ray, *Raja clavata*, in the southern North Sea. *J. Mar. Biol. Assoc. United Kingdom* 85, 1095–1105. doi:10.1017/S0025315405012142.

Hussey, N. E., Kessel, S. T., Aarestrup, K., Cooke, S. J., Cowley, P. D., Fisk, A. T., et al. (2015). Aquatic animal telemetry: a panoramic window into the underwater world. *Science* 348, 1255642–10. doi:10.1126/science.1255642.

Hutchison, Z. L., Sigray, P., He, H., Gill, A. B., King, J., and Gibson, C. (2018a). Electromagnetic field (EMF) impacts on elasmobranch (shark, rays, and skates) and american lobster movement and migration from direct current cables. Sterling (VA): U.S. Department of the Interior, Bureau of Ocean Energy Management. OCS Study BOEM 2018-00.

Hutchison, Z., Sigray, P., He, H., Gill, A., King, J., and Gibson, C. (2018b). Electromagnetic field (EMF) impacts on elasmobranch (shark, rays, and skates) and american lobster movement and migration from direct current cables. Sterling (VA) Available at: https://tethys.pnnl.gov/sites/default/files/publications/Hutchison2018.pdf.

Hyatt, M. W., Anderson, P. A., and O'Donnell, P. M. (2016). Behavioral release condition score of bull and bonnethead sharks as a coarse indicator of stress. *J. Coast. Res.* 32, 1464–1472. doi:10.2112/JCOASTRES-D-15-00108.1.

Hyndes, G. A., Platell, M. E., Potter, I. C., and Lenanton, R. C. J. (1999). Does the composition of the demersal fish assemblages in temperate coastal waters change with depth and undergo consistent seasonal changes? *Mar. Biol.* 134, 335–352. doi:10.1007/s002270050551.

Iglésias, S. P., Toulhoat, L., and Sellos, D. Y. (2010). Taxonomic confusion and market mislabelling of threatened skates: important consequences for their conservation status. *Aquat. Conserv. Mar. Freshw. Ecosyst.* 20, 319–333. doi:10.1002/aqc.1083.

International Hydrographic Organization (2020). *International Hydrographic Organization standards for hydrographic surveys. IHO Publication No. 44*. 6th ed. Principauté de Monaco: International Hydrographic Organization Available at: https://iho.int/uploads/user/pubs/Drafts/S-44_Edition_6.0.0-Final.pdf.

Jackson, J. B. C., Kirby, M. X., Berger, W. H., Bjorndal, K. A., Botsford, L. W., Bourque, B. J., et al. (2001). Historical Overfishing and the Recent Collapse of Coastal Ecosystems. *Science* 293, 629–638. doi:10.1126/science.1059199.

Jackson, L. J., Trebitz, A. S., and Cottingham, K. L. (2000). An introduction to the practice of ecological modeling. *Bioscience* 50, 694–706. doi:10.1641/0006-3568(2000)050[0694:AITTPO]2.0.CO;2.

Jacoby, D. M. P., Croft, D. P., and Sims, D. W. (2012). Social behaviour in sharks and rays: analysis, patterns and implications for conservation. *Fish Fish.* 13, 399–417. doi:10.1111/j.1467-2979.2011.00436.x.

Jacoby, D. M. P., Fear, L. N., Sims, D. W., and Croft, D. P. (2014). Shark personalities? Repeatability of social network traits in a widely distributed predatory fish. *Behav. Ecol. Sociobiol.* 68, 1995–2003. doi:10.1007/s00265-014-1805-9.

Jahn, A. E., Cueto, V. R., Fontana, C. S., Guaraldo, A. C., Levey, D. J., Marra, P. P., et al. (2020). Bird migration within the Neotropics. *Auk* 137, ukaa033. doi:10.1093/auk/ukaa033.

Johnson, M., Aguilar de Soto, N., and Madsen, P. T. (2009). Studying the behaviour and sensory ecology of marine mammals using acoustic recording tags: a review. *Mar. Ecol. Prog. Ser.* 395, 55–73. doi:10.3354/meps08255.

Johnson, M. P., Lordan, C., and Power, A. M. (2013). "Chapter Two - habitat and ecology of *Nephrops norvegicus*," in *Advances in Marine Biology*, eds. M. L. Johnson and M. P. B. T.-A. in M. B. Johnson (Academic Press), 27–63. doi:10.1016/B978-0-12-410466-2.00002-9.

Jordan, L. K., Mandelman, J. W., McComb, D. M., Fordham, S. V, Carlson, J. K., and Werner, T. B. (2013). Linking sensory biology and fisheries bycatch reduction in elasmobranch fishes: a review with new directions for research. *Conserv. Physiol.* 1, cot002. doi:10.1093/conphys/cot002.

Kabasakal, H. (2010). Post-release behavior and anthropogenic injuries of the bluntnose sixgill shark, *Hexanchus griseus* (Bonnaterre, 1788) (Chondrichthyes: Hexanchidae) in Turkish waters. *Ann. Ser. Hist. Nat.* 20, 39–46.

Kawabe, R., Naito, Y., Sato, K., Miyashita, K., and Yamashita, N. (2004). Direct measurement of the swimming speed, tailbeat, and body angle of Japanese flounder (*Paralichthys olivaceus*). *ICES J. Mar. Sci.* 61, 1080–1087. doi:10.1016/j.icesjms.2004.07.014.

Kays, R., Crofoot, M. C., Jetz, W., and Wikelski, M. (2015). Terrestrial animal tracking as an eye on life and planet. *Science* 348, aaa2478. doi:10.1126/science.aaa2478.

Keen, E., Falcone, E., Andrews, R. D., and Schorr, G. (2019). Diel dive behavior of fin whales (*Balaenoptera physalus*) in the Southern California Bight. *Aquat. Mamm.* 45, 233–243. doi:10.1578/AM.45.2.2019.233.

Kéry, M., and Schmidt, B. R. (2008). Imperfect detection and its consequences for monitoring for conservation. *Community Ecol.* 9, 207–216. doi:10.1556/ComEc.9.2008.2.10.

Kessel, S. T., Cooke, S. J., Heupel, M. R., Hussey, N. E., Simpfendorfer, C. A., Vagle, S., et al. (2014). A review of detection range testing in aquatic passive acoustic telemetry studies. *Rev. Fish Biol. Fish.* 24, 199–218. doi:10.1007/s11160-013-9328-4.

Kessel, S. T., Hussey, N. E., Crawford, R. E., Yurkowski, D. J., O'Neill, C. V, and Fisk, A. T. (2016). Distinct patterns of Arctic cod (*Boreogadus saida*) presence and absence in a shallow high Arctic embayment, revealed across open-water and ice-covered periods through acoustic telemetry. *Polar Biol.* 39, 1057–1068. doi:10.1007/s00300-015-1723-y.

Kinney, M. J., and Simpfendorfer, C. A. (2009). Reassessing the value of nursery areas to shark conservation and management. *Conserv. Lett.* 2, 53–60. doi:10.1111/j.1755-263X.2008.00046.x.

Klöcker, C. A. (2019). *From Transmissions to Detections: The impact of environmental variation on acoustic detection probability and its implications for spatial management in a Marine Protected Area.* MSc Thesis. University of St Andrews.

Kneebone, J., Chisholm, J. M., and Skomal, G. (2012). Seasonal residency, habitat use, and site fidelity of juvenile sand tiger sharks *Carcharias taurus* in a Massachusetts estuary. *Mar. Ecol. Prog. Ser.* 471, 165–181. doi:10.3354/MEPS09989.

Knip, D. M., Heupel, M. R., Simpfendorfer, C. A., Tobin, A. J., and Moloney, J. (2011a). Ontogenetic shifts in movement and habitat use of juvenile pigeye sharks *Carcharhinus*

amboinensis in a tropical nearshore region. *Mar. Ecol. Prog. Ser.* 425, 233–246. doi:10.3354/meps09006.

Knip, D. M., Heupel, M. R., Simpfendorfer, C. A., Tobin, A. J., and Moloney, J. (2011b). Wet-season effects on the distribution of juvenile pigeye sharks, *Carcharhinus amboinensis*, in tropical nearshore waters. *Mar. Freshw. Res.* 62, 658–667. doi:10.1071/MF10136.

Kock, A. A., Photopoulou, T., Durbach, I., Mauff, K., Meÿer, M., Kotze, D., et al. (2018). Summer at the beach: spatio-temporal patterns of white shark occurrence along the inshore areas of False Bay, South Africa. *Mov. Ecol.* 6, 7. doi:10.1186/s40462-018-0125-5.

Kohler, N. E., and Turner, P. A. (2001). Shark Tagging: a review of conventional methods and studies. *Environ. Biol. Fishes* 60, 191–224. doi:10.1023/A:1007679303082.

Kotwicki, S., and Weinberg, K. L. (2005). Estimating capture probability of a survey bottom trawl for Bering Sea skates (*Bathyraja* spp.) and other fish. *Alaska Fish. Res. Bull.* 11, 135–145.

Kranstauber, B., Kays, R., Lapoint, S. D., Wikelski, M., and Safi, K. (2012). A dynamic Brownian bridge movement model to estimate utilization distributions for heterogeneous animal movement. *J. Anim. Ecol.* 81, 738–746. doi:10.1111/j.1365-2656.2012.01955.x.

Kronfeld-Schor, N., Dominoni, D., de la Iglesia, H., Levy, O., Herzog, E. D., Dayan, T., et al. (2013). Chronobiology by moonlight. *Proc. R. Soc. B Biol. Sci.* 280, 20123088. doi:10.1098/rspb.2012.3088.

Krumme, U. (2009). "Diel and tidal movements by fish and decapods linking tropical coastal ecosystems," in *Ecological Connectivity among Tropical Coastal Ecosystems*, ed. I. Nagelkerken (Dordrecht: Springer Netherlands), 271–324. doi:10.1007/978-90-481-2406-0_8.

Kuempel, C. D., Jones, K. R., Watson, J. E. M., and Possingham, H. P. (2019). Quantifying biases in marine-protected-area placement relative to abatable threats. *Conserv. Biol.* 33, 1350–1359. doi:10.1111/cobi.13340.

Kuhnz, L. A., Bizzarro, J. J., and Ebert, D. A. (2019). In situ observations of deep-living skates in the eastern North Pacific. *Deep Sea Res. Part I Oceanogr. Res. Pap.* 152, 103104. doi:/10.1016/j.dsr.2019.103104.

Kynoch, R. J., Fryer, R. J., and Neat, F. C. (2015). A simple technical measure to reduce bycatch and discard of skates and sharks in mixed-species bottom-trawl fisheries. *ICES J. Mar. Sci.* 72, 1861–1868. doi:10.1093/icesjms/fsv037.

Langton, R., Stirling, D. A., Boulcott, P., and Wright, P. J. (2020). Are MPAs effective in removing fishing pressure from benthic species and habitats? *Biol. Conserv.* 247, 108511. doi:10.1016/j.biocon.2020.108511.

Larmet, V. (2019). cppRouting: Fast implementation of Dijkstra algorithm in R. R package version 2.0. Available at: https://github.com/vlarmet/cppRouting.

Last, P. R., Weigmann, S., and Yang, L. (2016). "Changes to the nomenclature of the skates (Chondrichthyes: Rajiformes)," in *Rays of the World* (CSIRO Australian National Fish Collection).

Lauria, V., Gristina, M., Attrill, M. J., Fiorentino, F., and Garofalo, G. (2015). Predictive habitat suitability models to aid conservation of elasmobranch diversity in the central Mediterranean Sea. *Sci. Rep.* 5, 13245. doi:10.1038/srep13245.

Lavender, E. (2020a). prettyGraphics: Pretty graphics with R. R package version 0.1.0. Available at: https://github.com/edwardlavender/prettyGraphics.

Lavender, E. (2020b). flapper: Routines for the analysis of passive acoustic telemetry data. R package version 0.1.0. Available at: https://github.com/edwardlavender/flapper.

Lavender, E. (2020c). Tools4ETS: Tools for ecological time series. R package version 0.1.0. Available at: https://github.com/edwardlavender/Tools4ETS.

Lavender, E. (2020d). MEFS: The Movement Ecology of Flapper Skate (MEFS) Project Datasets. R package version 0.1.0. Available at: https://github/edwardlavender/MEFS.

Lavender, E. (2020e). fvcom.tbx: An R toolbox for the unstructured grid Finite Volume Community Ocean Model (FVCOM). R package version 0.1.0. Available at: https://github.com/edwardlavender/fvcom.tbx.

Lavender, E., Aleynik, D., Dodd, J., Illian, J., James, M., Wright, P. J., et al. (2021a). Movement patterns of a Critically Endangered elasmobranch (*Dipturus intermedius*) in a Marine Protected Area. *Aquat. Conserv. Mar. Freshw. Ecosyst.* 32, 348–365. doi:10.1002/aqc.3753.

Lavender, E., Fox, C. J., and Burrows, M. T. (2021b). Modelling the impacts of climate change on thermal habitat suitability for shallow-water marine fish at a global scale. *PLoS One* 16, e0258184. doi:0.1371/journal.pone.0258184.

Lawson, C. L., Halsey, L. G., Hays, G. C., Dudgeon, C. L., Payne, N. L., Bennett, M. B., et al. (2019). Powering ocean giants: the energetics of shark and ray megafauna. *Trends Ecol. Evol.* 34, 1009–1021. doi:10.1016/j.tree.2019.07.001.

Lawson, G. L., Hückstädt, L. A., Lavery, A. C., Jaffré, F. M., Wiebe, P. H., Fincke, J. R., et al. (2015). Development of an animal-borne “sonar tag” for quantifying prey availability: test deployments on northern elephant seals. *Anim. Biotelemetry* 3, 22. doi:10.1186/s40317-015-0054-7.

Lazaridis, E. (2014). lunar: Lunar phase & distance, seasons and other environmental factors. R package version 0.1-04. Available at: http://statistics.lazaridis.eu.

Le Port, A., Sippel, T., and Montgomery, J. C. (2008). Observations of mesoscale movements in the short-tailed stingray, *Dasyatis brevicaudata* from New Zealand using a novel PSAT tag attachment method. *J. Exp. Mar. Bio. Ecol.* 359, 110–117. doi:10.1016/j.jembe.2008.02.024.

Lea, J. S. E., Humphries, N. E., von Brandis, R. G., Clarke, C. R., and Sims, D. W. (2016). Acoustic telemetry and network analysis reveal the space use of multiple reef predators and enhance marine protected area design. *Proc. R. Soc. B Biol. Sci.* 283, 20160717. doi:10.1098/rspb.2016.0717.

Lear, K. O., Whitney, N. M., Morgan, D. L., Brewster, L. R., Whitty, J. M., Poulakis, G. R., et al. (2019). Thermal performance responses in free-ranging elasmobranchs depend on habitat use and body size. *Oecologia* 191, 829–842. doi:10.1007/s00442-019-04547-1.

Lees, K. J., MacNeil, M. A., Hedges, K. J., and Hussey, N. E. (2021). Estimating demographic parameters for fisheries management using acoustic telemetry. *Rev. Fish Biol. Fish.* 31, 25–51. doi:10.1007/s11160-020-09626-8.

Levin, S. A. (1992). The problem of pattern and scale in ccology: the Robert H. MacArthur award lecture. *Ecology* 73, 1943–1967. doi:10.2307/1941447.

Little, W. (1995). Common skate and tope: first results of Glasgow museum’s tagging study. *Glas. Nat.* 22, 455–466.

Little, W. (1997). Common skate in the Sound of Mull. *Glaucus* 8, 42–43.

MacKeracher, T., Diedrich, A., and Simpfendorfer, C. A. (2019). Sharks, rays and marine protected areas: a critical evaluation of current perspectives. *Fish Fish.* 20, 255–267. doi:10.1111/faf.12337.

Martin, C. S., Vaz, S., Ellis, J. R., Lauria, V., Coppin, F., and Carpentier, A. (2012). Modelled distributions of ten demersal elasmobranchs of the eastern English Channel in relation to the environment. *J. Exp. Mar. Bio. Ecol.* 418–419, 91–103. doi:10.1016/j.jembe.2012.03.010.

Martin, R. A. (2007). A review of shark agonistic displays: comparison of display features and

implications for shark–human interactions. *Mar. Freshw. Behav. Physiol.* 40, 3–34. doi:10.1080/10236240601154872.

Mate, B. R., Ilyashenko, V. Y., Bradford, A. L., Vertyankin, V. V, Tsidulko, G. A., Rozhnov, V. V, et al. (2015). Critically endangered western gray whales migrate to the eastern North Pacific. *Biol. Lett.* 11, 20150071. doi:10.1098/rsbl.2015.0071.

Matern, S. A., Cech, J. J., and Hopkins, T. E. (2000). Diel movements of bat rays, *Myliobatis californica*, in Tomales Bay, California: evidence for behavioral thermoregulation? *Environ. Biol. Fishes* 58, 173–182. doi:10.1023/A:1007625212099.

Matley, J. K., Klinard, N. V, Barbosa Martins, A. P., Aarestrup, K., Aspillaga, E., Cooke, S. J., et al. (2022). Global trends in aquatic animal tracking with acoustic telemetry. *Trends Ecol. Evol.* 37, 79–94. doi:10.1016/j.tree.2021.09.001.

McCauley, D. J., Pinsky, M. L., Palumbi, S. R., Estes, J. A., Joyce, F. H., and Warner, R. R. (2015). Marine defaunation: animal loss in the global ocean. *Science* 347, 1255641. doi:10.1126/science.1255641.

McLeod, K. L., Lubchenco, J., Palumbi, S. R., and Rosenberg, A. A. (2005). Scientific consensus statement on marine ecosystem-based management. Signed by 221 academic scientists and policy experts with relevant expertise and published by the Communication Partnership for Science and the Sea. Available at: http://compassonline.org/?q=EBM.

Mercker, M., Schwemmer, P., Peschko, V., Enners, L., and Garthe, S. (2021). Analysis of local habitat selection and large-scale attraction/avoidance based on animal tracking data: is there a single best method? *Mov. Ecol.* 9, 20. doi:10.1186/s40462-021-00260-y.

Merrifield, M., Gleason, M., Bellquist, L., Kauer, K., Oberhoff, D., Burt, C., et al. (2019). eCatch: Enabling collaborative fisheries management with technology. *Ecol. Inform.* 52, 82–93. doi:10.1016/j.ecoinf.2019.05.010.

Metcalfe, J. D., Arnold, G. P., and Webb, P. W. (1990). The energetics of migration by selective tidal stream transport: an analysis for plaice tracked in the southern North Sea. *J. Mar. Biol. Assoc. United Kingdom* 70, 149–162. doi:10.1017/S0025315400034275.

Migaud, H., Davie, A., and Taylor, J. F. (2010). Current knowledge on the photoneuroendocrine regulation of reproduction in temperate fish species. *J. Fish Biol.* 76, 27–68. doi:10.1111/j.1095-8649.2009.02500.x.

Milligan, R. J., Scott, E. M., Jones, D. O. B., Bett, B. J., Jamieson, A. J., O'Brien, R., et al. (2020).

Evidence for seasonal cycles in deep-sea fish abundances: a great migration in the deep SE Atlantic? *J. Anim. Ecol.* 89, 1593–1603. doi:10.1111/1365-2656.13215.

Mittelbach, G. G., Ballew, N. G., and Kjelvik, M. K. (2014). Fish behavioral types and their ecological consequences. *Can. J. Fish. Aquat. Sci.* 71, 927–944. doi:10.1139/cjfas-2013-0558.

Mohan, J. A., Jones, E. R., Hendon, J. M., Falterman, B., Boswell, K. M., Hoffmayer, E. R., et al. (2020). Capture stress and post-release mortality of blacktip sharks in recreational charter fisheries of the Gulf of Mexico. *Conserv. Physiol.* 8, coaa041. doi:10.1093/conphys/coaa041.

Molina, J. M., and Cooke, S. J. (2012). Trends in shark bycatch research: current status and research needs. *Rev. Fish Biol. Fish.* 22, 719–737. doi:10.1007/s11160-012-9269-3.

Moll, A., and Radach, G. (2003). Review of three-dimensional ecological modelling related to the North Sea shelf system: Part 1: models and their results. *Prog. Oceanogr.* 57, 175–217. doi:10.1016/S0079-6611(03)00067-3.

Monk, C. T., Bekkevold, D., Klefoth, T., Pagel, T., Palmer, M., and Arlinghaus, R. (2021). The battle between harvest and natural selection creates small and shy fish. *Proc. Natl. Acad. Sci.* 118, e2009451118. doi:10.1073/pnas.2009451118.

Mora, T., Walczak, A. M., Del Castello, L., Ginelli, F., Melillo, S., Parisi, L., et al. (2016). Local equilibrium in bird flocks. *Nat. Phys.* 12, 1153–1157. doi:10.1038/nphys3846.

Morel, G. M., Shrives, J., Bossy, S. F., and Meyer, C. G. (2013). Residency and behavioural rhythmicity of ballan wrasse (*Labrus bergylta*) and rays (*Raja* spp.) captured in Portelet Bay, Jersey: Implications for Marine Protected Area design. *J. Mar. Biol. Assoc. United Kingdom* 93, 1407–1414. doi:10.1017/S0025315412001725.

Morrissey, J. F., and Gruber, S. H. (1993). Habitat selection by juvenile lemon sharks, *Negaprion brevirostris*. *Environ. Biol. Fishes* 38, 311–319. doi:10.1007/BF00007524.

Mucientes, G. R., Queiroz, N., Sousa, L. L., Tarroso, P., and Sims, D. W. (2009). Sexual segregation of pelagic sharks and the potential threat from fisheries. *Biol. Lett.* 5, 156–159. doi:10.1098/rsbl.2008.0761.

Mullen, E. J., Schoen, A. N., Hauger, M. D., Murray, L., and Anderson, W. G. (2020). Angler experience and seasonal effects on the response of the lake sturgeon to catch-and-release angling. *Trans. Am. Fish. Soc.* 149, 709–720. doi:10.1002/tafs.10266.

Mullen, R. J., Monekosso, D., Barman, S., and Remagnino, P. (2009). A review of ant algorithms.

Expert Syst. Appl. 36, 9608–9617. doi:10.1016/j.eswa.2009.01.020.

Musyl, M. K., and Gilman, E. L. (2019). Meta-analysis of post-release fishing mortality in apex predatory pelagic sharks and white marlin. *Fish Fish.* 20, 466–500. doi:10.1111/faf.12358.

Nathan, R., Getz, W. M., Revilla, E., Holyoak, M., Kadmon, R., Saltz, D., et al. (2008). A movement ecology paradigm for unifying organismal movement research. *Proc. Natl. Acad. Sci.* 105, 19052–19059. doi:10.1073/pnas.0800375105.

Nathan, R., Monk, C. T., Arlinghaus, R., Adam, T., Alós, J., Assaf, M., et al. (2022). Big-data approaches lead to an increased understanding of the ecology of animal movement. *Science* 375, eabg1780. doi:10.1126/science.abg1780.

NatureScot (2021). Protection of flapper skate - NatureScot advice to the Scottish Government regarding flapper skate eggs in the Inner Sound. Available at: https://www.gov.scot/binaries/content/documents/govscot/publications/advice-and-guidance/2021/03/protection-flapper-skate-naturescot-advice-scottish-government-regarding-flapper-skate-eggs-inner-sound/documents/protection-flapper-skate-naturescot-advice-s.

Neat, F. C., Wright, P. J., Zuur, A. F., Gibb, I. M., Gibb, F. M., Tulett, D., et al. (2006). Residency and depth movements of a coastal group of Atlantic cod (*Gadus morhua* L.). *Mar. Biol.* 148, 643–654. doi:10.1007/s00227-005-0110-6.

Neat, F., Pinto, C., Burrett, I., Cowie, L., Travis, J., Thorburn, J., et al. (2015). Site fidelity, survival and conservation options for the threatened flapper skate (*Dipturus cf. intermedia*). *Aquat. Conserv. Mar. Freshw. Ecosyst.* 25, 6–20. doi:10.1002/aqc.2472.

Neilson, J. D., and Perry, R. I. (1990). “Diel vertical migrations of marine fishes: an obligate or facultative process?,” in *Advances in Marine Biology*, eds. J. H. S. Blaxter and A. J. Southward (Cambridge, MA: Academic Press), 115–168. doi:10.1016/S0065-2881(08)60200-X.

Nichol, D. G., and Chilton, E. A. (2006). Recuperation and behaviour of Pacific cod after barotrauma. *ICES J. Mar. Sci.* 63, 83–94. doi:10.1016/j.icesjms.2005.05.021.

Niella, Y., Flávio, H., Smoothey, A. F., Aarestrup, K., Taylor, M. D., Peddemors, V. M., et al. (2020). Refined Shortest Paths (RSP): incorporation of topography in space use estimation from node-based telemetry data. *Methods Ecol. Evol.* 11, 1733–1742. doi:10.1111/2041-210X.13484.

Nosal, D. C., Cartamil, D. C., Long, J. W., Luhrmann, M., Wegner, N. C., and Graham, J. B. (2013). Demography and movement patterns of leopard sharks (*Triakis semifasciata*) aggregating near the head of a submarine canyon along the open coast of southern California, USA. *Environ. Biol. Fishes* 96, 865–878. doi:10.1007/s10641-012-0083-5.

O'Leary, B. C., Ban, N. C., Fernandez, M., Friedlander, A. M., García-Borboroglu, P., Golbuu, Y., et al. (2018). Addressing criticisms of large-scale marine protected areas. *Bioscience* 68, 359–370. doi:10.1093/biosci/biy021.

Ogburn, M. B., Harrison, A.-L., Whoriskey, F. G., Cooke, S. J., Mills Flemming, J. E., and Torres, L. G. (2017). Addressing challenges in the application of animal movement ecology to aquatic conservation and management. *Front. Mar. Sci.* 4, 70. doi:10.3389/fmars.2017.00070.

Oliver, S., Braccini, M., Newman, S. J., and Harvey, E. S. (2015). Global patterns in the bycatch of sharks and rays. *Mar. Policy* 54, 86–97. doi:10.1016/j.marpol.2014.12.017.

Orlov, A. (2003). Diets, feeding habits, and trophic relations of six deep-benthic skates (Rajidae) in the western Bering Sea. *J. Ichthyol. Aquat. Biol.* 7, 45–60.

Orrell, D. L., and Hussey, N. E. (2022). Using the VEMCO Positioning System (VPS) to explore fine-scale movements of aquatic species: applications, analytical approaches and future directions. *Mar. Ecol. Prog. Ser.* 687, 195–216. doi:10.3354/meps14003.

Pacoureau, N., Rigby, C. L., Kyne, P. M., Sherley, R. B., Winker, H., Carlson, J. K., et al. (2021). Half a century of global decline in oceanic sharks and rays. *Nature* 589, 567–571. doi:10.1038/s41586-020-03173-9.

Padian, K. (2018). Narrative and "anti-narrative" in science: how scientists tell stories, and don't. *Integr. Comp. Biol.* 58, 1224–1234. doi:10.1093/icb/icy038.

Papastamatiou, Y. P., Bodey, T. W., Friedlander, A. M., Lowe, C. G., Bradley, D., Weng, K., et al. (2018a). Spatial separation without territoriality in shark communities. *Oikos* 127, 767–779. doi:10.1111/oik.04289.

Papastamatiou, Y. P., Friedlander, A. M., Caselle, J. E., and Lowe, C. G. (2010). Long-term movement patterns and trophic ecology of blacktip reef sharks (*Carcharhinus melanopterus*) at Palmyra Atoll. *J. Exp. Mar. Bio. Ecol.* 386, 94–102. doi:10.1016/j.jembe.2010.02.009.

Papastamatiou, Y. P., and Lowe, C. G. (2012). An analytical and hypothesis-driven approach to elasmobranch movement studies. *J. Fish Biol.* 80, 1342–1360. doi:10.1111/j.1095-

8649.2012.03232.x.

Papastamatiou, Y. P., Watanabe, Y. Y., Bradley, D., Dee, L. E., Weng, K., Lowe, C. G., et al. (2015). Drivers of daily routines in an ectothermic marine predator: hunt warm, rest warmer? *PLoS One* 10, e0127807. doi:10.1371/journal.pone.0127807.

Papastamatiou, Y. P., Watanabe, Y. Y., Demšar, U., Leos-Barajas, V., Bradley, D., Langrock, R., et al. (2018b). Activity seascapes highlight central place foraging strategies in marine predators that never stop swimming. *Mov. Ecol.* 6, 9. doi:10.1186/s40462-018-0127-3.

Pardini, A. T., Jones, C. S., Noble, L. R., Kreiser, B., Malcolm, H., Bruce, B. D., et al. (2001). Sex-biased dispersal of great white sharks. *Nature* 412, 139–140. doi:10.1038/35084125.

Parsons, D. M., Morrison, M. A., and Slater, M. J. (2010). Responses to marine reserves: Decreased dispersion of the sparid *Pagrus auratus* (snapper). *Biol. Conserv.* 143, 2039–2048. doi:10.1016/j.biocon.2010.05.009.

Parton, K. J., Galloway, T. S., and Godley, B. J. (2019). Global review of shark and ray entanglement in anthropogenic marine debris. *Endanger. Species Res.* 39, 173–190. doi:10.3354/esr00964.

Patrick, S. C., Bearhop, S., Grémillet, D., Lescroël, A., Grecian, W. J., Bodey, T. W., et al. (2014). Individual differences in searching behaviour and spatial foraging consistency in a central place marine predator. *Oikos* 123, 33–40. doi:10.1111/j.1600-0706.2013.00406.x.

Patrick, S. C., and Weimerskirch, H. (2014). Personality, foraging and fitness consequences in a long lived seabird. *PLoS One* 9, e87269. doi:10.1371/journal.pone.0087269.

Patterson, T. A., Parton, A., Langrock, R., Blackwell, P. G., Thomas, L., and King, R. (2016). Statistical modelling of individual animal movement: an overview of key methods and a discussion of practical challenges. doi:10.1007/s10182-017-0302-7.

Patterson, T. A., Parton, A., Langrock, R., Blackwell, P. G., Thomas, L., and King, R. (2017). Statistical modelling of individual animal movement: an overview of key methods and a discussion of practical challenges. *AStA Adv. Stat. Anal.* 101, 399–438. doi:10.1007/s10182-017-0302-7.

Pecl, G. T., Araújo, M. B., Bell, J. D., Blanchard, J., Bonebrake, T. C., Chen, I., et al. (2017). Biodiversity redistribution under climate change: Impacts on ecosystems and human well-being. *Science* 9214. doi:10.1126/science.aai9214.

Pedersen, E. J., Miller, D. L., Simpson, G. L., and Ross, N. (2019). Hierarchical generalized

additive models in ecology: an introduction with mgcv. *PeerJ* 7, e6876. doi:10.7717/peerj.6876.

Pedersen, M. W., Righton, D., Thygesen, U. H., Andersen, K. H., and Madsen, H. (2008). Geolocation of North Sea cod (*Gadus morhua*) using hidden Markov models and behavioural switching. *Can. J. Fish. Aquat. Sci.* 65, 2367–2377. doi:10.1139/F08-144.

Pedersen, M. W., and Weng, K. C. (2013). Estimating individual animal movement from observation networks. *Methods Ecol. Evol.* 4, 920–929. doi:10.1111/2041-210X.12086.

Peklova, I., Hussey, N. E., Hedges, K. J., Treble, M. A., and Fisk, A. T. (2014). Movement, depth and temperature preferences of an important bycatch species, Arctic skate *Amblyraja hyperborea*, in Cumberland Sound, Canadian Arctic. *Endanger. Species Res.* 23, 229–240. doi:10.3354/esr00563.

Phillips, N. D., Garbett, A., Wise, D., Loca, S. L., Daly, O., Eagling, L. E., et al. (2021a). Evidence of egg-laying grounds for critically endangered flapper skate (*Dipturus intermedius*) off Orkney, UK. *J. Fish Biol.* 99, 1492–1496. doi:10.1111/jfb.14817.

Phillips, N. M., Devloo-Delva, F., McCall, C., and Daly-Engel, T. S. (2021b). Reviewing the genetic evidence for sex-biased dispersal in elasmobranchs. *Rev. Fish Biol. Fish.* 31, 821–841. doi:10.1007/s11160-021-09673-9.

Phillips, R. A., Croxall, J. P., Silk, J. R. D., and Briggs, D. R. (2007). Foraging ecology of albatrosses and petrels from South Georgia: two decades of insights from tracking technologies. *Aquat. Conserv. Mar. Freshw. Ecosyst.* 17, S6–S21. doi:10.1002/aqc.906.

Pieraccini, M., Coppa, S., and De Lucia, G. A. (2017). Beyond marine paper parks? Regulation theory to assess and address environmental non-compliance. *Aquat. Conserv. Mar. Freshw. Ecosyst.* 27, 177–196. doi:10.1002/aqc.2632.

Pimiento, C., Leprieur, F., Silvestro, D., Lefcheck, S. J., Albouy, C., Rasher, D. B., et al. (2020). Functional diversity of marine megafauna in the Anthropocene. *Sci. Adv.* 6, eaay7650. doi:10.1126/sciadv.aay7650.

Pincock, D. G. (2012). False detections: what they are and how to remove them from detection data. Amirix Document DOC-004691 Version 03. Available at: http://vemco.com/wp-content/uploads/2012/11/false_detections.pdf.

Pinto, C., and Spezia, L. (2016). Markov switching autoregressive models for interpreting vertical movement data with application to an endangered marine apex predator. *Methods Ecol. Evol.*

7, 407–417. doi:10.1111/2041-210X.12494.

Pinto, C., Thorburn, J., Neat, F., Wright, P. J., Wright, S., Scott, B. E., et al. (2016). Using individual tracking data to validate the predictions of species distribution models. *Divers. Distrib.* 22, 682–693. doi:10.1111/ddi.12437.

Powell, R. A., and Mitchell, M. S. (2012). What is a home range? *J. Mammal.* 93, 948–958. doi:10.1644/11-MAMM-S-177.1.

Powell, S. G., Baker, K. R., and Lawson, B. (2008). A critical review of the literature on spreadsheet errors. *Decis. Support Syst.* 46, 128–138. doi:10.1016/j.dss.2008.06.001.

Pyke, G. H. (2015). Understanding movements of organisms: it's time to abandon the Lévy foraging hypothesis. *Methods Ecol. Evol.* 6, 1–16. doi:10.1111/2041-210X.12298.

Queiroz, N., Humphries, N. E., Couto, A., Vedor, M., da Costa, I., Sequeira, A. M. M., et al. (2019). Global spatial risk assessment of sharks under the footprint of fisheries. *Nature* 572, 461–466. doi:10.1038/s41586-019-1444-4.

Quick, N. J., Cioffi, W. R., Shearer, J. M., Fahlman, A., and Read, A. J. (2020). Extreme diving in mammals: first estimates of behavioural aerobic dive limits in Cuvier's beaked whales. *J. Exp. Biol.* 223, jeb222109. doi:10.1242/jeb.222109.

R Core Team (2020). R: a language and environment for statistical computing. Available at: https://r-project.org.

Radach, G., and Moll, A. (2003). Review of three-dimensional ecological modelling related to the north sea shelf system. Part II: Model validation and data needs. *Oceanogr. Mar. Biol.* 44, 1–60. doi:10.1016/S0079-6611(03)00067-3.

Ramsay, J. O., Graves, S., and Hooker, G. (2020). fda: Functional data analysis. R package version 5.1.5.1. Available at: https://cran.r-project.org/package=fda.

Randall, J. E. (1997). Contribution to the biology of the whitetip reef shark (*Triaenodon obesus*). *Pacific Sci.* 31, 143–164.

Raoult, V., Williamson, J., Smith, T., and Gaston, T. (2019). Effects of on-deck holding conditions and air exposure on post-release behaviours of sharks revealed by a remote operated vehicle. *J. Exp. Mar. Bio. Ecol.* 511, 10–18. doi:10.1016/j.jembe.2018.11.003.

Rechisky, E. L., Porter, A. D., Winchell, P. M., and Welch, D. W. (2020). Performance of a high-frequency (180 kHz) acoustic array for tracking juvenile Pacific salmon in the coastal ocean. *Anim. Biotelemetry* 8, 19. doi:10.1186/s40317-020-00205-z.

Régnier, T., Dodd, J., Benjamins, S., Gibb, F. M., and Wright, P. J. (2021). Age and growth of the Critically Endangered flapper skate, *Dipturus intermedius*. *Aquat. Conserv. Mar. Freshw. Ecosyst.* 31, 2381–2388. doi:10.1002/aqc.3654.

Reynolds, A. M. (2018). Current status and future directions of Lévy walk research. *Biol. Open* 7, bio030106. doi:10.1242/bio.030106.

Rhodes, K. L., Baremore, I., and Graham, R. T. (2019). Grouper (Epinephelidae) spawning aggregations affect activity space of grey reef sharks, *Carcharhinus amblyrhynchos*, in Pohnpei, Micronesia. *PLoS One* 14, e0221589. doi:10.1371/journal.pone.0221589.

Rigby, R. A., and Stasinopoulos, D. M. (2005). Generalized additive models for location, scale and shape. *J. R. Stat. Soc. Ser. C (Applied Stat.* 54, 507–554. doi:10.1111/j.1467-9876.2005.00510.x.

Rindorf, A., Gislason, H., Burns, F., Ellis, J. R., and Reid, D. (2020). Are fish sensitive to trawling recovering in the Northeast Atlantic? *J. Appl. Ecol.* 57, 1936–1947. doi:10.1111/1365-2664.13693.

Riotte-Lambert, L., and Matthiopoulos, J. (2020). Environmental predictability as a cause and consequence of animal movement. *Trends Ecol. Evol.* 35, 163–174. doi:10.1016/j.tree.2019.09.009.

Ritchie, J. (1923). Migrations in the sea - hake. *Scottish Nat.* 133–134, 15–17.

Roche, D. G., Careau, V., and Binning, S. A. (2016). Demystifying animal personality (or not): why individual variation matters to experimental biologists. *J. Exp. Biol.* 219, 3832–3843. doi:10.1242/jeb.146712.

Rodríguez-Cabello, C., and Sánchez, F. (2017). Catch and post-release mortalities of deep-water sharks caught by bottom longlines in the Cantabrian Sea (NE Atlantic). *J. Sea Res.* 130, 248–255. doi:0.1016/j.seares.2017.04.004.

Rogers, P. J., Knuckey, I., Hudson, R. J., Lowther, A. D., and Guida, L. (2017). Post-release survival, movement, and habitat use of school shark *Galeorhinus galeus* in the Great Australian Bight, southern Australia. *Fish. Res.* 187, 188–198. doi:10.1016/j.fishres.2016.11.011.

Rojo, I., Sánchez-Meca, J., and García-Charton, J. A. (2019). Small-sized and well-enforced Marine Protected Areas provide ecological benefits for piscivorous fish populations worldwide. *Mar. Environ. Res.* 149, 100–110. doi:10.1016/j.marenvres.2019.06.005.

Roycroft, E. J., Le Port, A., and Lavery, S. D. (2019). Population structure and male-biased dispersal in the short-tail stingray *Bathytoshia brevicaudata* (Myliobatoidei: Dasyatidae). *Conserv. Genet.* 20, 717–728. doi:10.1007/s10592-019-01167-3.

Rutz, C., Loretto, M.-C., Bates, A. E., Davidson, S. C., Duarte, C. M., Jetz, W., et al. (2020). COVID-19 lockdown allows researchers to quantify the effects of human activity on wildlife. *Nat. Ecol. Evol.* 4, 1156–1159. doi:10.1038/s41559-020-1237-z.

Saeedi, H., Costello, M. J., Warren, D., and Brandt, A. (2019). Latitudinal and bathymetrical species richness patterns in the NW Pacific and adjacent Arctic Ocean. *Sci. Rep.* 9, 9303. doi:10.1038/s41598-019-45813-9.

Schlaff, A. M., Heupel, M. R., and Simpfendorfer, C. A. (2014). Influence of environmental factors on shark and ray movement, behaviour and habitat use: a review. *Rev. Fish Biol. Fish.* 24, 1089–1103. doi:10.1007/s11160-014-9364-8.

Scott, J. D., Courtney, M. B., Farrugia, T. J., Nielsen, J. K., and Seitz, A. C. (2016). An approach to describe depth-specific periodic behavior in Pacific halibut (*Hippoglossus stenolepis*). *J. Sea Res.* 107, 6–13. doi:10.1016/j.seares.2015.06.003.

Scottish Natural Heritage (2013). Scottish MPA project data confidence assessment: Loch Sween Possible Nature Conservation MPA. Available at: https://apps.snh.gov.uk/sitelink-api/v1/sites/10419/documents/50.

Scottish Natural Heritage (2014). Scottish MPA project assessment against the MPA selection guidelines: Loch Sunart to the Sound of Jura Nature Conservation MPA. Available at: https://apps.snh.gov.uk/sitelink-api/v1/sites/10418/documents/51.

Secor, D. H., Bailey, H., Carroll, A., Lyubchich, V., O'Brien, M. H. P., and Wiernicki, C. J. (2021). Diurnal vertical movements in black sea bass (*Centropristis striata*): endogenous, facultative, or something else? *Ecosphere* 12, e03616. doi:10.1002/ecs2.3616.

Semmens, J. M., Kock, A. A., Watanabe, Y. Y., Shepard, C. M., Berkenpas, E., Stehfest, K. M., et al. (2019). Preparing to launch: biologging reveals the dynamics of white shark breaching behaviour. *Mar. Biol.* 166, 95. doi:10.1007/s00227-019-3542-0.

Sempere-Valverde, J., Sedano, F., Megina, C., García-Gómez, J. C., and Espinosa, F. (2019). Feeding behaviour of *Patella caerulea* L. and *P. rustica* L. under spring and neap simulated tides. An innovative approach for quick quantification of grazing activity. *Ethol. Ecol. Evol.* 31, 283–292. doi:10.1080/03949370.2018.1561525.

Sepulveda, C. A., Heberer, C., Aalbers, S. A., Spear, N., Kinney, M., Bernal, D., et al. (2015). Post-release survivorship studies on common thresher sharks (*Alopias vulpinus*) captured in the southern California recreational fishery. *Fish. Res.* 161, 102–108. doi:10.1016/j.fishres.2014.06.014.

Shaw, A. K. (2020). Causes and consequences of individual variation in animal movement. *Mov. Ecol.* 8, 12. doi:10.1186/s40462-020-0197-x.

Shepard, E., Ahmed, M., Southall, E. J., Witt, M., Metcalfe, J., and Sims, D. (2006). Diel and tidal rhythms in diving behaviour of pelagic sharks identified by signal processing of archival tagging data. *Mar. Ecol. Prog. Ser.* 328, 205–213. doi:10.3354/meps328205.

Shiffman, D. S., Gallagher, A. J., Boyle, M. D., Hammerschlag-Peyer, C. M., and Hammerschlag, N. (2012). Stable isotope analysis as a tool for elasmobranch conservation research: a primer for non-specialists. *Mar. Freshw. Res.* 63, 635–643. doi:10.1071/MF11235.

Sidortsov, M., Morgenstern, Y., and Be'er, A. (2017). Role of tumbling in bacterial swarming. *Phys. Rev. E* 96, 22407. doi:10.1103/PhysRevE.96.022407.

Silva, J. F., Ellis, J. R., and Catchpole, T. L. (2012). Species composition of skates (Rajidae) in commercial fisheries around the British Isles and their discarding patterns. *J. Fish Biol.* 80, 1678–1703. doi:10.1111/j.1095-8649.2012.03247.x.

Simpfendorfer, C. A., Heupel, M. R., and Hueter, R. E. (2002). Estimation of short-term centers of activity from an array of omnidirectional hydrophones and its use in studying animal movements. *Can. J. Fish. Aquat. Sci.* 59, 23–32. doi:10.1139/f01-191.

Simpfendorfer, C. A., Huveneers, C., Steckenreuter, A., Tattersall, K., Hoenner, X., Harcourt, R., et al. (2015). Ghosts in the data: false detections in VEMCO pulse position modulation acoustic telemetry monitoring equipment. *Anim. Biotelemetry* 3, 55. doi:10.1186/s40317-015-0094-z.

Simpfendorfer, C. A., Yeiser, B. G., Wiley, T. R., Poulakis, G. R., Stevens, P. W., and Heupel, M. R. (2011). Environmental influences on the spatial ecology of juvenile smalltooth sawfish (*Pristis pectinata*): results from acoustic monitoring. *PLoS One* 6, e16918. doi:10.1371/journal.pone.0016918.

Simpson, S. J., Humphries, N. E., and Sims, D. W. (2020). The spatial ecology of Rajidae from mark-recapture tagging and its implications for assessing fishery interactions and efficacy of Marine Protected Areas. *Fish. Res.* 228, 105569. doi:10.1016/j.fishres.2020.105569.

Sims, D. W., Southall, E. J., Humphries, N. E., Hays, G. C., Bradshaw, C. J. A., Pitchford, J. W., et al. (2008). Scaling laws of marine predator search behaviour. *Nature* 451, 1098–1102. doi:10.1038/nature06518.

Sims, D. W., Wearmouth, V. J., Southall, E. J., Hill, J. M., Moore, P., Rawlinson, K., et al. (2006). Hunt warm, rest cool: bioenergetic strategy underlying diel vertical migration of a benthic shark. *J. Anim. Ecol.* 75, 176–190. doi:10.1111/j.1365-2656.2005.01033.x.

Siskey, M. R., Shipley, O. N., and Frisk, M. G. (2019). Skating on thin ice: identifying the need for species-specific data and defined migration ecology of Rajidae spp. *Fish Fish.* 20, 286–302. doi:10.1111/faf.12340.

Skatespotter (2021). Data summary report - September 2021. Available at: https://skatespotter.sams.ac.uk/news/2019/Skatespotter summary Sep 2021.pdf.

Skomal, G. B. (2007). Evaluating the physiological and physical consequences of capture on post-release survivorship in large pelagic fishes. *Fish. Manag. Ecol.* 14, 81–89. doi:10.1111/j.1365-2400.2007.00528.x.

Smale, M. J., Sauer, W. H. H., and Hanlon, R. T. (1995). Attempted ambush predation on spawning squids *Loligo vulgaris reynaudii* by benthic pyjama sharks, *Poroderma africanum*, off South Africa. *J. Mar. Biol. Assoc. United Kingdom* 75, 739–742. doi:10.1017/S002531540003914X.

Smale, M., Sauer, W., and Roberts, M. (2001). Behavioural interactions of predators and spawning chokka squid off South Africa: towards quantification. *Mar. Biol.* 139, 1095–1105. doi:10.1007/s002270100664.

Smith, L. E. (2018). Plastic ingestion by *Scyliorhinus canicula* trawl captured in the North Sea. *Mar. Pollut. Bull.* 130, 6–7. doi:10.1016/j.marpolbul.2018.03.001.

Solandt, J.-L., Mullier, T., Elliott, S., and Sheehan, E. (2020). “Chapter 9 - Managing marine protected areas in Europe: Moving from ‘feature-based’ to ‘whole-site’ management of sites,” in *Marine Protected Areas: Science, Policy and Management*, eds. J. Humphreys and R. W. E. Clark (Oxford: Elsevier), 157–181. doi:10.1016/B978-0-08-102698-4.00009-5.

Sousa, I., Baeyaert, J., Gonçalves, J. M. S., and Erzini, K. (2019). Preliminary insights into the spatial ecology and movement patterns of a regionally critically endangered skate (*Rostroraja alba*) associated with a marine protected area. *Mar. Freshw. Behav. Physiol.* 52, 283–299. doi:10.1080/10236244.2019.1705805.

Sousa, I., Gonçalves, J. M. S., Claudet, J., Coelho, R., Gonçalves, E. J., and Erzini, K. (2018). Soft-bottom fishes and spatial protection: findings from a temperate marine protected area. *PeerJ* 6, e4653. doi:10.7717/peerj.4653.

Speed, C. W., Field, I. C., Meekan, M. G., and Bradshaw, C. J. A. (2010). Complexities of coastal shark movements and their implications for management. *Mar. Ecol. Prog. Ser.* 408, 275–293. doi:10.3354/meps08581.

Stasinopoulos, M., Rigby, B., Voudouris, V., and Kiose, D. (2020). gamlss.add: Extra additive terms for Generalized Additive Models for Location Scale and Shape. R package version 5.1-6. Available at: https://cran.r-project.org/package=gamlss.add.

Steven, G. A. (1947). The British Rajidae. *Sci. Prog.* 35, 220–236.

Stokes, D., Gerritsen, H., O'Hea, B., Moore, S. J., and Dransfeld, L. (2014). Irish Groundfish Survey Cruise Report, Sept. 24th – Dec. 17th, 2014. Available at: https://oar.marine.ie/handle/10793/1064.

Stuart-Smith, R. D., Edgar, G. J., and Bates, A. E. (2017). Thermal limits to the geographic distributions of shallow-water marine species. *Nat. Ecol. Evol.* 1, 1846–1852. doi:10.1038/s41559-017-0353-x.

Subbey, S., Michalsen, K., and Nilsen, G. K. (2008). A tool for analyzing information from data storage tags: the continuous wavelet transform (CWT). *Rev. Fish Biol. Fish.* 18, 301–312. doi:10.1007/s11160-007-9078-2.

Sun, C. C., Fuller, A. K., and Royle, J. A. (2014). Trap configuration and spacing influences parameter estimates in spatial capture-recapture models. *PLoS One* 9, e88025. doi:10.1371/journal.pone.0088025.

Sundström, L. F., Gruber, S. H., Clermont, S. M., Correia, J. P. S., de Marignac, J. R. C., Morrissey, J. F., et al. (2001). "Review of elasmobranch behavioral studies using ultrasonic telemetry with special reference to the lemon shark, *Negaprion brevirostris*, around Bimini Islands, Bahamas," in *The behavior and sensory biology of elasmobranch fishes: an anthology in memory of Donald Richard Nelson*, eds. T. C. Tricas and S. H. Gruber (Dordrecht: Springer Netherlands), 225–250. doi:10.1007/978-94-017-3245-1_13.

Swearer, S., Treml, E., and Shima, J. (2019). "A review of biophysical models of marine larval dispersal," in *Oceanography and Marine Biology* (CRC Press), 325–356. doi:10.1201/9780429026379-7.

Tennessen, J. B., Holt, M. M., Hanson, M. B., Emmons, C. K., Giles, D. A., and Hogan, J. T. (2019). Kinematic signatures of prey capture from archival tags reveal sex differences in killer whale foraging activity. *J. Exp. Biol.* 222, jeb191874. doi:10.1242/jeb.191874.

Teo, S. L. H., Boustany, A., Blackwell, S., Walli, A., Weng, K. C., and Block, B. A. (2004). Validation of geolocation estimates based on light level and sea surface temperature from electronic tags. *Mar. Ecol. Prog. Ser.* 283, 81–98. doi:10.3354/meps283081.

The Loch Sunart to the Sound of Jura Marine Conservation Order (2016). Available at: https://www.legislation.gov.uk/ssi/2016/90/made.

Thieurmel, B., and Elmarhraoui, A. (2019). suncalc: Compute Sun Position, Sunlight Phases, Moon Position and Lunar Phase. R package version 0.5.0. Available at: https://cran.r-project.org/package=suncalc.

Thorburn, J., Neat, F., Burrett, I., Henry, L.-A., Bailey, D. M., Jones, C. S., et al. (2019). Ontogenetic variation in movements and depth use, and evidence of partial migration in a benthopelagic elasmobranch. *Front. Ecol. Evol.* 7, 353. doi:10.3389/fevo.2019.00353.

Thorburn, J., Wright, P. J., Lavender, E., Dodd, J., Neat, F., Martin, J. C. A., et al. (2021). Seasonal and ontogenetic variation in depth use by a Critically Endangered benthic elasmobranch and its implications for spatial management. *Front. Mar. Sci.* 8, 656368. doi:10.3389/fmars.2021.656368.

Tiktak, G. P., Butcher, D., Lawrence, P. J., Norrey, J., Bradley, L., Shaw, K., et al. (2020). Are concentrations of pollutants in sharks, rays and skates (Elasmobranchii) a cause for concern? A systematic review. *Mar. Pollut. Bull.* 160, 111701. doi:10.1016/j.marpolbul.2020.111701.

Torkamani, S., and Lohweg, V. (2017). Survey on time series motif discovery. *WIREs Data Min. Knowl. Discov.* 7, e1199. doi:10.1002/widm.1199.

Treep, J., de Jager, M., Bartumeus, F., and Soons, M. B. (2021). Seed dispersal as a search strategy: dynamic and fragmented landscapes select for multi-scale movement strategies in plants. *Mov. Ecol.* 9, 4. doi:10.1186/s40462-020-00239-1.

Treloar, M. A., Laurenson, L. J. B., and Stevens, J. D. (2007). Dietary comparisons of six skate species (Rajidae) in south-eastern Australian waters. *Environ. Biol. Fishes* 80, 181. doi:10.1007/s10641-007-9233-6.

Turchin, P. (1998). *Quantitative Analysis of Movement*. Sunderland, MA: Sinauer.

Udyawer, V., Dwyer, R. G., Hoenner, X., Babcock, R. C., Brodie, S., Campbell, H. A., et al.

(2018). A standardised framework for analysing animal detections from automated tracking arrays. *Anim. Biotelemetry* 6, 17. doi:10.1186/s40317-018-0162-2.

Ullah, S., and Finch, C. F. (2013). Applications of functional data analysis: A systematic review. *BMC Med. Res. Methodol.* 13, 43. doi:10.1186/1471-2288-13-43.

Valdimarsson, S. K., and Metcalfe, N. B. (2001). Is the level of aggression and dispersion in territorial fish dependent on light intensity? *Anim. Behav.* 61, 1143–1149. doi:10.1006/anbe.2001.1710.

Valletta, J. J., Torney, C., Kings, M., Thornton, A., and Madden, J. (2017). Applications of machine learning in animal behaviour studies. *Anim. Behav.* 124, 203–220. doi:10.1016/j.anbehav.2016.12.005.

Vaudo, J. J., and Lowe, C. G. (2006). Movement patterns of the round stingray *Urobatis halleri* (Cooper) near a thermal outfall. *J. Fish Biol.* 68, 1756–1766. doi:10.1111/j.0022-1112.2006.01054.x.

Wang, J.-L., Chiou, J.-M., and Müller, H.-G. (2016). Functional data analysis. *Annu. Rev. Stat. Its Appl.* 3, 257–295. doi:10.1146/annurev-statistics-041715-033624.

Wearmouth, V. J., and Sims, D. W. (2009). Movement and behaviour patterns of the critically endangered common skate *Dipturus batis* revealed by electronic tagging. *J. Exp. Mar. Bio. Ecol.* 380, 77–87. doi:10.1016/j.jembe.2009.07.035.

Wearmouth, V. J., and Sims, D. W. (2010). Sexual segregation in elasmobranchs. *Biol. Mar. Mediterr.* 17, 236–239.

Weber, D. N., Frazier, B. S., Whitney, N. M., Gelsleichter, J., and Sancho, G. (2020). Stress response and postrelease mortality of blacktip sharks (*Carcharhinus limbatus*) captured in shore-based and charter-boat-based recreational fisheries. *Fish. Bull.* 118, 297–314. doi:10.7755/FB.118.3.8.

Weng, K. C., O'Sullivan, J. B., Lowe, C. G., Winkler, C. E., Dewar, H., and Block, B. A. (2007). Movements, behavior and habitat preferences of juvenile white sharks *Carcharodon carcharias* in the eastern Pacific. *Mar. Ecol. Prog. Ser.* 338, 211–224. doi:10.3354/meps338211.

West, G. J., and Stevens, J. D. (2001). Archival tagging of school shark, *Galeorhinus Galeus*, in Australia: initial results. *Environ. Biol. Fishes* 60, 283–298. doi:10.1023/A:1007697816642.

Wetherbee, B. M., Gruber, S. H., and Rosa, R. S. (2007). Movement patterns of juvenile lemon

sharks *Negaprion brevirostris* within Atol das Rocas, Brazil: a nursery characterized by tidal extremes. *Mar. Ecol. Prog. Ser.* 343, 283–293. doi:10.3354/meps06920.

Wheeler, A. (1969). *The fishes of the British Isles and NW Europe*. London: MacMillan & Co. Ltd.

Wheeler, C. R., Gervais, C. R., Johnson, M. S., Vance, S., Rosa, R., Mandelman, J. W., et al. (2020). Anthropogenic stressors influence reproduction and development in elasmobranch fishes. *Rev. Fish Biol. Fish.* 30, 373–386. doi:10.1007/s11160-020-09604-0.

White, E. R. (2019). Minimum time required to detect population trends: the need for long-term monitoring programs. *Bioscience* 69, 40–46. doi:10.1093/biosci/biy144.

Whitney, N. M., Lear, K. O., Morris, J. J., Hueter, R. E., Carlson, J. K., and Marshall, H. M. (2021). Connecting post-release mortality to the physiological stress response of large coastal sharks in a commercial longline fishery. *PLoS One* 16, e0255673. doi:10.1371/journal.pone.0255673.

Whitney, N. M., White, C. F., Gleiss, A. C., Schwieterman, G. D., Anderson, P., Hueter, R. E., et al. (2016). A novel method for determining post-release mortality, behavior, and recovery period using acceleration data loggers. *Fish. Res.* 183, 210–221. doi:10.1016/j.fishres.2016.06.003.

Whitney, N., White, C., Anderson, P., Hueter, R., and Skomal, G. (2017). The physiological stress response, postrelease behavior, and mortality of blacktip sharks (*Carcharhinus limbatus*) caught on circle and J-hooks in the Florida recreational fishery. *Fish. Bull.* 115, 532–543. doi:10.7755/FB.115.4.9.

Whitty, J. M., Morgan, D. L., Peverell, S. C., Thorburn, D. C., and Beatty, S. J. (2009). Ontogenetic depth partitioning by juvenile freshwater sawfish (*Pristis microdon*: Pristidae) in a riverine environment. *Mar. Freshw. Res.* 60, 306–316. doi:10.1071/MF08169.

Wickham, H. (2015). *R packages: organize, test, document, and share your code*. 1st ed. Sebastopol: O'Reilly Media.

Wiegand, J., Hunter, E., and Dulvy, N. K. (2011). Are spatial closures better than size limits for halting the decline of the North Sea thornback ray, *Raja clavata*? *Mar. Freshw. Res.* 62, 722–733. doi:10.1071/MF10141.

Wild, M. (2009). Global dimming and brightening: a review. *J. Geophys. Res. Atmos.* 114. doi:10.1029/2008JD011470.

Wilkinson, M. D., Dumontier, M., Aalbersberg, Ij. J., Appleton, G., Axton, M., Baak, A., et al. (2016). The FAIR Guiding Principles for scientific data management and stewardship. *Sci. Data* 3, 160018. doi:10.1038/sdata.2016.18.

Williams, H. J., Taylor, L. A., Benhamou, S., Bijleveld, A. I., Clay, T. A., de Grissac, S., et al. (2020). Optimizing the use of biologgers for movement ecology research. *J. Anim. Ecol.* 89, 186–206. doi:10.1111/1365-2656.13094.

Williams, J. J., Papastamatiou, Y. P., Caselle, J. E., Bradley, D., and Jacoby, D. M. P. (2018). Mobile marine predators: an understudied source of nutrients to coral reefs in an unfished atoll. *Proc. R. Soc. B Biol. Sci.* 285, 20172456. doi:10.1098/rspb.2017.2456.

Williamson, M. J., Tebbs, E. J., Dawson, T. P., Curnick, D. J., Ferretti, F., Carlisle, A. B., et al. (2021). Analysing detection gaps in acoustic telemetry data to infer differential movement patterns in fish. *Ecol. Evol.* 11, 2717–2730. doi:10.1002/ece3.7226.

Wilson, A. M., Hubel, T. Y., Wilshin, S. D., Lowe, J. C., Lorenc, M., Dewhirst, O. P., et al. (2018). Biomechanics of predator–prey arms race in lion, zebra, cheetah and impala. *Nature* 554, 183–188. doi:10.1038/nature25479.

Winslade, P. (1974). Behavioural studies on the lesser sandeel *Ammodytes marinus* (Raitt) II. The effect of light intensity on activity. *J. Fish Biol.* 6, 577–586. doi:10.1111/j.1095-8649.1974.tb05101.x.

Winton, M. V, Kneebone, J., Zemeckis, D. R., and Fay, G. (2018). A spatial point process model to estimate individual centres of activity from passive acoustic telemetry data. *Methods Ecol. Evol.* 9, 2262–2272. doi:10.1111/2041-210X.13080.

Wood, S. N. (2017). *Generalized additive models: an introduction with R*. London: Chapman and Hall/CRC.

Wood, S. N., Goude, Y., and Shaw, S. (2015). Generalized additive models for large data sets. *J. R. Stat. Soc. Ser. C Appl. Stat.* 64, 139–155. doi:10.1111/rssc.12068.

Wood, S. N., Li, Z., Shaddick, G., and Augustin, N. H. (2017). Generalized additive models for gigadata: modeling the U.K. black smoke network daily data. *J. Am. Stat. Assoc.* 112, 1199–1210. doi:10.1080/01621459.2016.1195744.

Wright, P. J., Jensen, H., and Tuck, I. (2000). The influence of sediment type on the distribution of the lesser sandeel, *Ammodytes marinus*. *J. Sea Res.* 44, 243–256. doi:10.1016/S1385-1101(00)00050-2.